NTNU
Norwegian University of
Science and Technology

An analysis of facies in the De Geerdalen Formation and provenance across the Middle to Late Triassic boundary on Spitsbergen, Svalbard

Bård Heggem

Geology
Submission date: May 2017
Supervisor: Atle Mørk, IGP
Co-supervisor: Arild Andresen, UiO
Snorre Olaussen, UNIS

Norwegian University of Science and Technology
Department of Geoscience and Petroleum

Abstract

At the end of the Paleozoic era, Svalbard and the Barents Sea were part of a large shallow embayment on the northern margin of Pangea. During the Triassic period, the embayment was filled with sediments from a large deltaic system that progressed across the Barents Shelf. The De Geerdalen Formation on Spitsbergen was deposited during the Carnian stage of the Late Triassic, and is composed of sediments that were deposited in a distal part of the deltaic system. This study documents and discusses the depositional environment of the De Geerdalen Formation through facies analysis of outcrops in the Fulmardalen area on Central Spitsbergen. The study builds on previous work, and aims to extend the present understanding of the environmental evolution on Svalbard during the Late Triassic.

A total of 6 measured section from Fulmardalen are presented. The facies analyses display a general upwards shallowing environment, dominated by prodelta and open marine deposits in the lower part, shallow marine and delta front deposits in the middle part, and delta plain deposits in the upper part. The data indicate deposition in a highly dynamic environment, with significant facies variations both laterally and vertically. Laterally extensive sandstone bodies dominate the lower part of the De Geerdalen Formation in Fulmardalen, and are interpreted as barrier bars deposited in a shallow marine and delta front setting. Compared to more fluvial influenced sandstone bodies from the De Geerdalen Formation on the eastern islands of Svalbard, sandstone bodies in Fulmardalen are generally thin, with sedimentary structures that indicate a domination of basinal processes such as wave- and tidal energy. This may indicate that the deposition happened in a low accommodation space setting, where basinal processes could control the sediment distribution.

In addition to facies data from Fulmardalen, detrital zircon U-Pb age data from Middle and Upper Triassic sandstones from the Festningen section are presented. In combination with existing detrital zircon age data, sedimentological, stratigraphic, and seismic data, the zircon ages are used to investigate provenance for the Triassic succession at Festningen. The data indicate a western source in northern Greenland for the Early and Middle Triassic deposits. At the transition between the Middle and Late Triassic, the data indicate a distinct shift in provenance. The deposits of the Upper Triassic De Geerdalen Formation show zircon ages that suggest domains within the Uralides and the Taimyr region as main sediment sources, with additional input from the Timanides and Caledonides. The presence of near-syn-depositional zircon ages in samples from the De Geerdalen Formation may reflect rapid transportation rates, deposition as airborne volcanic ash, or the presence of a proximal active margin.

Sammendrag

Ved slutten av den paleozoiske æraen var Svalbard og Barentshavet del av en stor grunnhavsbukt på den nordlige kanten av Pangea. I løpet av den triassiske perioden ble bukten fylt med sedimenter fra et stort deltaisk system som prograderte over Barentshav-sokkelen. De Geerdals-formasjonen ble avsatt under carnium stadiet i sen-trias, og er bygget opp av sedimenter som ble avsatt i en distal del av det deltaiske systemet. Dette studiet dokumenterer og diskuterer avsetningsmiljøet til De Geerdals-formasjonen gjennom facies-analyser av blotninger fra Fulmardalen-området på sentrale Spitsbergen. Studiet bygger på tidligere arbeider, og har som formål å utvide den nåværende forståelsen av miljøutviklingen på Svalbard i sen-trias.

Totalt 6 oppmålte seksjoner fra Fulmardalen er presentert. Facies-analysene viser et generelt oppover-grunnende miljø, dominert av prodelta og åpen-marine avsetninger i nedre del, grunnmarine- og delta front avsetninger i midtre del, og delta slette avsetninger i øvre del. Dataene indikerer avsetning i et veldig dynamisk miljø, med betydelige facies-variasjoner både lateralt og vertikalt. Lateralt utstrakte sandsteinskropper dominerer i den nedre del av De Geerdals-formasjonen i Fulmardalen, og de er tolket som barrierebanker, avsatt i en grunnmarin og delta front setting. Sammenlignet med de mer fluvial-påvirkede sandsteinskroppene fra De Geerdals-formasjonen fra de østlige øyene på Svalbard, er sandsteinskroppene i Fulmardalen generelt tynne, med sedimentære strukturer som indikerer en dominans av basseng-prosesser som bølge- og tidevannsenergi. Dette indikerer trolig at avsetning skjedde i et miljø med lite akkomodasjonsrom, hvor bassengprosesser kontrollerer sediment-fordelingen.

I tillegg til facies-data fra Fulmardalen, så er detrital zirkon U-Pb aldersdata fra midt- og sen triasiske sandsteiner fra Festningen seksjonen presentert i denne oppgaven. I kombinasjon med eksisterende detrital-zirkon aldersdata, samt sedimentologisk, stratigrafisk og seismisk data, er aldersdataene brukt til å undersøke provenance for den triasiske lagrekka på Festningen. Dataene indikere en vestlig kilde på nordlige Grønland for avsetningene fra tidlig- og midt-trias. I overgangen mellom midt- og sen-trias indikerer zikon-alder populasjonene et distinkt provenance-skifte. Sedimentene i De Geerdals-formasjonen viser alderspopulasjoner som peker på domener i Uralidene og Taimyr-regionen som hovedkilder for sedimentene, i tillegg til input fra Timanidene og Kaledonidene. Tilstedeværelsen av zirkon-aldere som nærmest sammenfaller med avsetningsalderen til prøvene fra De Geerdals-formasjonen kan reflektere høye transport-hastigheter, avsetning som luftbåren vulkansk aske, eller tilstedeværelsen av en nærliggende aktiv plategrense.

Preface

This thesis is part of a Master's degree in geology at the Department of Geoscience and Petroleum at the Norwegian University of Science and Technology (NTNU). The main supervisor for this thesis has been Atle Mørk, *Professor II* at NTNU. Arild Andresen, *Professor emeritus* at the University of Oslo (UiO), and Snorre Olaussen, *Professor* at the University Centre in Svalbard (UNIS), has been co-supervisors.

The work presented herein is partly written in collaboration with master student Cathinka Schaanning Forsberg. Both Cathinka and I have studied the same geological formation, and worked closely together during fieldwork. As a natural consequence, Chapters 4, 5, 6 and 7 are therefore also presented in Cathinka's thesis, although minor differences may occur.

All photographs presented in the thesis have been taken by NTNU-students that attended fieldwork in 2016, unless otherwise stated.

Trondheim, 15.06.2017

Bård Heggem

Acknowledgements

First I would like to extend my thanks to my main supervisor Atle Mørk, *Professor II* at NTNU, for allowing me to partake in his projects on Svalbard. Being a part of his research team has allowed me to explore remote and exotic areas on the Svalbard archipelago, and it gives me great pleasure to look back at exciting memories from my fieldwork. Atle has a lot of experience both as a geoscientist and as a supervisor, something of which I have benefitted a lot. His honest and constructive feedback and guidance has been indispensable.

I would also like to thank co-supervisor Arild Andresen, *Professor Emeritus* at the University of Oslo (UiO), for his support and guidance on the detrital zircon age analysis. Arild has been nothing but helpful and kind during the process of writing my thesis, and has provided excellent feedback on my work. Thanks also to my second co-supervisor Snorre Olaussen, *Professor* at the University Centre in Svalbard (UNIS), for useful help and comments.

Several institutions have contributed to the funding of this thesis. The Norwegian Petroleum Directorate provided financial support for ship-transportation to fieldwork localities both in 2015 and 2016. The Svalbard Science Forum funded helicopter transportation to fieldwork in Fulmardalen 2016. UNIS and their logistics department are also thanked for providing fieldwork equipment, supplies and assistance in organizing fieldwork logistics.

A special thanks to my friend and fellow master student Cathinka S. Forsberg, for great collaboration during the countless hours we've spent together on fieldwork and thesis writing.

Nina Bakke, Sofie Bernhardsen, Jostein Røstad and Martijn Vermeer are thanked for great cooperation and assistance on fieldwork in Fulmardalen 2016. Turid Haugen, Sondre K. Johansen and Simen J. Støen are also thanked for joyful days in the field in August 2015. Special thanks are also forwarded to PhD-candidate Gareth S. Lord for helpful advice and guidance on fieldwork as well as through the whole thesis writing process. Furthermore, my good friends and classmates at "Kontoret" are thanked for all the good times during the years we have spent together studying at NTNU.

I would also like to thank all the kind people at the Department of Geosciences at UiO who helped with my detrital zircon analysis. A special thanks to Magnus Kristoffersen, who has been extremely helpful with the analysis, interpretation and presentation of zircon age data.

Finally, I wish to thank my family and friends for their continuous support, encouragements and tireless efforts to keep me motivated. Also, a huge "thank you" to my dear girlfriend Eirin Eidem, who saved the day when my MacBook decided to crash, just four days before the thesis deadline.

Table of Contents

List of Figures

List of Tables

1 Introduction

1.1 Study area

The archipelago of Svalbard represents the north-westernmost land-exposure in the Barents Sea (Figure 1.1). Covering around 1.3 million km^2, the Barents Sea is one of the largest continental shelf areas in the world (Doré, 1995). Geologically, the shelf can be divided into two major and highly disparate provinces. The eastern province is composed of large depositional basins, while the western province consists of a complex mosaic of basins, platforms, and structural highs (Faleide et al., 1984; Worsley, 2008). This mosaic, including the emerged Svalbard archipelago, reflects upon major tectonic movements that has affected the western and north-western margins of the Eurasian continental plate through time, and Svalbard is often regarded as an uplifted corner of the Barents Sea shelf (Worsley, 2008; Dallmann, 2015).

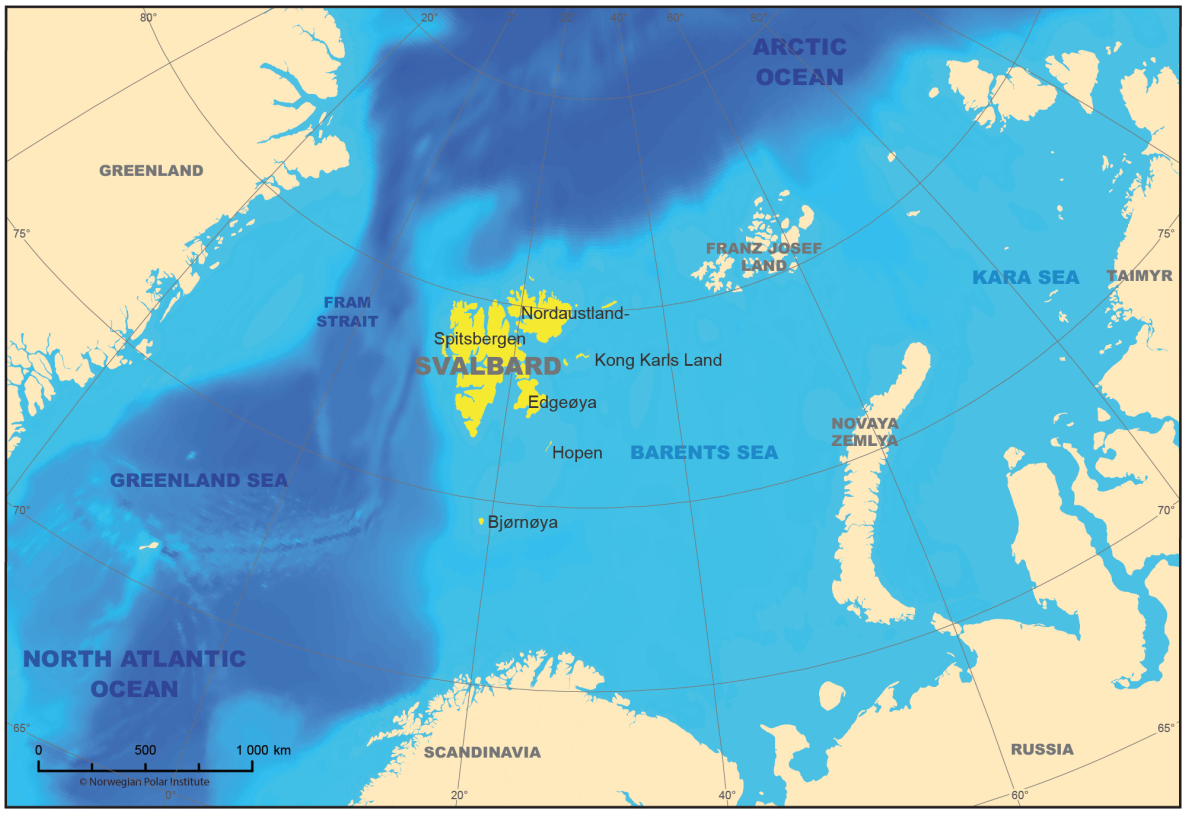

Figure 1.1 *Map overview of the Barents Sea region. The map illustrates Svalbard's present day position in the north-western corner of the Barents Sea. From Dallmann (2015).*

The archipelago of Svalbard consists of 8 major and several smaller islands. The data presented in this thesis concern exposed Triassic strata from two separate areas on Spitsbergen, which is the largest island of the archipelago. For facies analysis, flat lying strata from the mountain slopes of Fulmardalen, a northwest-southeast trending side valley of Sassendalen on

Central Spitsbergen, has been studied. The second dataset that will be presented in this thesis was collected from the Festningen section, a geological locality situated in outer Isfjorden on the west-coast of Spitsbergen.

1.2 Aim of Study

The work presented in this thesis was conducted with an overall aim of achieving the following two objectives:

i. Investigate the depositional environment of the Late Triassic De Geerdalen Formation and construct a representative facies-model for the Fulmardalen area. This will then enable a correlation to datasets that has previously been presented from other areas with Late Triassic exposures on Svalbard.
ii. Apply detrital zircon geochronology to investigate sedimentary provenance for the Triassic succession at Festningen section. More specifically, the study will try to pinpoint the stratigraphic position of a shift in provenance at the transition between the Middle and Late Triassic succession, previously suggested by Bue and Andresen (2014). The data will enable a discussion on source areas and basin fill models. The application of detrital zircon geochronology as a method in a provenance research will also be evaluated.

1.3 Previous research – Sedimentology and Stratigraphy

The initial geoscientific investigations of Triassic successions on Svalbard dates all the way back to the second half of the 19th century, when Swedish scientists dominated the research efforts and contributed with important stratigraphic and paleontological work (Vigran et al., 2014). Much of this work was later synthesized by Nathorst (1910). Since then, Svalbard's scientifically and politically open status has allowed the archipelago to become a study site for international collaboration. Thus, the current understanding of the Triassic succession on Svalbard is based on the work of geoscientists from various nations, but especially from Sweden, Britain, Russia, Poland and Norway (Vigran et al., 2014).

During the 1970's, the realization of a large petroleum potential for the Barents Sea led to a renewed and increased interest in post-Caledonian outcrops on Svalbard (Vigran et al., 2014), which serve as great analogues to the offshore subsurface strata (Worsley, 2008). A rapidly growing amount of both onshore and offshore data were collected and published. As a consequence, Mørk et al. (1999a) found it necessary to revise previous lithostratigraphic proposals in order to create an integrated lithostratigraphic scheme that would ease correlation

between the different studies. The lithostratigraphic nomenclature presented in Mørk et al. (1999a) is at present the accepted scheme for the Triassic stratigraphy on Svalbard, only with a few additions (Krajewski, 2008; Mørk et al., 2013; Lord et al., 2014a). This scheme has also been applied as the stratigraphical framework in this thesis.

Amongst the studies of the Triassic succession on Svalbard, previous studies has been focussing on outcrops from western and central Spitsbergen (Buchan et al., 1965; Knarud, 1980; Mørk et al., 1982; Pčelina, 1983; Rød et al., 2014; Lord et al., 2017a), eastern Spitsbergen (Buchan et al., 1965; Knarud, 1980; Mørk et al., 1982; Lord et al., 2017a), Edgeøya, Barentsøya and Wilhelmøya (Buchan et al., 1965; Flood et al., 1971; Lock et al., 1978; Knarud, 1980; Winsnes and Worsley, 1981; Mørk et al., 1982; Rød et al., 2014; Lord et al., 2017a) and Hopen (Flood et al., 1971; Pčelina, 1972; Worsley, 1973; Smith et al., 1975; Mørk et al., 2013; Klausen and Mørk, 2014; Lord et al., 2014a,b; Paterson and Mangerud, 2015). Ongoing petroleum exploration has also resulted in several publications on seismic- and core data from analogue successions in the Barents Sea (Leith et al., 1992; Mørk et al., 1993; Vigran et al., 1998; Mørk and Elvebakk, 1999; Bugge et al., 2002; Riis et al., 2008; Glørstad-Clark et al., 2010, 2011; Glørstad-Clark, 2011; Høy and Lundschien, 2011; Anell et al., 2014b; Lundschien et al., 2014; Klausen et al., 2015). Palynological and sedimentological studies conducted on the Triassic succession on Svalbard and in the Barents Sea are summarized in Vigran et al. (2014).

The sedimentological dataset presented in this thesis stems from the Fulmardalen area on central Spitsbergen. Due to its remote position, quite far inland on Spitsbergen, the study site has remained one of the lesser visited areas for geological research. With the exception of a log from Storfjellet (Knarud, 1980) and a log from Raggfjellet (Klausen et al., 2015; Lord et al., 2017a), very little data has been published from the area. During the fieldwork seasons of 2007-2009, fieldwork was conducted on mountains on the southern side of Sassendalen and Tempelfjorden, a couple of kilometres west-north-west of Fulmardalen. The resulting data has been presented in (Rød et al., 2014). During the summer of 2015, several students form NTNU, including the author of this thesis, conducted fieldwork on mountains on the east-coast of Spitsbergen, Wilhelmøya, Barentsøya and Edgeøya. This work resulted in the master theses of Johansen (2016), Haugen (2016) and Støen (2016), which are summarized in Lord et al. (2017a). Geographically speaking, Fulmardalen is located in between the aforementioned study areas.

1.4 Detrital zircon provenance studies from the Arctic

The second objective in this thesis is to investigate provenance of the Triassic succession at Festningen. In this section, the most relevant detrital zircon (DZ) provenance studies that previously has been published will be summarized. A more detailed description of the geology of proposed source areas that are mentioned in this section is given in Section 2.5.

The application of DZ geochronology as a tool in provenance studies is a relatively young method. Over the last decade there has been a rapid increase in the number of DZ geochronology studies with focus on potential source areas for late Paleozoic to Early Mesozoic sediments in and around the Arctic basins. Miller et al. (2013) provides a summary of Triassic detrital zircon data the Arctic, with focus on their implications for paleo-drainage systems. But also in more recent years, several studies presenting DZ geochronology datasets relevant to this thesis have been published from various areas in the Arctic.

Soloviev et al. (2015) presents DZ age data Franz Josef Islands, and suggest that the main sources clastic material for the Northern Barents Sea in the Middle-Late Triassic were domains within the Uralian Fold Belt, with additional sources from the East European Craton, the Timanides and Taimyr. Zhang et al. (2016) investigates DZs from sandstones in Southern Taimyr, and found that the age signatures in the Triassic-Jurassic succession displayed a gradual transition from a dominant Uralian source in the Triassic, to a predominantly Siberian Trap related dominance in the Early Jurassic. In the Sverdrup Basin, both Miller et al. (2006) and Omma et al. (2011) present evidence of a potential Triassic sediment transport pathway between the Sverdrup basin and the Uralian Orogeny. Anfinson et al. (2016), working with samples from the northern part of the Sverdrup basin, discuss evidence of a characteristic DZ signature for a hypothetical northern source area, often referred to as Crockerland (Embry, 1993). Based on the occurrence of volcanic ash layers and near-syn-sedimentary DZ ages in Triassic strata on Axel Heiberg Island in the Sverdrup Basin, Midwinter et al. (2016) suggest that a northern source associated with an active convergent margin could have existed north of the basin in the Triassic. It is furthermore suggested that this margin were actively sourcing sediments to the Sverdrup basin for at least 50 Myr.

Paleogeographic reconstructions from Triassic times (e.g. Gee and Teben'kov, 2004; Riis et al., 2008; Smelror et al., 2009) put Svalbard in a relatively proximal position to Greenland and the Sverdrup Basin. Røhr et al. (2008) and Røhr et al. (2010) presents DZ age data of samples from Lower Cretaceous sedimentary formations from the Wandel Sea Basin and from the Sverdrup Basin, respectively. According to these studies, the data presented therein allows for an identification of zircon age-populations typical for the Greenlandic

Caledonides and the Greenland–Canadian Shield. Furthermore, Røhr and Andersen (2009) suggest that Greenland to be the most likely source for DZs in the Lower Cretaceous Helvetiafjellet Formation on Svalbard. All three aforementioned studies have a high interpretative value to the data presented in this thesis as they may act as references for identifying Greenland as a potential source area.

Wells drilled by petroleum companies in recent years has allowed for DZ provenance studies from subsurface strata in the southern and southwestern Barents Sea. Fleming et al. (2016) present sample-data from wells in the south-western Barents Sea, and concludes that Triassic sands of the Snadd Formation has a strong Uralian signature. It is also pointed out that the sand show a slightly different DZ age signature than what is found age-equivalent sands in Svalbard and Franz Josef Land, and suggest Taimyr and Severnaya Zemlya to have been important source areas for the the Traissic succession on these archipelagos. Klausen et al. (2016), also working on samples from the Norwegian Barents Sea, discuss the presence of "young" detrital zircon ages in Late Triassic – Early Jurassic formations. Their data shows many zircon ages falling close to the interpreted depositional age of the sampled rocks. It is suggested that the ages may be indicate the presence of a dynamic and magmatically active source area in the east during the Triassic, potentially situated in or around the Novaya Zemlya protrusion of the Uralide Orogen. Klausen et al. (2016) propose that this region could have been sourcing sediments to the Norwegian Barents Sea as late as until the Early Jurassic.

The most relevant data for this thesis, however, are published in Bue and Andresen (2014). In their paper, DZ age data from Triassic and Jurassic samples collected from various localities on Svalbard, including from the Festningen profile on western Spitsbergen, is presented. The samples that were analysed in this paper were collected from several stratigraphic levels within the Triassic and Jurassic succession on Svalbard, and the data demonstrate significant changes in provenance signatures with time. Sediments that were deposited in the Early to Middle Triassic (in the Vardebukta and Tvillingodden formations) are found to reflect derivation from westerly located sources, most likely within northern Greenland and potentially northern Canada. DZ age data form the De Geerdalen Formation are interpreted to suggest that easterly located sources became dominant in the Late Triassic, mainly with sediments coming from the northern Uralides and the Taimyr region, with additional input from the Timanides and the Caledonides. Samples from the Late Triassic to Early Jurassic Wilhelmøya Subgroup are interpreted to display a mix of the detrital zircon ages, suggesting that older sediments may have been reworked and redeposited, potentially accompanied by

renewed sediment influx from a westerly source. Bue and Andresen (2014) point out that that the Early to Middle Triassic provenance signatures show a strong resemblance to the signatures derived from Early Cretaceous sandstones on Svalbard (Røhr and Andersen, 2009), and that a similar, westerly located source was dominant both in the Early to Middle Jurassic and in the Early Cretaceous.

The findings presented in Bue and Andresen (2014) form the very foundation behind the provenance research questions that will be addressed in this thesis. The aim of the work presented in this thesis has been to investigate and refine the proposed provenance shift from a western to an eastern source across the Middle to Late Triassic boundary. In order pinpoint this shift to a stratigraphic position, a combination of detrital zircon geochronology data and a sedimentological understanding of the succession has been applied.

2 Regional Geology for Svalbard and the Barents Sea Shelf

The geology of Svalbard (Figure 2.1) and the Barents Sea records a long and complex history, and the Svalbard archipelago is often regarded as an emerged north-western window into the subsurface geology of the Barents Sea. The "basement" geology on Svalbard, collectively referred to as "Hekla Hoek", is composed of a complex mosaic of Late Archean to Early Palaeozoic sediments, metasediments, and igneous rocks (Worsley, 2008; Elvevold and Dallmann, 2015a), which all were to a varying degree affected by deformational events during the build-up of the Caledonian Orogeny (Elvevold and Dallmann, 2015b).

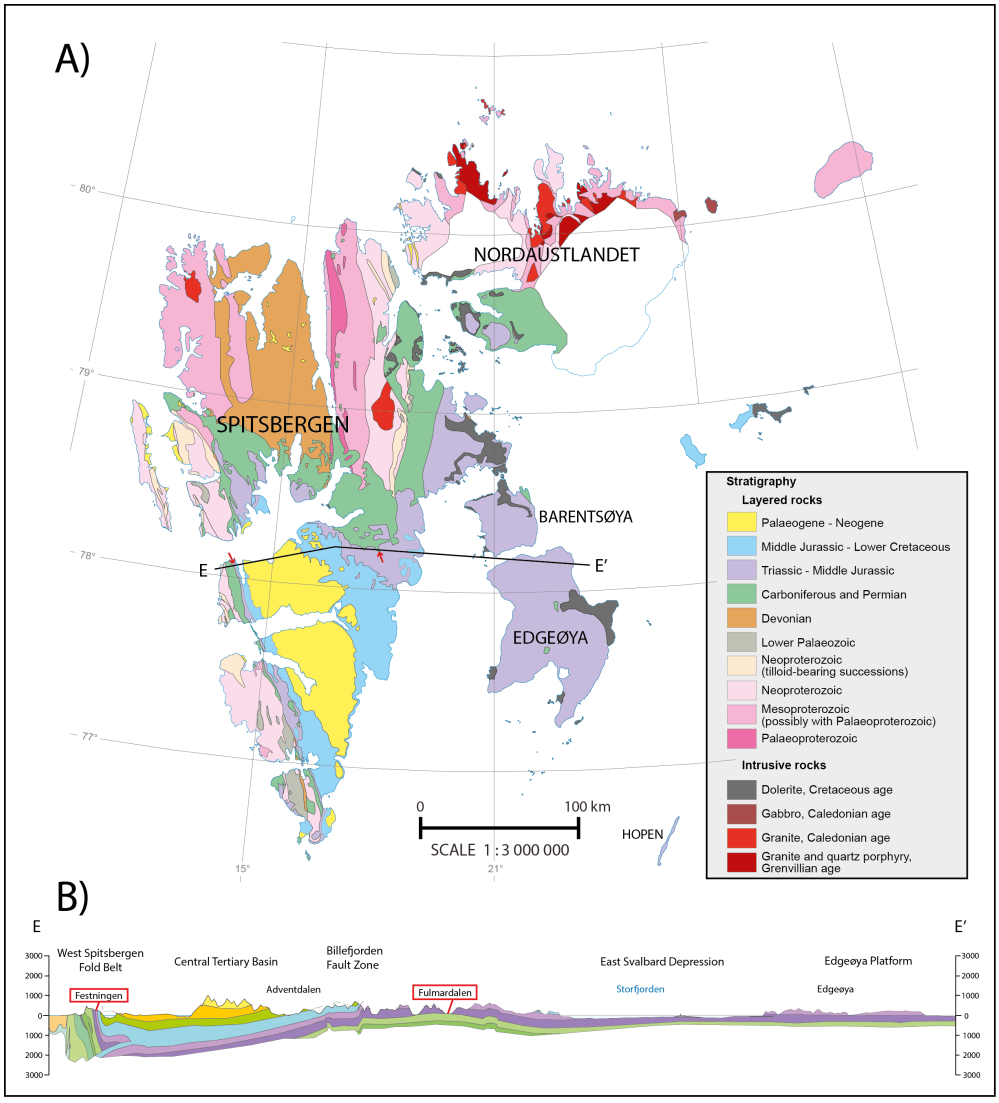

Figure 2.1 *Geological map of the Svalbard archipelago and an east-west profile from Dallmann (2015).* ***(A)*** *The map is based on the major stratigraphic division on Svalbard. The location of profile E-E' has been indicated with a black line. The small red arrows mark the position of the Festningen section (to the west) and Fulmardalen (to the east).* ***(B)*** *Vertically exaggerated profile across Spitsbergen and Edgeøya. The position of Festningen and Fulmardalen are indicated.*

On top of the basement rests an almost complete sedimentary succession of Devonian to Cenozoic age (Worsley, 2008; Dallmann, 2015). Continuous northwards drift due to plate-tectonic movements (Figure 2.2) has brought Svalbard through several climatic zones (Elvevold et al., 2007; Worsley, 2008). Svalbard has drifted from approximately 40°S in the Cambrian, to its present-day position at around 79°N. The drifting that has resulted in significant changes to the depositional environments with time, and has left behind a highly diverse sedimentary succession. A concise review on the post-Caledonian development of Svalbard and the western Barents Sea is presented in Worsley (2008), and later also summarized in (Dallmann, 2015). In the remaining sections of Chapter 2, parts of the post-Caledonian succession on Svalbard that are most relevant to this thesis will be presented. This includes an overview of the Upper Permian – Middle Jurassic stratigraphy (Figure 2.5), with special emphasis on the Upper Triassic to Middle Jurassic Kapp Toscana Group and the depositional environments represented therein. A short review of post-Palaeozoic events that later have affected the Triassic succession will also be presented.

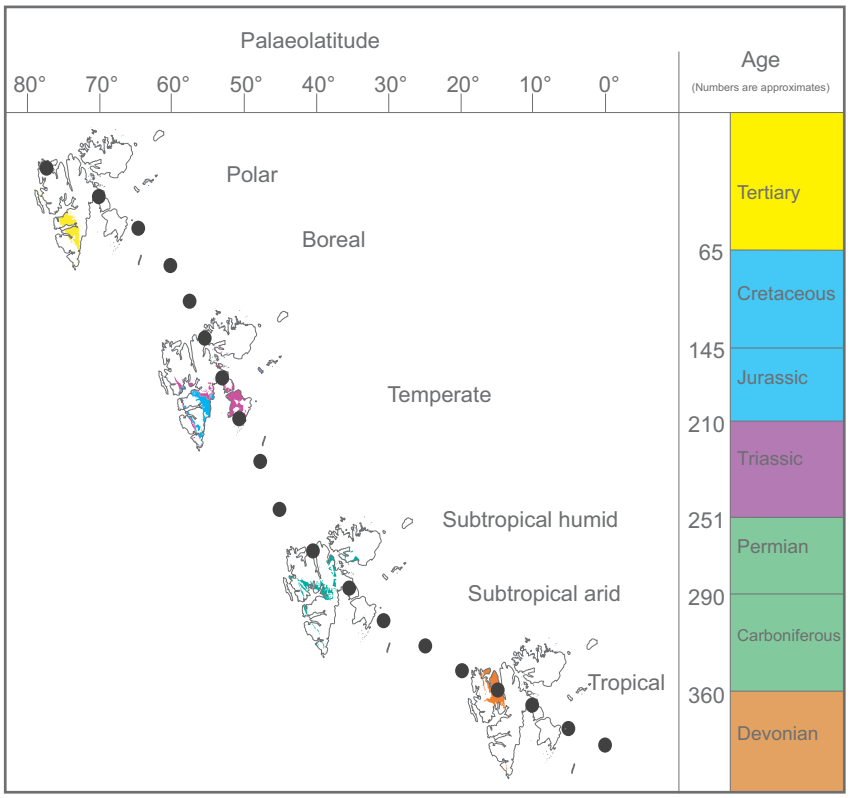

Figure 2.2 *Graphical presentation of Svalbard's continuous northward drift. From Paleozoic to Cenozoic times, Svalbard has drifted through several climatic zones. This drift has resulted in the highly diverse sedimentary succession that is exposed on the archipelago. From (Elvevold et al., 2007)*

2.1 From Late Permian biogenic sediments to Early Triassic clastics

After being part of a large carbonate platform with deposition of warm-water carbonates and evaporites from the Late Carboniferous to the Early Permian, Svalbard experienced a climatic shift towards the Late Permian (Blomeier, 2015). The climatic shift was connected to the build-up of the Uralide Orogeny in the east and the opening of intracratonic seaways along the western shelf margins (Worsley, 2008). From relatively calm, shallow marine, warm and arid conditions, the Svalbard area now became part of an open marine shelf with temperate to cold-water and high energy conditions. Carbonate precipitating organism that thrived in the warm-water conditions in the Early Permian became less dominant, and were replaced by siliceous sponges that produced enormous amounts of spicules. Accumulations of these spicules have formed thick biogenic chert-layers, and such layers, inter-fingering with black shales and dark siltstones are characteristic for the Late Permian Kapp Starostin Formation on Svalbard (Worsley, 2008; Blomeier, 2015). Towards the end of the Permian, life on earth suffered through a major mass extinction (Worsley, 2008). This extinction also affected the sedimentation style on Svalbard (Blomeier, 2015; Mørk, 2015). The biological influence on the sedimentation became more or less completely absent, and in the Upper Permian and Lowermost Triassic succession on Svalbard, fine grained deposits of non-siliceous shales are dominant (Mørk et al., 1982; Mørk et al., 1999a,b; Worsley, 2008).

2.2 Lower to Middle Triassic – the Sassendalen Group

Going in to the Mesozoic, the Barents Sea region was part of a large and shallow epicontinental embayment (Figure 2.3) in the north-western corner of the supercontinent Pangea (Buiter and Torsvik, 2007; Worsley, 2008; Lundschien et al., 2014). The embayment was bordered by Laurentia in the west, present day Novaya Zemlya in the east, and the Fennoscandian Shield in the south, with an opening to the Phantalassa Ocean in the northwest (Riis et al., 2008; Mørk, 2015).

The Lower to Middle Triassic succession in Svalbard and the western Barents Sea belongs to the Sassendalen Group. The fact that the Sassendalen Group has been subdivided into ten formations reflects upon both lateral and vertical facies variations (Mørk et al., 1999a). On Svalbard, the Sassendalen Group represents an overall transgressive trend, punctuated by repeated coastal progradations (Mørk et al., 1982, 1999a; Worsley, 2008). The rhytmic pattern of this coastal progradations were caused by major transgressive-regressive cycles that can be traced and correlated across the Arctic (Mørk et al., 1989; Egorov and Mørk, 2000; Mørk and

Smelror, 2001). On Svalbard, the cycles are most evident in the western parts of Spitsbergen, where coastal, shallow shelf to deltaic sequences are making up the Vardebukta, Tvillingodden and Bravaisberget formations (Mørk et al., 1982; Mørk et al., 1999a). On central and eastern Svalbard, the coastal development seen in the west are replaced by a more distal development, dominated by shelf mudstone deposits in the Vikinghøgda and Botneheia Formations (Mørk et al., 1999a,b; Vigran et al., 2014).

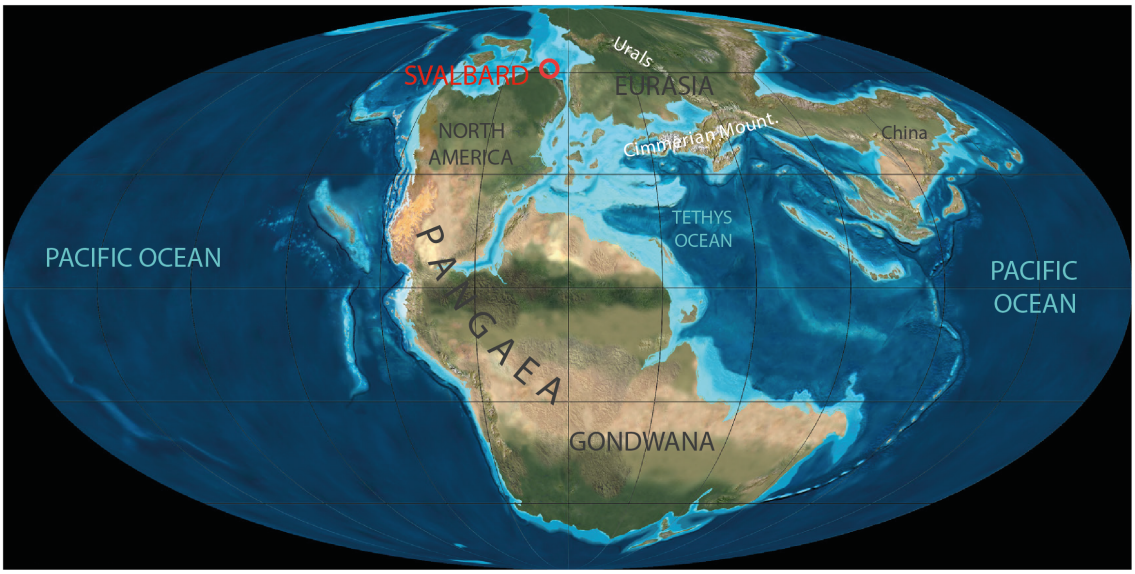

Figure 2.3 *Global paleogeography during the late Triassic. Svalbard was located in a shallow embayment in the north-western corner of Pangea, with an opening to the Panthalassa Ocean (named Pacific Ocean on figure) in the north. At the time, Svalbard was situated at around 55°N. From (Dallmann, 2015).*

Organic-rich shales of the Middle Triassic Bravaisberget and Botneheia formations represent the most promising hydrocarbon source-rocks on Svalbard (Mørk and Bjorøy, 1984; Mørk et al., 1999a; Krajewski, 2008). The Bravaisberget Formation, which is exposed along western Spitsbergen, represents a large upwards shallowing unit, coarsening from marine shale to shallow-water silt and fine sandstones (Mørk et al., 1999a; Krajewski et al., 2007). Similar to the older formations in the Sassendalen Group, facies and sedimentological data has indicated that the sediments were derived from a source located west of Svalbard (e.g. Mørk et al., 1982). This will be discussed further in Chapter 9. The Botneheia Formation, which is exposed in central and eastern Svalbard, represent a more distal development of the deltaic progradations from the west, mainly grading up from laminated mudstones to siltstones (Mørk et al., 1982; Mørk et al., 1999a). Total organic carbon values of up to 12% and abundant phosphate nodules occur in the Botneheia Formation, and has been interpreted to reflect locally restricted water circulation and periodic sediment starvation in a marine shelf environment for the Middle Triassic (Mørk and Bjorøy, 1984; Mørk et al., 1999a; Mørk and Bromley, 2008).

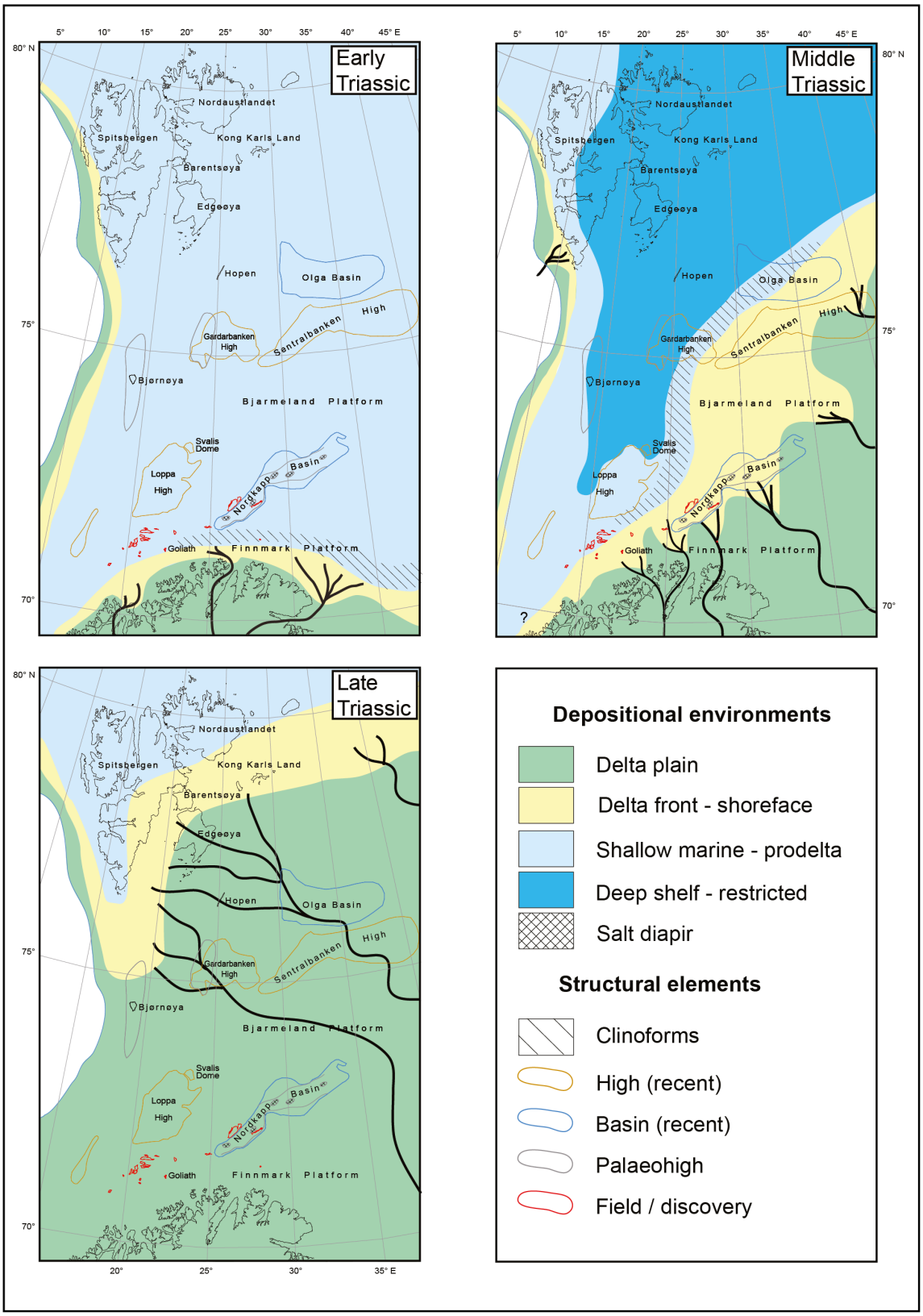

Figure 2.4 *Paleogeographic reconstruction of the Triassic on the Barents Sea Shelf. The reconstruction suggests domination of a western source for the Early and Middle Triassic, but in the Late Triassic, the area mainly received sediments from the southeast. From Lundschien et al. (2014).*

2.3 Late Triassic to Middle Jurassic – The Kapp Toscana Group

The transition from the Early and Middle Triassic Sassendalen Group to the Late Triassic to Middle Jurassic Kapp Toscana Group reflects a major change in the sedimentation pattern on Svalbard and in the Barents Sea (Mørk et al., 1999a; Riis et al., 2008; Lundschien et al., 2014). This transition is illustrated in Figure 2.4. The Kapp Toscana Group are divided into two major subdivisions, namely the Storfjorden and Wilhelmøya Subgroups, both representing quite different depositional regimes (Vigran et al., 2014).

2.3.1 The Storfjorden Subgroup

The lowermost part of the Storfjorden Subgroup is composed of grey, silty shales with red weathering nodules, belonging to the Tschermakfjellet Formation. This formation is dated to be of Early Carnian age (Vigran et al., 2014), and interpreted to represent a shallowing upwards, pro-delta depositional environment (Mørk et al., 1999a). On Svalbard, the Tschermakfjellet Formation has a somewhat variable thickness, but appears to be thicker on the eastern islands compared to western Spitsbergen, where it appears to be locally absent (Mørk et al., 1982, 1999a; Vigran et al., 2014).

The base of the Carnian to Early Norian De Geerdalen Formation (Tozer and Parker, 1968; Korčinskaja, 1982; Vigran et al., 2014) has been defined at the base of the first occurring prominent sandstone unit in the Storfjorden Subgroup (Flood et al., 1971; Lock et al., 1978; Mørk et al., 1999a). The formation is collectively described as a series of stacked upwards coarsening sequences, typically coarsening from shale to sandstone, and has been interpreted to reflect deposition in a shallow shelf to deltaic environment (Mørk et al., 1999a; Vigran et al., 2014; Lord et al., 2017a). As a unit, the De Geerdalen Formation thicken east- and north-eastwards over the Svalbard archipelago (Vigran et al., 2014). The De Geerdalen Formation correlates to the Snadd Formation from the Barents Sea Shelf, where it is considered as one of the most promising hydrocarbon reservoir formations (Worsley et al., 1988; Riis et al., 2008; Høy and Lundschien, 2011; Lord et al., 2014b; Lundschien et al., 2014; Klausen et al., 2015).

The upper part of the De Geerdalen Formation on western, central and eastern Spitsbergen, and on Wilhelmøya, is constituted by the Early Norian Isfjorden Member (Pčelina, 1983; Mørk et al., 1999a; Haugen, 2016; Lord et al., 2017a). The base of the Isfjorden Member was previously defined as the base of siltstone bivalve coquina bed occurring above a thick crossbedded sandstone unit (Mørk et al., 1999a), but recent investigations of the member has found this is definition to be inconsistent (Haugen, 2016). This is further discussed in Section 7.2.1. Lithologically, the Isfjorden Member is dominated by shales and mudrocks, with

relatively thin silt- and sandstone beds. Multi-coloured red and green shales and mudstones, siderite nodule beds, bivalve coquina beds, carbonate beds are characteristic for the Isfjorden Member (Mørk et al., 1999a; Haugen, 2016; Lord et al., 2017a). Calcrete profiles are also present, but are unevenly distributed (Haugen, 2016). The Isfjorden Member is interpreted to have been deposited in a shallow marine shelf, possibly lagoonal environment (Pčelina, 1983; Mørk et al., 1999a). Certain beds within the Isfjorden Member have been interpreted as calcrete, vastly different from other paleosol profiles found at lower levels in the De Geerdalen Formation (Haugen, 2016; Lord et al., 2017a). The occurrence of calcrete may indicate a climatic shift to a more arid environment on Svalbard in the late Carnian, or a significant change in the drainage pattern that resulted in a different type of pedogenesis (Haugen, 2016).

2.3.2 The Wilhelmøya and Realgrunnen Subgroups

The Storfjorden Subgroup and the De Geerdalen Formation is terminates with the occurrence of a calcareous sand- and siltstone, polymict conglomerate bed with locally abundant phosphatic nodules (Mørk et al., 1999a). This bed is known as the Slottet Bed and marks the onset of the Wilhelmøya Subgroup. The bed has been dated to be of Early Norian age (Korčinskaja, 1980). The Wilhelmøya Subgroup exhibits a succession of relatively thin and condensed formations in the western parts of Spitsbergen, with several hiatuses and low sedimentation rates (Worsley, 2008). This has resulted in the subdivision into only one formation with a composite vertical thickness between 3 – 25 m for this area (Mørk et al., 1999a). As a collective unit, the Wilhelmøya Subgroup thickens toward the east (Worsley, 2008), where it is composed of a more complete succession, reaching up to 230 m in vertical thickness on Kong Karls Land in the easternmost part of Svalbard (Mørk et al., 1999a).

The Uppermost Triassic to Middle Jurassic succession in the Norwegian part of the Barents Sea Shelf shows a similar but more complete development compared to on Svalbard (Worsley et al., 1988). The offshore equivalent to the Wilhelmøya Subgroup in the Barents Sea is defined as the Realgrunnen Subgroup (Worsley et al., 1988; Mørk et al., 1999a). Sandstone units in both subgroups are mineralogically and texturally more mature that the underlying sandstones of the De Geerdalen Formation, and has been interpreted to reflect deposition of reworked sediments in shallow marine and coastal environments (Bergan and Knarud, 1993; Worsley, 2008; Vigran et al., 2014). Recent hydrocarbon discoveries in sandstones of the Realgrunnen Subgroup in the Hoop area of the Barents Sea, have led to renewed attention on outcrop-analogues from the Wilhelmøya Subgroup on Svalbard (Lord et al., 2017c).

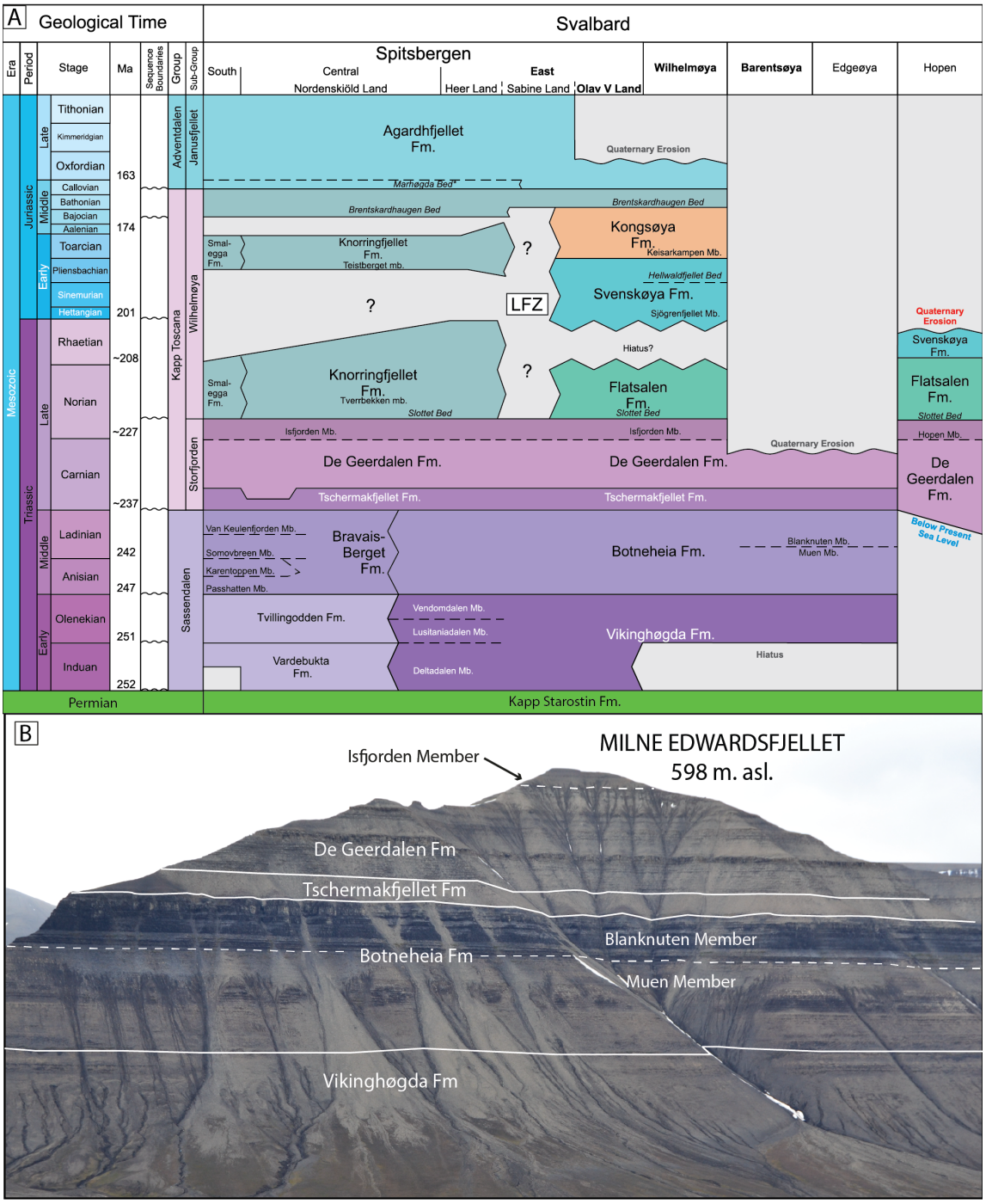

Figure 2.5 *Stratigraphic chart of the Triassic – Middle Jurassic on Svalbard.* ***(A)*** *Stratigraphic chart from various areas on Svalbard, from Lord et al. (2017a). The stratigraphic development in Fulmardalen are most like the one displayed under Heer Land.* ***(B)*** *Overview picture of the Lower to Upper Triassic succession at Milne Edwardsfjellet in Fulmardalen. The Lower Triassic Vikinghøgda Formation is poorly exposed at the location, while the dark shales of the Middle Triassic Botneheia Formation form a well exposed cliff in the mountainside. The cliff is overlain by stacked upwards coarsening units in the Upper Triassic De Geerdalen Formation. The uppermost part of the section is interpreted to belong to the Isfjorden Member.*

2.4 Post-Paleozoic tectonics, magmatic influence and erosion

The Triassic to mid-Jurassic period is generally regarded as a tectonically quiescent period on Svalbard and in the Barents Sea, and basin fill patterns were mainly controlled by inherited paleotopography from the Late Palaeozoic (Mørk et al., 1982; Faleide et al., 1984, 2008; Gabrielsen et al., 1990; Riis et al., 2008; Glørstad-Clark et al., 2010, 2011; Henriksen et al., 2011; Høy and Lundschien, 2011; Klausen and Mørk, 2014). Recent work from the eastern islands of Svalbard (Anell et al., 2013; Osmundsen et al., 2014) have found evidence of growth faulting in the late Triassic De Geerdalen Formation. Osmundsen et al. (2014) suggest that the presence of the faults may contradict the theory of a quiescent phase on the northern Barents Shelf during the Triassic, but this interpretation remains controversial. Rød et al. (2014) also studies the same faults on Edgeøya, but do not find evidence of any faults cutting through the Botneheia Formation, and suggested the faults to be a result of high sedimentation rates that led to syn-sedimentary faulting in a delta front setting during the Late Triassic.

Early Cretaceous dolerite dikes and sills of the Diabasodden Suite have intruded strata of all older ages on Svalbard (Mørk et al., 1999a; Maher, 2001). The intrusions occur frequently and at several stratigraphic levels within the Triassic strata, and the magmatic events have been related to the formation of a High Arctic Large Igneous Province in the Cretaceous (Maher, 2001). In addition to the Diabasodden Suite on Svalbard, evidence of such a High Arctic Large Igneous Province has been found on Franz Josef Land, adjacent shelf areas, Axel Heiberg and Ellesmere Islands, and perhaps on North Greenland (Maher, 2001). Recent U-Pb age analysis of the Diasbasodden Suite has given Lower Cretaceous ages at around 124.5 Ma (Corfu et al., 2013; Senger et al., 2014).

In the Late Cretaceous there are no sedimentary record from Svalbard. At this time, large parts of the Arctic, including the Svalbard archipelago, was uplifted and eroded, forming a regional unconformity on the Archipelago (Grundvåg, 2015).

In the Early Cenozoic, transpressional stresses caused by motion between the Barents Sea Shelf and the north-eastern edge of Greenland, led to the formation of the Central Tertiary Basin (CTB), a major depression that was filled with sediments from the early Palaeocene to the Oligocene (Steel et al., 1981; Steel and Worsley, 1984; Müller and Spielhagen, 1990; Worsley, 2008). Due to continuous plate-motion in the Eocene, a fold-and-thrust belt developed along the western rim of the CTB (Braathen et al., 1999; Smelror et al., 2009; Dallmann, 2015). Remnants of an equivalent Eurekan fold-and-thrust belt are also found in Ellesmere Island and on northern Greenland (Dallmann et al., 2015). In Svalbard the fold-and-thrust belt is

collectively known as the West Spitsbergen Fold Belt (Dallmann et al., 2015). Recent detrital zircon provenance analysis have shown that the formation of the fold and thrust belt to a large extent controlled the sedimentation pattern in the CTB (Petersen et al., 2016). Resulting structures from the Cenozoic deformational stresses that affected Svalbard are most visible along the western parts of Spitsbergen (e.g. at Festningen). However, deformational structures are also seen in areas further east, where tectonic stresses have created decollement zones with duplex structures in the soft shales of the Botneheia Formation (Andresen et al., 1992).

The Cenozoic movements between the Greenland and the Barents Sea ultimately led to the opening of the Norwegian-Greenland Sea in Early Eocene (Faleide et al., 1984; Smelror et al., 2009), and the sea-floor spreading continued into Neogene and Quaternary time (Hormes and Dallmann, 2015). In the Quaternary period, a cooler climate resulted in repeated glaciations on the Barents Sea Shelf. Ice-sheets covered Svalbard at several stages, and has left a denudated and erosion-dominated landscape that prevails on the archipelago today (Hormes and Dallmann, 2015).

2.5 Crystalline geology of potential Triassic source areas

In order to understand the detrital zircon signatures and provenance of the sedimentary successions on Svalbard it is important to understand the geological evolution of the surrounding areas. Figure 2.6 displays a simplified map of the Arctic region, including the Svalbard archipelago, with major crustal domains highlighted. In the following chapter, a brief overview of the geology of potential source areas for the Triassic deposits on Svalbard will be presented, with focus on their apparent zircon age signatures.

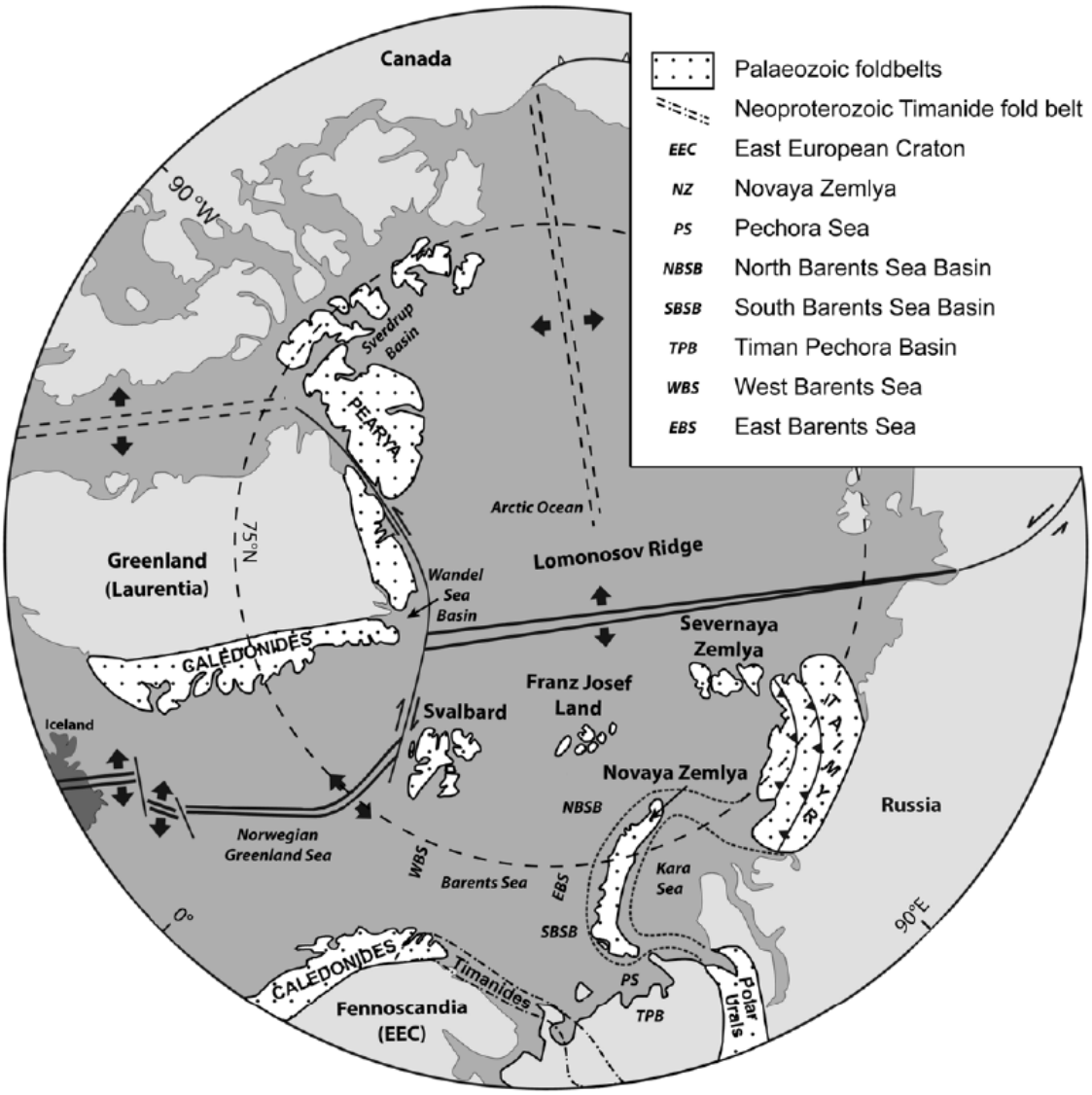

Figure 2.6 *Simplified map with major crustal domains surrounding the Barents Sea. Having a control on the geology of these areas is important in order to identify their zircon age signatures and potential as sediment sources.*

2.5.1 Archean and Proterozoic Cratons

Laurentia and the East European Craton formed around Archaean nuclei and grew through successive addition of juvenile crust and accretion of continental terrains (Bue and Andresen, 2014). At present, the cratons hold a complex geology, with ages spanning from the Eoarchean to the Neoproterozoic (Gee et al., 2006; Bue and Andresen, 2014). The oldest rocks known from the cratons are found on Greenland, where rocks of Eoarchean (>3.6 Ga) ages have been reported (Whitehouse and Kamber, 2005). On the East European Craton, Archean ages are not common, but sparse examples do exist. Ages around 3.6 Ga has been found from detrital zircons in sediments on the Kola Peninsula (Myskova et al., 2005) and from magmatic Archean complexes in Karelia (Lauri et al., 2011). On Svalbard itself, Archean ages are rare. Here, the oldest age recorded came from zircon grains in a basement quartz monzanite of the Atomfjella Complex, which yielded an age of 2710 Ma (Hellman et al., 2001; Elvevold and Dallmann, 2015a).

From the Neoarchean to the Paleoproterozoic, a wide range of ages are found from intrusive and metamorphic rocks in both Laurentia and the East European Craton (Bue and Andresen, 2014 and references therein). The northern parts of the East European Craton typically expose Paleo-Mesoproterozoic ages (approximately 2.5 - 1.0 Ga), but similar ages are also present in the northern parts of Laurentia (Bue and Andresen, 2014 and references therein). Domains yielding Grenvillian/Sweconorwegian ages (1.14 - 0.9 Ga) are dominant in any of the areas surrounding the Barents Sea, but have occasionally been reported from the Pearya Terrain (Figure 2.6), from Svalbard, from plutons within the Kalak Nappe, from the Taimyr Peninsula, and from Novaya Zemlya (Bue and Andresen, 2014 and references therein). Zircons of similar ages are also present in granitoids within the Caledonides on East Greenland (e.g. Kalsbeek et al., 2000; Watt and Thrane, 2001) and in granites from Southern Baltica (Andersen et al., 2002) and eastern Canada (Gower et al., 1990; Gower and Krogh, 2002). Geological domains yielding Neoproterozoic ages have been found in Svalbard, the Kalak Nappe, the Taimyr Fold Belt, from Novaya Zemlya, from the western parts of the Sibirian Craton and from the Timanide orogeny (Bue and Andresen, 2014 and references therein).

2.5.2 The Timanides

The Timanide orogeny refers to an orogenic event that took place between the Late Neoproterozoic and the Cambrian, and it has been suggested that to have formed as a result of a collision between the ancient continental plates Baltica and Arctida (Gee et al., 2006; Kuznetsov et al., 2007). Remnants of the orogeny are at present located along the northern and

eastern rim of the East European Craton (Kuznetsov et al., 2007), and can be traced from northern Russia to the Varanger Peninsula in northern Norway, where it has been truncated by the Caledonian orogenic front (Gee et al., 2006). Magmatic rocks related to the formation of the Timanide orogeny represent a significant source for Neoproterozoic aged (ca. 610 – 540 Ma) zircons for the Barents Sea region (Larionov et al., 2004; Pease, 2011; Soloviev et al., 2015). Remnant parts of the Timanide orogeny may also be present as complexes within the polar Urals, including at Novaya Zemlya.

2.5.3 The Caledonides

Gradual oblique convergence between the continental plates Baltica and Laurentia led to collision, subduction of the Baltic plate, and the formation of an orogeny during Silurian to Early Devonian time (Roberts, 2003). At present, remnants of the Caledonian Orogeny cover large areas both in Scandinavia and on the eastern margin of Greenland. The formation of the orogeny involved several magmatic and metamorphic events, providing zircon ages ranging from ca. 500 to 390 Ma (Bue and Andresen, 2014 and references therein). A north-south trending Caledonian suture has also been interpreted to extend northwards into the Barents Sea, stretching from northern Norway to somewhere between Svalbard and Franz Josef Land (Gee et al., 2006). Studies of pre-Devonian basement rocks on Svalbard (Gee and Teben'kov, 2004) and Caledonian domains on eastern Greenland (Higgins and Leslie, 2000) has indicated a strong correlation, suggesting that the basement on Svalbard to a large extent represents a direct northerly continuation of the Caledonides represented on eastern Greenland (Gee et al., 2006).

The Caledonides on north-eastern Greenland are mainly composed of Proterozoic sediments and gneisses (Kalsbeek et al., 1993; Pedersen et al., 2002), whereas areas further to the south expose Neo- and Mesoproterozoic sediments (e.g. Kalsbeek et al., 2000; Watt et al., 2000). Caledonian aged (440-420 Ma) granitoids are present in areas south of 76°N (Kalsbeek et al., 2001; Andresen et al., 2007; Røhr et al., 2010). Granitic intrusions and volcanic rocks of Caledonian age (500-390 Ma) have also been reported from the Pearya Terrain (Gee and Teben'kov, 2004). Similar ages have also been described from granitoids in Severnaya Zemlya (Harstad, 2016, and references therein).

2.5.4 The Uralides

The Uralide Orogeny formed between the Late Devonian and the Late Permian, and is thought to represent a significant detrital zircon producing event in the areas surrounding the Barents Sea (Bue and Andresen, 2014). The Uralide orogeny emerged as a result of convergence,

subduction and collision of the plates of Baltica, Kazakhstania and Siberia (Puchkov, 2009). Uralide granitoids formed at an almost constant rate from 370 Ma to 250 Ma, generally represented with older ages in the southern parts of the orogeny than in the north (Vernikovskij et al., 1995; Bea et al., 2002). The northern part of the Uralide orogeny, the part that is adjacent to the Barents Sea, starts with the Polar Urals in Siberia, stretches through Novaya Zemlya, and culminates in the Taimyr region (Gee et al., 2006; Puchkov, 2009). The tectonic evolution of the orogeny was initiated with the collision of an island arc and eastward subduction of oceanic lithosphere from the Middle-Late Devonian (Ritzmann and Faleide, 2009). It has been suggested that the creation of the Pai-Koi – Novaya Zemlya Fold Belt, a convergent zone with deformation dated to Late Triassic/Early Jurassic, potentially marks the final development of the Uralian event (Ritzmann and Faleide, 2009).

2.5.5 Siberian Traps Large Ingeous Province and Taimyr Igneous Complex

The decline of the main collisional phase during the Uralian event is marked with the emplacement of Sibirian Traps Large Igneous Province. This province formed when enormous volumes of flood basalts erupted over a 22 - 26 Myr long period, starting around the Permo-Triassic boundary (Renne and Basu, 1991; Puchkov, 2009). The emplacement of the Sibirian Traps was accompanied by syenitic magmatism happening approximately between 249 - 232 Ma. Such syenitic rocks are known from the Taimyr Peninsula and from Islands in the Kara Sea (Bue and Andresen, 2014 and references therein). Granitic rocks are present in the western parts of Taimyr, and has been dated to 249-233 Ma (Czamanske et al., 2000; Vernikovskij et al., 2003). Extrusive volcanic rocks and sills in Southern Taimyr are often regarded as the northernmost expression of the Siberian Traps volcanism, and was emplaced between 230 and 220 Ma (Walderhaug et al., 2005). However, these intrusives post-dates the main pulse of the Siberian Traps (251-249 Ma; Renne and Basu, 1991; Dalrymple et al., 1995; Czamanske et al., 2000) with around 20 Myr, and may rather be related to an Early Mesozoic tectonic event in this area (Walderhaug et al., 2005). Whatever the cause, post Sibirian Trap related magmatic rocks may give the Taimyr region a relatively distinct signature as a potential provenance area for Triassic deposits (Zhang et al., 2016).

2.5.6 Crockeland

The name Crockerland refers to a hypothetical landmass that are thought to have been located north of Svalbard and Ellesmere Island (Embry, 1993). It has been proposed that Crockerland may have been an important source area for Late Paleozoic and Mesozoic sediments in the Sverdrup Basin (Embry, 1993; Miller et al., 2006; Embry, 2009; Omma et al., 2011; Anfinson

et al., 2016). As there are no landmasses in this proposed source area at present, it is challenging to identify any distinct age signatures for Crockerland. Anfinson et al. (2016), have suggested that age-populations around 700-500 Ma and 450 – 370 Ma are representative U-Pb ages for the crustal domain of Crockerland. However, due to the fact that these age-populations are also found in other potential source areas adjacent to Svalbard and the Barents Sea, it is not possible to distinguish the enigmatic Crockerland from other sources based on age signatures alone (Bue and Andresen, 2014).

3 Methodology

3.1 Fieldwork logistics

3.1.1 Fulmardalen

Sedimentological fieldwork was conducted in the Fulmardalen area during a nine-day long period from the 12th to the 21st of August 2016. The fieldwork campaign was planned and organized as a co-operation between the Norwegian University of Science and Technology (NTNU) and the University Centre on Svalbard (UNIS). Fieldwork equipment was provided by UNIS Logistics, while helicopter transportation to the fieldwork area was provided by Lufttransport AS, Svalbard. The camp site was located at the mountain Dyrhø, from which logging-localities were reached by foot. The field party consisted of master students Cathinka Schaanning Forsberg, Nina Bakke and Bård Heggem, and the three fieldwork assistants Sofie Bernhardsen, Jostein Røstad and Martijn Vermeer. During the time spent in Fulmardalen the field party investigated the mountain slopes of Wallenbergfjellet, Dyrhø, Milne Edwardsfjellet, Ryssen, Storfjellet and Raggfjellet. All six of the mountains hold exposed sections of the De Geerdalen Formation, and all sections were systematically logged and sampled.

3.1.2 Festningen

A second fieldwork campaign was conducted at Festningen in the outer Isfjorden area on the 24th of August 2016. The fieldwork area was reach with transportation by the vessel MS *Stålbas,* which was on an excursion with the Norwegian Petroleum Directorate (NPD) arranged by UNIS. A small field party, consisting of *Professor emeritus* Arild Andresen and master student Bård Heggem, spent one day at Festningen for strategic collection of sandstone samples that has been used for detrital zircon provenance analysis. Specific intervals for sampling were chosen in advance after consultation with *Professor II* Atle Mørk.

3.2 Logging procedure

All sedimentological observations were taken following guidelines from Tucker (2011). GPS coordinates in UTM were recorded at the start and end of every log (Appendix A). All sections were measured using a meter-stick and the logs were drawn in the scale of 1:100. The logs were drawn in field notebooks, but have later been redrawn and digitalized using Adobe Illustrator. As described in Section 2.3.1, the De Geerdalen Formation can be described as a series of alternating shale and sandstone units. Because shale-dominated intervals are often heavily weathered and poorly exposed, the field observations are mainly focussed around the sandstone units. Digital cameras were used to document the observations. The outcrop-observations are

mainly focussing on lithology, grain size, sedimentological structures, unit thicknesses, bed geometry, bed contacts, bed colour, stratigraphic relationships and other physical features and relationships. Grain size variations were estimated with help from a hand-lens and a standard grain size sheets, while hydrochloric acid was applied on the sandstones to check for carbonate cementation. All other observation and investigations were done visually.

Six recorded logs were measured from at different localities in Fulmardalen, ranging from 21 m to 261 m in length. All logs are presented in Chapter 5. The exact log traces were chosen after visual investigations of the mountain slopes from a distance, where focus was put on finding the best exposed sections from each mountain. Most of the logs start around the top of the cliff-forming Blanknuten Member of the Botneheia Formation (Figure 2.5). Where it was possible, the Tschermakfjellet Formation was measured and included in the logs. The logs end where the gradient of the slopes, and consequently the exposed strata, tapers into scree towards the plateau-shaped mountain tops. All measured sections has been interpreted to end somewhere within the De Geerdalen Formation, suggesting that outcrops from the Wilhelmøya Subgroup were not measured at any of the log-localities. Lateral variations and geometries of the sandstone units were primarily observed and estimated in a distance from the log trace.

All measured sections from Fulmardalen were systematically sampled. Mudrock dominated intervals with exposed outcrops were sampled for potential palynology studies or Rock-Eval pyrolysis, while sandstone samples were collected for provenance and thin section analysis. However, most of the samples were collected with the purpose of being available for future work, and only a few samples have undergone any further analysis (see Chapter 8).

3.2.1 Sources of error

The major sources of error for the data collected during fieldwork in Fulmardalen are related to the "human factor". Most observations of sedimentological structures and other features within the outcrops are to a large extent subjective, and may therefore vary from person to person. Thickness-measurements carried out with a simple measuring stick may should also be considered as a potential source of error, as the accuracy of these measurements may vary. As previously mentioned, scree-cover poses as a common challenge when investigating the De Geerdalen Formation. Large section of the Formation is composed of shale-dominated intervals which are more easily a subject to weathering. Important facies details may therefore be hidden underneath scree-cover. This problem becomes very visible when working with the Isfjorden Member, where the characteristic red and green mudstone intervals are very often covered and

not exposed (Haugen, 2016). The degree of exposure is strongly linked to the steepness of the slopes, which again tends to be connected to lithology.

3.3 Optical Microscopy

Petrographic thin-sections from two potential calcrete profiles were produced at IGP, taken from the De Geerdalen Formation in Fulmardalen. A standard optical microscope with plan- and cross-polarized light was used to study the texture and mineralogy of the samples.

3.4 Rock-Eval pyrolysis

Rock-Eval pyrolysis was carried out on two samples from the upper part of the De Geerdalen Formation. The pyrolysis was carried out at Applied Petroleum Technology AS (APT) at Kjeller in Norway. The purpose of the analysis was to investigate the origin of the organic matter in the samples in order to understand the depositional environment of the shale units.

3.5 Detrital zircon analysis

All analytical work concerning samples from the Festningen profile, including sample preparation and isotope measurements, was conducted at the Department of Geosciences, University of Oslo, Norway. A total of 11 samples were collected from the Festningen profile, whereof 3 were chosen for analysis. One of the samples did however not contain any zircons, meaning that only two of the samples where therefore fully analysed.

3.5.1 Sample preparation

All analysed zircons were extracted from the samples using standard methods. After first being washed in an ultrasonic bath for 10 minutes and dried in an oven at 45°C over night, the samples were crushed to a coarse grain size (<1cm) using a jaw crusher. The grain size was further reduced to approximately 0.5mm using a Retch percussion mill. In order to separate the heavy mineral fraction from minerals of lower density, the crushed material was first "washed" in a jar with running water. This method was used to avoid losing any heavy minerals, which may be an issue when working with relatively fine-grained samples. After being washed, the heavy fraction was further isolated by applying heavy liquid (sodium heteropolytungstate $\rho = 2.80 \pm 0.02$ g ml^{-1}). No magnetic separation was performed, as this method may introduce an artificial bias to the samples (Sircombe and Stern, 2002; Andersen et al., 2011). Zircon grains were randomly hand-picked under a binocular microscope and placed on a double-adhesive tape. The grains were further mounted in epoxy resin, polished, and imaged by cathodoluminescence

applying a JEOL JSM 6460LV scanning electron microscope.

3.5.2 U-Pb analysis

LA-ICP-MS analysis was conducted in accordance with the procedures described in Kristoffersen et al. (2016), following analytical protocols from Andersen et al. (2009). U-Pb analysis was carried out using laser ablation inductively coupled plasma mass spectrometer (LA-ICP-MS) using a Nu Plasma HR multi-collector mass spectrometer equipped with a Cetac LSX-213 G2+ laser microprobe. Ablation conditions for the Cetac LSX-213 G2+ laser microprobe were beam diameter 40 μm (aperture imaging mode), pulse frequency 10Hz and beam fluence <0.78Jcm^{-2}, using static ablation. For data reduction, an interactive, in-house Microsoft Excel 2003 spreadsheet program were used for the U-Pb data.

Calculations of U-Pb ages were done using the decay constants of Steiger and Jäger (1977), while discordance percentages were calculated following methods presented in Kristoffersen et al. (2014). Ages are given using the ages with the lowest degree of uncertainty, meaning that ^{206}Pb-^{238}U ages are used when this uncertainty is lower or equal to the ^{207}Pb-^{206}Pb age uncertainty, otherwise ^{207}Pb-^{206}Pb ages are used. Grains with more than ±10% central discordance have not been included.

During the LA-ICP-MS analysis, standard zircons placed on separate epoxy pucks were used as U-Pb standards. These zircons were GJ-1 (^{207}Pb-^{206}Pb age = 609± 1 Ma; Jackson et al., 2004), 91500 (^{207}Pb-^{206}Pb age = 1065± 1 Ma; Wiedenbeck et al., 1995) and A382 (concordia age = 1876± 2Ma; Huhma et al., 2012). All three in-house reference standards were analysed at the start and at the end of each run, while analyses of GJ-1 were also repeated at approximately every half hour.

3.5.3 Data handling

For graphical presentation of the data, concordia plots and ages were calculated using Isoplot (Ludwig, 2008). Histograms, kernel density estimates (KDE), empirical cumulative distribution function (ECDF) and likeness-tests (Satkoski et al., 2013) were constructed using R programming language and statistical computing environment (R Development Core Team, 2015), following procedures described in Andersen et al. (2017).

4 Facies in the De Geerdalen Formation

The following four chapters have been written in collaboration with master student Cathinka Schaanning Forsberg, and based on data collected on fieldwork that was conducted in Fulmardalen on Svalbard during the summer of 2016.

The chapters may be regarded as a continuation of the work that was presented in the collaboration chapters presented in the Master's theses of Haugen (2016), Johansen (2016) and Støen (2016). Their chapters were based on field work that was conducted in areas to the east of Fulmardalen in August 2015. Both authors of the following four chapters presented in this thesis also participated in the fieldwork of 2015, but later spent time on exchange studies and were therefore not involved in processing and presenting the data that was collected.

Detailed work on the facies of the De Geerdalen Formation was already presented in Knarud (1980), and laid the foundation for any subsequent studies that has been conducted on the formation. The work that will be presented in this chapter stands as a part of a comprehensive project that has had an overall aim of extending the current understanding of the facies of the Upper Triassic sedimentary succession in Svalbard.

The project was initiated with fieldwork on Hopen, Edgeøya and Central Spitsbergen in 2008, 2009 and 2010 and was presented in Hynne (2010), Rød (2011) and Rød et al. (2014). This work was further extended and presented in the master theses of Enga (2015), Haugen (2016), Johansen (2016) and Støen (2016). The data presented in the latter three theses are summarized in (Lord et al., 2017a). In Figure 4.1, the location of Fulmardalen in relation to the aforementioned studies are shown.

In Lord et al. (2017a), 14 different facies types have been described and interpreted from the De Geerdalen Formation (Table 4.1). The different facies types are also found to be highly representative for the formation in Fulmardalen. The following chapter will mainly focus on discrepancies between the facies observations from Fulmardalen and those presented in the table, with the purpose of establishing a representative facies-model for the De Geerdalen Formation in Fulmardalen. Hence, facies that have the same appearance in Fulmardalen as elsewhere on Svalbard will not be described in detail in this chapter, but all facies types are illustrated with figures. Furthermore, the interpretations of the facies types are consistent with those presented in Table 4.1, unless otherwise is stated.

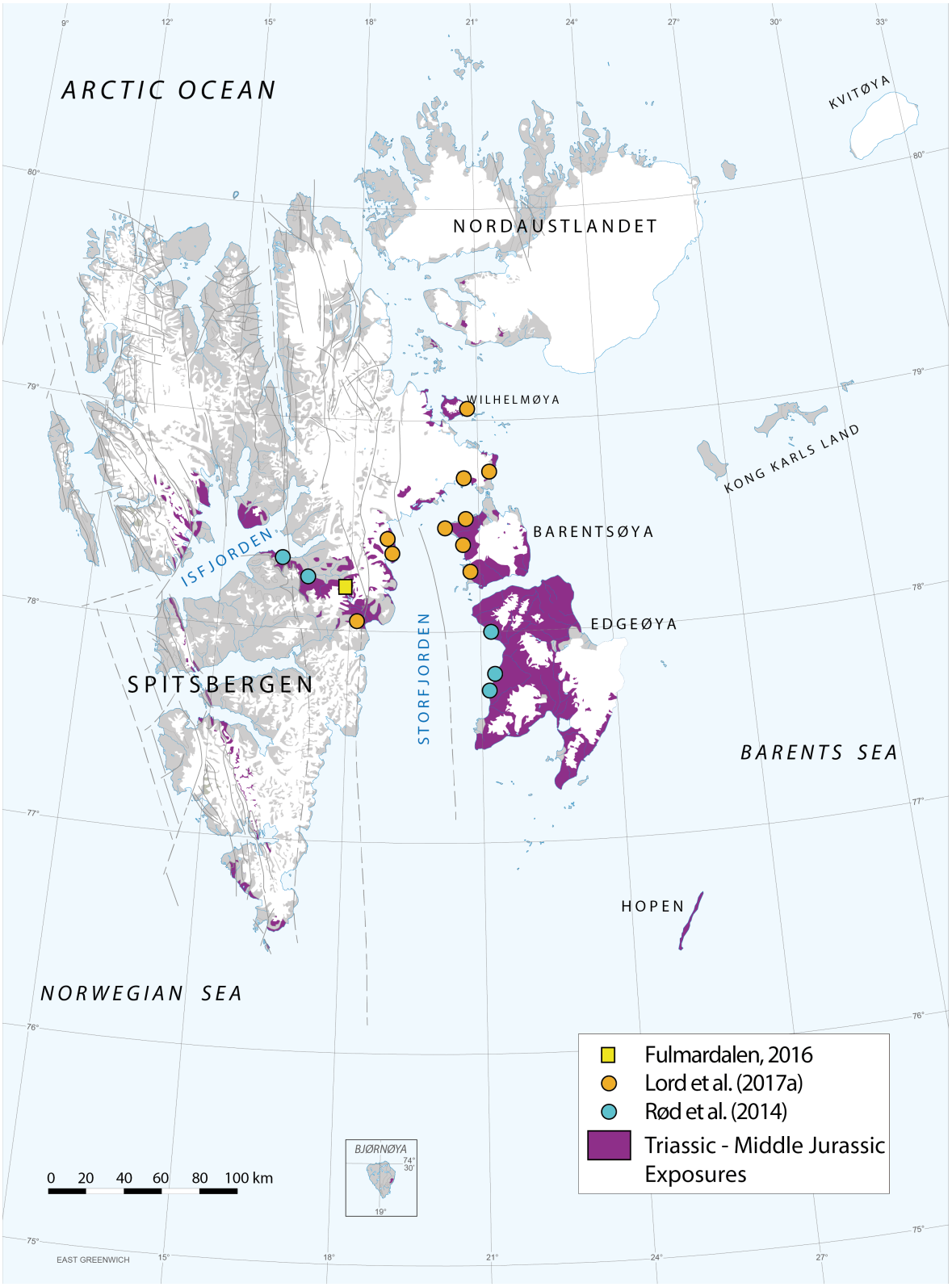

Figure 4.1 *Overview map of Triassic-Middle Jurassic exposures on Svalbard. Fieldwork localities from previous studies (Rød et al., 2014; Lord et al., 2017a) are indicated. The figure shows how Fulmardalen is located between these localities, linking the data from western and eastern Svalbard together.*

4.1 The meaning of "Facies" and "Facies analysis"

The word "facies" comes from the Latin language and means face, figure, appearance, aspect, look and condition (Miall, 2016), and was first introduced to geological literature by Steno (1669). The modern way of understanding the term stems back to a definition that was presented by Gressly (1838). Since then, the usage of the facies term in a geological setting has been much debated (e.g. Teichert, 1958; Middleton, 1973). In more recent years, publications from Reading and Levell (1996), Dalrymple (2010) and Miall (2016) provide good summaries of how the facies concept is applied in modern day sedimentology.

There are different kinds of facies, depending on which features in a sedimentary rock the observations are focussed around. While biofacies is mainly considering fossil- and trace fossil components in a rock unit, lithofacies focus on describing rocks based on lithological features such as composition, grains size, stratification characteristics and sedimentary structures (Miall, 2016). Microfacies is term typically used when facies features are identified from thin sections. All the latter facies types are classified as descriptive types of facies. However, the facies term can also be used in a more genetic way, with emphasis on the depositional processes that were active at the time when the rock was deposited (Reading and Levell, 1996). "Fluvial facies" and "tidal facies" are examples of such genetic facies types.

Individual facies may be of varying value for interpretation purposes, with some facies (e.g. a coal seam) holding stronger environmental implications than others (e.g. a dark shale). However, all individual facies have their interpretative limitations, and in order to propose environmental interpretations, it is important that the individual facies are seen in relation to the surrounding facies (Reading and Levell, 1996).

Facies analysis forms a foundation for modern day stratigraphy. The importance of understanding facies sequences was already recognized by Walther (1894), where it was stated that the conformable vertical progression of facies is a result of successive depositional environments that are laterally juxtaposed to each other (López, 2015). This is a principle that has become so important in sedimentary geology that it often is just referred to as "Walther's Law". By analysing the facies that occur in sedimentary successions, a base for correlation between rock units both vertically and horizontally is created. Observations of spatial and temporal relationships in sedimentary rocks are easiest recognized from outcrops. Facies is therefore best described in a way that makes it possible to correlate it to what can be seen in the field (Walker, 2006).

4.2 Facies in Fulmardalen

Table 4.1 *Overview of the 14 facies defined for the Upper Triassic succession in eastern Svalbard, modified from Lord et al. (2017a). The table is expanded from the work of Rød et al. (2014), and is also representative for the De Geerdalen Formation in Fulmardalen.*

#	Description	Interpretation
A	**Mudstone (0.1 – 10's m)** Clay and silt, laminated (shale) or non-laminated (mudstone). Thickness varies from a few centimetres to tens of metres. Laminated mudstones are most common and may encase thin beds of silty to very fine sandstone. Colour is dominantly grey or black, but may also be yellow, white or purple colour with weathering of siderite cement. The facies is characterised by horizontal and gently undulating laminae. Load structures and irregular lamination are occasionally observed. Concretions of calcite or siderite are common. Organic content may be high at some intervals. Ammonoids and marine vertebrate fossils are common.	Pelagic shale and mudstone deposited from suspension in low energy environments where clay and silt flocculate and settle on the sea floor (Collinson et al., 2006; Boggs, 2011). Also forms background sedimentation in shallow marine environments closer to the shoreline.
B	**Heterolithic Bedding (0.01 – 10's m)** Heterolithic bedding is observed as thin beds of very fine to fine sandstone and siltstone alternating with mudstones often forming coarsening upwards units. The thickness of mud and sand layers generally range from 1 mm to a few centimetres, however thicker packages are evident. Units are up to 10-15 m thick. Sedimentary structures preserved in the sandstones of heterolithic successions are commonly hummocky cross-stratification and ripple cross-stratification. Bioturbation is common towards the top of units and *Skolithos* may be present.	Heterolithic bedding indicates alternating flow regime where sand and mud is available (Davis Jr, 2012). Mud is deposited from suspension, while sand is deposited during current or wave activity (Reineck and Singh, 1980). This facies can form in the transition zone when mud interacts with sand introduced by periods of higher flow and sedimentation.
C	**Hummocky Cross-Stratified VF-F Sandstone (0.1 – 1 m)** Very fine to fine grained sandstones featuring hummocky and swaley cross-stratification. Consists of 10 cm to 1 m thick sandstone beds and are characterised by cross-laminae in undulating sets. Individual laminae sets are commonly between 5 and 20 cm thick. The sandstones are typically grey to yellow or orange to reddish brown colour. Beds are usually moderately to intensely bioturbated with *Skolithos* and *Diplocraterion*. Hummocky cross-stratified sandstones are common in upwards coarsening sequences in the lower part of the De Geerdalen Formation throughout the study area.	Hummocky cross-stratification shows a distinct undulating geometry of lamination formed by the migration of low- relief bed forms in one direction due to wave surge and unidirectional currents (Nøttvedt and Kreisa, 1987). This facies is widely recognised as being characteristic of tempestite deposition in shallow marine, storm-dominated inner shelf, to lower shoreface settings (Midtgaard, 1996; Yang et al., 2006). Hummocks form below the fair weather wave base and above, but are most common near storm weather wave base (Dumas and Arnott, 2006).
D	**Sandstone with Soft Sediment Deformation (0.3 – 1.5 m)** Erosive based, very fine to fine grained sandstones characterised by abundant soft sediment deformation. Units can be laterally restricted but also extensive thickness ranges from 0.3 to 1.5 m. Irregular lamination seen within the sandstone bodies are also present in the upper parts of the underlying, deformed, mudstones. Sandstones are typically green-grey in colour and lack bioturbation. Soft sediment deformed beds are relatively rare throughout the study area, with the most extensive beds occurring at the locality of Mistakodden.	Soft sediment deformation structures typically generate from gravitational processes such as downslope sliding and slumping or rapid loading of sediment (Reineck and Singh, 1980; Bhattacharya and MacEachern, 2009). Likely form the base of distributary mouth bar deposits, where large volumes of sediments are deposited rapidly in front of distributary systems and reworked by wave or fluvial processes.

#	Description	Interpretation
E	**Wave Rippled Sandstone (0.1 – 4 m)** Very-fine to fine grained sandstone with symmetrical ripple lamination. Thicknesses range from tens of cm up to ca. 4 m, individual beds can be 10 to 30 cm in thickness. Sandstones have grey, yellow or red weathering colour. Fresh surfaces are light grey. Carbonate cement (calcite/dolomite) or siderite is common. Sandstone beds of this facies are normally graded and wave ripples are often observed on the upper surfaces in coarsening upwards successions. The crests tend to be continuous and straight. Mud drapes are common and expose ripple foresets. Facies is commonly found interbedded with heterolithic bedding or overlying horizontally bedded sandstone. Moderate bioturbation and *Rhizocorallium* or *Skolithos* trace fossils are present.	Wave ripples are commonly found in shallow marine settings. They are formed by the oscillatory movement of currents at normal wave base (upper shoreface) where swash and backwash currents produce symmetrically shaped ripples (Boggs, 2011). Mud drapes on the foresets of ripples indicate a tidal influence.
F	**Current Rippled Sandstone (0.1 – 4 m)** Very fine to fine grained sandstone with asymmetric ripples forming individual beds or units composed entirely of ripple cross stratification up to 4 m in thickness. Sandstone is yellow, orange and brownish colour. Sandstone beds in this facies are typically normally graded and have sharp lower contacts, whereas contacts to upper facies are gradual. In some instances, this facies may fine upwards. Facies is often observed to overlay large-scale cross-bedded and small-scale cross-bedded, normal graded sandstones and itself is overlain by fining upwards beds of horizontally bedded sandstone.	Current ripples occur with the aggradation of ripples under contemporary downstream migration during unidirectional flow. Sets arranged into climbing ripples form under the same regime but with the angle of climb reflecting rate of aggradation (Collinson et al., 2006). Current ripples are commonly found in environments such as fluvial floodplains, with sub-environments such as; crevasse splays and point bars. They are also present in seasonally flooded river deltas (Reading and Collinson, 1996). In marine environments they are usually formed in the shoaling wave zone.
G	**Carbonate Cemented Sandstone (0.2 – 2 m)** Very fine to fine grained, normally graded, sandstones characterised by structures formed during diagenesis. Sandstone units are commonly hard and heavily cemented with calcite, dolomite or siderite, making observations of primary sedimentary structures difficult, thickness is typically 0.2 – 2 m. Secondary sedimentary structures include cone-in-cone, siderite beds and calcareous concretions. Colour variation between grey, brown and red are observed. Scarce to heavy bioturbation is noticed. Cemented sandstone forms benches in the topography or distinctive layers, that may be laterally continuous for several tens of metres prior to pinching out.	Sources of calcite cement may be dissolved bivalves and coquinas. Recent studies by Tugarova and Fedyaevsky (2014) suggests a genesis driven by micro-organisms and a biochemical precipitation of carbonates during early diagenesis in a shallow marine environment. Siderite occurs in organic-rich brackish to meteoric pore-waters depleted of SO_2 and is commonly found in fine grained deltaic to coastal sediments (Morad, 1998). Siderite concretions and layering might indicate a continental influence on marine sedimentation with organic-rich stagnant waters close to the delta front (Pettijohn et al., 1987).

#	Description	Interpretation
H	**Plane Parallel Laminated Sandstone (0.3 – 2 m)** Sandstones with horizontal, plane parallel lamination or plane parallel stratification. Mostly very fine to fine grained sand, but can also be silty and medium grained. Units range between 30 cm and 2 m in thickness, with mm-thin lamina and cm-thick beds. Parting lineation (primary current lineation), is present on bedding surfaces. Stratification varies from lamination to bedding. Colour is grey to pale yellow, but weathers brown to red. Lower boundaries are typically sharp, while the upper are commonly more gradual. Units are often observed towards the top of sandstone benches. Bioturbation is rare in lower parts, but occurs towards the upper part of units. *Skolithos, Diplocraterion* and *Rhizocorallium* also observed.	Plane parallel stratification occurs in various environments and is not a unique environmental indicator (Boggs, 2011). The structure form by settling of fine grains from suspension or traction of sand as bed-load in the upper flow regime (Collinson et al., 2006; Boggs, 2011). Laminae are defined by grain size variations or assembling of mica, representing subtle variations in depositional environment (Collinson et al., 2006). It is commonly found in rivers and streams with a high flow (Boggs, 2011), but it can also result from settling of sand grains from suspension.
I	**Low Angle Cross-Stratified Sandstone (0.1 – 1.5 m)** Very fine to fine grained sand, forming gently inclined sets of planar parallel stratification or lamination, with wedge-shaped set boundaries. The colour is usually grey to red-brown when weathered and grey on fresh surfaces. Unit thickness is usually between tens of cm to 1.5 m, while set thickness range between 5 and 15 cm. Individual sets are composed of both beds and lamina, where the former is the most common. These sandstones are commonly bioturbated and contain plant fragments and rare fish remains. It is frequently found overlying or interbedded with wave rippled sandstones, or heterolithic bedding.	Low angle cross-stratification is not considered a diagnostic sedimentary structure as it can be seen occurring in a range of depositional environments. However, the presence of bioturbation and plant fragments are interpreted as indicators of a proximal position in the shallow marine environment, most likely the upper shoreface or beach foreshore (Reading and Collinson, 1996). Low angle cross-stratified sandstones typically exhibit a gentle dip seaward when found in foreshore and backshore settings (Reading and Collinson, 1996).
J	**Tabular Cross-Stratified Sandstone (0.1 – 1.5 m)** Very fine to fine grained sandstones with tabular cross-stratification or cross-lamination, arranged in foresets with bedforms of 2 to 10 cm thickness and stacked in units that are up to 1.5 m thick. Calcite cementation is common and varies from vague to pervasive resulting in differences in appearance within facies. Sparse bioturbation is occasionally observed towards the top of units and plant fragments are common. Grey, yellow, brown and reddish colours are observed. Weathering of finer material on sandstone bounding surfaces is interpreted as draping mud or finer sand. Facies J is commonly found overlying large-scale trough cross bedded sandstones in fining upwards units. It is also often found within heterolithic bedded units.	Tabular cross-stratification forms by unidirectional currents of the lower flow regime in shallow waters (Collinson et al., 2006; Boggs, 2011). Environments of formation are fluvial and shallow marine where rip-currents, longshore currents, tidal currents and breaking waves creates unidirectional currents (Reading and Collinson, 1996). Plant fragments, low abundance of trace fossils and close proximity to palaeosols in upper sections indicates that this facies is most likely associated with terrestrial depositional environments.
K	**Trough Cross-Stratified Sandstone (0.2 – 4 m)** Fine to medium grained trough cross-stratified sandstones with sharp erosive base, displaying a fining upwards trend. Cross set thicknesses range from 20 to 80 cm, whereas stacking of sets results in unit thicknesses of 0.2 to 4 meters. Rip-up clasts and plant fragments are frequent in the basal parts of units and scours. Observed colours are grey, yellow and brown, with reddish and dark colours appearing occasionally on weathered surfaces. Upper parts of sandstones may be sparsely bioturbated, whereas lower parts are essentially free of traces. Trace fossils observed within this facies are *Skolithos* and *Diplocraterion.*	Formed by migration of 3D dunes, in unidirectional currents in the lower flow regime (Reading and Collinson, 1996; Boggs, 2011). Complexity of dune morphology is thought to increase at higher current velocities and shallower waters (Reading and Collinson, 1996; Boggs, 2011) and stacking of co-sets represent superimposed bed-forms (Reineck and Singh, 1980). Facies is interpreted as migrating dunes in a subaqueous environment due to unidirectional current. Mud drapes are attributed to slight changes in current velocity, possibly implemented by tidal activity or seasonal changes in stream discharge.

#	Description	Interpretation
L	**Bioclastic Sandstone and Mudstone (0.1 – 0.5 m)** The unit consists mainly of disarticulated and fragmented bivalves (coquina), lacking sedimentary structures. Thickness is from 10 to 50 cm. All the observed units are cemented and display orange and purple weathering colours. Bioclastic beds are found as discrete laterally continuous layers sandwiched between mud and locally as minor shell accumulations within sandstone bodies. Bioclastic beds are typically restricted to the lower parts of the Isfjorden Member, but are also seen at some localities in the lower part of the De Geerdalen Formation.	Fragmented shells indicate a relatively high energy environment. Mass erosion and transportation of shells can lead to concentration of shell fragments in beds where the hydrodynamic energy is low enough for deposition (Reineck and Singh, 1980). The Isfjorden Member is interpreted to be deposited in a shallow marine and lagoonal environment. Based on associated facies, field observations also point towards a proximal shallow marine origin, and coquina beds may represent wave reworked shallow marine shell banks accumulated by currents or waves.
M	**Coal and Coal Shale (0.1 – 0.2 m)** Units of coal and coal shale are from 1 to 20 cm thick. The units often appear laterally continuous over tens of metres. Coal and coal shales are usually found in close proximity to the top of larger sandstones. Coals are distinguished from coal shales by being more consolidated and vitrinous, reflecting a higher proportion of organic material. Coal and coal shales are commonly associated with underlying palaeosols, but coal shale surrounded by grey shale is observed on Wilhelmøya and Hahnfjella. Rhizoliths are also commonly observed in the coals. The facies is found at all localities, but only in the middle and upper parts of the De Geerdalen Formation.	Coal seams found in the De Geerdalen Formation typically overlie palaeosols, indicating they are formed in place (histic epipedons) (Retallack, 1991). Coal and coal shale beds found in the De Geerdalen Formation are thin and laterally discontinuous. Coal and coal shales are here interpreted to originate from mires on a dynamic delta plain setting in a humid palaeoclimate with seasonal variations in precipitation, following the conclusions of Enga (2015).
N	**Palaeosols and Calcrete (0.2 – 1 m)** Palaeosols are found at all localities. The thickness is in the range of 0.2 to 1.0 metres. Roots and wood fragments up to 20 cm in diameter can be found. The colour varies from brown to reddish brown and yellow. Non-calcareous palaeosols are composed of mudstone and weather red or green and are 0.2 to 1 m in thickness. The structure of these mudstones is blocky or gravelly with weathering and mottles being common. Palaeosols occur both in grey mudstone and on top of sandstone beds. A gradual contact at the base and sharper contact at the top is typical for palaeosols (Boggs, 2011) and is frequently observed in the outcrops. The palaeosols are commonly overlain by coal or coal shale.	Palaeosols form due to physical, biological and chemical modification of soil during periods of subaerial exposure. Palaeosols are continental (Boggs, 2009), but can form in marine strata following sea level fall and sub-aerial exposure (Webb, 1994). Palaeosols represent an unconformity, formed in a degrading landscape (Kraus, 1999). Red mudstone beds are interpreted as calcrete horizons formed in a semi-arid environment. Calcretes also imply periods of non-deposition. Red and green colours may result from fluctuations in groundwater and shifts between oxic to anoxic conditions.

Facies A – Mudstone

Mudstones (facies A) in Fulmardalen (Figure 4.2A) fit the description given in Table 4.1. Facies A is interpreted as the most dominant facies in the De Geerdalen Formation in Fulmardalen. Detailed investigations of the facies are, however, challenging due to extensive scree cover and weathering.

Facies B – Heterolithic Bedding

The description of heterolithic bedding (facies B) from previous studies on Svalbard (Table 4.1) is consistent with the observations of this facies in Fulmardalen (Figure 4.2). Intervals of alternating sandstones, siltstones and mudstones occur throughout the formation at all localities (e.g. Figure 4.2C). Sedimentary structures preserved in sandstone and siltstone layers are mainly wave ripples (Figure 4.2D) and hummocky cross-stratification (Figure 4.2E). Erosive-based and deformed sandstone lenses (facies D) are commonly found in these intervals as well.

Facies C – Hummocky Cross-Stratified VF-F Sandstone

Hummocky and swaley cross-stratified sandstones (facies C) in Fulmardalen (Figure 4.2E) are commonly observed in the lower part of the De Geerdalen Formation. Hummocks and swales are dominating structures in the coarser beds within heterolithic sections, which are consistent with previous descriptions of the facies on Svalbard.

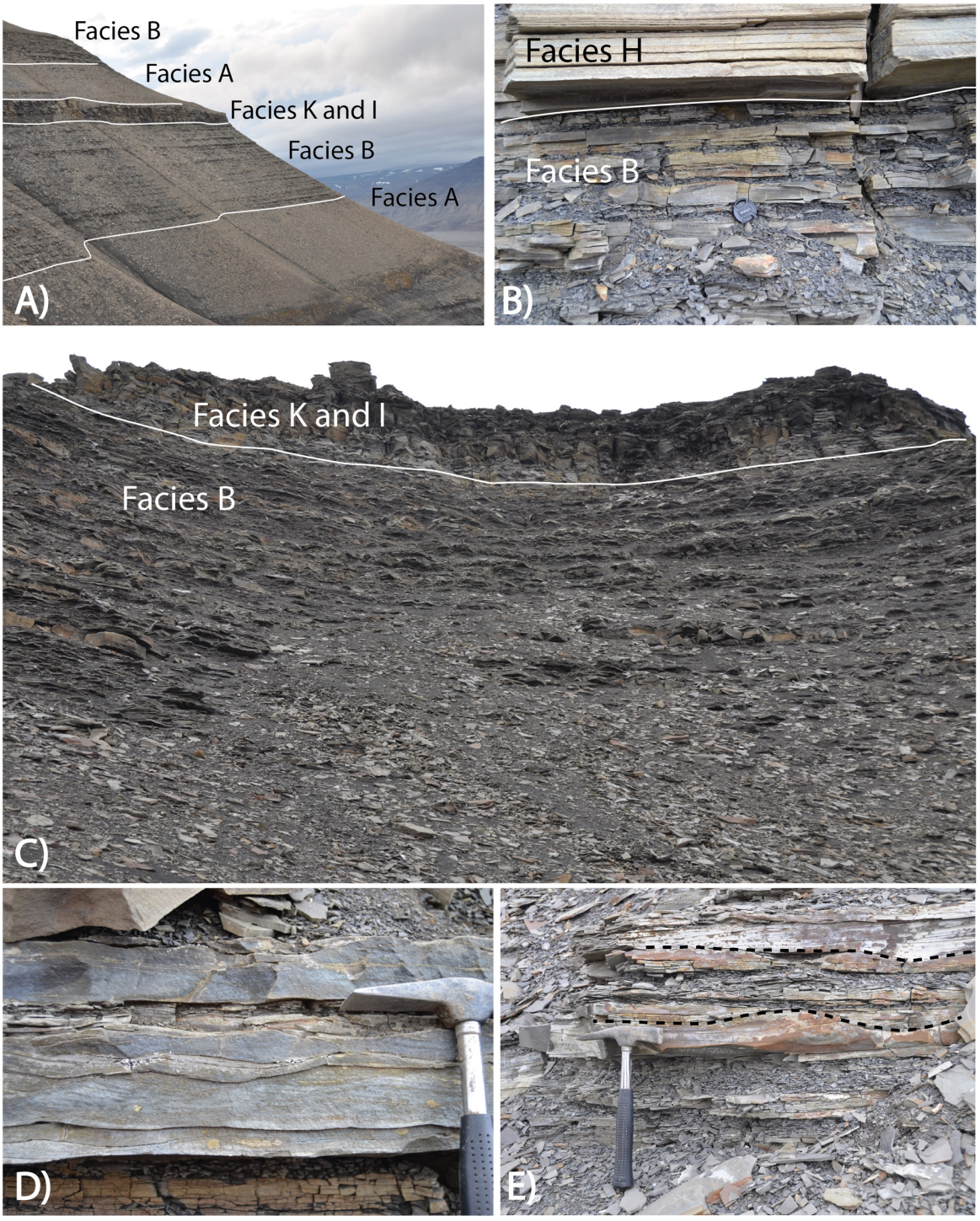

Figure 4.2 *Facies A, B and C.* ***(A)*** *Slope of Milne Edvardsfjellet, displaying two repeated upwards coarsening units with mudstones (facies A) in the lower part, heterolithic bedding (facies B) in the middle part and sandstone in the upper part.* ***(B)*** *Outcrop from Dyrhø, displaying the alternating lithological appearance of a heterolithic bedding (facies B) overlain by a planar laminated sandstone (facies H).* ***(C)*** *Slope section at Milne Edwardsfjellet, displaying heterolithic bedding (facies B) gradually coarsening upwards into a sandstone-dominated unit.* ***(D)*** *Outcrop from Dyrhø, showing climbing ripples in a sandstone within a heterolithic unit.* ***(E)*** *Outcrop from Storfjellet, showing hummocky cross-stratified sandstone (facies C) within a heterolithic unit. Dashed lines indicate the hummocky appearance of the lamination.*

Facies D – Sandstone with Soft Sediment Deformation

Soft sediment deformation in sandstones (facies D) is commonly observed in the lower part of the formation at multiple locations in Fulmardalen. Following the division from Oliveira et al. (2011), it is possible to distinguish between two different types of soft sediment deformation structures. The first of these two types are called "detached soft sediment deformation structures", which is a product of lateral movement of slides, slump and debris flow deposits (Figure 4.3A, B, C, D, H). The other type is called "*in situ* soft sediment deformation structures", and is mainly a result of vertical movements forming flame structures, load structures, water-escape structures, convolute bedding etc. (Figure 4.3E, F, G). In Fulmardalen, detached soft sediment deformation structures often occur as erosive based sandstone lenses within mudstones (facies A) and the heterolithic parts (facies B) of upward coarsening sequences. *In situ* soft sediment deformation structures are less common than the detached ones, and are only present in the lowermost major sandstone intervals at Storfjellet and Ryssen. Compared to the findings of Lord et al. (2017a), detached soft sediment deformation structures in sandstone bodies capsuled by mudstones appear to be more common in Fulmardalen than in the eastern areas. Especially at Milne Edwardsfjellet, such deformed sandstone lenses are well preserved and exposed in the lowermost part of the De Geerdalen Formation. While *in situ* soft sediment deformation structures are well described in Lord et al. (2017a), detached soft sediment deformation structures can be more precisely described from the outcrops in Fulmardalen.

All detached soft sediment deformed sandstone outcrops in Fulmardalen appear to be very fine grained. Geometrically the bodies mainly come in two different shapes, with one type being lense-shaped, ranging from 0.5 m to 3 m in width, while the other type has a more sheet-like geometry and reaches up to 20 m in width. The bodies are between 0.2 and 2 m thick. The intensity of deformation tends to vary locally within the lenses and sheets. Laminations and stratifications within the sandstones are in most cases preserved, displaying complex and laterally elongated folding patterns. Some of the deformed sandstone units may also resemble ball and pillow structures (e.g. Reineck and Singh, 1980). Plant fragments and mud flakes are commonly observed within the strucutures, while bioturbation and wave-ripples are present on top of the units. In contrast to what was observed from a similar outcrop at Muen on Edgeøya (Johansen, 2016) (see Figure 7.2), carbonate cementation and cone-in-cone structures were not observed in this sub-facies in Fulmardalen.

Oliveira et al. (2011) concludes that the position of the different soft sediment deformation strucutures can be related to their position on clinoforms. It is suggested that *in*

situ soft sediment deformation structures mainly form due to high sedimentation rates on a relatively stable delta front/clinoform rollover. Detached soft sediment deformation structures requires a higher degree of sediment instability, and such conditions are more abundant on the delta slope/clinoform slope. Folding patterns in detached soft sediment deformation structures are mainly a result of "freezing" of slump deposits, and such structures are common in front of migrating sandbars (Oliveira et al., 2011). This seems to be consistent with the findings from Fulmardalen, where the detached soft sediment deformation structures are interpreted as delta slope deposits, while the *in situ* soft sediment deformation structures are found in what has been interpreted as delta front barrier sand deposits. The relative content of deformed sandstone observed at the different localities varies, which may be a result of varying proximity to sand distributaries, or due to a varying degree of scree cover.

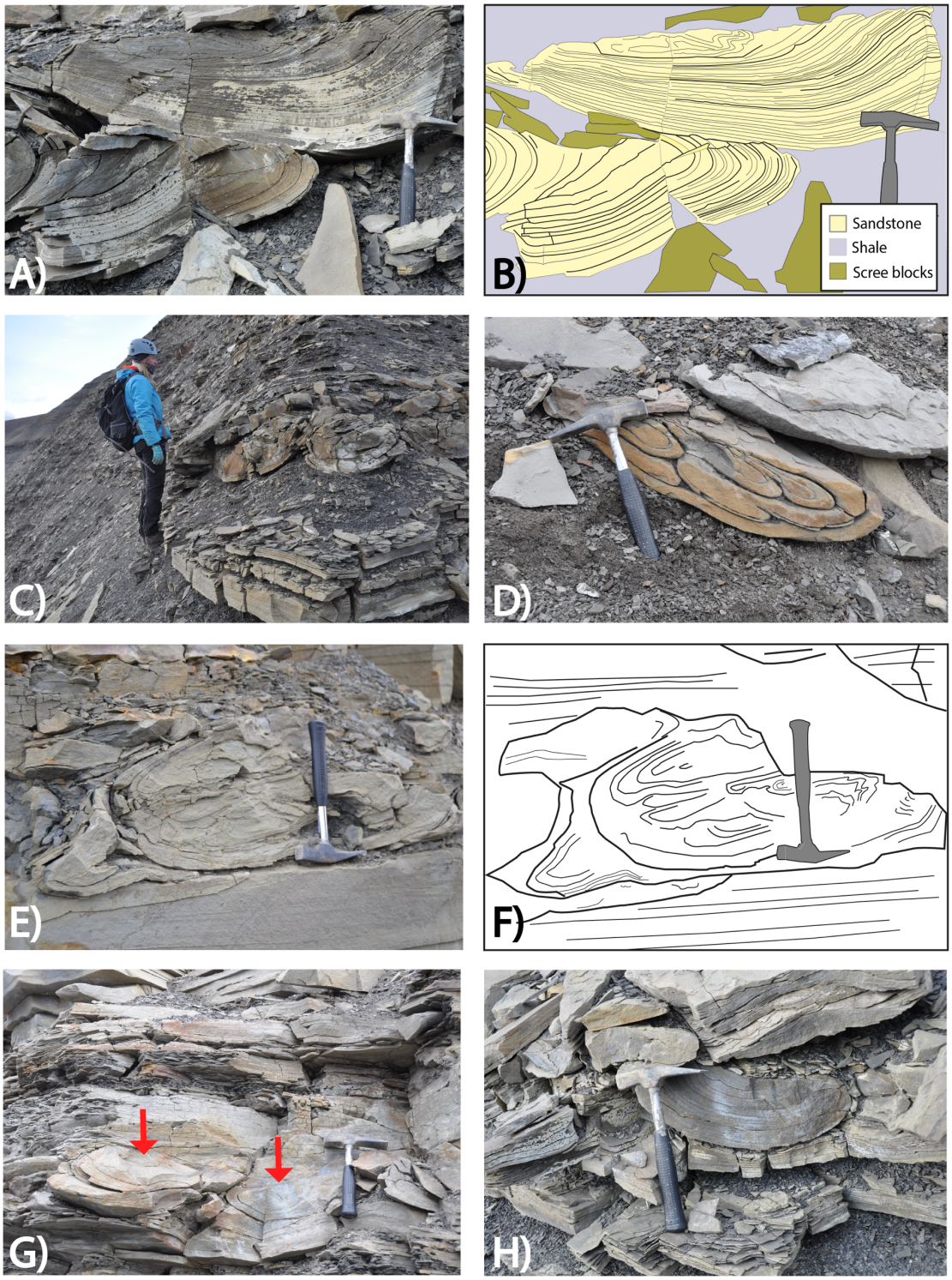

Figure 4.3 *Soft sediment deformed sandstones (facies D) in Fulmardalen. Both detached soft sediment deformation structures (DS) and in-situ soft deformation structures (IS) are displayed.* ***(A)*** *DS from Milne Edwardsfjellet, resembling ball and pillow structures* ***(B)*** *Sketch of the sandstone in A.* ***(C)*** *DS in a laterally restricted sandstone at Milne Edwardsfjellet.* ***(D)*** *DS from Storfjellet.* ***(E)*** *IS from Ryssen.* ***(F)*** *Sketch of the sandstone in E.* ***(G)*** *IS from Storfjellet.* ***(H)*** *DS from Milne Edwardsfjellet.*

Facies E – Wave Rippled Sandstone

The wave rippled sandstones in Fulmardalen (Figure 4.4) fit well to the description of facies E in Table 4.1. However, the unit-thickness appear to be slightly larger in Fulmardalen. *Diplocraterion* is observed in addition to *Skolithos* and *Rhizocorallium*. The facies are found at every location visited and at all stratigraphic levels in the formation.

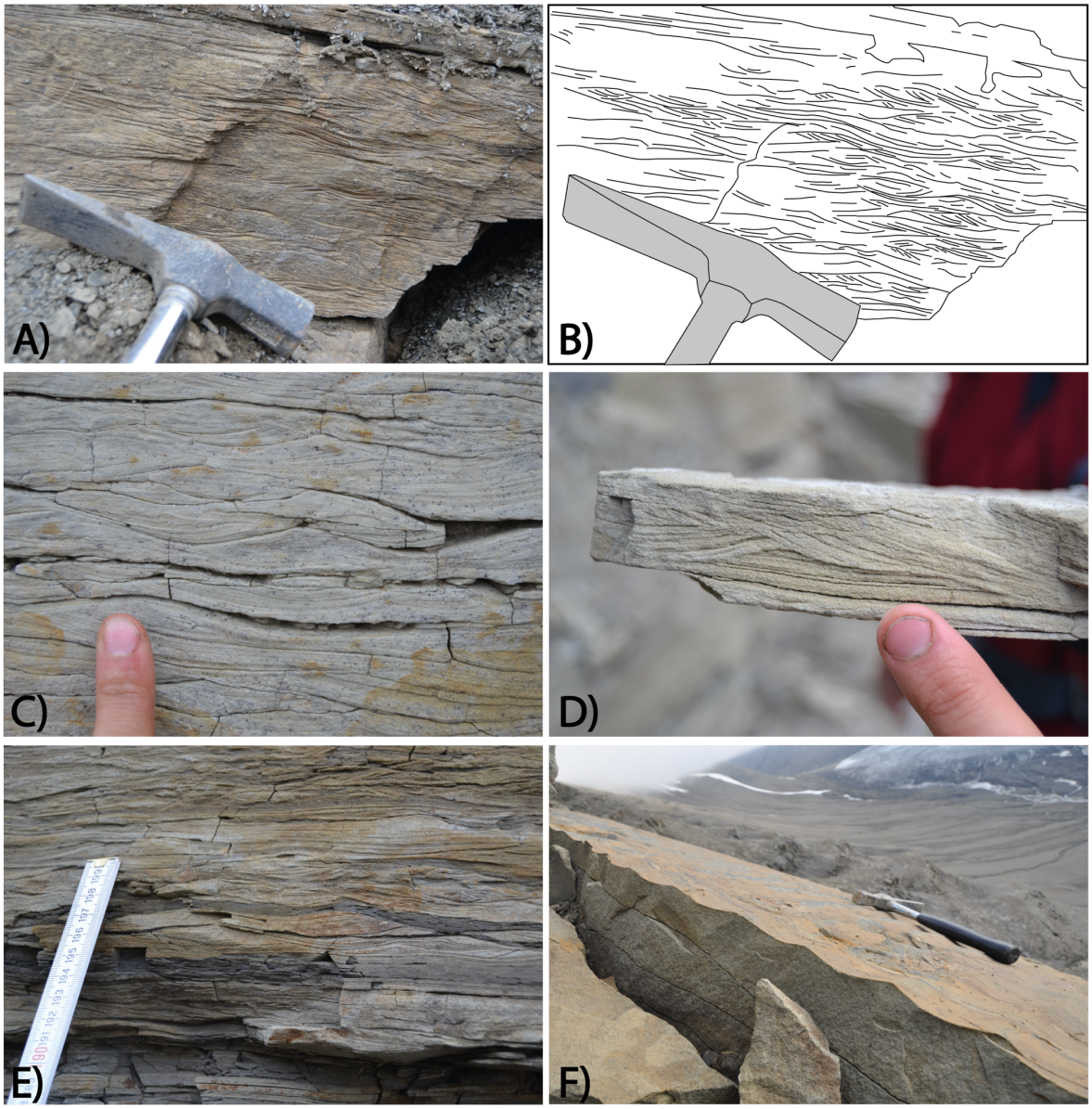

Figure 4.4 *Wave rippled sandstones (facies E) in Fulmardalen.* ***(A)*** *Wave rippled sandstone at Ryssen.* ***(B)*** *Sketch of the sandstone in A.* ***(C)*** *and* ***(D)*** *Wave rippled sandstone at Ryssen. Notice the well exposed symmetrical shape.* ***(E)*** *Wave rippled sandstone at Dyrhø. Notice the mud draping in some of the ripple crests.* ***(F)*** *Wave rippled sandstone at Storfjellet, displaying symmetrical ripple crests in 3D.*

Facies F – Current Rippled Sandstone

Current rippled sandstones (facies F) are observed in relatively few outcrops in Fulmardalen (Figure 4.5). Where present, the facies resemble descriptions from previous studies in having undulating, parallel wavy to straight stratification/set boundaries without apparent cross-stratification (e.g. Johansen, 2016).

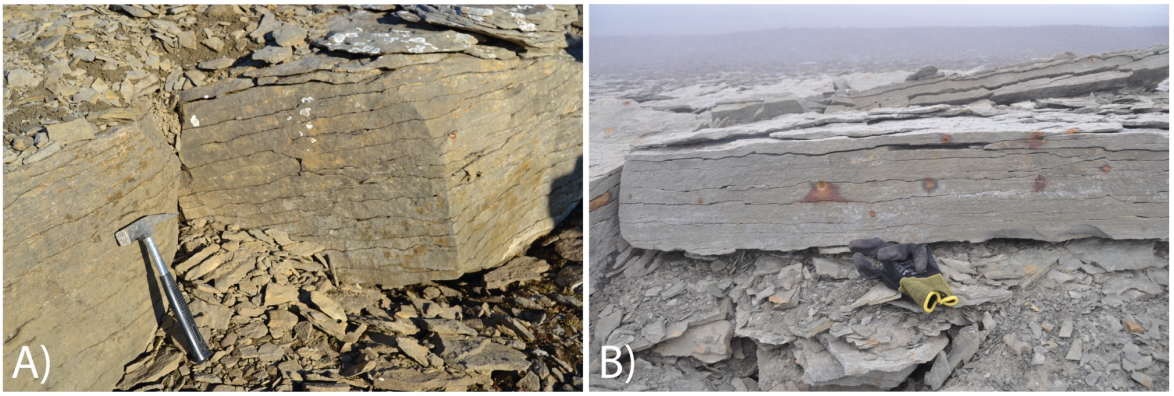

Figure 4.5 *Current rippled sandstones in Fulmardalen at* ***(A)*** *Wallenbergfjellet and* ***(B)*** *Storfjellet.*

Facies G – Carbonate Cemented Sandstone

Carbonate cemented sandstones (facies G) are observed especially in the middle and upper part of the logged sections in Fulmardalen (Figure 4.6). Cone-in-cone structures (Figure 4.6B), siderite beds and calcareous concretions (Figure 4.6C) are observed to fit the descriptions from Table 4.1. Furthermore, the units are hard and laterally extensive (Figure 4.6A), often with a red to brown weathering colour. Shell fragments which may be assigned to facies L, bioclastic sandstone, occur locally within carbonate cemented sandstones. Additionally, structures interpreted as desiccation cracks are found within facies G in Fulmardalen (Figure 4.7). Such structures are not described from facies G in Table 4.1, and will be described in more detail in the following section.

Potential desiccation cracks in the De Geerdalen Formation

In Fulmardalen, structures resembling desiccation cracks are only found in the upper part of the De Geerdalen Formation, within a rusty-red carbonate cemented unit found below a shale unit with a characteristic dark colour. The layer is illustrated with an orange colour in the logs presented in Chapter 5. Desiccation cracks have also been described from the De Geerdalen Formation in central and eastern Spitsbergen by Knarud (1980), and are indicative of periodical sub-aerial exposure.

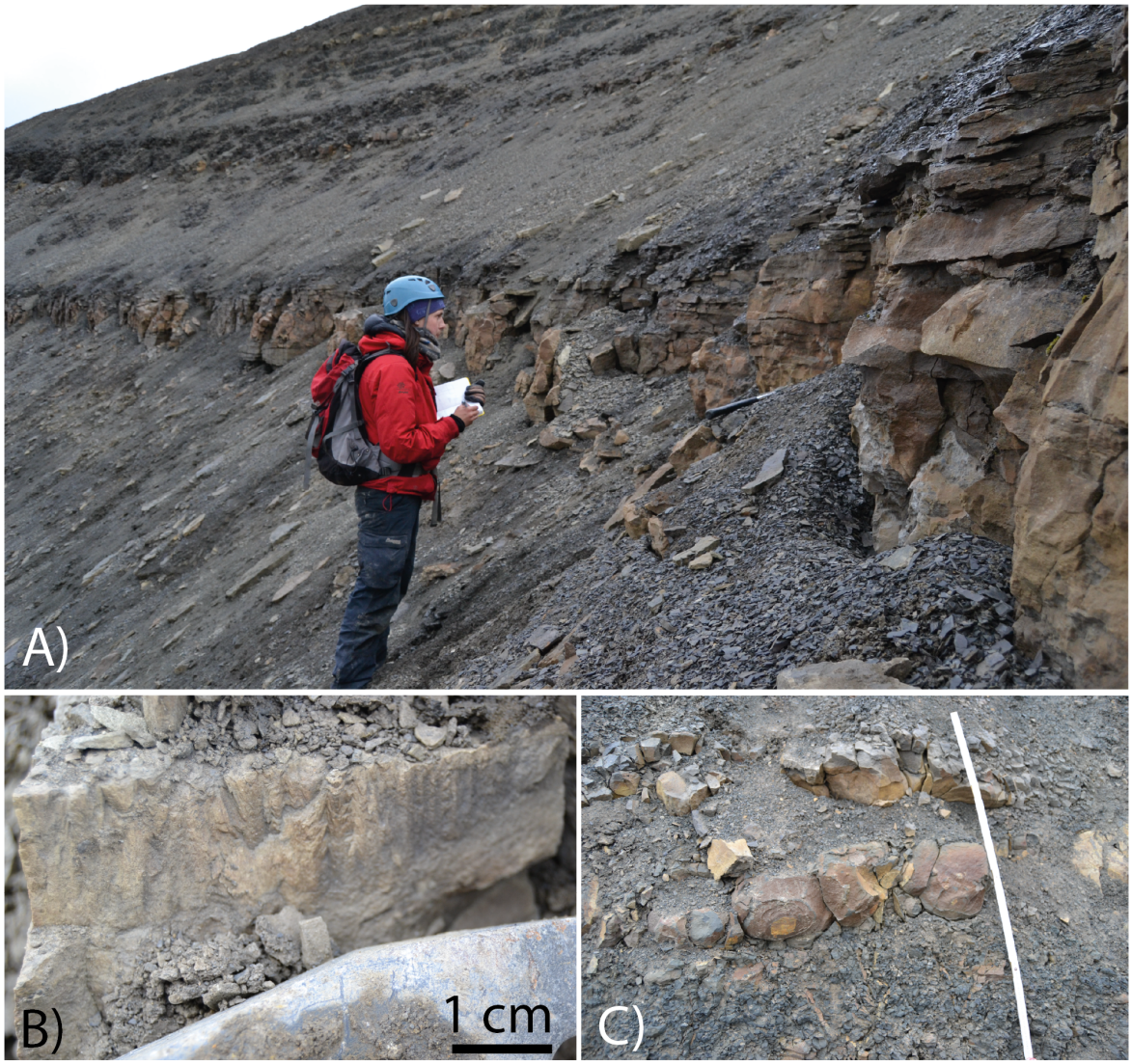

Figure 4.6 *Carbonate cemented sandstones (Facies G) in Fulmardalen.* ***(A)*** *Carbonate cemented sandstone at Dyrhø. Notice its lateral continuity.* ***(B)*** *Cone-in-cone structures at Ryssen.* ***(C)*** *Siderite concretion layer at Dyrhø.*

The rusty-red unit in Fulmardalen often shows alternating light and dark coloured laminations representing mud and sand, respectively. At the mountain Ryssen, the mud is interrupted by multiple deformed downward-tapering cracks filled with sand (Figure 4.7), interpreted as desiccation cracks that have been compacted. The structures often have sharp edges and the mud seems to have been pulled apart, which indicates a shrinkage mechanism. Desiccation cracks develop under sub-aerial conditions when muddy sediment dries out (Nichols, 2009). Desiccation crack patterns are typically polygonal, and are most clearly preserved in sedimentary rocks when they are filled with sand or silt transported by wind or water (Nichols, 2009). The sand filled cracks observed at Ryssen are to some extent polygonal

(Figure 4.7E), but are often straight, spindle-shaped or slightly curved tapering cracks (Figure 4.7F) as well. For the latter example it is possible that the polygonal crack pattern did not have time to fully develop before a new portion of sand covered the mud. The area between the cracks is sometimes curved upward into a concave shape (Figure 4.7D), which is typical for desiccation cracks (Boggs, 2011). However, the concave appearance may also be a result of mud draping wave ripple crests. An inter-tidal setting is a likely candidate for the depositional environment. The thickness of the mud is relatively thin, and it is reasonable to imagine that it could have easily dried out when exposed during low tide.

On the other hand, the observed crack shapes are also typical for syneresis cracks (Nichols, 2009; Boggs, 2011). In contrast to desiccation cracks, syneresis cracks are shrinkage cracks that form under water in clayey sediment when the clay settles and compacts (Nichols, 2009). They commonly occur in thin mudstones interbedded with sandstones (Boggs, 2011). The sand-mud ratio in the lamination at Ryssen is high, which could imply that the cracks are syneresis cracks rather than desiccation cracks. Syneresis cracks are typical in carbonate or carbonates or carbonate cemented sandstones.

The undulating light and dark coloured lamination of the host rock resembles a carbonate cemented unit that was observed in the upper part of the De Geerdalen Formation during field work in 2015 in eastern Spitsbergen. Støen (2016) presents petrographic data of a sample from this unit from Klementievfjellet in Agardhbukta, which is located 20 km SE of Ryssen (see Figure 7.1). Thin-section microscopy reveals that the laminas result from alternating micritic calcite and detrital siliciclastic clasts dispersed in the micritic calcite.

Støen (2016) suggests that the laminations could be stromatolitic structures. Such structures form in shallow to marginal marine environments by trapping and binding of sediments as well as chemical action of cyanobacteria (Hofmann, 1973). The laminated organic material and cavities seen in the thin-sections are typical for microbial formation (Boggs, 2009). Støen (2016) points out that these findings are consistent with the study of Tugarova and Fedyaevsky (2014). In their paper it is suggested that micro-organisms and biochemical precipitation in connection to cyanobacterial mats are the main mechanism for calcite cementation within siliciclastic intervals in the De Geerdalen Formation on Edgeøya.

If the undulating laminations seen in Fulmardalen in the rusty-red layer are stromatolitic structures, the depositional environment must have been shallow to marginal marine, or possibly lacustrine. Modern stromatolites are restricted to shallow subtidal, intertidal and supratidal zones, as well as to lacustrine environments, where cyanobacteria have sufficient sunlight to carry out photosynthesis (Boggs, 2011). Co-existing shell fragments within the same

unit could support the interpretation of a shallow marine environment. Wave ripples are also observed in the unit (Figure 4.7B), possibly indicating that the undulating lamination is a result of wave activity rather than the formation of stromatolites. The fact that the portion of mud is

Figure 4.7 *Structures interpreted as desiccation cracks, or potentially as syneresis cracks, at Ryssen.* ***(A)*** *Oblique view. Muddy areas are outlined with dashed lines.* ***(B)*** *Side view. Wave ripples are indicated with a dashed line.* ***(C)*** *Top view.* ***(D)*** *Side view. Notice the concave shape (indicated with dashed lines) and the deformed downward tapering cracks.* ***(E)*** *Top view. A partly polygonal pattern can be seen.* ***(F)*** *Top view. Notice the straight to spindle-shaped cracks.*

low in comparison to sand may imply an environment with relatively high energy level, with occasional calm periods where carbonate mud is deposited from suspension.

In general, all the interpretations are consistent with deposition in a shallow marine and tidal setting, suggesting that such conditions may have prevailed during deposition of the respective layer.

Facies H – Plane Parallel Laminated Sandstone

Plane parallel laminated sandstones (facies H) in Fulmardalen (Figure 4.8) share most of the same characteristics as described in Table 4.1. The facies often dominate in relatively thin sandstone units surrounded by mudstones, but also occurs together with facies J, F, E and I in thicker sandstone units. The main difference in how facies H appears in Fulmardalen compared to in compared to elsewhere on Svalbard is related to the level of bioturbation and trace fossils observed. In Fulmardalen the intensity of bioturbation is relatively low, and very few trace fossils are observed, especially when compared to on eastern Svalbard.

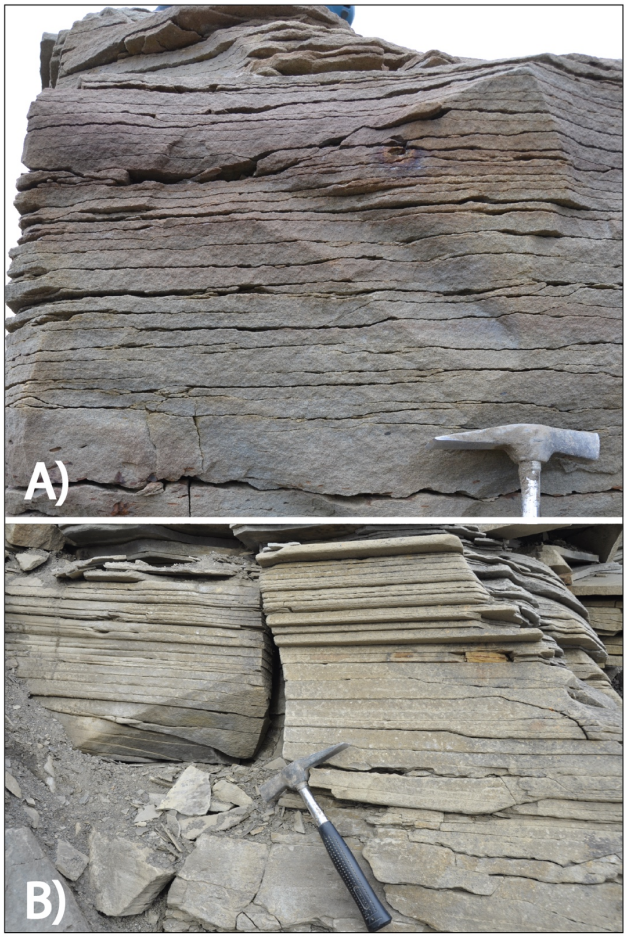

Figure 4.8 *Planar parallel stratified sandstone (facies H) in Fulmardalen at* ***(A)*** *Ryssen and* ***(B)*** *Storfjellet.*

Facies I – Low Angle Cross-Stratified Sandstone

Low angle cross-bedded sandstones (facies I) in Fulmardalen (Figure 4.9) are frequently observed. The description from Table 4.1 is also representative for Fulmardalen. However, minor differences are found. Firstly, mud flakes are occasionally observed in this facies. Secondly, the units are thicker in Fulmardalen, up to 3 m. Finally, bioturbation is not observed within low angle cross-stratified sandstones.

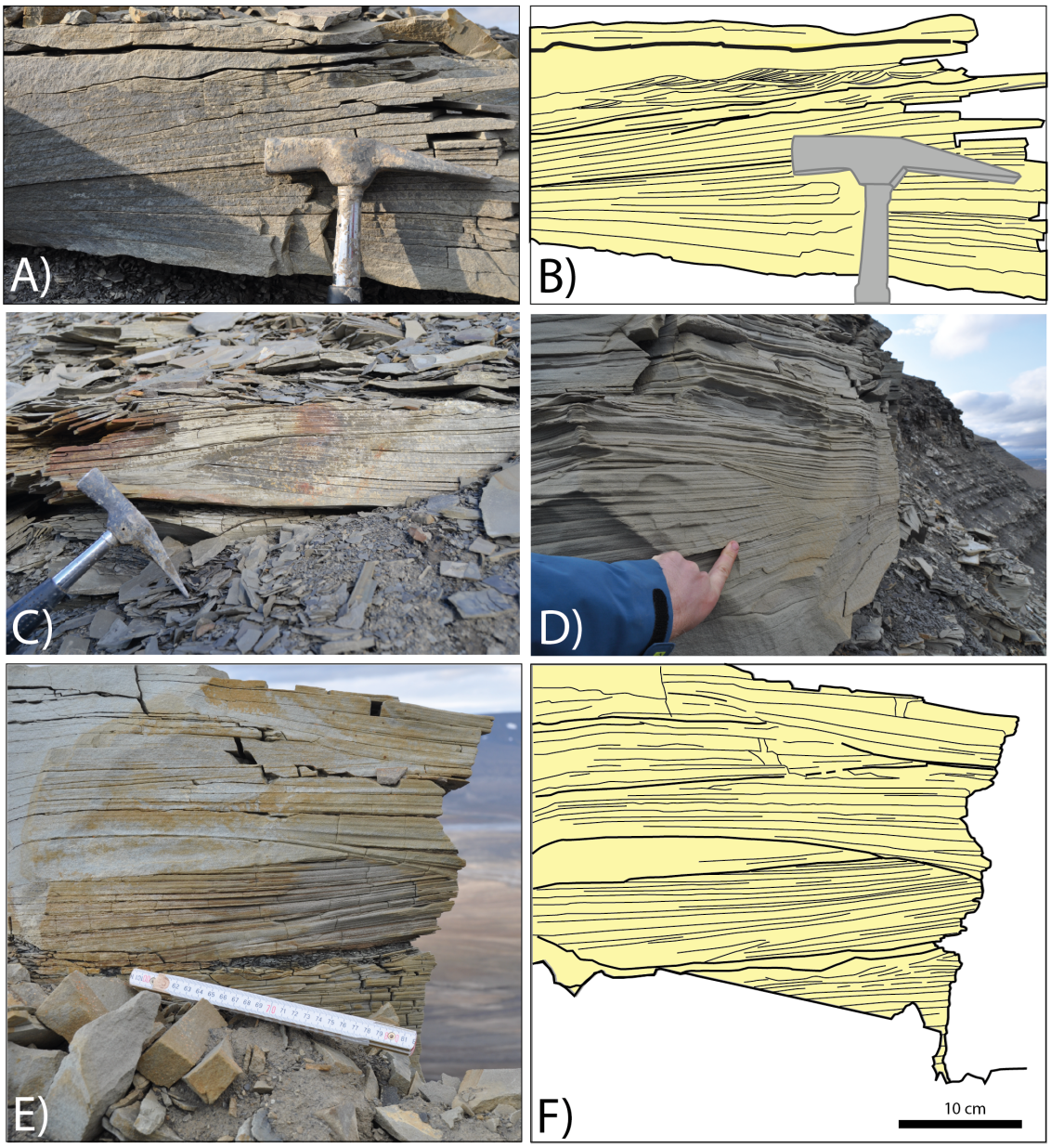

Figure 4.9 *Low angle cross-stratified sandstone (facies I) in Fulmardalen.* ***(A)*** *Outcrop at Milne Edwardsfjellet. Notice ripples towards the top of the unit.* ***(B)*** *Sketch of the sandstone in A.* ***(C)*** *Outcrop at Storfjellet.* ***(D)*** *Outcrop at Milne Edwardsfjellet.* ***(E)*** *Outcrop at Milne Edwardsfjellet.* ***(F)*** *Sketch of the sandstone in E.*

Facies J & K – Tabular & Trough Cross-Stratified Sandstone

In Fulmardalen, tabular and trough cross stratified sandstones (facies J and facies K) (Figure 4.10), share many of the characteristics with outcrops from elsewhere on Svalbard (Table 4.1). The two facies often occur within the same sandstone units, and often are tabular cross-stratified sandstones found overlying trough cross-stratified sandstones. Minor sandstone units with facies J and K may display an erosive base and often have a laterally restricted geometry, tapering into scree. In units where tabular cross stratification is overlying trough cross-stratified sandstones, the cross-stratification tends to get more tabular as the grain size gets finer upwards. In Fulmardalen facies J and K are also commonly observed in laterally extensive and upward coarsening sandstone units, especially in the lower part of the formation. These sandstones typically include facies E, I and H as well, and have gradual lower boundaries to a heterolithic succession (facies B). Herringbone structures are also observed at Storfjellet (Figure 4.10A). Such structures have not commonly been reported from the De Geerdalen Formation, but Rød et al. (2014) do describe herringbone structures from Edgeøya on eastern Svalbard (see Figure 4.1).

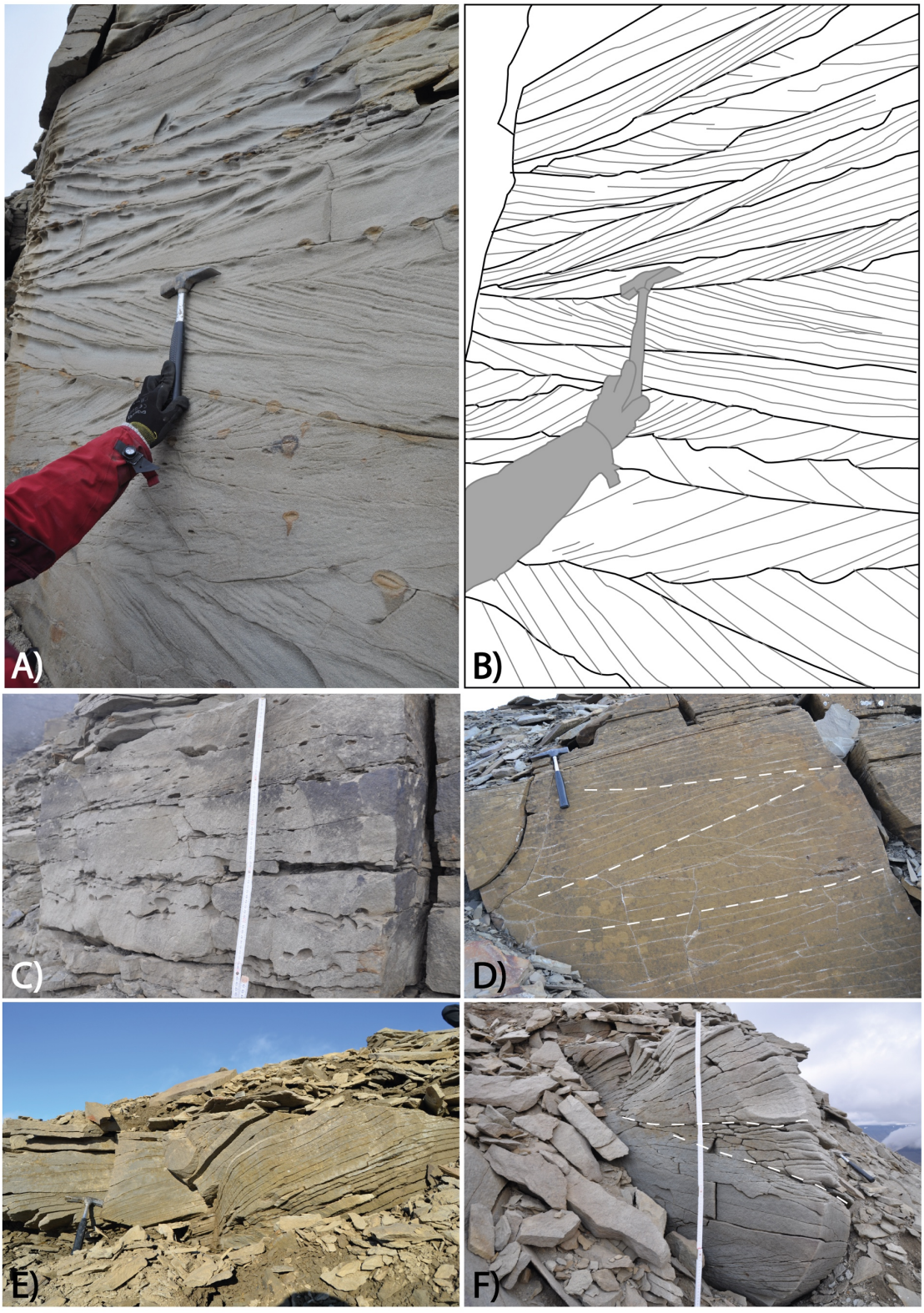

Figure 4.10 *Tabular and trough cross-stratified sandstones (facies J and K) in Fulmardalen.* ***(A)*** *Bi-directional tabular to trough cross-stratified sandstone at Storfjellet.* ***(B)*** *Sketch of the sandstone in A.* ***(C)*** *Trough cross-stratified sandstone with mud clasts at Storfjellet.* ***(D)*** *and* ***(E)*** *Tabular cross-stratified sandstones at Wallenbergfjellet.* ***(F)*** *Trough cross-stratified sandstone at Milne Edwardsfjellet.*

Facies L – Bioclastic Sandstone and Mudstone

In Fulmardalen bioclastic sandstones (facies L) (Figure 4.11) are only observed at Storfjellet and Ryssen in the middle to upper part of the logged sections. This is consistent with description from elsewhere on Svalbard (Table 4.1), where such beds are typically restricted to the lower part of Isfjorden Member (e.g. Mørk et al., 1999a; Haugen, 2016). Bioclastic beds are found encapsulated within mudstone and locally as accumulations in distinct layers within carbonate cemented sandstones (facies G).

Figure 4.11 *Bioclastic sandstones in Fulmardalen at* ***(A)*** *Ryssen,* ***(B)*** *Ryssen and* ***(C)*** *Storfjellet.*

Facies M – Coal and Coal Shale

Coal shale is only found at one locality in Fulmardalen – in the upper part of Ryssen (Figure 4.12). It appears as a 5 cm thick layer and is associated with underlying paleosol and dark shale within the Isfjorden Member. The lateral continuity of the layer is uncertain due to scree cover. No coal layers or beds are observed in Fulmardalen.

Figure 4.12 *Coal shale in Fulmardalen at Ryssen.*

Facies N – Paleosols and Calcrete

Paleosols and calcrete are frequently observed in the upper part of the De Geerdalen Formation, within the Isfjorden Member in Fulmardalen (Figure 4.13).

Wood fragments are not found in this facies in Fulmardalen, which is in contrast to what has been described from other localities on Svalbard (e.g. on Wilhelmøya, Lord et al., 2017a). Two different types of paleosols dominate this facies the study area; non-calcareous red and green mudstones (Figure 4.13A, B) and carbonate soils (calcretes) (Figure 4.13B, D). The colour alternation in the mudstones is thought to be related to a change in the redox regime during formation, where red mudstone occurs in oxidising conditions and green and grey mudstone in reduced environments (Haugen, 2016). Calcrete in Fulmardalen appears as 0.5-1.5 m thick laterally extensive carbonate units, often interbedded in red and green mudstone.

Calcrete forms in semi-arid to arid climate, when $CaCO_3$ precipitates from oversaturated water within the soil (Wright and Tucker, 1991). Calcareous nodules (Figure 4.13C, D, E) are found within both of the soil types in Fulmardalen and are thought to be a result of local precipitation of calcite around roots, caused by an oversaturation of calcite when water is drained from the soil.

Figure 4.13 *Paleosols and calcrete in Fulmardalen.* ***(A)*** *Red and green mudstones of the Isfjorden Member at Storfjellet.* ***(B)*** *Calcrete and underlying green mudstone at Dyrhø.* ***(C)*** *Irregular-shaped nodule found in green mudstones at Dyrhø.* ***(D)*** *Calcrete at Raggfjellet. Notice its irregular shape and mottled appearance.* ***(E)*** *Nodules that have weathered out from red mudstones at Storfjellet.*

5 Logged sections from Fulmardalen

As mentioned in Chapter 4, the sedimentological data from the Triassic exposures in Fulmardalen can create a link between previously collected data from central Spitsbergen and eastern Svalbard. The new dataset from Fulmardalen may be regarded as the last missing piece of the "Triassic puzzle" on Svalbard.

The dataset from Fulmardalen consists of 6 sedimentological logs (location shown in Figure 5.1) ranging from 21 to 261 m in length. This chapter presents each mountain visited together the corresponding logged sections. The logs have been sub-divided into intervals based on trends and similarities, with the purpose of making the description and interpretation of the logs easier to follow.

The logs are presented with a lithology- and a grain-size column. The colours in the grain size column try to illustrate the actual colour-variations observed between different outcrops. A log-legend is presented in Appendix B.

Figure 5.1 *Overview map of Fulmardalen with the start and end positions of the logs indicated. Base map retrieved from Norwegian Polar Institute.*

5.1 Wallenbergfjellet

Wallenbergfjellet (Figure 5.2) is a mountain on the corner between Sassendalen and Fulmardalen, limited by Skrottbreen in NE, Lumpen in E, and Lumpbreen in SE (Figure 5.1). The top is plateau shaped and the highest point reaches 674 masl. The south-western mountain-side of Wallenbergfjellet faces Fulmardalen and holds exposures of Vikinghøgda, Botneheia, Tschermakfjellet and De Geerdalen formations. However, the exposures are not of the best kind. The De Geerdalen Formation, which is the target of this study, only comprises the upper part of the mountain and is relatively poorly exposed compared to most of the other mountains visited.

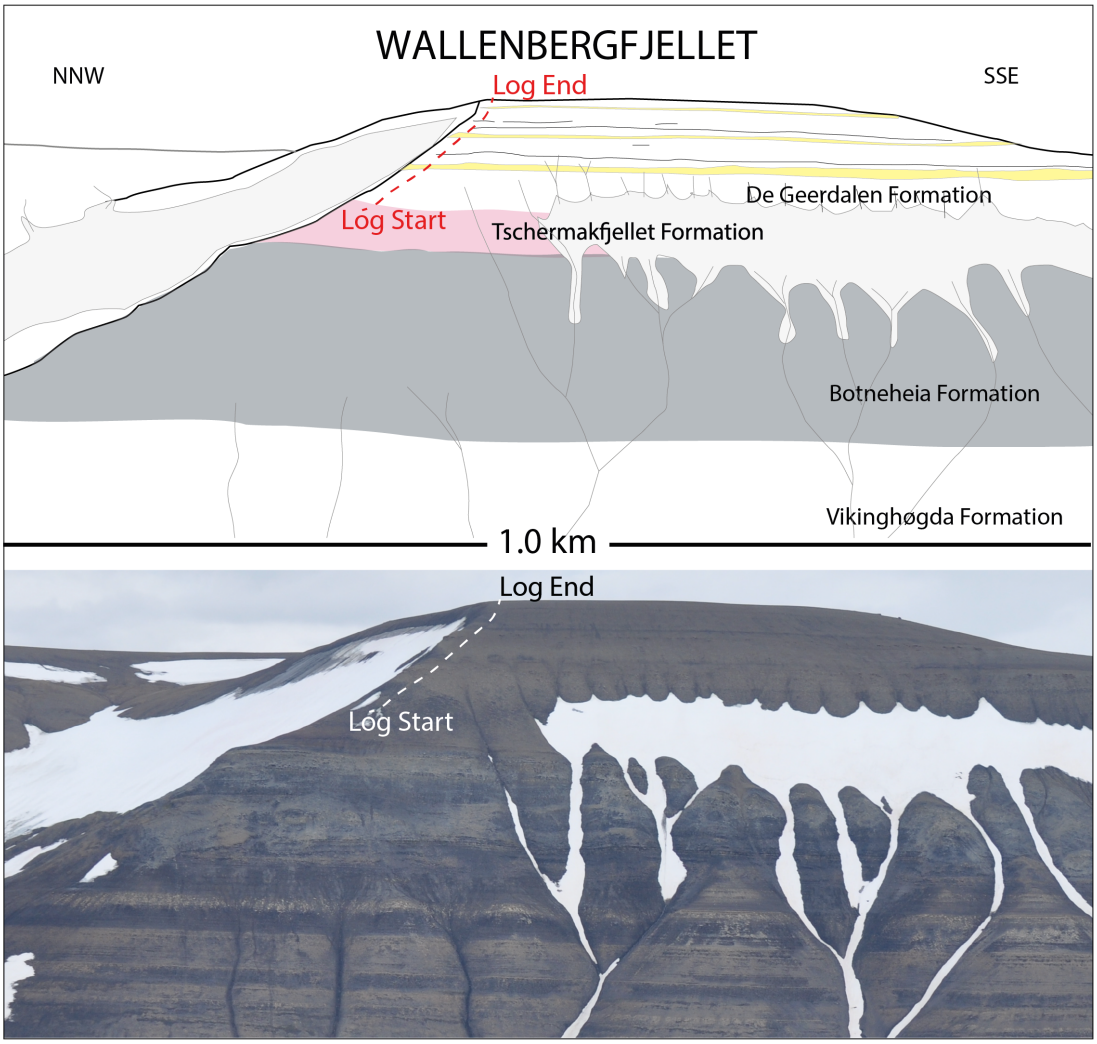

Figure 5.2 *Geological sketch and corresponding overview photo of Wallenbergfjellet. Formation names and stratigraphic boundaries have been indicated. Yellow areas within the De Geerdalen Formation mark major sandstone intervals. Log trace indicated with a dashed line.*

The logged section (Wal 16-1; Figure 5.3) is 98 m long and is located along a ridge in the south-western slope of Wallenbergfjellet. It starts in the Tschermakfjellet Formation and continues upwards into the De Geerdalen Formation and ends on the plateau. The characteristic red and green mudstones of Isfjorden Member are not observed. Briefly described, the De Geerdalen Formation on Wallenbergfjellet consist of three major upwards coarsening units (Figure 5.4).

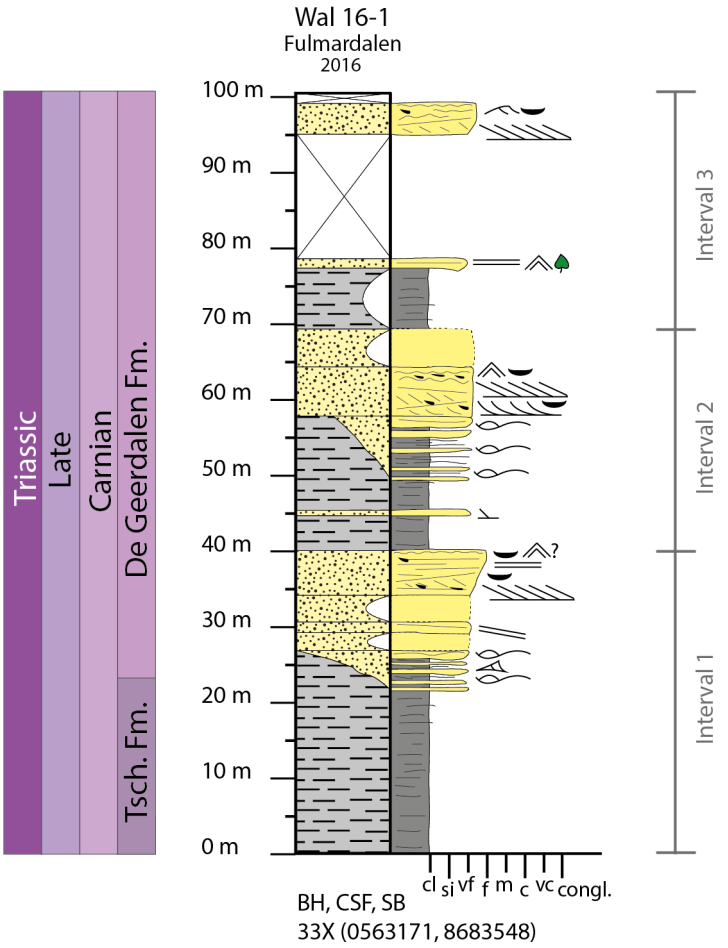

Figure 5.3 *Log from the measured section at Wallenbergfjellet. Depositional age has been interpreted following Mørk et al. (1999a). Interval sub-division is indicated.*

Log Wal 16-1

Interval 1 (0 – 40)

Description: The interval is an upward coarsening sequence. The first 23 m consist of partly scree covered grey shale and siltstone beds (facies A). The next 4 m are heterolithic deposits

(facies B) where decimetre thick very fine sandstones with hummocky cross-stratification (facies C) are interbedded in shales and siltstones. There is an upward coarsening partly scree covered 13 m thick very fine to fine sandstone dominated unit on top of the heterolithic package. Whether the lower boundary is sharp or gradual is hard to say due to scree-cover. The lower part of the sandstone is heavily scree covered. Low angle cross-stratification is observed in the intact part further up. The upper part of the sandstone is cemented and shows a change from tabular cross-stratification (facies J) to plane parallel stratification (facies H) along with a decrease in bed thickness; from 5 cm to 1 cm. Mud flakes are found at the base of a bed. The uppermost part of the sandstone has signs of wave ripples (facies E) and is heavily fractured. The sandstone unit is laterally extensive and can be traced several hundred meters.

Interpretation: The interval is interpreted to represent a transition from a prodelta to a delta front environment. The basal 23 m of the section measured at Wallenbergfjellet is interpreted to belong to the marine pro-delta deposits of the Tschermakfjellet Formation (Mørk et al., 1982, 1999a). The hummocky cross-stratified sandstones in the overlying heterolithic package are interpreted to be storm generated beds in the offshore transition zone to lower shoreface (Reading and Collinson, 1996) and are thought to reflect the base of the De Geerdalen Formation (Mørk et al., 1982, 1999a). The sandstone at the top is thought to reflect delta front to upper shoreface sands, more specifically a barrier bar or shallow subaqueous bank deposit. A relatively thin and laterally continuous geometry is typical for such deposits (Rød et al., 2014; Lord et al., 2017a).

Interval 2 (40 – 68.5m)

Description: The following interval is also an upwards coarsening sequence. The lowermost 9 m consist of partly scree covered grey shales and siltstones (facies A) enclosing a 20 cm thick siderite cemented very fine sandstone layer. Above is a 9 m heterolithic unit (facies B). The sandstones within the heterolithic unit are very fine with sharp bases and hummocky cross-stratification (facies C). The sandstones increase both in thickness and frequency upwards. The heterolithic unit has an upper sharp boundary to a cemented, brown, very fine sandstone dominated unit of 6 m thickness. The lower part of the sandstone unit has large scale cross bedding with mud flakes along set boundaries. The geometry of the cross beds changes from troughs (facies K) to tabular (facies J) upwards, along with a decreasing bed thickness in the range of 7 to 1 cm. The upper part of the sandstone is wave rippled (facies E) and mud flakes

are observed. The uppermost 4.5 m of the interval consists of sandstone scree. The sandstone unit can be traced laterally for several hundred meters.

Interpretation: The boundary to the underlying interval is interpreted to represent a relative sea level rise and a change back to an environment in the offshore transition zone to lower shoreface. Here, clay is deposited from suspension during relatively calm periods, and silt and sand during periods with higher energy such as storm episodes (Johnson and Baldwin, 1996; Bhattacharya et al., 2004). The sandstone above the heterolithic unit is believed to be delta front to shoreface sands. Its lower boundary may appear sharper than it actually is, due to the contrast between its hard, cemented appearance and the more easily weathered heterolithic unit below. Based on the upward coarsening nature and geometry of the sandstone unit, in addition to the sedimentological structures observed, it is likely that this unit represents a barrier bar or subaqueous bank, similar to the sandstone in the underlying interval.

Interval 3 (68.5 – 98m)

Description: Overlying the sandstone scree there are 8.5 m of partly scree covered shales and siltstones (facies A). A very fine sandstone of 25 cm is found above the scree. It is planar stratified (facies H) and plant fragments are observed. The following 18 m are totally scree covered. A very fine sandstone of 3 m is found above the scree. It is tabular cross bedded (facies J) with mud flakes in the lower part and asymmetrical ripple laminated (facies F) in the upper part.

Interpretation: The partly covered shale is interpreted to represent deposits in the offshore transition zone to lower shoreface. The sandstones are interpreted as shoreface to delta front deposits. Tabular cross-stratification typically forms by unidirectional currents of the lower flow regime in shallow waters (Collinson et al., 2006; Boggs, 2011).

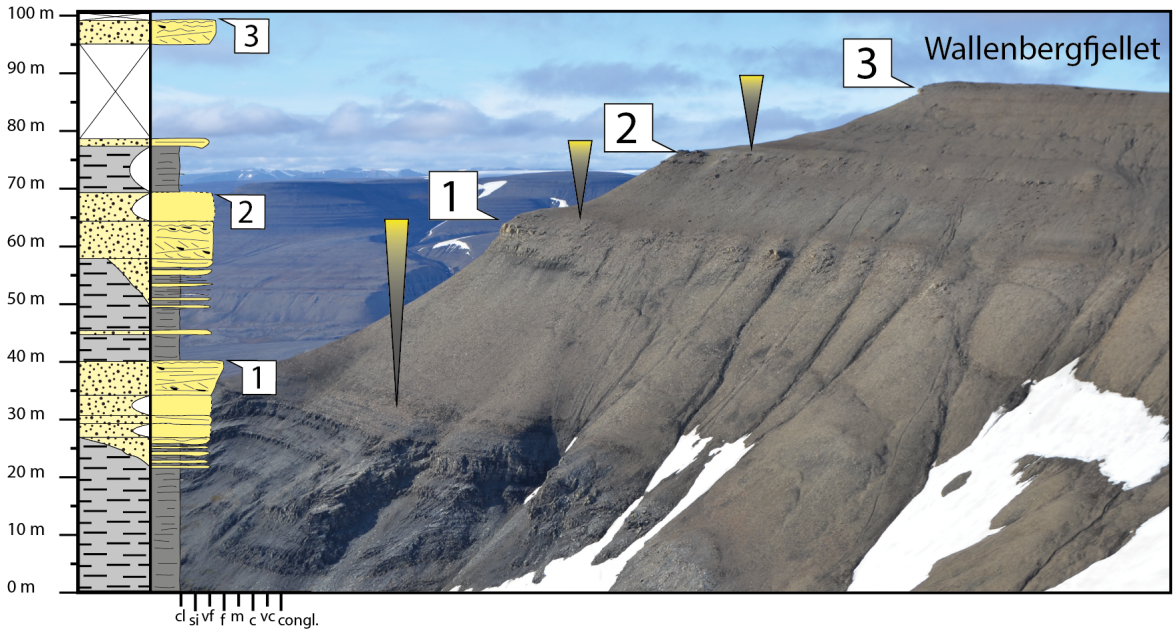

Figure 5.4 *Log and picture correlation from Wallenbergfjellet. The figure shows three major coarsening upwards sequences, typical for the lower part of the De Geerdalen Formation. The top of each sequence is indicated.*

5.2 Dyrhø

Dyrhø (Figure 5.5) is the innermost mountain in the south-western side of Fulmardalen (see Figure 5.1). The summit of the mountain is situated at 680 masl, where the top extends out from a glacier to the west of the measured profile. The slopes facing Fulmardalen hold exposures of the Botneheia Formation, the Tschermakfjellet Formation and the De Geerdalen Formation.

The section measured at Dyrhø (Dyr 16-1; Figure 5.6) is 190 m long, and starts in the upper part of the Tschermakfjellet Formation close to the base of the De Geerdalen Formation. Characteristic features of the Isfjorden Member (e.g. Pčelina, 1983; Mørk et al., 1999a; Haugen, 2016) are found in the upper reaches of the measured slope, indicating that the log terminates somewhere in the upper parts of the De Geerdalen Formation.

The De Geerdalen Formation at Dyrhø consists of one major coarsening upwards sequence in the lower part, followed by an interval of several minor coarsening upwards sequences. The upper part of the formation is dominated by shale, interbedded with relatively thin and often carbonate cemented sandstone benches.

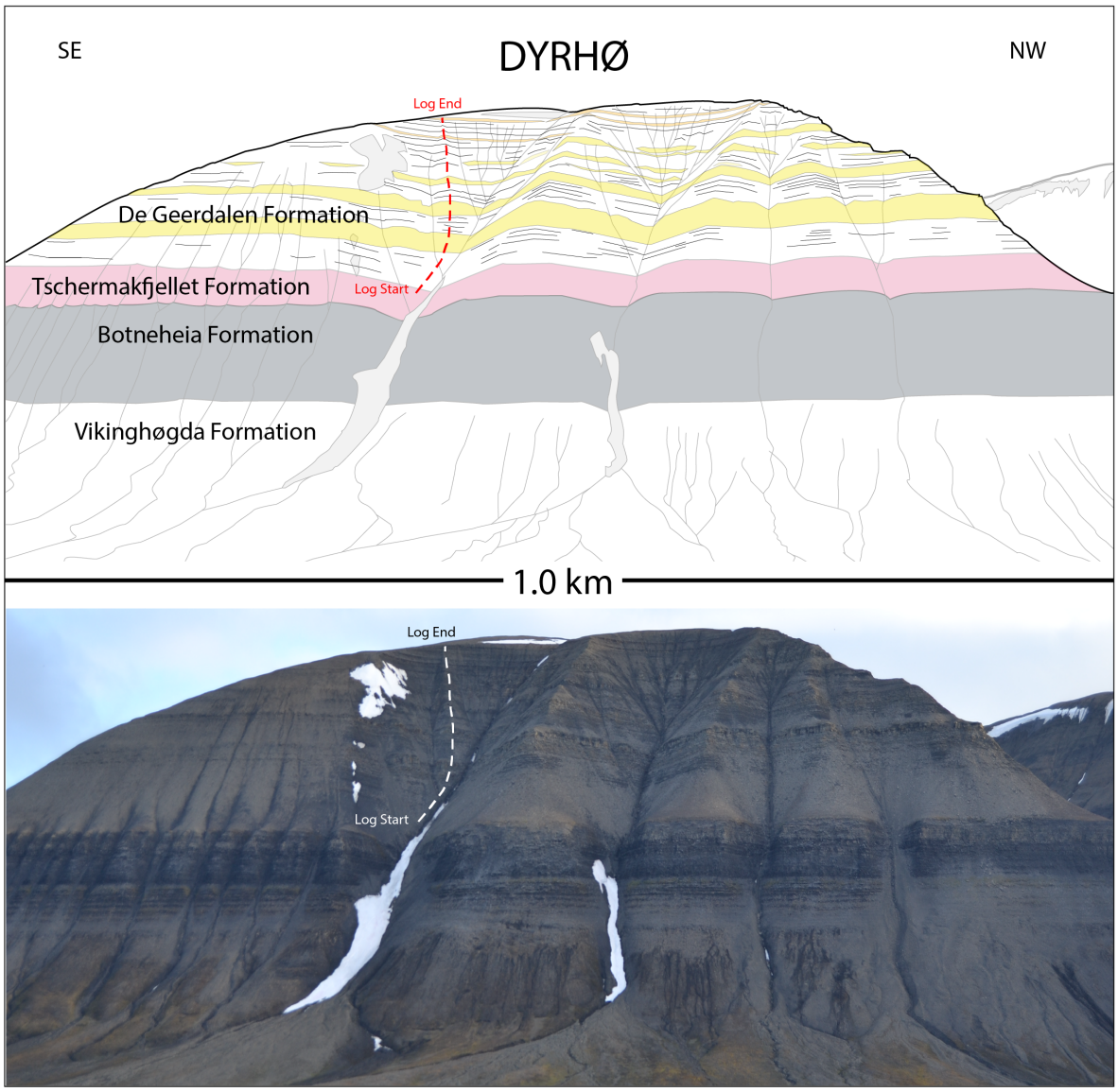

Figure 5.5 *Geological sketch and corresponding overview photo of Dyrhø. Formation names and stratigraphic boundaries have been indicated. Yellow areas within the De Geerdalen Formation mark major sandstone intervals. The log trace is indicated with a dashed line.*

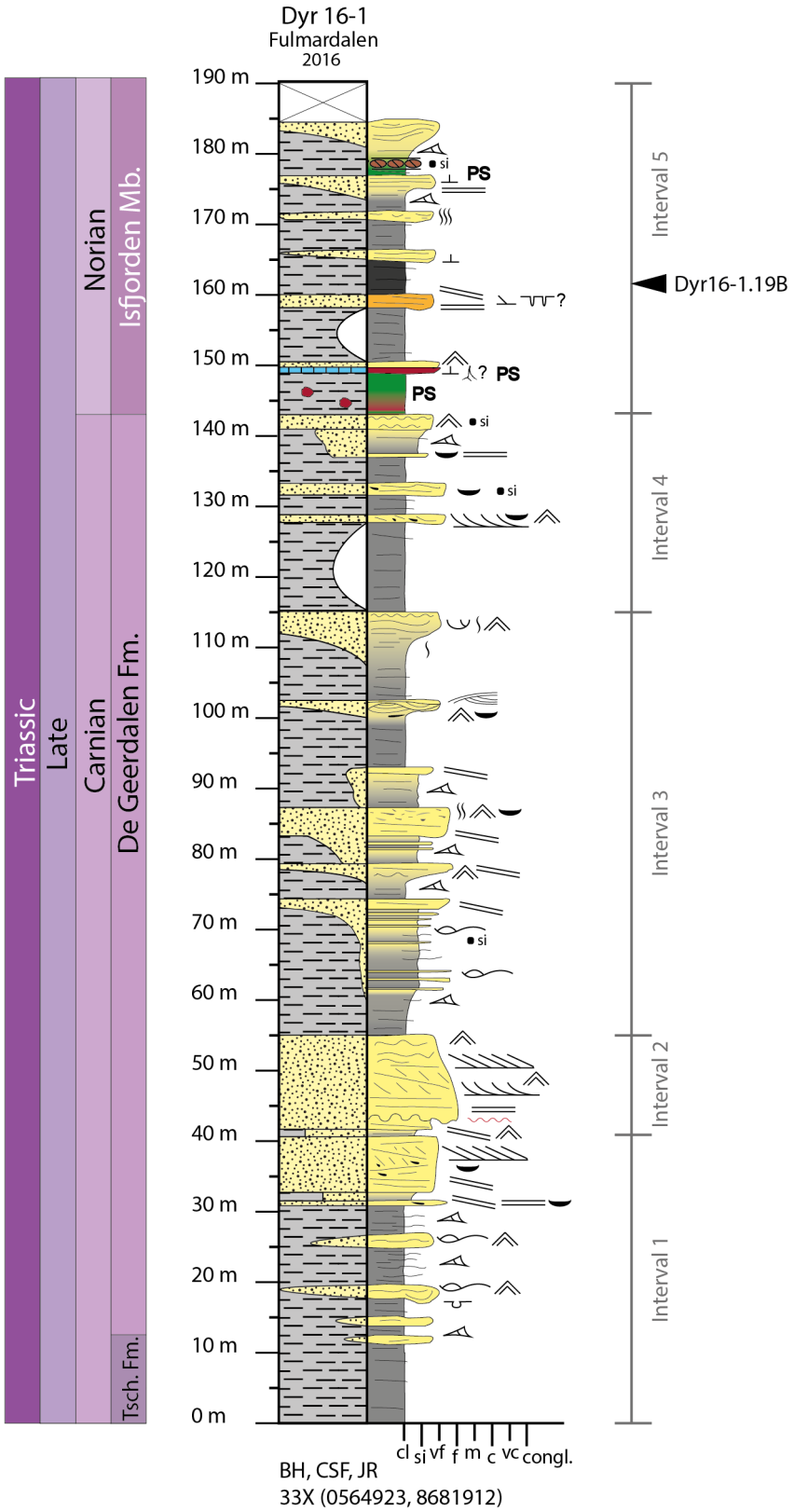

Figure 5.6 *Log from the measured section at Dyrhø. Depositional age has been interpreted following Mørk et al. (1999a). Interval sub-division and the postion of sample Dyr16-1.19B are indicated.*

Log Dyr 16-1

Interval 1 (0 – 41m)

Description: The first 41 m of log Dyr 16-1 represents an upwards coarsening sequence. The lowermost 10 m consists of mudstone. The following 21 m of the interval consist of mainly heterolithic bedding (facies B) and mudstones (facies A). Minor sandstones with thicknesses ranging from 0.5-2.5 m occur within this section. The sandstones are very fine in grain size, and display hummocky cross-stratification (facies C) topped by wave ripples (facies E) and plane parallel lamination (facies H). Erosive surfaces and evidence of soft sediment deformation (facies D) are also observed. The sandstone bodies are laterally restricted, ranging from 2-20 m in width. The interval is gradually coarsening upwards into a sandstone dominated unit. The sandstone unit is very fine to fine grained with low angle cross-stratification (facies I) and large scale tabular cross-stratification (facies J). Mud flakes and thin layers of shale are present. It is laterally extensive and can be followed for several hundred metres.

Interpretation: The lower mud-dominated sequence in the basal part is interpreted as prodelta deposits, assigned to the Tschermakfjellet Formation. The base of the De Geerdalen Formation is interpreted to be the first prominent sandstone bench at the base of the heterolithic unit (Mørk et al., 1999a). The sedimentary structures within the sandstones indicate rapid deposition, potentially as storm deposits or gravity flows within a muddy environment in a prodelta setting (Reading and Collinson, 1996). The upwards coarsening, laterally extensive, low angle and tabular cross bedded sandstone unit in the upper part of the interval is interpreted as a barrier bar and correlates to the lowermost sand dominated units at the other mountains in Fulmardalen. The mud flakes herein are probably deposited as a result of tidal- or wave activity. In tidal settings, parts of semi-consolidated mud may be ripped up by high energy currents (Dalrymple and Choi, 2007; Rød et al., 2014). The presence of thin layers of shale within the sandstone unit may indicate variations in flow velocities during deposition, probably supporting influence from tidal activity (Dalrymple and Choi, 2007).

Interval 2 (41 – 55m)

Description: A short heterolithic unit followed by an 11 m thick, erosive based and upwards fining sandstone (Figure 8.5C) overlies the sandstone from the previous interval. The erosive surface is covered with mud flakes. The grain size changes upwards from medium to fine sand. The sandstone displays plane parallel stratification (facies H), wave ripples (facies E) and large

scale trough cross-stratification (facies K). The cross-stratification gets more tabular (facies J) upwards as the grain size decreases. The sandstone is topped by wave ripples (facies E).

Interpretation: The sandstone is interpreted as a tidal inlet cutting through a barrier bar. The interpretation is based on the upwards fining trend, the erosional base with mud flakes and the relatively coarse grain size, in addition to large scale cross-stratification. Similar tidal inlet deposits have been described from the Upper Cretaceous St. Mary River Formation in southern Alberta by Young and Reinson (1975) (see Figure 5.7).

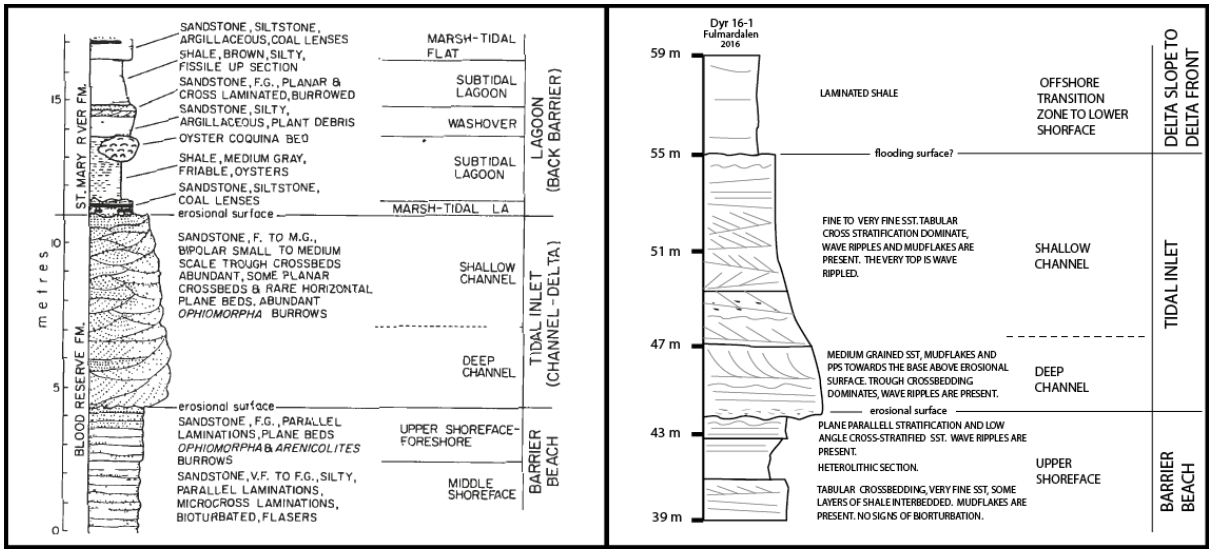

Figure 5.7 *Barrier inlet log sections. The Figure illustrate a comparison of a log through a barrier inlet complex from the Upper Cretaceous Blood Reserve – St Mary River Formation in Southern Alberta (Young and Reinson, 1975), and a similar complex from the Upper Triassic De Geerdalen Formation at Dyrhø. The main difference between the two logs is the interpreted depositional environment of the fine grained facies in the upper part of the logged sections.*

Interval 3 (55 – 115m)

Description: The following 60 m in Dyr 16-1 are represented by series of small coarsening upwards units. Ranging from 5-19 m in length, the sequences are typically composed of shales (facies A) in the lower part, followed by a heterolithic sequence (facies B) containing thin sandstones with hummocky cross-stratification and some siderite concretions. The sandstones capping each sequence are very fine to fine in grain size, with a typical thickness between 0.5-4 m. Structures such as low angle cross-stratification (facies I) and wave ripples (facies E) are common. Mud flakes occur in several of the sandstones, and some of the units also show signs of sparse to moderate bioturbation. Large scale hummocky cross-stratification and mud-drapes are also present. The uppermost sandstone shows mud drapes in addition to wave ripples and

sparse bioturbation (Figure 5.8B). The geometry of the sandstone bodies varies, with some of them being laterally extensive, stretching across the whole mountainside. Other units have a more restricted lateral appearance.

Interpretation: The contact to the underlying sandstone interval marks a change to deposition of mudstones. The contact is interpreted to represent a relative sea level rise and a change to an offshore transition zone to lower shoreface environment. Hummocky cross-stratification indicates deposition of sand in the offshore transition zone to lower shoreface setting. Wave rippled and low angle cross-stratified sandstones are interpreted as barrier bars in a delta front setting. Mud drapes in the uppermost sandstone unit may indicate a tidal influence on the deposition (Boggs, 2011).

Interval 4 (115 – 143m)

Description: This interval has a lower part dominated by mudstone (facies A). The upper part has three relatively thin sandstone units (< 2m), in which structures such as large scale trough cross-stratification (facies K), planar lamination (facies H) and wave ripples (facies E) occur, as well as features like siderite concretions and mud flakes.

Interpretation: A dominance of mud in interval 4 suggests deposition in a low energy regime. Fine grained deposits may occur in interdistributary areas which may contain tidal flats, bays, lagoons and floodplains (Rød et al., 2014). Alternatively the mudstones represent deposition in a lower shoreface to offshore environment. However, thin sandstones containing sedimentary structures like trough cross-stratification and mud flakes abruptly interbedded are found within the mudstone interval. This may imply that the interval represents deposition in an interdistributary area, like a lagoon or bay with thin sandstones deposited as wash-over fans from storm episodes. Small to medium scale cross beds and low angle to planar stratification characterize the sedimentary structures in such deposits (Reinson, 1984). The sandstones could also reflect small channels on a mud dominated tidal flat (Reineck and Singh, 1980).

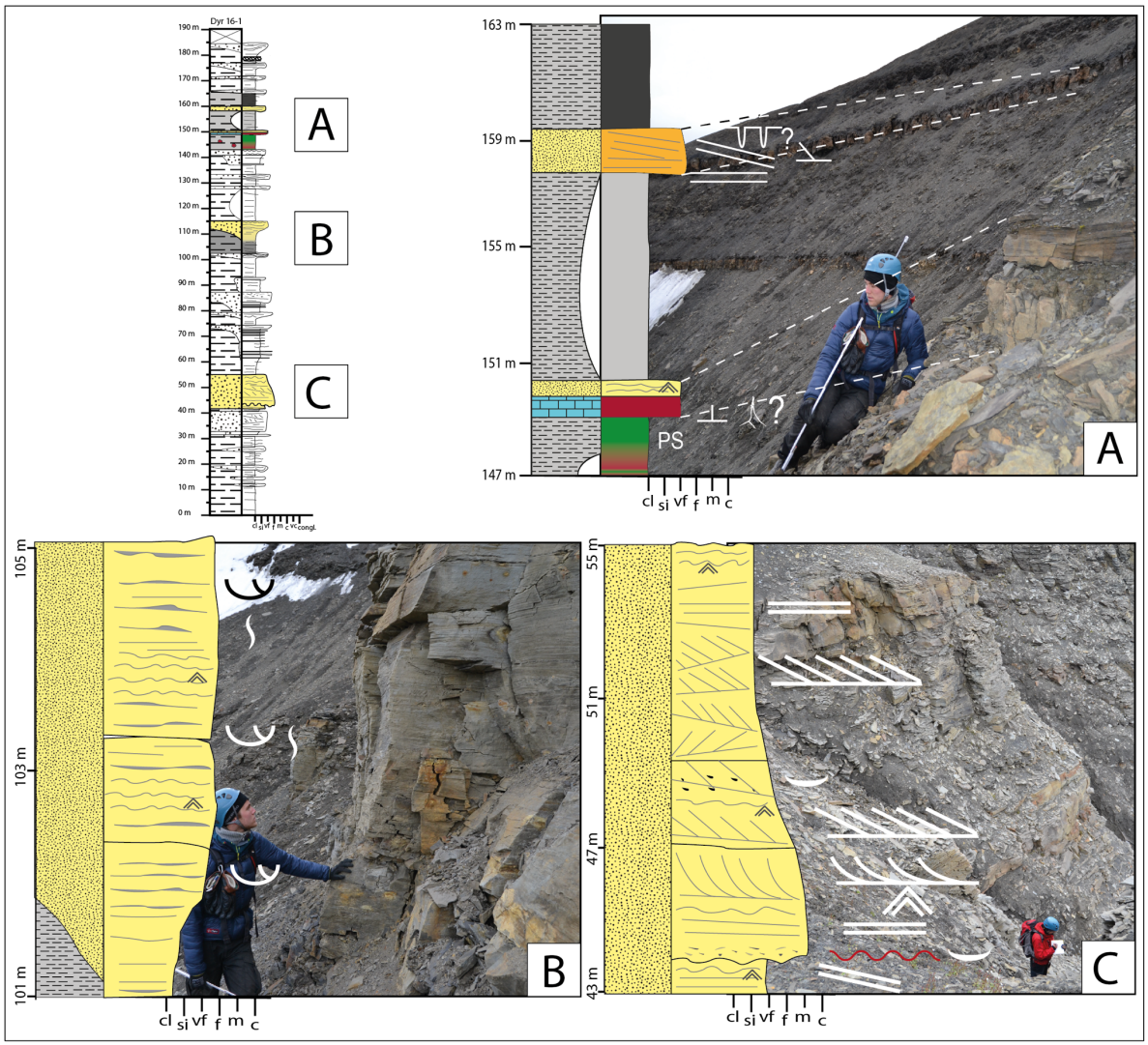

Figure 5.8 *Log and picture correlation from Dyrhø.* ***(A)*** *A shale-dominated sequence with thin carbonate cemented sandstones, a calcrete profile, and red and green mudrocks. These deposits are typical for the Isfjorden Member.* ***(B)*** *Sandstone interval deposited with a tidal influence.* ***(C)*** *A thick sandstone interval in the lower part of the De Geerdalen Formation, interpreted as a barrier bar complex with an inlet cutting through.*

Interval 5 (143 – 190m)

Description: The uppermost 47 m of the measured section at Dyrhø are shale dominated (facies A), with relatively thin and carbonate cemented sandstones (facies G). The interval starts with green mudstone with nodules (facies N). Above there is a sequence of deposits that can be fully or partly recognized at Milne Edwardsfjellet, Ryssen and Storfjellet. At Dyrhø the sequence (shown in Figure 5.8A) starts with a distinct 1 m thick carbonate rich unit with a red weathering colour containing potential root structures or vertical trace fossils. It forms a laterally extensive bench in the mountain side and is topped by a wave rippled (facies E) sandstone. The sequence continues with 10 m of grey shale followed by a 2 m thick rusty-red carbonate cemented

sandstone with an overlying very dark shale. The rusty-red layer sticks out in the terrain and is laterally extensive. It shows signs of low angle and planar parallel cross-laminations, but the structures are poorly preserved due to heavy cementation. Additionally, it has lighter coloured mud laminations with possible desiccation cracks. The top of a dark shale marks the end of the sequence that has also been recognized from other mountains in Fulmardalen. The uppermost 13 m of the interval consist of green mudstone (facies N) capped by a very fine sandstone with overlying scree. A laterally continuous 20-40 cm thick layer of siderite concretions is found within the green mudstone. The concretions are 10-20 cm in diameter. A similar concretion-layer are also observed at Storfjellet.

Interpretation: The interval is interpreted to represent the Isfjorden Member, deposited in a restricted marine to lagoonal environment. Bioturbation, low angle cross-stratification and carbonate cementation reflect upon a shallow marine origin. Green shales with nodules and overlying carbonate-rich deposits are interpreted paleosols and calcrete, respectively. Such deposits are typically found in ancient delta plain environments (Enga, 2015; Haugen, 2016).

5.3 Ryssen

Ryssen (Figure 5.9) is located on the south-eastern side of Fulmardalen, with Storfjellet to the south and Wallenbergfjellet to the northwest (Figure 5.1). The mountain has a plateau-shaped top with a glacier towards the east. The highest point on the mountain is found at 605 masl. The slopes facing Fulmardalen hold good exposures of the upper parts of the Botneheia Formation, Tschermakfjellet Formation, as well as an almost complete section of the De Geerdalen Formation.

The section measured from Ryssen (Rys 16-1; Figure 5.10) is 261 m long and was recorded from a ridge in the middle of the slope facing Fulmardalen. Tschermakfjellet Formation constitutes the lowermost 34 m of the log, while the rest is considered belonging to the De Geerdalen Formation. Red and green mudstones characteristic for the Isfjorden Member (Pčelina, 1983; Mørk et al., 1999a; Haugen, 2016) were found close to the summit of the mountain. This means that the deposits from Wilhelmøya Subgroup are absent at Ryssen.

Broadly speaking, the lower part of the De Geerdalen Formation at Ryssen consists of two major coarsening upwards sequences from shale to fine and medium sandstone. The upper part is more complex with several smaller sequences, thinner sandstone bodies, coquina beds and orange carbonate-cemented sandstones. Most sandstone bodies are laterally continuous and some can be traced to sections on the neighbouring mountains. Magmatic intrusions have

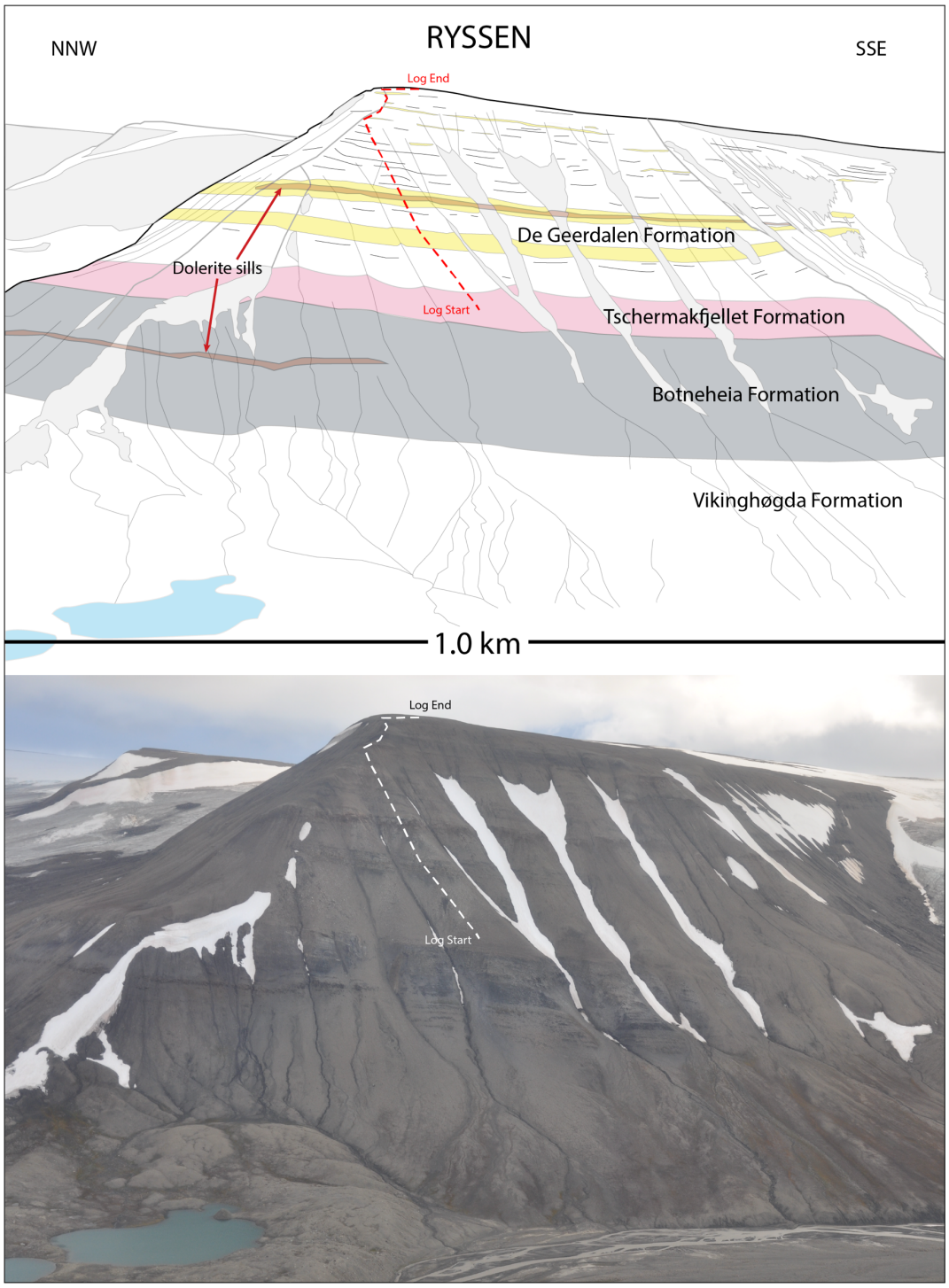

Figure 5.9 *Geological sketch and corresponding overview photo of Ryssen. Formation names and stratigraphic boundaries have been indicated. Yellow areas within the De Geerdalen Formation mark major sandstone intervals. Log trace indicated with a dashed line. Dolerite sills of the Diabasodden Suite appears at two stratigraphic levels.*

affected the Triassic succession at several levels on the north-eastern side of Fulmardalen, and a dolerite sill has also intruded the middle part of the De Geerdalen Formation at Ryssen.

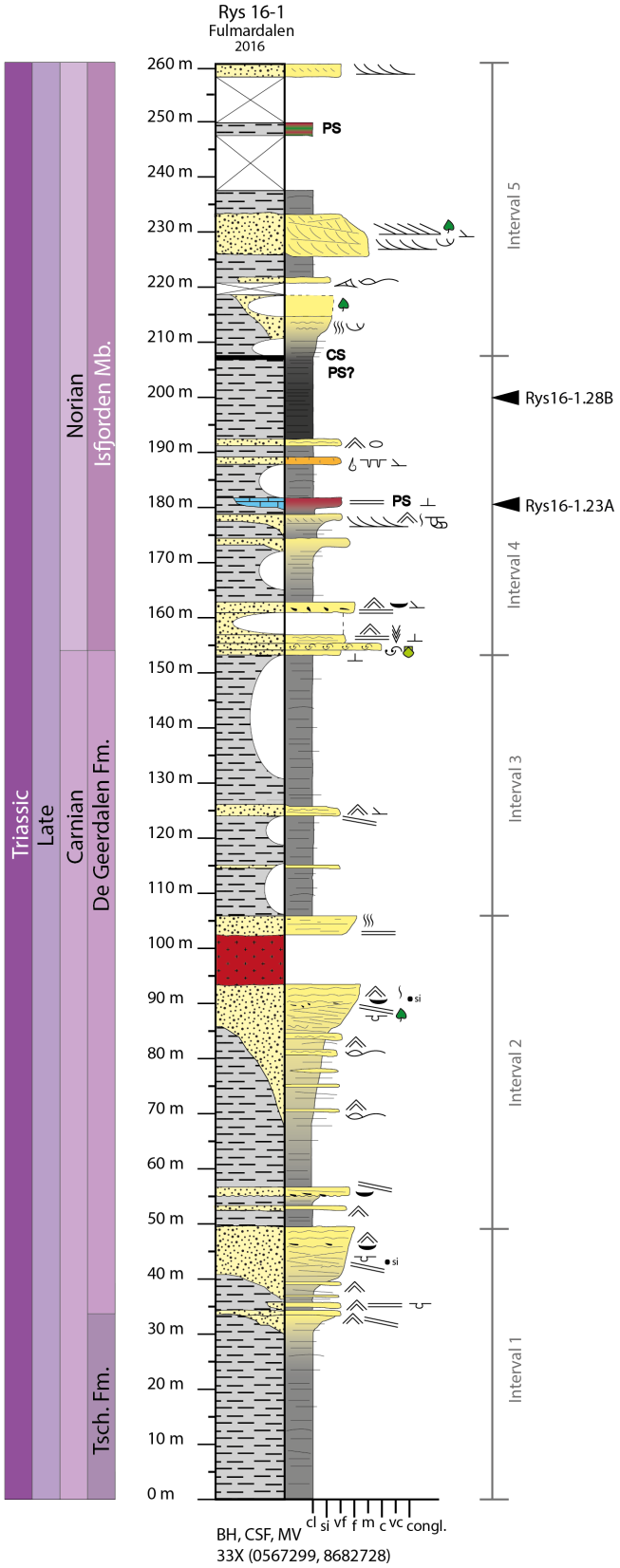

Figure 5.10 *Log from the measured section at Ryssen. Depositional age has been interpreted following Mørk et al. (1999a). Interval sub-division and the position of samples (Rys16-1.23A, 28B) are indicated.*

Log Rys 16-1

Interval 1 (0 – 50m)

Description: The interval is an upwards coarsening sequence. The lower part consists of grey shales and siltstones (facies A), which gradually coarsen upwards into a heterolithic bedding (facies B). Sandstones within the heterolithic bedding are up to a metre thick, with planar parallel stratification (facies H), mud flakes and loading structures (facies D). The heterolithic sequence coarsens upward into an 8.5 m thick very fine to fine sandstone. This is the most sand-rich interval at Ryssen, similar to that which was observed at approximately the same stratigraphic levels in the successions at Storfjellet, Milne Edwardsfjellet, Dyrhø and Wallenbergfjellet. The lower part of the sandstone is dominated by low angle cross-lamination (facies I) and wave ripples (facies E). Soft sediment deformation structures (facies D) are found within the sandstone unit, in addition to mud flakes and a siderite concretion. The very top of the sandstone is wave rippled (facies E).

Interpretation: The lower grey shales and siltstones are interpreted as the prodeltaic deposits of the Tschermakfjellet Formation (Mørk et al., 1999a). Sharply based and relatively thin (<15 cm) siltstone layers are interpreted as storm deposits (Bhattacharya et al., 2004). The transition to the De Geerdalen Formation is found at the first prominent sandstone bench (Mørk et al., 1999a) at the base of a heterolithic section. This transition marks a development to a more proximal and shallow depositional environment, probably in an offshore transition zone to shoreface setting. The sand dominated unit above is interpreted as a barrier bar complex. Soft sediment deformational structures within the sandstone could indicate rapid loading of sediment (Reineck and Singh, 1980; Bhattacharya and MacEachern, 2009), which may be typical in delta front environments. Wave ripples support a shallow marine environment.

Interval 2 (50 – 107m)

Description: The sandstone unit from the underlying interval is capped by 18 m of mudstone (facies A) which mark the onset of a new coarsening upwards sequence. Two 1 m thick sandstone beds with wave ripples (facies E), low angle cross-stratification (facies I) and mud flakes are found within the mudstone unit. The interval gets progressively sandier upwards, turning into a heterolithic section (facies B) with thin layers (< 30 cm) of very fine sandstones. These sandstones are characterized by hummocky cross-stratification (facies C) in the lower part and wave ripples (facies E) in the upper part. The heterolithic section is overlain by an

upwards coarsening 9 m thick low angle cross-stratified sandstone (facies I), also with deformation structures (facies D), plant fragments, sparse bioturbation and siderite nodules, as well as with wave ripples (facies E) at the top. The following 9 m consists of a dolerite intrusion. Above the intrusion there is a 3 m thick fine sandstone unit with plane parallel stratification (facies H) at the base, a massive and structureless middle part and an intensely bioturbated upper part.

Interpretation: The transition from the underlying barrier bar complex is interpreted as a flooding surface. A similar stratigraphic surface is noted in the logs from the other mountains in Fulmardalen. Such distinct changes in depositional environment may be related to autogenic delta processes (Martinius et al., 2014). The interval is interpreted to reflect a transition from the offshore transition zone to a shoreface to delta front setting. The sand dominated unit in the upper part has the same characteristics as the deposits interpreted as a barrier bar from the underlying interval. The sandstone is laterally extensive and can be partly recognized in the other logs from Fulmardalen. The dolerite intrusion is interpreted to belong to the Diabasodden Suite of Late Jurassic to Early Cretaceous age (Mørk et al., 1999a).

Interval 3 (107 – 153m)

Description: Interval 3 is dominated by partly covered mudstones (facies A). The mudstones are interrupted by two thin sandstone beds, ranging from approximately 0.4-2 m in thickness. One of the sandstones is low angle cross-stratified (facies I), wave rippled (facies E) and siderite cemented. The similar stratigraphic level at the other mountains seems to contain more sandstones than at Ryssen, especially at Storfjellet.

Interpretation: The interval is interpreted to reflect a low-energy environment. The low amount of sandstones at Ryssen in this interval compared to at the same stratigraphic level on other mountains may indicate that this part of the succession at Ryssen reflect a locally sheltered marine environment, such as a small lagoon or interdistributary bay. Bioturbation is often intense in lagoons protected by barriers (Reineck and Singh, 1980), which could explain the bioturbation in the upper part of the sandstone in the underlying interval. Thin low angle cross-stratified and wave rippled sandstone units in the lower part of the interval may represent wash-over deposits from storms. Modern studies of wash-over deposits indicate subhorizontal to planar stratification as one of the dominant sedimentary structures (Reinson, 1984).

Interval 4 (153 – 209m)

Description: The interval starts with a laterally extensive and carbonate cemented sandstone (facies G) with wave ripples, planar lamination and cone-in-cone structures. A 20 cm thick coquina bed (facies L) with fragmented shells is interbedded in the sandstone. The upper part of the sandstone is less carbonate cemented, and siderite cemented mud flakes are found at the base of a bed within the sandstone. The rest of the interval is mud dominated with a few interbedded and relatively thin sandstones. One of these sandstones has trough cross stratification (facies K), wave ripples (facies E) and the marine trace fossil *Rhizocorallium*. A depositional sequence that also can be fully or partly recognized at Milne Edwardsfjellet, Dyrhø and Storfjellet comprises the upper part of the interval. At Ryssen this sequence starts with a 0.5 m thick carbonate rich unit (calcrete) with a red weathering colour. Above there are 7 m of grey shale with a 1 m thick rusty-red carbonate cemented sandstone (facies G) on top. This sandstone is laterally extensive, has sporadic shell fragments and potential desiccation cracks observed within a lighter coloured muddy lamination. The rest of the sequence is dominated by very dark grey shales, capped by a paleosol (facies N) and coal shale (facies M).

Interpretation: The interval is interpreted to display a continuation of a marginal marine to lagoonal environment. The occurrence of coquina beds, carbonate beds and red and green mudstones is typical for the Isfjorden Member (Mørk et al., 1999a; Haugen, 2016). Shell bearing organisms such as molluscs typically thrive in environments with low sedimentation rates (Eyles and Lagoe, 1989). Reinson (1984) described coquina beds from lagoonal deposits of the Upper Cretaceous St. Mary Formation in southern Alberta. A fragmented appearance of the shells indicates that the shells may have been reworked and transported away from their original growing position (Reineck and Singh, 1980). A possible scenario is that shell banks accumulate at or close to a beach or barrier bar. During high energy episodes these fragments, together with sand, may be transported into the lagoon as wash-over fan deposits (Boggs, 2011). *Rhizocorallium* trace fossils in one of the sandstones represents a marine trace fossil, belonging to the Cruziana ichnofacies, commonly found in lagoonal and shelf environments with medium to low energy conditions (Boggs, 2011). The high concentration of carbonate in the sandstones could originate from dissolution and re-precipitation of shell material in starved sediment conditions (Ketzer et al., 2003; Støen, 2016). The dark shale in the upper part may reflect deposition in an interdistributary area with restricted energy conditions. Poor water circulation

may have created periodically anoxic conditions, allowing the preservation of accumulated organic material and the resulting dark colour. Associated coal shale and paleosol support a marginal marine to delta plain depositional setting.

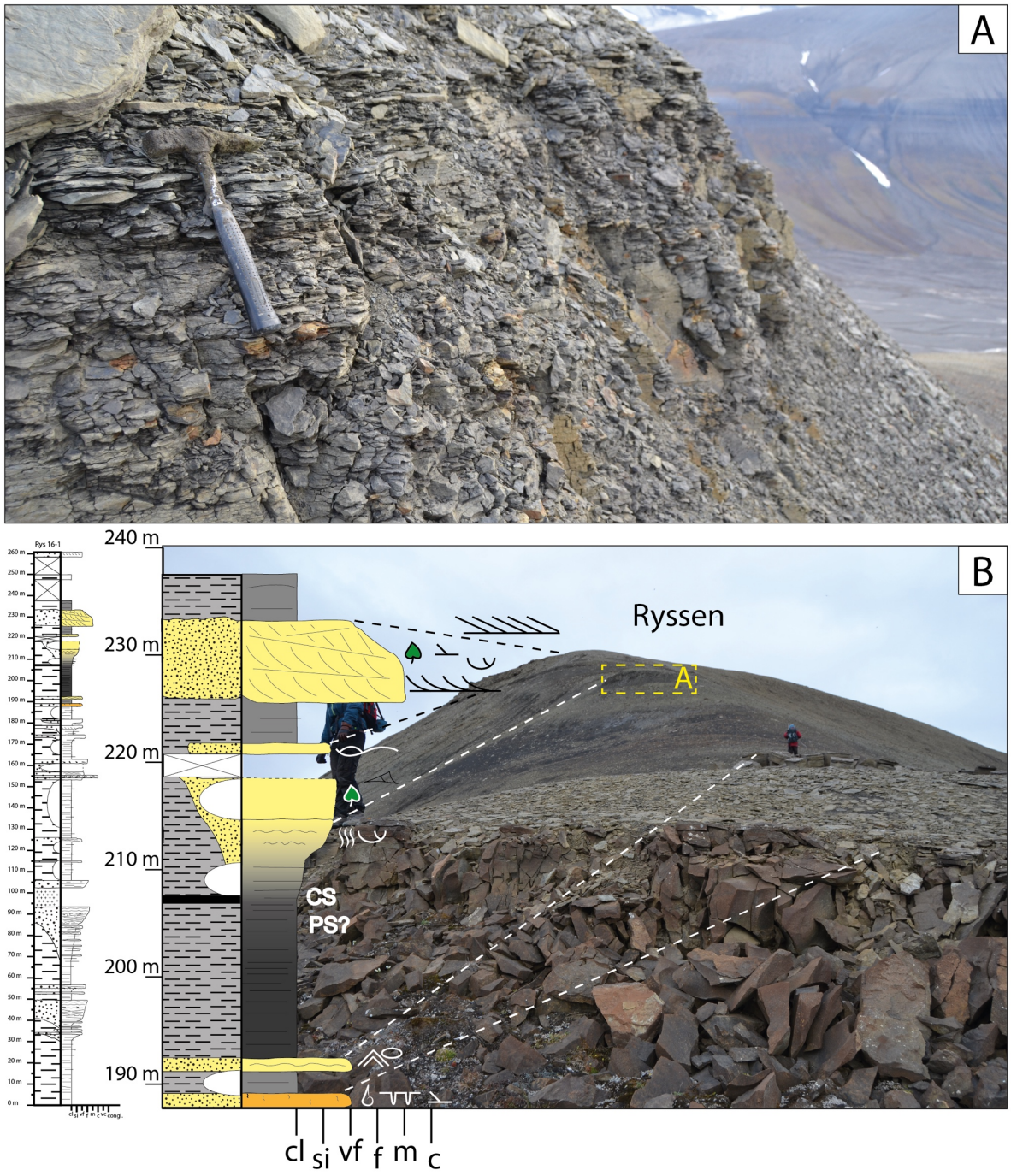

Figure 5.11 *Log and picture correlation from Ryssen.* ***(A)*** *An intensely bioturbated and heterolithic section.* ***(B)*** *A rusty-red carbonate cemented bed with desiccation cracks and shell fragments. Section (A) is seen in the background, laying above of a distinct, very dark shale. Geologists for scale.*

Interval 5 (209 – 261 m)

Description: The dark shale from the underlying interval gradually coarsens upwards into a bioturbated and mud draped siltstone to very fine sandstone unit (Figure 5.11). A plant fragment is found at the surface of a scree block. 8 m of shale (facies A) separates this lower sandstone unit from an upwards fining sandstone with trough and tabular cross-stratification (facies K and J). The grain size in this sandstone changes from medium to very fine upwards. It is 6.5 m thick and has a laterally restricted geometry. The upper part of the interval is recorded from a very flat and scree covered terrain with very few outcrops. However, red and green mudstones (facies N) are found after digging into the scree. The uppermost outcrop found at Ryssen is a 1.5 m thick laterally restricted very fine sandstone with trough cross-stratification (facies K).

Interpretation: The interval is interpreted to represent deposition in a marginal marine to delta plain environment. Intense bioturbation and mud-drapes in the lower siltstone unit may indicate a marine low energy environment with a potential tidal influence (e.g. De Raaf and Boersma, 2007). Mudstone intervals are interpreted as interdistributary deposits. The upwards fining and cross-stratified sandstone with mud drapes may be interpreted as a distributary channel with tidal influence (Reading and Collinson, 1996). The uppermost cross-stratified sandstone is interpreted as a small channel deposit as well. The laterally restricted geometry of the sandstones is typical for channel deposits (Collinson, 1996; Lord et al., 2014b). The red and green mudstones in the upper that part indicate that the deposits belong to the Isfjorden Member (Mørk et al., 1999a; Haugen, 2016).

5.4 Milne Edwardsfjellet

Milne Edwardsfjellet (Figure 5.12) is a 598 m high mountain situated in the north-western corner of Fulmardalen (Figure 5.1). The slopes facing Fulmardalen are relatively steep and hold good exposures of the Botneheia, Tschermakfjellet and the De Geerdalen formations. Due to a very steep gradient on the mountain slope, the transition from the Tschermakfjellet Formation to the De Geerdalen Formation is relatively well exposed at Milne Edwardsfjellet.

The log recorded from Milne Edwardsfjellet (Mil 16-1; Figure 5.13) is 230 m long, and the log trace follows a narrow ridge at the easternmost side of the mountain (Figure 5.12). It covers the uppermost 10 m of the Botneheia Formation, the entire Tschermakfjellet Formation (24 m) and 196 m of the De Geerdalen Formation. The log ends at the summit of the mountain, somewhere in the uppermost part of the De Geerdalen Formation.

The De Geerdalen Formation on Milne Edwardsfjellet can be described as several upwards coarsening sequences, with shales coarsening up to fine and medium grained sandstones. Each of the sandstone bodies are capped by shales, marking the onset of a new coarsening upward sequence. Geometrically, the sandstone bodies are laterally continuous and relatively thin. The thickest sandstone intervals are found in the lower part of the formation.

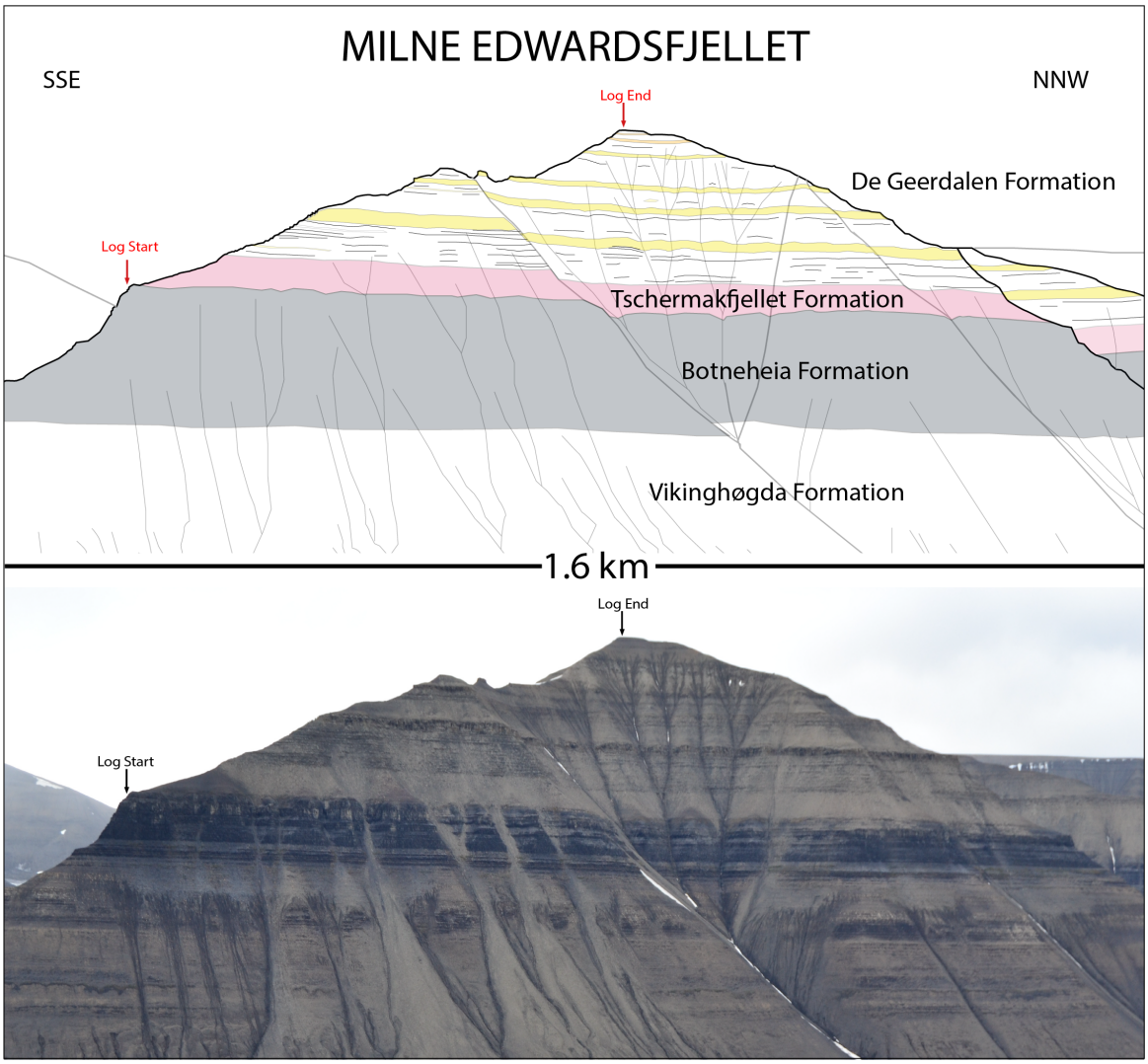

Figure 5.12 *Geological sketch and corresponding overview photo of Milne Edwardsfjellet. Formation names and stratigraphic boundaries have been indicated. Yellow areas within the De Geerdalen Formation mark major sandstone intervals. The log trace follows the ridge between the Log Start and Log End arrows.*

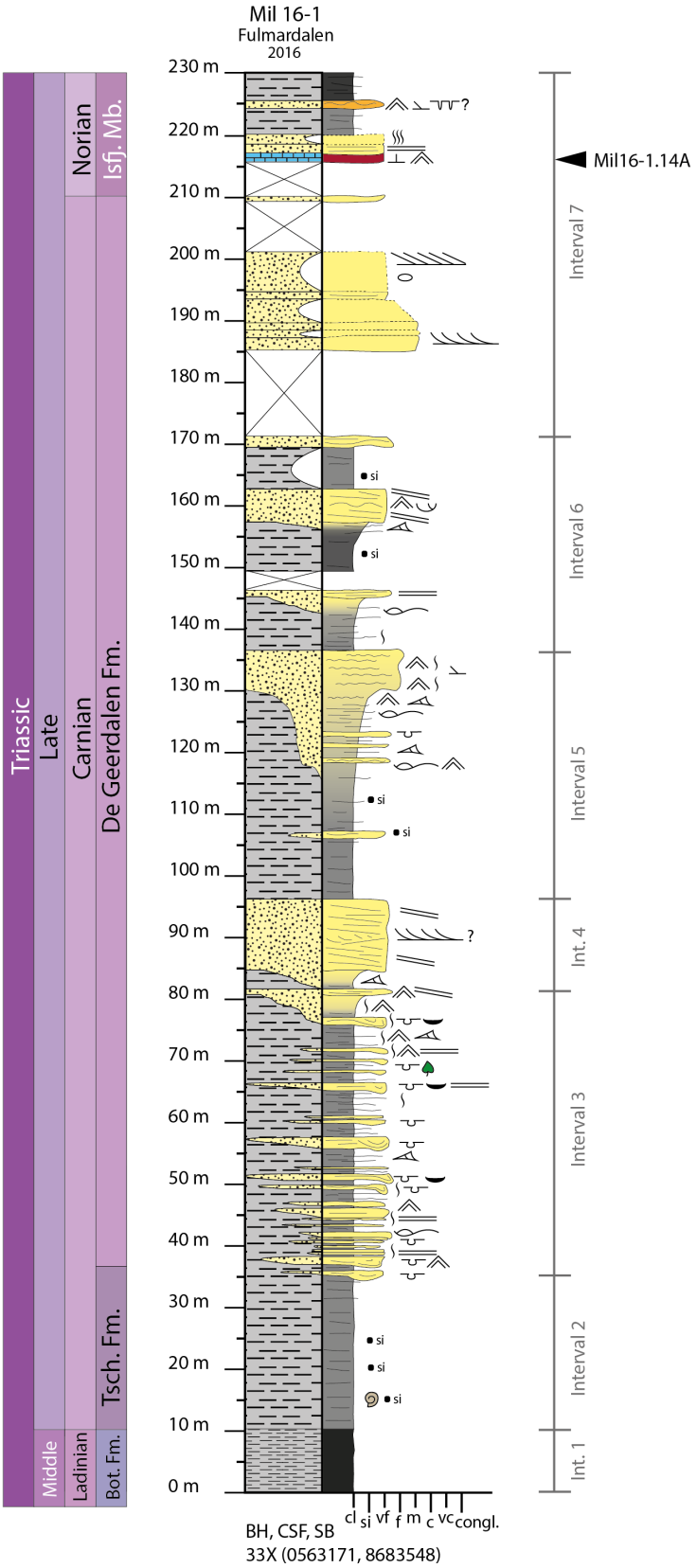

Figure 5.13 *Log from the measured section at Milne Edwardsfjellet. Depositional age has been interpreted following Mørk et al. (1999a). Interval sub-division and position of sample Mil16-1.14A are indicated.*

Log Mil 16-1

Interval 1 (0 – 10m)

Description: Interval 1 consists of 10 m dark grey to black coloured, finely laminated paper shale. The colour of the shale is distinctly darker than the shale in the overlying intervals.

Interpretation: The dark coloured paper shale belongs to the Blanknuten Member of the Botneheia Formation. This formation reflects a deltaic influenced, regressive shelf deposit with restricted water circulation conditions (Mørk et al., 1982, 1989, 1999a).

Interval 2 (10 – 34m)

Description: This interval consists of grey shales (facies A) with siderite nodules and some thin (<10 cm thick) siltstone beds. The nodules weather with a distinct purple and red colour, making it possible to trace the formation laterally. Ammonoid fossil imprints are present in the siderite nodules.

Interpretation: The grey shales with siderite nodules overlying the dark paper shales belong to the Tschermakfjellet Formation. The formation represents a shale-dominated, prodelta depositional environment (Mørk et al., 1999a). The observed imprints of ammonoid fossils support a marine origin for the interval.

Interval 3 (34 – 81m)

Description: The grey shale of the Tschermakfjellet Formation is followed by a 47 m thick heterolithic succession of alternating very fine sandstones and shales (facies B). The sandstones are characterized by soft sediment deformation structures (facies D), hummocky cross-stratification (facies C) and wave ripples (facies E). Bed thicknesses vary from 0.2-1.5 m. The deformed sandstones often hold plant fragments and mud flakes. Sparse bioturbation and wave ripples are typically found towards the top of the sandstone beds. The intensity of the bioturbation is generally sparse through the whole interval. The sandstone bodies are laterally restricted, ranging from two to several tens of metres in width.

Interpretation: The base of the interval is interpreted to represent the base of the De Geerdalen Formation at Milne Edwardsfjellet. The interval is interpreted to record deposition in an offshore transition and lower shoreface setting. Sandstones with erosive bases and soft sediment deformation structures are interpreted as deposits from gravitational processes such as slumping

and sliding at the delta front and prodelta (Mills, 1983; Reading and Collinson, 1996). The relatively short lateral geometry of the sandstone bodies may originate from slumps and slides that moved downward into a muddier substrate. Plant fragments incorporated within deformed sandstones are interpreted to have been transported and deposited by mass movement processes. Hummocky cross-stratified and laminated sand- and siltstones with wave ripples and sparse bioturbation on top are interpreted to be storm-generated beds, while mudstone intervals have been deposited from suspension under fair weather conditions.

The fact that the De Geerdalen Formation at Milne Edwardsfjellet has much more sandstone bodies in the lower part with deformational structures compared to the other localities in Fulmardalen, could indicate that this locality was located in a more proximal position to a distributary channel outlet. As a result the area may have experienced high sedimentation rates at the delta front, resulting in mass movements and soft sediment failures on the prodelta slope (Reading and Collinson, 1996).

Interval 4 (81 – 96m)

Description: The heterolithic section from the underlying interval is gradually replaced by a 12 m thick very fine sandstone dominated by low angle cross-stratification (facies I) and trough cross-stratification (facies K) (Figure 5.14). The sandstone shows a weak coarsening upwards trend and is the thickest sandstone body observed at Milne Edwardsfjellet. Due to the very steep nature of this sandstone outcrop, it was not possible to carry out any detailed investigations of the middle and upper part of the unit. The sandstone body is laterally continuous and can be traced along the whole mountainside and over to the neighbouring mountains.

Interpretation: The sandstone is interpreted to belong to the same barrier bar complex identified in the lower part of the measured sections at the other mountains in Fulmardalen.

Interval 5 (96 – 136m)

Description: Interval 5 can be considered as an new upwards coarsening sequence, and is shown in Figure 5.14. The lower part is dominated by mudstone (facies A) and heterolithic bedding (facies B) with very fine sandstone beds ranging from 5-50 cm in thickness. Hummocky cross-stratification (facies C), wave ripples (facies E) and deformation structures (facies D) are observed within the sandstones. The upper part consists of a 6 m thick intensely wave rippled sandstone (facies E) with sparse bioturbation.

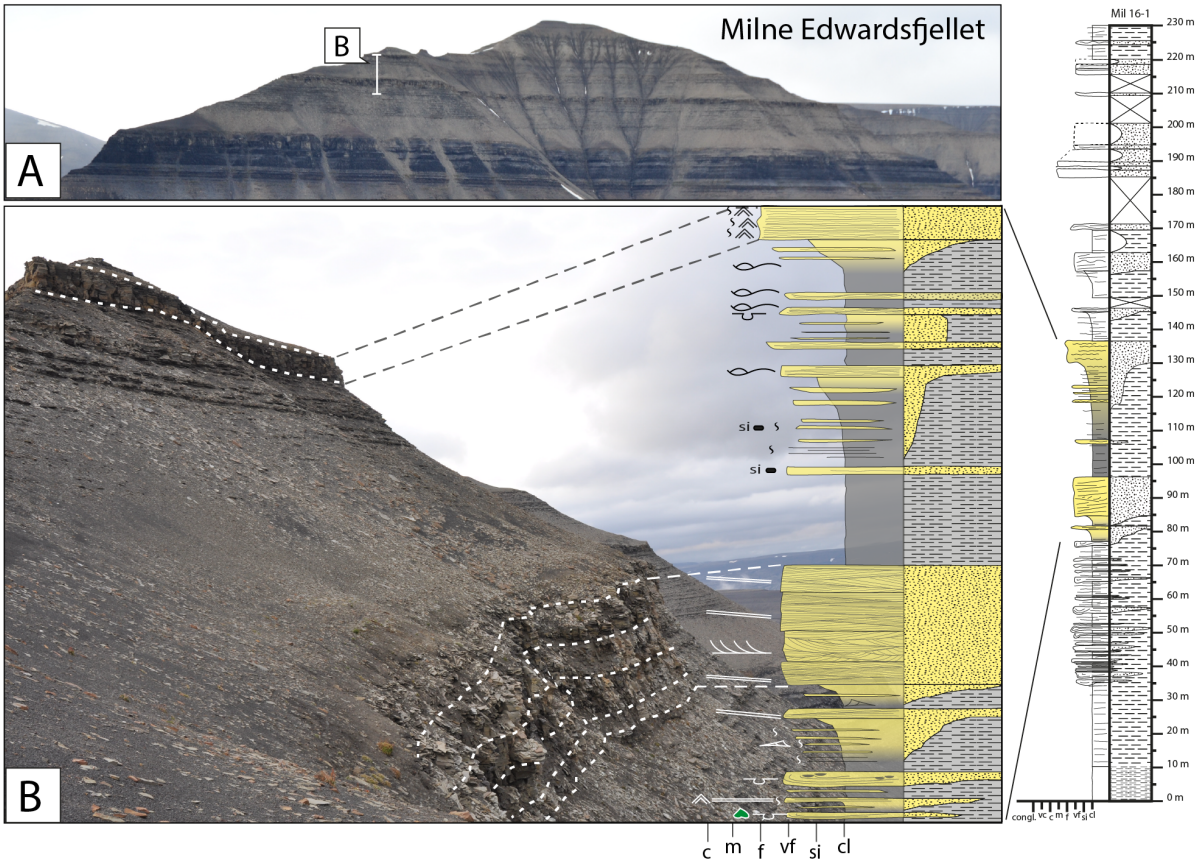

Figure 5.14 *Log and picture correlation from Milne Edwardsfjellet.* ***(A)*** *Image of the mountain indicating the location of figure B.* ***(B)*** *A lower sand-dominated section interpreted as a barrier bar complex, followed by an upwards coarsening unit. The uppermost sandstone has been interpreted as a shallow marine subaqueous bank.*

Interpretation: The boundary to the underlying interval is interpreted as a flooding surface and a shift back to a lower shoreface to offshore setting, where mud is deposited during calm periods and sand during episodic storm events. The wave rippled sandstone towards the top indicates a change to a higher energy environment with time, where wave processes have reworked and redistributed the sediments. It possibly reflects a proximal delta front deposit, such as a shallow subaqueous bank (e.g. Knarud, 1980). Stacked upwards coarsening sequences with relatively low bioturbation rates, like the sequences observed especially in the lower half of the De Geerdalen Formation in Fulmardalen, are typically formed in delta front settings (Hori et al., 2002).

Interval 6 (135 – 171m)

Description: Interval 6 consists of minor upwards coarsening units, with mudstones (facies A) in the lower part and very fine sandstones in the upper part. There are siltstone beds displaying

hummocks (facies C), whereas the sandstones are characterized by planar stratification (facies H), low angle cross-stratification (facies I) and wave ripples (facies E). Mud draped foresets are observed in addition to short intervals of flaser- and wavy bedding within the larger sandstone unit in the top.

Interpretation: Interval 6 is interpreted to represent deposition from small migrating bars with a stronger tidal influence on the deposits compared to the underlying interval. Mud drapes, flaser- and wavy bedding are typical in tidal environments. In such settings, mud is deposited in slack-water conditions, while sand is deposited by currents created by tidal and wave energy. Alternatively, such deposits are also known to form in marine delta front environments where sediment supply and current velocities may fluctuate (Boggs, 2011).

Interval 7 (171 – 230m)

Description: The next interval consists of large sections that are totally scree-covered. Within the scree cover, there is an upwards fining sandstone unit that partly consists of unconsolidated sand. The grain size changes from medium to very fine sand upwards. The intact parts of the sandstone show large-scale trough cross-stratification (facies K) and tabular cross-stratification (facies J). Large, grey and sandy concretions are observed within the sandstone.

The part of the interval above the scree cover consists of a sequence of deposits that can be recognized at Dyrhø, Ryssen and Storfjellet. It starts with a 2 m thick lateral continuous layer, consisting of carbonate in the lower part and a planar laminated sandstone in the upper part (facies H). The bed is topped by 2 m of an intensely bioturbated sandstone. The sandstone is capped by 4 m of grey shale (facies A), followed by a 1 m thick, laterally extensive and rusty-red carbonate rich sandstone (facies G) with wave ripples and potential desiccation cracks. The final 4 m consist of very dark shale (facies A).

Interpretation: The large scree-covered sections are thought to be mud-dominated, reflecting deposition in a low-energy environment, potentially in an interdistributary area. Poorly exposed large scale trough cross bedded sandstones in the upper reaches of the interval may represent deposition in a distributary channel. Relatively thin sandstones and carbonate cemented beds alternating with muddy intervals are interpreted to represent deposition in a paralic environment from shallow marine to lower delta plain, possibly in a lagoonal setting. Desiccation cracks in one of the sandbodies indicates periods of sub-aerial exposure, while intense bioturbation in

another sandstone unit may reflect upon marine influence. A very distinct, dark colour of the uppermost shale sequence may be a result of a high organic content, suggesting a low-energy, potentially lagoonal, depositional environment, where organic material could accumulate. Carbonate beds and thin sand and siltstones are characteristic for the Isfjorden Member (Mørk et al., 1999a). The section is therefore interpreted to display a part of the Isfjorden Member, despite lacking the most characteristic red and green mudstones.

5.5 Storfjellet

Storfjellet (Figure 5.15) is a mountain located in the southeastern part of Fulmardalen with Ryssen bordering to the north (see Figure 5.1). The glacier, Veitbreen flows across the plateau shaped top, separating Storfjellet from the mountain ridge Prospektryggen to the east. The highest point is 556 masl and is located at the northern margin of the plateau. The slopes facing W-NW into Fulmardalen are relatively steep and hold good exposures of the De Geerdalen Formation.

The logged section at Storfjellet (Stor 16-1; Figure 5.16) is 245 m long and recorded from the W-NW facing slope at the northern part of the mountain. The log starts in Tschermackfjellet Formation and continues into the De Geerdalen Formation. The Isfjorden Member is found in the upper part.

Knarud (1980) also presents a log from Storfjellet (see Appendix C), which were recorded relatively close to the section presented herein (Atle Mørk, pers. comm., 2017).

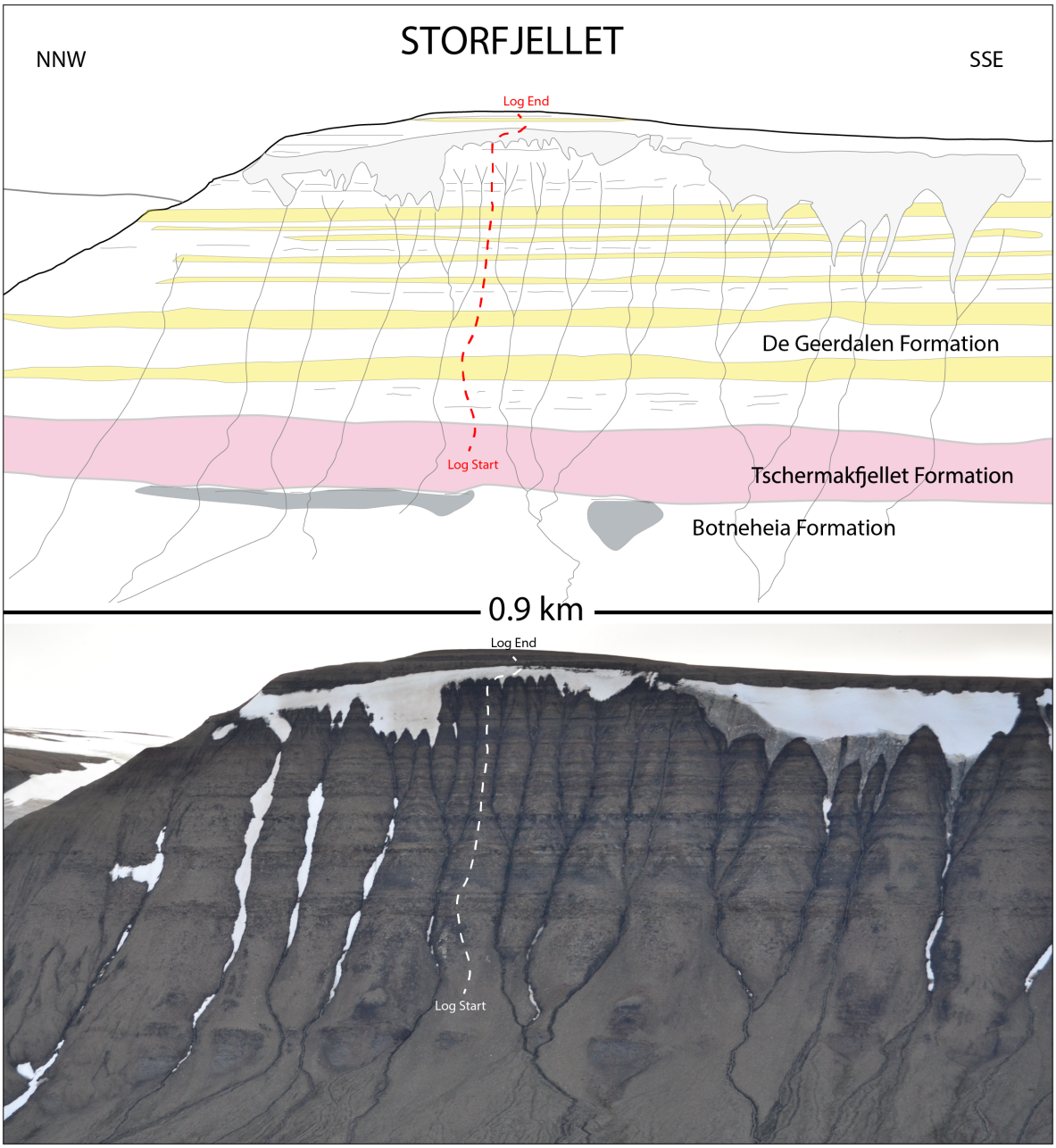

Figure 5.15 *Geological sketch and corresponding overview photo of Storfjellet. Formation names and stratigraphic boundaries have been indicated. Yellow areas within the De Geerdalen Formation mark major sandstone intervals. Log trace is indicated with a dashed line.*

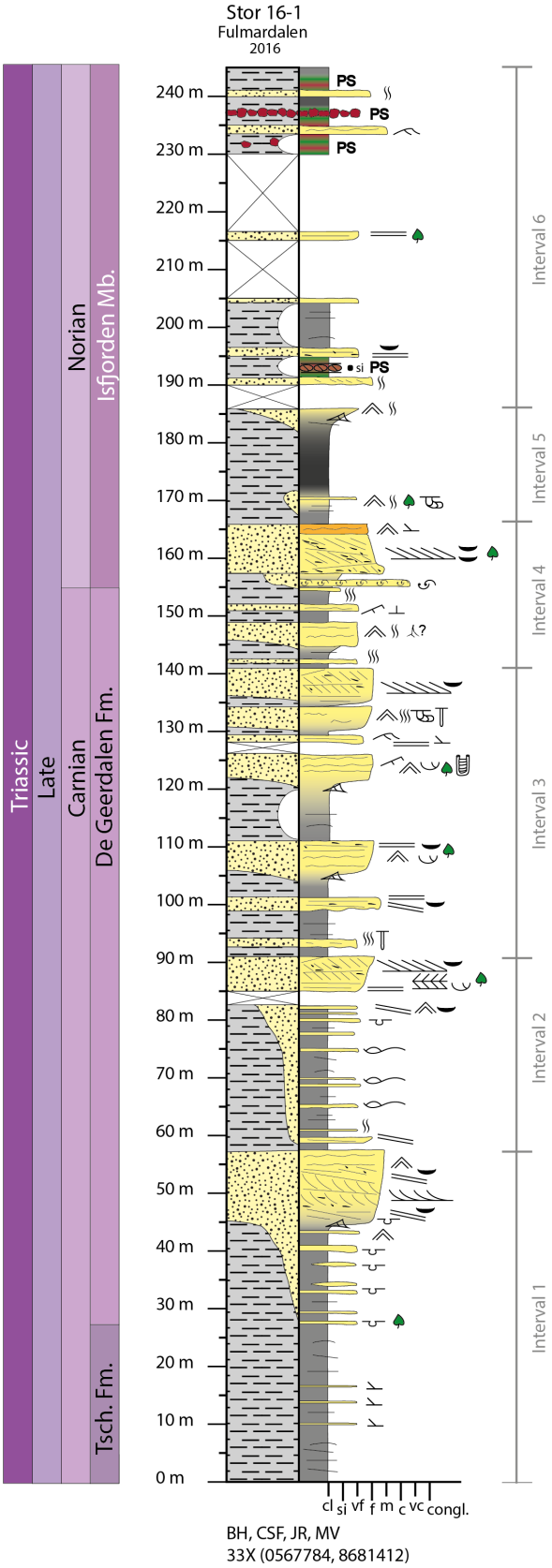

Figure 5.16 *Log from the measured section at Storfjellet. Depostional age has been interpreted following Mørk et al. (1999a). Interval sub-division are indicated.*

Log Stor 16-1

Interval 1 (0 – 56m)

Description: The interval is an upwards coarsening unit. The lowermost 28 m of Stor 16-1 consist of grey shales (facies A) with centimetre scale thick siltstone beds and 0.2-0.5 m thick very fine siderite cemented sandstone units. Above there is a 17 m thick heterolithic succession (facies B) with 0.5-1 m thick very fine sandstone units that become thicker in the upper part. The sandstones show soft sediment deformation structures (facies D) and are laterally restricted, varying from one m to several tens of m in width. Plant fragments are evident within these sandstones. Above the heterolithic package there is an 11 m thick, laterally continuous sandstone unit coarsening upwards from very fine to medium grained sand. Its base is gradual. Soft sediment deformation structures (facies D) are observed close to the base. The unit is mainly low angle cross-stratified (facies I), but large scale trough cross-stratification (facies K) is also observed with bed thicknesses of 10 cm. Mud flakes are observed throughout the whole sandstone unit, often at the interface between beds. Wave ripples (facies E) are only found in the upper part.

Interpretation: The lowermost part of the interval hosts the characteristics of the Tschermakfjellet Formation, representing a marine pro-delta environment (Mørk et al., 1999a). The base of the De Geerdalen Formation at Storfjellet is interpreted to be at the base of the heterolithic succession. The laterally restricted sandstones with soft sediment deformation structures are interpreted to be generated from gravitational processes in an offshore transition to lower shoreface setting (e.g. Hori et al., 2002; Oliveira et al., 2011). The overlying sandstone is interpreted to represent a barrier bar deposit, possibly cut by a tidal channel in a delta front to upper shoreface setting, similar to what has been observed at the other mountains in Fulmardalen. Knarud (1980) interpreted this interval at Storfjellet as a shallow marine bank deposit, with the most important processes being controlled by marine currents, wind and storm activity and by fluctuating clastic input from land.

Interval 2 (56 – 91m)

Description: This interval is also an upward coarsening unit. The lowermost 25 m comprise a heterolithic package (facies B) of alternating grey shale and siltstone (facies A) and 0.2-0.5 m thick hummocky cross-stratified (facies C) very fine sandstone units. One of the sandstones show soft sediment deformation structures (facies D). The uppermost 10 m of the interval are

mainly an upward coarsening sandstone unit, but the bottom part is scree covered. The grain size changes from very fine to fine sand upwards. The lower part of the sandstone is planar parallel stratified (facies H) with mud flakes, mud drapes and plant fragments occurring at the interface between beds, whereas the upper part is large scale tabular cross-stratified (facies J). Successive sets are occasionally bidirectional. Mud flakes are observed throughout the whole unit.

Interpretation: The contact to the underlying interval is interpreted to represent a flooding surface with marine shales, silt and sand being deposited under pulsating energy conditions in the offshore transition zone to lower shoreface (Knarud, 1980). Deformation structures in sandstones are likely due to rapid deposition of sand on a muddy substrate, as described in Section 4.2. The thick sandstone dominated unit at the top of the interval is interpreted to reflect shallow marine delta front to upper shoreface deposits. The planar stratification overlain by bidirectional cross-stratification could reflect a barrier bar cut by a tidal channel where both ebb and flow tide deposits are preserved (Boggs, 2011). Knarud (1980) interprets similar outcrops at Dalsnuten in central Spistbergen (see Figure 7.1) as point-bar deposits from a migrating tidal channel.

Interval 3 (91 – 141m)

Description: The interval consists of multiple stacked upward coarsening sequences, where shales and siltstones are gradually replaced by sandstones (Figure 5.17). The larger sandstones display a variation between wave ripples (facies D), low angle cross-stratification (facies I), plane parallel stratification (facies H) and tabular cross-stratification (facies J). The thinner sandstones display asymmetrical ripples (facies F), planar stratification (facies H), low angle cross-stratification and are locally intensely bioturbated. The trace fossils *Diplocraterion, Skolithos* and *Rhizocorallium* occur in distinct sandstone units. Mud flakes, plant fragments and mud drapes are observed at several levels.

Interpretation: The main characteristic of progradational deltaic sequences is that they shallow and coarsen upwards from muds, through silts to various sand-dominated facies (Reading and Collinson, 1996). The stacked upwards coarsening sequences in this interval are interpreted as progradational subaquous sandbanks terminated by abandonment/flooding surfaces. The extent and nature of such surfaces depend on the process controlling relative sea-level rise. Each surface indicates a subsequent deepening, developing new accommodation space for further

progradation (Reading and Collinson, 1996). The sedimentary structures observed in the sandstones typically occur in shallow marine environments. The trace fossils *Diplocraterion* and *Skolithos* indicate deposition in an upper shoreface, high energy environment, whereas the occurrence of *Rhizocorallium* points towards a medium to low energy marine environment (Boggs, 2011), indicating variable energy conditions during deposition of the sandstones.

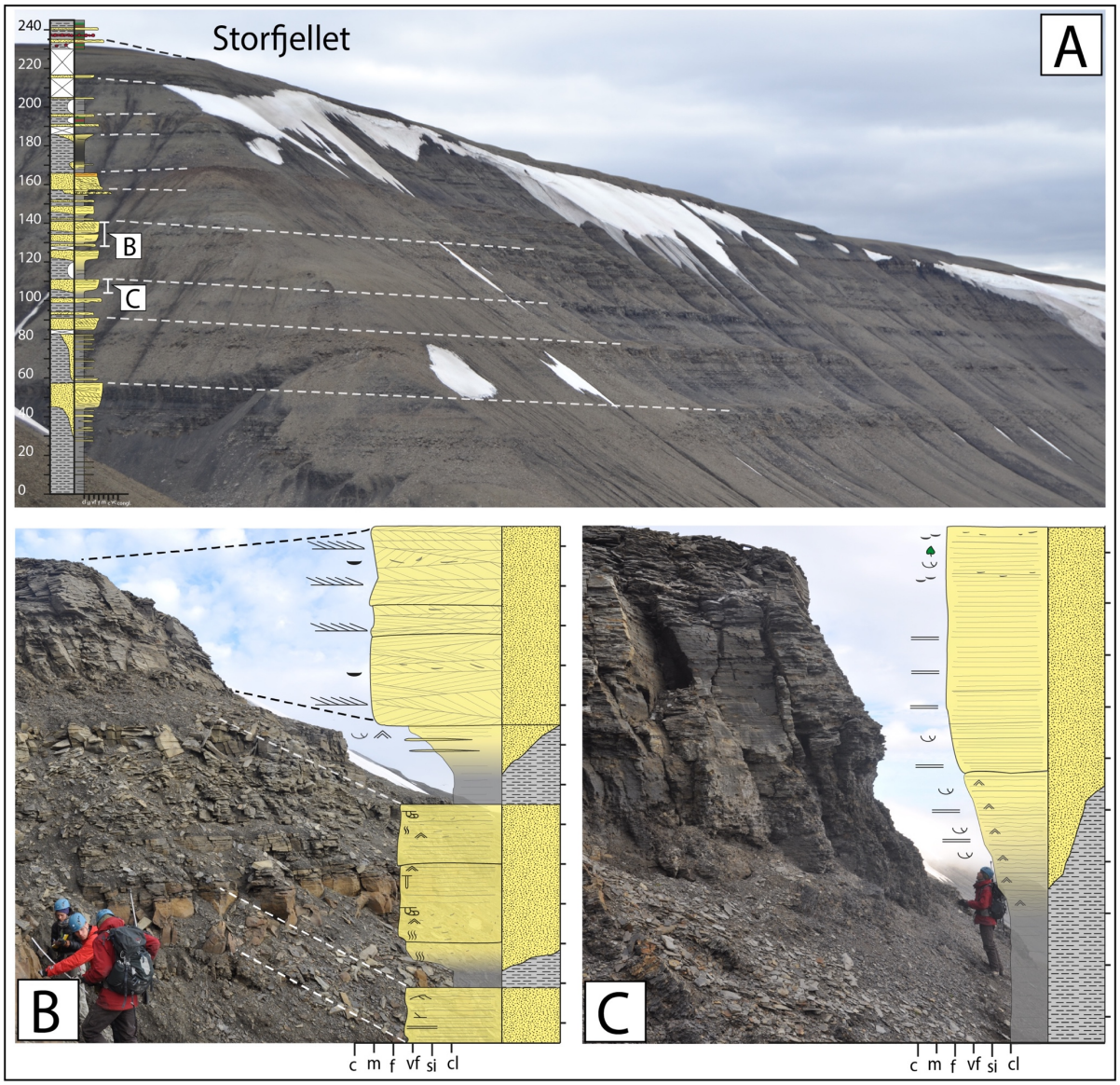

Figure 5.17 *Log and picture correlation from Storfjellet.* ***(A)*** *Storfjellet seen from Ryssen. The top of major sandstone units has been correlated between log and picture with dashed lines.* ***(B)*** *Small scale upwards coarsening units within a sandstone dominated interval.* ***(C)*** *Upwards coarsening sequence interpreted as a shallow marine distal bar, deposited with a combination of marine and deltaic processes.*

Knarud (1980) suggests that the sequences in this interval are distal shallow marine bars, in which the sediment supply is controlled by both deltaic sediment input and marine current processes. Furthermore, mud flakes within sandstones indicate that surrounding semi-consolidated muddy sediment have been ripped up by strong currents and quickly re-deposited together with sand (Spearing, 1976; Knarud, 1980).

Interval 4 (141 – 166.5m)

Description: The interval is initiated by a 15 m thick sequence of alternating sand- and mudstone units. The sandstones are very fine grained, intensely bioturbated and show signs of wave ripple lamination (facies E). The sandstones are thinner compared to those in the underlying interval. Potential rootlets are observed in the upper part of one of the sandstones. The upper part of the interval consists of a bioclastic sandstone with shell fragments (facies L) capped by an upwards fining, 8 m thick medium to fine grained sandstone with large scale tabular cross-stratification (facies J) and a high amount of rip-up mud clasts and flakes. Plant fragments are found within the sandstone and the top is intensely bioturbated. A 1.5 m thick rusty-red, heavily cemented, carbonate rich fine sandstone with signs of ripple lamination (facies G) is overlaying the cross bedded sandstone. The sandstone is sticking out in the terrain, and can be laterally traced to the neighbouring mountains.

Interpretation: The lower part of the interval displays features indicative of a calm and low-energy environment, interpreted as deposits in a protected shallow marine, potentially lagoonal, setting. Relatively thin and intensely bioturbated sandstones surrounded by mudstone, in addition to the presence of bioclastic sandstones, are common in such depositional settings (Reineck and Singh, 1980; Reinson, 1984; Boggs, 2011). Structures like ripples and undulating stratification in the sandstones may suggest periodical influence of higher energy processes. Root structures indicate sub-aerial exposure. However, the structures could also resemble vertical trace fossils belonging to the *Skolithos* ichnofacies, and Knarud (1980) describes *Skolithos* in a sandstone at similar stratigraphic levels at Storfjellet. The cross bedded sandstone in the upper part of the interval is interpreted to represent a distributary or tidal channel. The carbonate rich sandstone at the very top is interpreted to have been deposited in shallow marine waters during a period of low clastic input where carbonate producing microorganisms could thrive (Knarud, 1980).

Interval 5 (166.5 – 186m)

Description: The interval consists of 14 m of dark grey shale (facies A) that gradually coarsens upwards into a 2 m thick siltstone to very fine sandstone unit. The shale has a characteristic dark colour that are also recognized at neighbouring mountains. The silt- to sandstone is moderately bioturbated and discontinuous wave ripple lamination (facies E) is observed. A thin sandstone layer with wave ripples (facies E), moderate bioturbation, plant fragment and the trace fossil *Rhizocorallium* is found in the lower part of the interval.

Interpretation: The interval reflects a low energy depositional environment with dominance of fine grained material settling from suspension. *Rhizocorallium* indicate a marine medium to low energy environment, and typically occurs in lagoonal and shelf settings (Boggs, 2011). The very dark shale is interpreted as organic rich shale deposited in a lagoon or interdistributary area where water circulation was restricted. The upward coarsening sandstone is interpreted as a possible wash-over fan deposit into a lagoon, being reworked by organisms during calm periods.

Interval 6 (186 – 245m)

Description: The uppermost interval at Storfjellet is characterized by thin 0.5-1 m thick very fine to fine sandstones interbedded in scree or partly covered mudstones that have grey, green and red colours (facies N). Sedimentary structures observed in the sandstones are plane parallel stratification (facies H) and asymmetrical ripples (facies F) in addition to bioturbation. Plant fragments are also present. A layer of large round siderite concretions (10-30 cm in diameter) is found within red and green mudstones. A weathered carbonate rich horizon with red and green nodules that are 2-15 cm in diameter is found in the upper part. The nodules have an irregular shape.

Interpretation: The interval is thought to reflect a marginal marine, possibly lagoonal, low-energy environment belonging to the Isfjorden Member (Mørk et al., 1999a). The thin sandstones may represent small subaqueous banks or wash-over deposits. The nodule horizon is interpreted to be weathered carbonate soil (calcrete) with calcified nodules that may have formed around roots. Such nodules are commonly found in red-bed successions and especially in flood-plain deposits (Tucker, 2011). Haugen (2016) describes similar calcareous nodules in the Isfjorden Member, appearing as individual nodules within red and green mudstones, but

also within calcretes at localities from Agardhdalen in eastern Svalbard and from Deltaneset in central Spitsbergen. Red and green mudstones are interpreted as paleosols, where the colour-alternation may result from fluctuations in the groundwater table causing shifts in the redox regime (Haugen, 2016; Lord et al., 2017a). Paleosols have a high interpretative value as they indicate sub-aerial exposure (Kraus, 1999). Paleosols have been described from a variety of continental depositional settings (Kraus, 1999), and have also been found in marginal marine environments where sea level fall has left marine strata sub-aerially exposed (Lander et al., 1991; Webb, 1994; Wright, 1994).

5.6 Raggfjellet

Raggfjellet (Figure 5.18) is a mountain located in the southernmost part of Fulmardalen with Hellefonna located to the east and its tributary glaciers, Marmorbreen and Skruisbreen situated to the north and to the south, respectively (see Figure 5.1). Raggfjellet has a plateau shaped top, similar to many of the other mountains in the area, with the highest point at 571 masl.

The logged section at Raggfjellet (Rag 16-1; Figure 5.19) is only 21 m long and is recorded in the uppermost part of the slope facing north towards Marmorbreen. The lower part of the slope is extensively scree covered and was therefore not measured. The upper part holds exposures of the Isfjorden Member.

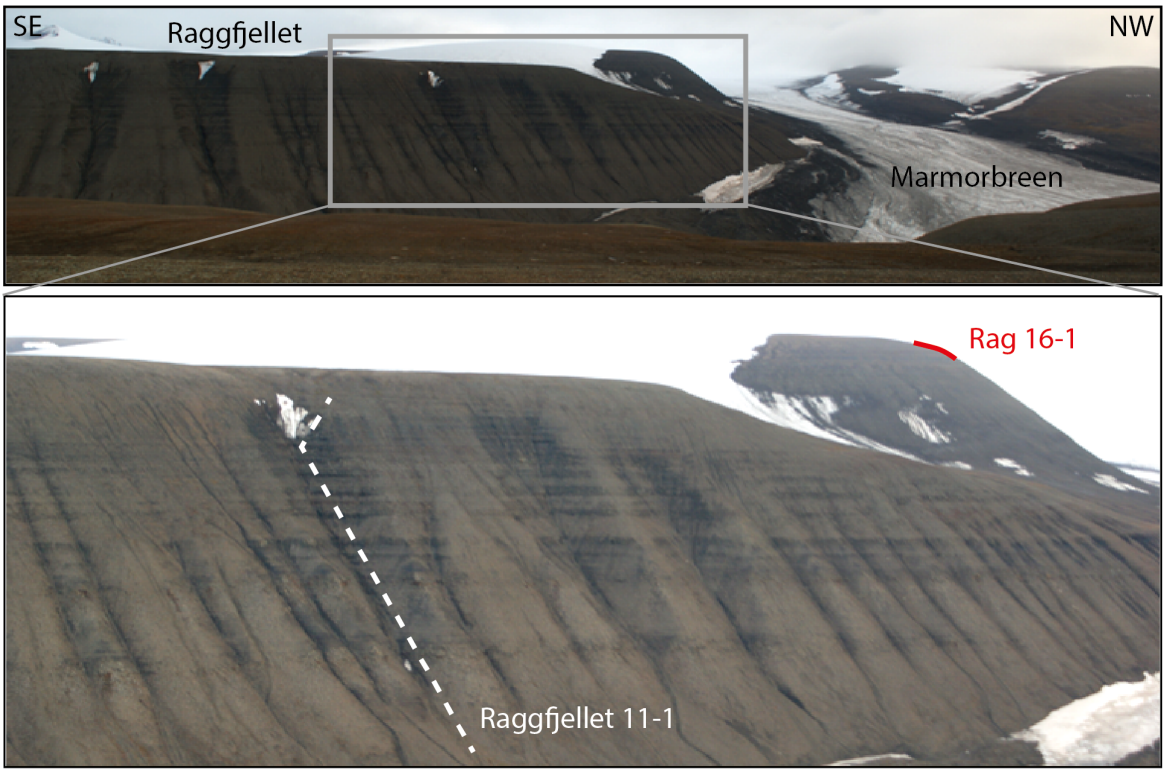

Figure 5.18 *Photo of Raggfjellet seen from Storfjellet. The location of the logs Rag 16-1 and Raggfjellet 11-1 is indicated. Note the stratigraphically higher position of Rag 16-1. Photo: Gareth S. Lord.*

A sedimentological log from Raggfjellet (Raggfjellet 11-1) is presented in Klausen et al. (2015) and Lord et al. (2017a). However, Raggfjellet 11-1 was recorded in the NE-facing slope of the mountain and is measured stratigraphically lower than Rag 16-1 (Figure 5.18). The logs will be further discussed in Section 7.3.

Log Rag 16-1

Description: The lower part of the log is characterized by red and green mudstones (facies N) interrupted by 0.5-1 m thick wave rippled (facies E) and bioturbated very fine sandstones. Irregular shaped and mottled nodules are found within the red mudstones in addition to a distinct carbonate layer containing similar nodules. The upper part of the log consists of grey shales (facies A) interrupted by a 60 cm thick very fine sandstone.

Interpretation: The red and green mudstones with nodules are interpreted as being paleosols belonging to the Isfjorden Member, and are interpreted to have been deposited under similar conditions to the succession in the upper part of Storfjellet. The nodular layer has been interpreted as calcrete with calcified nodules forming around roots.

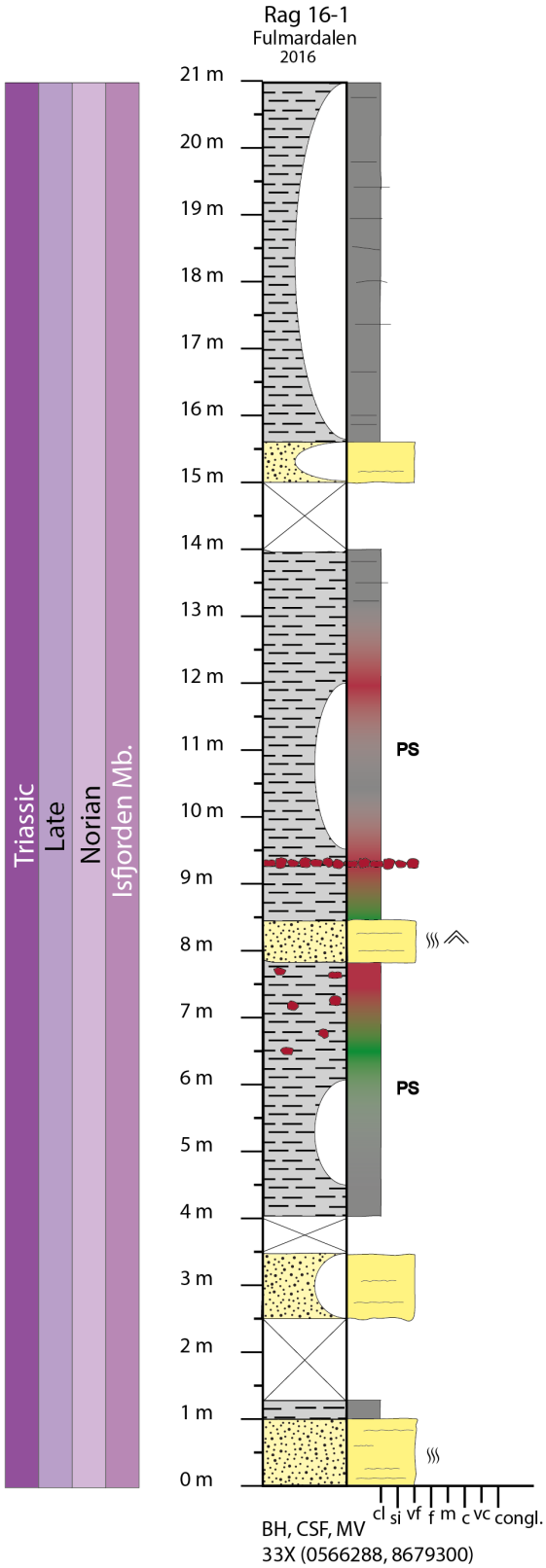

Figure 5.19 *Log from the measured section at Raggfjellet. Depositional age has been interpreted following Mørk et al. (1999a). It should be noted that the scale is different from on the other logs. Only the upper 21 m of Raggfjellet have been recorded.*

6 Laboratory results from Fulmardalen

6.1 Optical microscopy - calcrete

In order to investigate potential calcrete units from Fulmardalen, two petrographic thin sections were made from two separate carbonate units from within the Isfjorden Member. One of the samples was collected from Milne Edwardsfjellet (Mil16-1.14A; Figure 5.13), while another was collected from Ryssen (Rys16-1.23A; Figure 5.10). Thin section analyses of calcrete units from the Isfjorden Member have also been presented in Haugen (2016). Typical microfeatures from calcretes have been described by Alonso-Zarza and Wright (2010), where the features are sub-divided into alpha- and beta microfabrics.

Alpha-microfabrics are non-biogenetic features that form in supersaturated soil solution (Haugen, 2016), and is typically expressed as a groundmass of crystalline carbonate. The fabrics are thought to form as a result of carbonate replacement, recrystallization and precipitation of carbonate in pores (Alonso-Zarza and Wright, 2010; Haugen, 2016). Beta-microfabrics are mainly formed by biogenetic processes (Alonso-Zarza and Wright, 2010).

Thin section analyses of the samples from Fulmardalen (Figure 6.1) indicate the presence of both alpha- and beta-microfabrics. All samples show a groundmass of micrite which is interpreted to be a result of the aforementioned processes forming alpha-microfabrics. Additional beta-fabrics are thought to be present, but are less abundant. Potential alveolar structures have been interpreted in the sample from Milne Edwardsfjellet (Figure 6.1C). Such structures are mainly a product of fungal activity related to roots (Haugen, 2016). Other structures observed that may have formed by biogenic processes are coated grains. These structures, as seen in the samples from Fulmardalen, are interpreted to have formed as a result of precipitation of micrite around an organic substrate (like a root) that was later oxidized, leaving a void where sparitic calcite could grow (Figure 6.1D, E, F).

Müller et al. (2004) studied pedogenetic (soil forming) mud aggregates from dryland river systems in the North Sea. The study distinguishes between in-situ mud aggregates formed by soil processes in paleosols and aggregates that were reworked on the floodplain. Reworked beds of floodplain mud-rocks often loose internal aggregate texture and a massive and structureless appearance, and a heterogeneous appearance in thin section. *In-situ* formed beds, on the other hand, are characterized by mudrock aggregates with the same internal texture, separated by calcite cement (Müller et al., 2004). The calcrete from Ryssen has a relatively homogeneous texture (Figure 6.1D, E, F), which may imply that it is *in-situ*. However, the

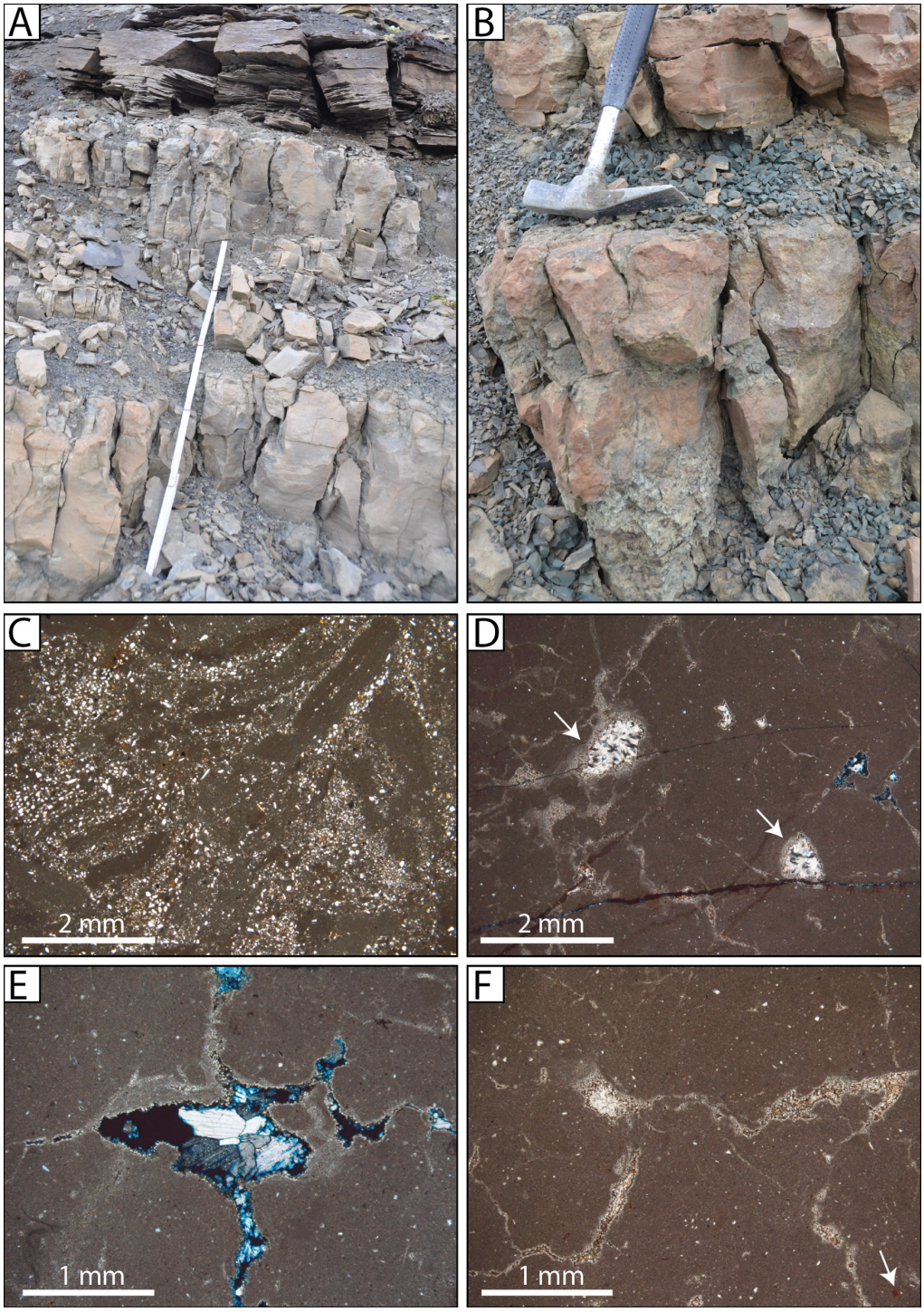

Figure 6.1 *Calcrete from Fulmardalen. Cross-polarized light = XPL. Plan-polarized light = PPL.* ***(A)*** *Calcrete from Milne Edwardsfjellet where sample Mil16-1.14A was taken.* ***(B)*** *Calcrete from Ryssen where sample Rys16-1.23A was taken.* ***(C)*** *Potential alveolar structures in beta-microfabrics in Mil16-1.14A. PPL.* ***(D)*** *A groundmass of micrite (alpha-microfabrics) in Rys16-1.23A. Additional irregular shaped patches of slightly coarser micritic calcite are present. These may have precipitated around an organic substrate that was later oxidized, creating a void that was later filled with sparitic calcite. XPL.* ***(E)*** *Large calcite crystals filling a void in Rys16-1.23A. Note the micritic grain coating. XPL.* ***(F)*** *Micritic groundmass (alpa-microfabrics) and voids filled with sparitic calcite in Rys16-1.23A. Arrow indicates a patch of brown material interpreted as organic remains. PPL.*

sample from Milne Edwardsfjellet (Figure 6.1C), has a more heterogeneous texture, and could represent reworked floodplain deposits rather than alveolar structures.

Observations from thin sections and outcrops from Fulmardalen are similar to those described from previously interpreted calcrete deposits in the De Geerdalen Formation by Haugen (2016). These calcrete observations were restricted to Spitsbergen, with the best developed calcretes found in the west (at Deltaneset, see Figure 7.1). Haugen (2016) suggests that this trend, together with more frequently observed coal seams in the east, point towards lateral semi regional variations in paleomoisture, with more arid conditions prevailing in the west. The calcrete outcrops from Fulmardalen are more poorly developed than those described from Deltaneset, and the present study supports the interpretations of Haugen (2016) of a lateral variation in the conditions controlling calcrete formation. A western uplift, causing better drainage of the soil, has been suggested as a possible explanation to the lateral trend (Haugen, 2016). Alternatively, paleotopography may have caused local variations in precipitation patterns. It could also indicate that calcretes of the Isfjorden Member on Spitsbergen were formed relatively far inland, further away from a more humid coastal climate.

6.2 Rock Eval anlaysis

A relatively distinct dark shale layer can be correlated between Milne Edwardsfjellet, Dyrhø, Ryssen and Storfjellet in Fulmardalen. The shale occurs within a succession that has been interpreted to mainly display delta plain facies in the Isfjorden Member, from which a lacustrine, lagoonal or marginal marine origin would be logical. However, marine flooding surfaces are also found at several levels in the De Geerdalen Formation. A Rock-Eval analysis was performed on two samples from the dark shale, at Ryssen (Rys16-1.28B; Figure 5.10) and Dyrhø (Dyr16-1.19B; Figure 5.6), with the aim of obtaining information about the depositional environment the shale layer represent. The results of the analysis can be found in Appendix D.

The hydrogen index (HI) and oxygen index (OI), which are retrieved from the Rock-Eval analysis, can be used as a measure to describe the quality of the organic matter (kerogen type) in the samples. Kerogen type I typically originates from algal material in lacustrine and lagoonal environments, type II kerogen from marine plankton, while type III is mainly derived from terrestrial woody material (Langford and Blanc-Valleron, 1990). Plotting the OI and HI indexes against each other in a van Krevelen diagram indicates a mixture of type II and III kerogen for the samples from Fulmardalen (Figure 6.2). However, both samples plot in the left corner of the diagram, close to where the van Krevelen curves converge. Moreover, the

positions of the curves are only approximate. The resulting cross plots of the samples should, in other words, be treated with care and not be conclusively assigned to one kerogen type or the other. The organic material in both samples has a very low OI, which is typical for algal derived material. It is possible that the samples reflect algal (kerogen I) material with influence of terrestrial (kerogen III) material, forcing the cross plots towards the kerogen III type in the van Krevelen diagram.

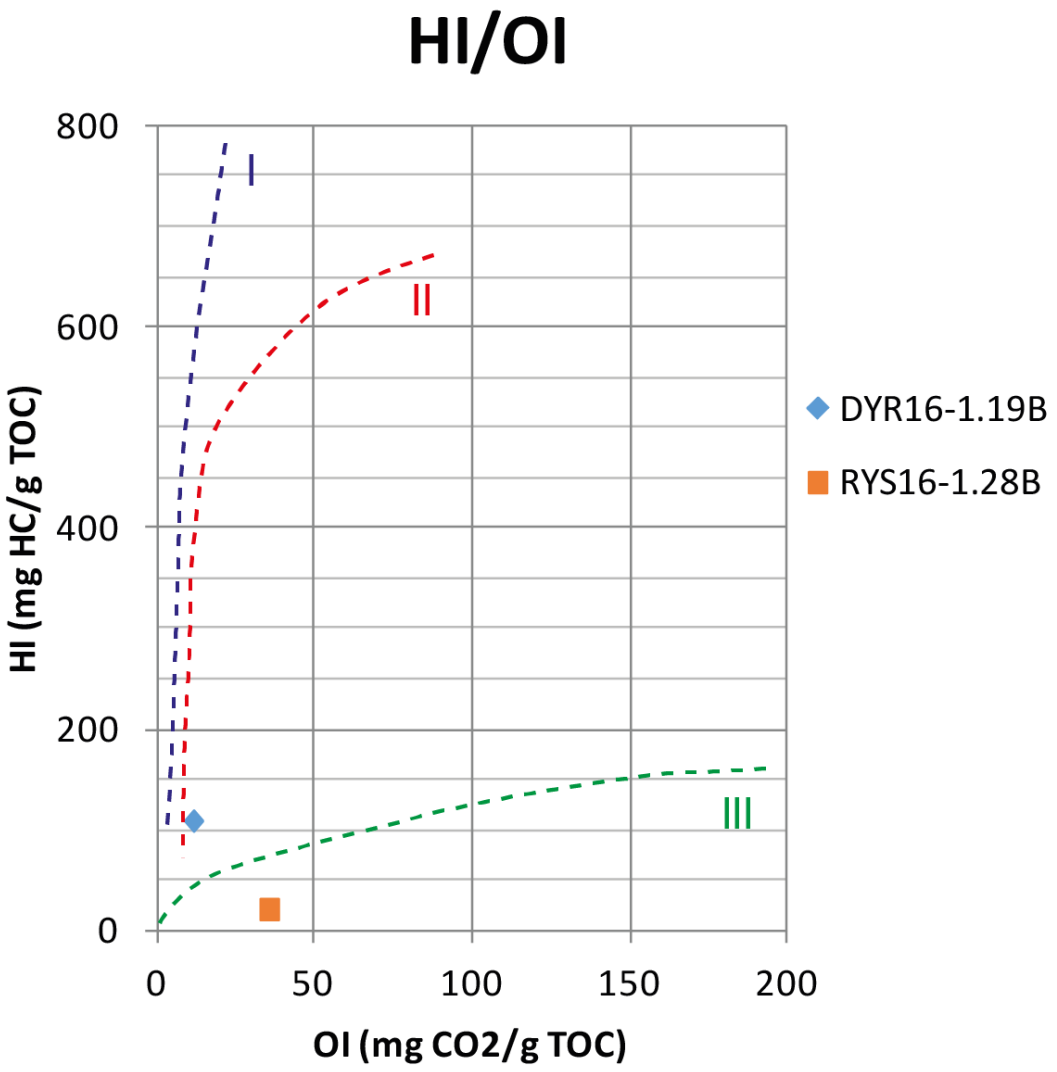

Figure 6.2 *Plot of Oxygen Index (OI) vs Hydrogen Index (HI) for the samples from Fulmardalen. Van Krevelen curves has been added to indicate zones of different kerogen types (I-III)*

7 Discussion – the De Geerdalen Formation in Fulmardalen

The following chapter will present a discussion on the implications of the observations from the De Geerdalen Formation in Fulmardalen. In Section 7.1, a modern understanding of deltaic sequences and the process that control them will be discussed. Section 7.2 discusses the facies distribution in Fulmardalen with the aim of constructing a model for the depositional environment. Section 7.3 extend the discussion to a more regional context, where the findings from Fulmardalen have been attempted to be fit into the established depositional models of the De Geerdalen Formation from other areas on Svalbard.

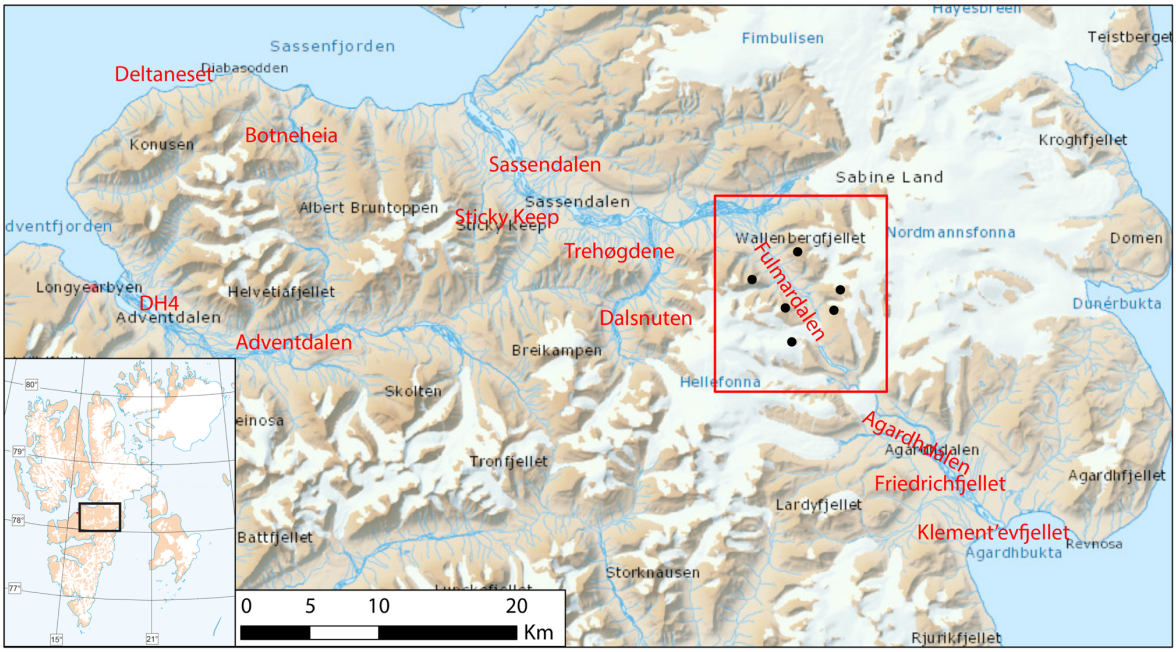

***Figure** 7.1 Map of central and eastern Spitsbergen. Relevant place names for the discussion are marked in red. The red square encloses Fulmardalen (zoomed in on in Figure 5.1). Base map retrieved from Norwegian Polar Institute.*

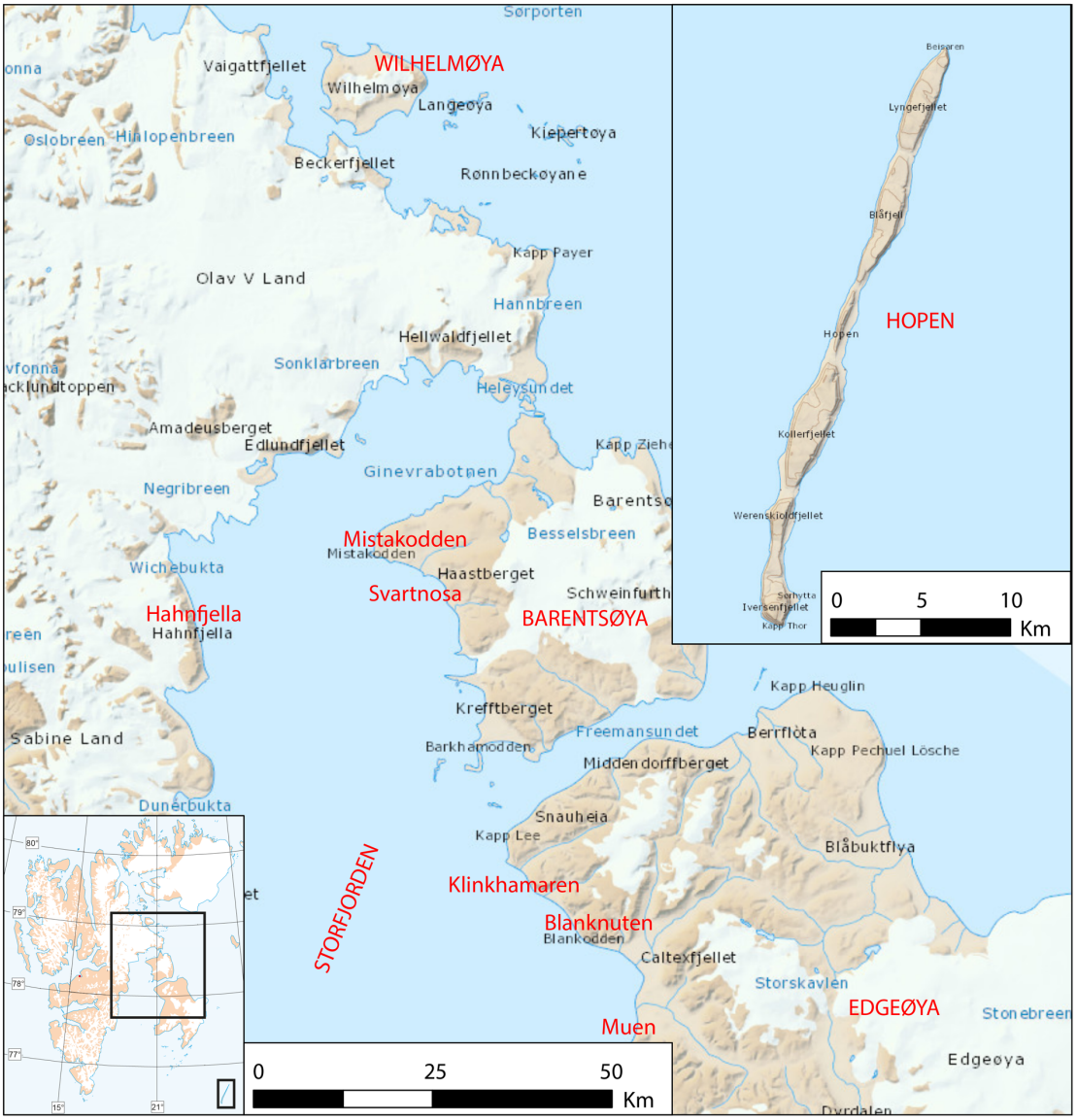

Figure 7.2 *Map of relevant areas on eastern Svalbard. Place names used in the discussion are marked in red. Base map retrieved from Norwegian Polar Institute.*

7.1 Delta classification and deltaic sequences

Deltas are often regarded as the single largest repository of sediment in sedimentary basins (Miall, 2016). Delta protuberances form at shorelines where rivers enter standing bodies of water and supplies sediments at a rate that is too high for the basinal processes, such as waves and tides, to redistribute (Elliott, 1986; Bhattacharya, 2006). In that sense, all deltas may be regarded as river-dominated and regressive in nature (Dalrymple, 1999), but the morphology and facies architecture of a delta is also largely dependent on the proportion of wave, tide and river processes, depth of the sedimentary basin, salinity contrasts between the river water and the basinal water, sediment discharge and sediment grain size (Reading and Collinson, 1996; Bhattacharya, 2006).

Several classification schemes for differentiating between delta-types have been proposed. A tripartite classification scheme, which classifies deltas based on the relative importance of fluvial input, wave modulation and tidal energy, was first introduced by Galloway (1975). This is at present one of the most commonly applied classification scheme. However, it does not come without controversy. Most deltas are influenced by each of the three processes to a varying degree, and while process dominance may be averaged over the entire delta, the dominating processes may vary more locally over short distances (Olariu, 2014). Bhattacharya and Giosan (2003) also point out a general tendency of delta examples being force-fitted into the endmembers of the tripartite process scheme, despite the fact that most deltas experience a mixed influence of all endmember processes.

The De Geerdalen Formation exhibits evidence of both fluvial-, wave- and tidal influence on the deposition. The formation displays a lateral variability in how strongly each of the processes has influenced the deposition, where a fluvial dominance has been interpreted from the eastern islands of Svalbard, opposed to a more wave and tidally influenced deposition on Spitsbergen (Knarud, 1980; Mørk et al., 1982; Rød et al., 2014; Lord et al., 2017a). Rød et al. (2014) suggest that this pattern reflected upon changes in the proximity to the source, differences in accommodation space, varying degree of sedimentation rates, wave- and tide modulation. Bhattacharya and Giosan (2003) point out that significant differences in the dominating deposition processes may occur between different deltaic lobes within the same deltaic system. Portions of large deltas may comprise several elements indicative of different depositional processes being dominant. Such elements can be tidal estuaries, beach-ridge strandplains, wave-formed shorefaces, barrier-islands and lagoons, offshore bars, as well as distributary mouth bars (Reading and Collinson, 1996; Bhattacharya, 2006), all potentially found within the same delta system. The De Geerdalen Formation comprises several of these elements, and represents an example of the difficulty in trying to classify ancient deltas as either fluvial-, wave- or tidally dominated. The problem with such classifications, lies largely with the scale that is under consideration and the objective of the study (Reading and Collinson, 1996; Bhattacharya, 2006).

Orton and Reading (1993) extend the process-based classification scheme by adding the dominant grain size as an important factor as to how deltas develop. Generally speaking, river deltas are characterized by deposition of mud, silt and sand, deposited in low and moderate gradient systems which allow basinal processes to affect the sedimentation (Reading and Collinson, 1996). The geometry of the basins that receive sediments and the proximity to a shelf

edge are controlling factors on the morphology and facies architecture of a delta (Bhattacharya, 2006). The De Geerdalen Formation reflects upon a relatively fine-grained system, with a general grain size variation between clay and medium sand. The formation has been interpreted to represent a distal part of a large deltaic systems that filled a relatively shallow (less than 500 m deep) Barents Sea Basin during the Triassic period (Klausen et al., 2015).

Another issue with delta classification has been the eagerness of finding suitable modern analogues to ancient deltas inferred from sedimentary deltaic sequences. Important controls on the deposition, such as the mean sea-level at the time of deposition, are fundamental to how deltas develop. Such controls change with time, and add controversy to correlations with modern delta examples, that were mainly formed under high eustatic sea level conditions during the Holocene (Clifton, 2006). In other words, large modern delta systems, as for example the Mississippi-Atchafalaya delta, the Ganges-Brahmaputra delta, the Nile delta, the Amazon delta and the Niger delta, prograde into much deeper waters compared to delta systems from the Triassic. The deltaic system that created the deposits of the Snadd and De Geerdalen formations must have represented a very large regressive system, as it filled the entire Barents Sea shelf over a course of approximately 50 million years. Few modern deltas have a similar extent, and representative modern analogues may thus not exist.

Sequences formed due to deltaic progradation, are characterized by an upward coarsening facies succession, with sandy delta front facies building over more fine grained deeper water facies (Bhattacharya, 2006). Repetitive or cyclic successions created as a result of repeated progradation and abandonment of deltaic lobes or of the entire delta, are typical for ancient deltaic deposits (Reading and Collinson, 1996). Facies sequences within deltaic deposits may occur on different scales. Large allocyclic sequences represent the development of the entire delta, and may be caused by tectonics, climatic changes, major river avulsions upstream, and eustatic sea-level changes (Reading and Collinson, 1996). Medium-scale sequences are mainly a result of delta lobes switching within the same deltaic system, while small-scale sequences may result from more restricted and local factors, such as differential subsidence on delta plains, lacustrine delta formation, crevassing of distributary channels and migration of tidal channels (Reading and Collinson, 1996). The De Geerdalen Formation comprises facies sequences at all three scales. The whole formation itself represents one large upwards shallowing unit, while medium-scale and small-scale sequences occur at all levels of the formation. In all modern deltas, the delta grades up from marine to non-marine facies following the principles of Walter's Law, but in low accommodation space settings the upper delta plain facies are often eroded and removed by wave and tidal activity during transgression

(Bhattacharya, 2006). In general, the inter-fingering facies elements and cyclic facies architecture of deltaic deposits reflect upon the dynamic nature of deltaic environments, where waves, rivers and tides continuously interact to form complex sequences (Bhattacharya and Giosan, 2003). Thus, local variations occur both laterally and vertically over short distances. Differences between river-, wave- and tidal-dominated deltas are most visible in the delta front facies association. Here, the interplay between fluvial and basinal processes is recorded (Reading and Collinson, 1996). Dependant on the portion and efficiency of each process, the delta front may hold facies of sub-environments such as distributary mouth bars, barrier bars, subaqueous levees, beach ridges, beach spits, tidal channels, ebb and flood tidal deltas (Reading and Collinson, 1996).

Sedimentation styles on deltaic coastlines are largely governed by depositional regressions and transgressions. The transgressive parts of deltaic systems will normally experience a large degree of subsidence and marine reworking, while regressive parts are characterised by a large fluvial sediment supply (Bhattacharya, 2006). Switching between transgressive stages and regressive stages causes cyclic deposition patterns, patterns that are typical, but not exclusive to deltaic sequences. Sequences that form as a result of repeated deltaic progradations are often referred to as parasequences. The concept of parasequences originates back to the work of (Van Wagoner et al., 1988, 1990), in which parasequences were defined as a succession of beds that recorded upwards shallowing and were bound by marine flooding surfaces. Following this definition, a single parasequence may include several minor upwards coarsening and fining units, also called sub-sequences. Both parasequences and sub-sequences are characteristic for the De Geerdalen Formation, and has recently quantified by (Lord et al., 2017b). A pattern of stacked upwards shallowing units, or parasequences, are characteristic for the De Geerdalen Formation, as well as for the Snadd Formation in the Barents Sea (Klausen et al., 2015), and have been interpreted as a result of auto-cyclic switching of deltaic lobes within a major delta system (Knarud, 1980; Riis et al., 2008).

7.2 Facies distribution in Fulmardalen

The dataset that was collected from Fulmardalen represents a narrowly spaced dataset, with only a couple kilometres between the logged sections. While previous sedimentological studies of the De Geerdalen Formation (e.g. Lord et al., 2017a) have presented correlations between localities often spaced by several tens of kilometres, a denser spacing in the dataset from

Fulmardalen enables a more detailed study of both local vertical and lateral facies variations within the formation.

The facies distribution in Fulmardalen reflects an overall shallowing upwards depositional environment, with open marine shelf and prodelta (DE 1) deposits in the lower part, belonging to the Botneheia and Tschermakfjellet Formations, shallow marine (DE 2) and delta front (DE 3) deposits in the middle part and delta plain (DE 4) deposits in the upper part, reflecting an overall a distal to a more proximal deltaic setting. This shallowing upwards trend is concordant with previous studies of the De Geerdalen and Snadd formations (Knarud, 1980; Mørk et al., 1982; Riis et al., 2008; Høy and Lundschien, 2011; Lundschien et al., 2014; Rød et al., 2014; Lord et al., 2017a). Each depositional environment represents a group of facies associations (Table 7.1 and Figure 7.3). For simplicity, the classification into depositional environments has been used to correlate the logs in the study area (Figure 7.4). Due to the paralic nature of the De Geerdalen Formation, individual facies associations may be difficult to correlate laterally (Lord et al., 2017a).

The lower half of the De Geerdalen Formation in Fulmardalen (DE 2-3), consists of laterally extensive, stacked upwards coarsening units which have been interpreted as parasequences, reflecting repeated switching between regressive and transgressive phases within an overall prograding deltaic system. Many of the sandstones in the upper part of the parasequences are thought to reflect ancient barrier bar complexes or shallow subaqueous bank deposits. Traditionally, barrier bars are associated with transgressive phases of a delta complex, when the regressive phase reaches a state of over-extension, leading to abandonment and reworking of sediments (Boyd and Penland, 1988; Bhattacharya, 2006). However, Bhattacharya and Giosan (2003) show that barrier bars/islands may form naturally in modern prograding wave-influenced deltaic systems. In other words, the barrier bars interpreted in the De Geerdalen Formation are not necessarily associated with transgressive phases. The deposits witness of depositional environment considerably influenced by marine processes (and to some extent by tidal processes), which is in accordance with previous studies from Spitsbergen (Knarud, 1980; Rød et al., 2014; Lord et al., 2017a).

The deposits from Fulmardalen fit well into the description of ancient wave-dominated deltas (e.g. Reading and Collinson, 1996). Laterally extensive coarsening upward sequences characterized by wave- and storm-dominated facies comprise the shallow marine to delta front environment in such deltas. Furthermore, typical delta plain elements in wave-dominated deltas include distributary channels, interdistributary lagoonal facies with minor bars and lagoonal beach deposits (Reading and Collinson, 1996), which is what has been interpreted from the

upper part of the measured sections in Fulmardalen, within the Isfjorden Member. In fact, the type locality of the Isfjorden Member is in Fulmardalen (Mørk et al., 1999a).

Table 7.1 *An overview of facies associations (FA) interpreted from the De Geerdalen Formation and facies incorporated therein. The facies associations have also been linked with their gross depositional environments (DE). From Lord et al. (2017a).*

DE	Facies Association (FA)	Facies Incorporated	Description	Geometry/Form
DE 1 – Open Marine Shelf & Prodelta	FA 1 – Open Marine Shelf Deposits	A	Pelagic, organic rich shales and marine shale deposits. Abundant fossils and bone fragments and thin interlaminae of silt.	Extensive in thickness and areal extent. Forms major units.
	FA 2 – Prodelta Slope Deposits	A, B, C & H	Marine shales and siltstones, minor sand and bioturbation. Tempestites may be present with minor hummocky cross-stratification and ripples.	Areally extensive throughout Svalbard. Forms stratigraphic unit with variable thickness. (10-130m)
DE 2 – Shallow Marine	FA 3 – Offshore Deposits	A, I & J	Mud and silt dominated distal deltaic sediments. Forms dark mudstone and heterolithic bedded units with minor storm induced sandstones and thin offshore bars.	1-10's of metres thick. Laterally extensive and grade into offshore transition or lower shoreface deposits.
	FA 4 – Offshore Transition Deposits	A, B, C & E	Thin beds of hummocky cross-stratified sandstone in fine-grained shale and siltstones. Wave and symmetrical ripples common. Bioturbation and shell fragments also present.	1-10 m thick, laterally extensive for 100's m. Grades laterally into offshore or lower shoreface deposits.
	FA 5 – Lower Shoreface Deposits	A, B, C, E, G & H	Below normal wave base deposits dominated by mudstone and siltstone, with storm induced sandstone beds. Wave rippled, carbonate cemented or plane parallel laminated sandstone beds are common.	1-5 m thick and laterally extensive. Grades laterally into upper shoreface deposits of fluvial distributary deposits.
DE 3 – Delta Front	FA 6 – Upper Shoreface Deposits	C, E, F, I & K (also G & L)	Sandstone and siltstone, showing re-working of sediment in a turbulent environment. Wave structures indicate marine processes. Mud drapes suggest tidal influence. Forms prominent sandstone benches.	1-5 m thick and laterally extensive. Overlies lower shoreface or offshore transition deposits.
	FA 7 – Distributary Mouth Bar Deposits	D, F, H, I, J & M	Soft sediment deformed sandstone with trough, low-angle and tabular cross stratified sandstones. Erosive base indicates rapid deposition. Reworking of sediment by wave or tide processes evident. Also amalgamated.	Laterally extensive sheets for 100's of m. Thickness varies but is in the order of 1-4 m. Grades into distributary facies.
	FA 8 – Barrier Bar Deposits	E, F, H, I & K	Upwards coarsening facies, with trough or low angle cross-stratified sandstone, with current or wave-rippled sandstone. Tidal indicators and bioturbation suggest a marine origin.	Laterally extensive. Thickness ca. 1-2 m. Grades laterally into shoreface or inter distributary deposits.
DE 4 - Delta Plain	FA 9 – Distributary Channel Deposits	F, H, J, K, M & N	Sharp erosive base, contains trough and tabular cross-stratified sandstone facies. Mud-flakes are common in this association. Often underlies palaeosol facies. Can also form lateral sheets with amalgamated channels.	Extensive sandstone bodies. Often less than 10 m in thickness. Grades laterally into floodplain deposits.
	FA 10 – Floodplain Deposits	A, E, F, J, M & N	Fine-grained floodplain deposits, or overbank fines. Silt with sandstone laminae common. Coal, coal-shale and palaeosols present in this FA.	Laterally extensive with variable thickness, ca. 0.2-1.5 m. Overlies or incised by fluvial distributary deposits.
	FA 11 – Inter-distributary Areas	A, L, M & N (with E, F, & H)	Fine-grained facies. Some rare sandstone incursions with hummocks or ripples may be present, facies generally suggest a low energy marine or lacustrine environment. Bioturbation and palaeosols common.	1-10's of metres thick, laterally extensive, grading laterally into shoreface or barrier bar deposits.

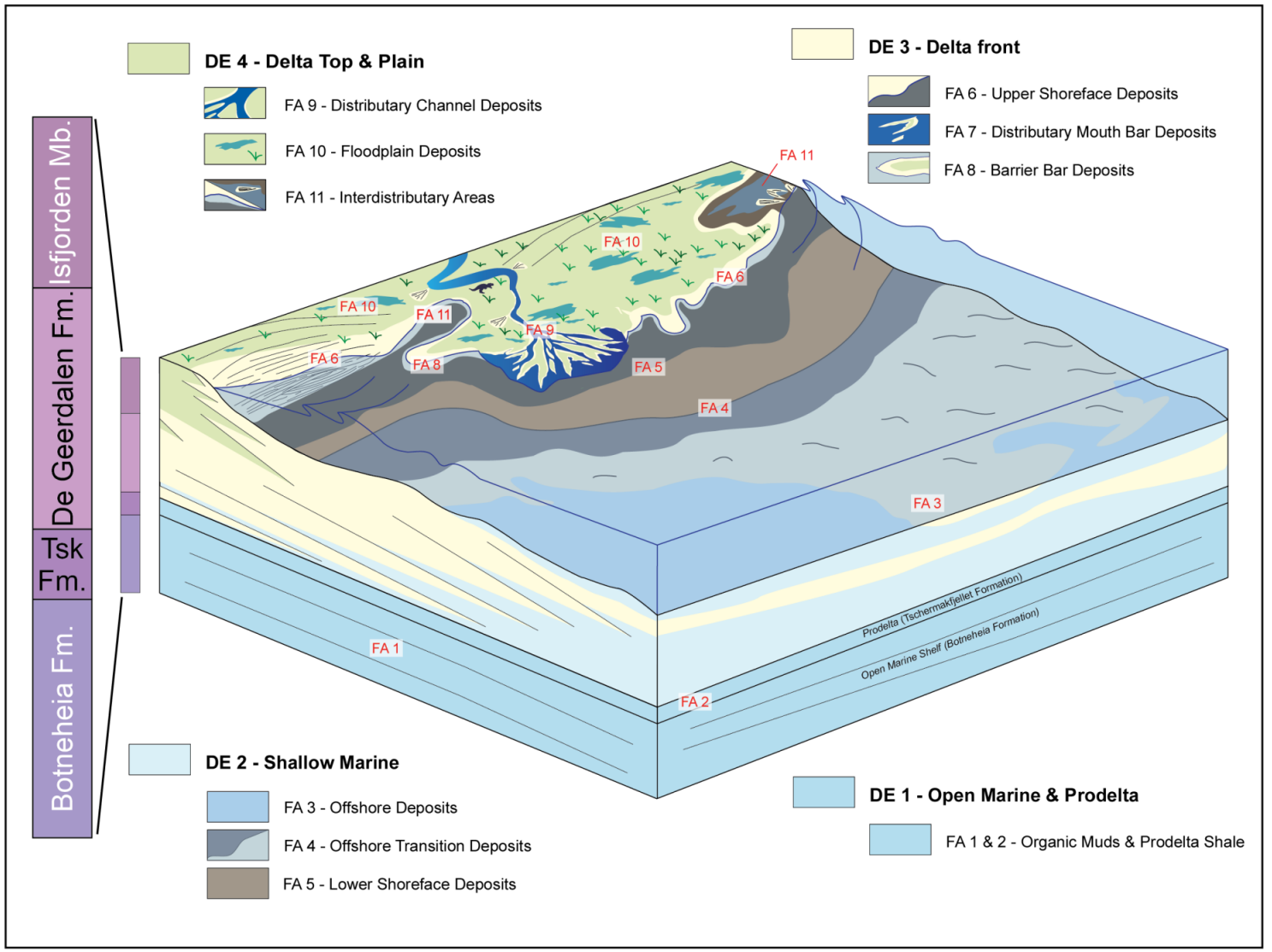

Figure 7.3 *A generalised, conceptual depositional model for the Botneheia, Tschermakfjellet and De Geerdalen formations, after Johansen (2016) retrieved from Lord et al. (2017a). The position of the facies associations in Table 7.1 are indicated. The model is based on concepts from Bhattacharya (1992), Reinson (1992), Howell et al. (2008), Glørstad-Clark et al. (2011) and Rød et al. (2014).*

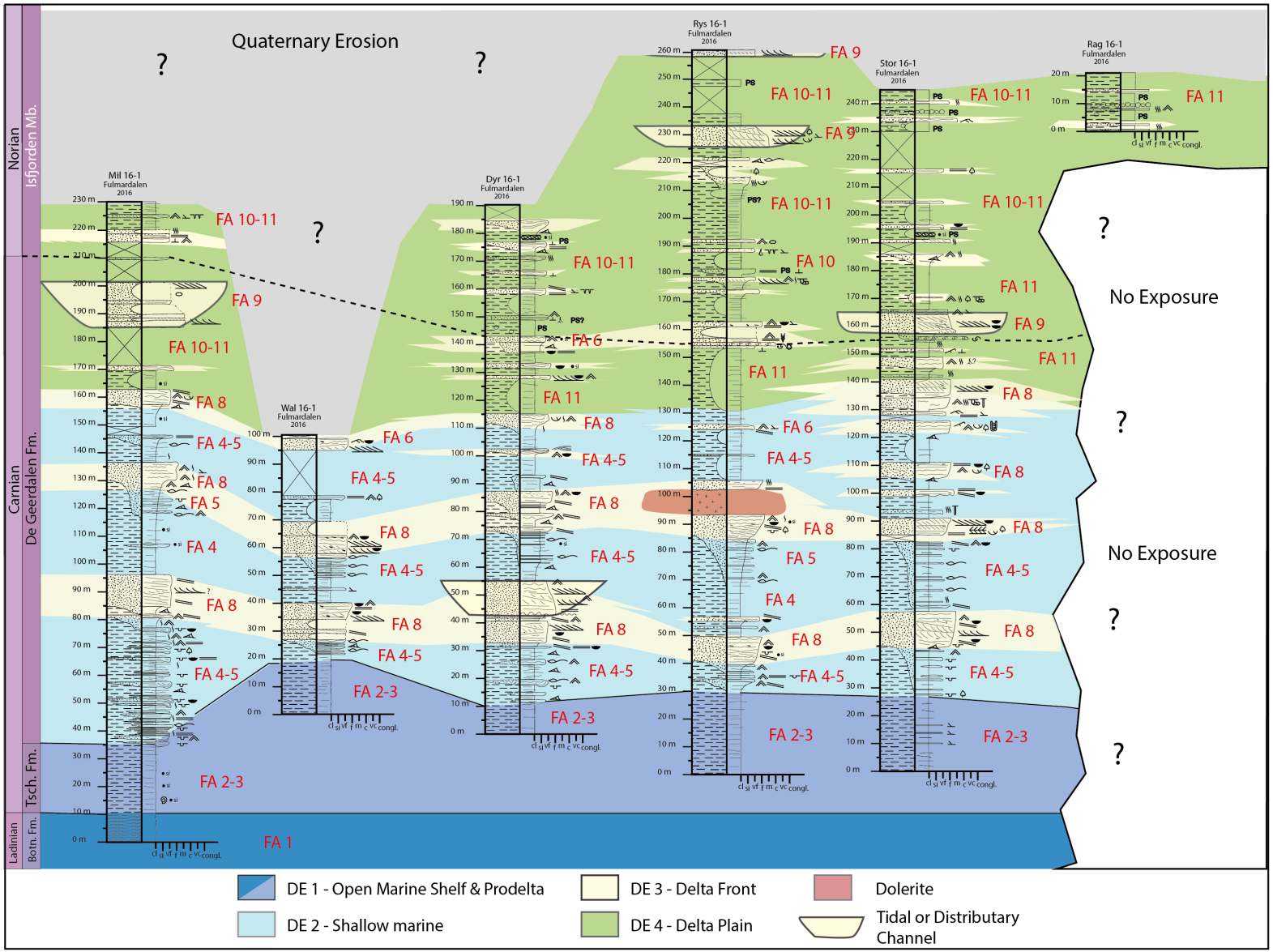

Figure 7.4 *Log correlations for sections measured in Fulmardalen. Positions of the individual logs are indicated in Figure 5.1. Depositional environments have been suggested based on facies and the interpreted facies associations.*

Issues related to the definition of the base of the Isfjorden Member are discussed in Section 7.2.1. It is important to remember that the deposits in Fulmardalen only represent a small portion of a large complex delta system which, depending on location, shows different dominating depositional processes. A more regional facies distribution discussion will be given in Section 7.3, putting the dataset from Fulmardalen into a larger scale context.

7.2.1 The base of the Isfjorden Member

Mørk et al. (1999a) suggest Storfjellet to be the type locality of the Isfjorden Member, where the lower boundary is defined by a bivalve coquina bed which occurs above a thick cross-bedded sandstone unit. This definition was based on the log from Storfjellet that was presented in Knarud (1980) (Appendix C). The rusty-red carbonate rich sandstone (without shell fragments) overlying a cross-bedded sandstone that were observed during fieldwork in 2016 (at 165 m in log Stor16-1), is most likely the same layer as the one that Knarud (1980) describes as a coquina bed. Local accumulations and/or dissolution of shell fragments may be the reason for these variations that seem to occur laterally over relatively short distances, and may explain the differences between Knarud's log and Stor16-1. This statement is supported by the fact that the correlative rusty-red layer observed at Ryssen (at 188 m in log Rys16-1) contains shell fragments (Figure 7.5). However, at Ryssen the coquina bed does not have any underlying cross-bedded sandstone, which makes the definition of the base of the Isfjorden Member questionable. Additionally, the work from Storfjellet observed the presence of a coquina bed that has not been described by Knarud (1980), located stratigraphically below the aforementioned cross-bedded sandstone at Storfjellet. A coquina bed was also observed at Ryssen at a lower stratigraphic level relative to the correlative layer defined as the base of the Isfjorden Member. Haugen (2016) studied the Isfjorden Member in eastern Svalbard and suggests that coquina beds are considered diagnostic features of the member. Furthermore, Haugen (2016) proposes that the lower boundary of the Isfjorden Member differs depending on facies associations and locality. This study is in accordance with those conclusions and suggests that the definition of the lower boundary of the Isfjorden Member following Mørk et al. (1999a) should be revised. Knarud's section from 1980 was not logged with the purposed of being a type section, a definition was later created by Mørk et al. (1999a) based on a re-interpretation of the original log (Atle Mørk, pers. comm., 2017). The fact that the defined lower boundary cannot be recognized even within the type locality area shows the necessity of a revision, and the definition proposed by Haugen (2016) seems more applicable.

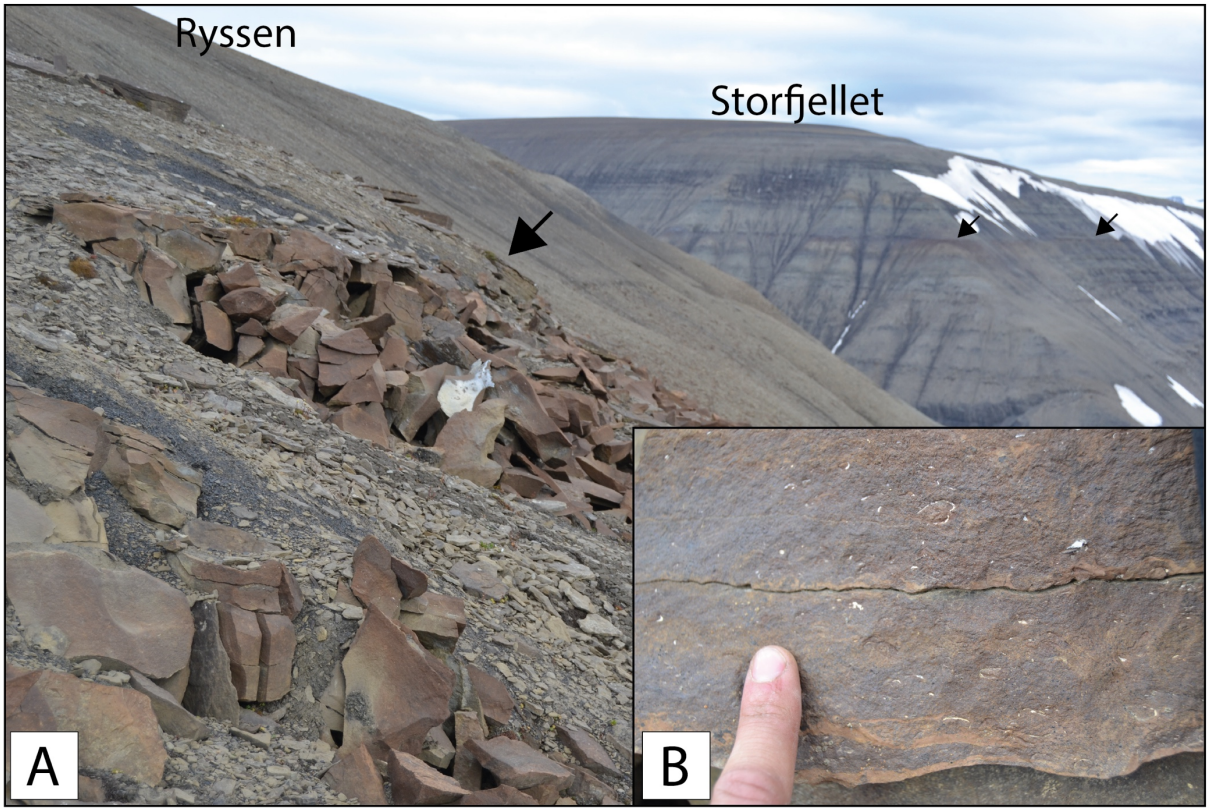

Figure 7.5 *Coquina and carbonate rich beds in the Isfjorden Member.* ***(A)*** *The rusty-red carbonate cemented sandstone at Ryssen can be laterally traced to Storfjellet (indicated by arrows). The layer occurs above a cross-bedded sandstone at Storfjellet where it defines the base of the Isfjorden Member according to the definition in Mørk et al. (1999a).* ***(B)*** *Shell framents in the rusty-red layer at Ryssen.*

7.3 Regional facies distribution

7.3.1 Spitsbergen

The new data presented from Fulmardalen provides important infill to previous work on the De Geerdalen Formation on Svalbard, and allows for data-comparison on a regional scale. A selection of representative logs from adjacent datasets from Botneheia, Sticky Keep and Trehøgdene on central Spitsbergen, and Klement'evfjellet and Friedrichfjellet in Agardhdalen, presented in Rød et al. (2014) and Lord et al. (2017a) respectively, are correlated and compared to new data from Fulmardalen in Figure 7.6.

The logs presented in the correlation panel are located on a NW-SE trending transect across Spitsbergen (see Figure 7.7). Fulmardalen represents a transition area that connects the observations from more westerly located areas on central Spitsbergen to Agardhdalen on eastern Spitsbergen. Rød et al. (2014) found that the De Geerdalen Formation in central

Spitsbergen was characterized by laterally continuous, blocky sandstone and siltstone layers interbedded with shale. The most adjacent log to Fulmardalen that was collected by Rød et al. (2014) on central Spitsbergen was measured from Trehøgdene (see Figure 7.7). In this section, low angle cross-stratified sandstone units are interpreted as barrier bar complexes in the lower part of the formation. This interpretation is consistent with the interpretation of barrier complexes occurring at similar stratigraphic levels in Fulmardalen. At Botneheia, which is a mountain located to the NW of Trehøgdene, the barrier complexes become absent or less prominent, but such deposits have been interpreted from the cores of well DH4 in Adventdalen (Rød et al., 2014), which is located west of Fulmardalen (see Figure 7.1).

In general, exposures of the De Geerdalen Formation NW of Fulmardalen show a tendency of being very fine grained, with a relatively low content of sand. The barriers and subaqueous banks that has been interpreted from the middle part of the De Geerdalen Formation in Fulmardalen seems to be less prominent at similar stratigraphic levels in this area. The middle part of the De Geerdalen Formation NW of Fulmardalen is generally characterised by thinner sandstone beds and a domination of shale, which could imply a more distal facies expression than displayed in the deposits in Fulmardalen. However, the differences between the deposits in the two areas are mainly related to the relative portion of sand and shale, and sandy units from both areas are characterized by the same structures and facies types. This could suggest a similar depositional regime for both Fulmardalen and the areas further NW on central Spitsbergen. Rød et al. (2014) argue that the sediments in central Spitsbergen were deposited in a setting with strong modulation from wave-energy, as well as with tidal influence. It seems likely that reworking and redistribution of sediments by basinal processes, especially wave activity, also played a major role in the depositional environment in Fulmardalen.

In Agardhdalen to the SE of Fulmardalen, the facies assemblages of the De Geerdalen Formation display a somewhat different trend compared to on central Spitsbergen. Here, the formation is dominated by more sandy intervals. The basal parts of the De Geerdalen Formation are generally poorly exposed in this area, but the deposits from the middle part of the succession and upwards have been interpreted to reflect upon a paralic nearshore setting dominated by delta front and shallow marine facies (Lord et al., 2017a). The sandstone geometries from the measured sections in Agardhdalen are described as thin and laterally continuous (Johansen, 2016), similar to sandstone bodies described from Fulmardalen and central Spitsbergen. Delta plain deposits in Agardhdalen include distributary channel facies, often associated with overlying paleosols, coal and coaly shales (Lord et al., 2017a). Indications of a more developed delta plain depositional environment are stronger in Agardhdalen than in Fulmardalen, where

comparatively few distributary channels, paleosol profiles and coal shale horizons have been interpreted. Fossil fragments of plants appear to be less abundant in Fulmardalen compared to in Agardhdalen. Although plant debris may be transported relatively far away from growth position, more frequent occurrences of fossilized plant debris in Agardhdalen may indicate a more developed delta plain, and proximal facies-expression towards the SE. Lord et al. (2017a) point out that a more developed delta plain environment, with paleosols, coal and coaly shales, requires time to develop in a relatively stable environment. If so, the data comparison could imply more stable conditions on the delta plain in Agardhdalen compared to in the Fulmardalen area. Additionally, higher bioturbation rates in Agardhdalen compared to in Fulmardalen may indicate a higher energy regime influencing the deposition in Fulmardalen, causing more restricted and harsher living-conditions.

Generally, the facies development found along the SE-NW directed transect (Figure 7.7) shows a development from a relatively proximal to distal facies expression. Johansen (2016) also suggests a more proximal facies expression in Agardhdalen compared to the observations of Rød et al. (2014) on central Spitsbergen, and base this interpretation on a higher amount of sand-rich facies in Agardhdalen. Fulmardalen represents a transition zone between these areas, both geographically and with regards to facies expression. However, a relatively high sand-content is also present in the De Geerdalen Formation at the Festningen section (Vigran et al., 2014), which is the westernmost exposure of the formation in Svalbard. This adds complexity to the sand distribution pattern, and may suggest that the aforementioned trend of a decreasing sand-content from east to west (or southeast to northwest) does not occur all over Svalbard.

Thickness trends has often been used a parameter for understanding the evolution of a deltaic system, where thick and thin deposits are associated with proximal and distal positions to the source area, respectively. However, variations in accommodation space and paleotopography are also controlling factors on basin fill patterns. Interpretations of deltaic evolution based on thickness-variations should be treated with care, and should not conclusively be associated with source proximity. Previous work has shown that the De Geerdalen Formation has a relatively uniform thickness across central Spitsbergen (e.g. Vigran et al., 2014; Lord et al., 2017b). Comparing thickness-measurements between localities on Svalbard is challenging due to the fact that very few areas display a complete succession of the formation. While the lower boundary of the formation is not exposed in Agardhdalen, the upper boundary is missing in both Fulmardalen and further NW on central Spitsbergen. This makes direct and quantitative

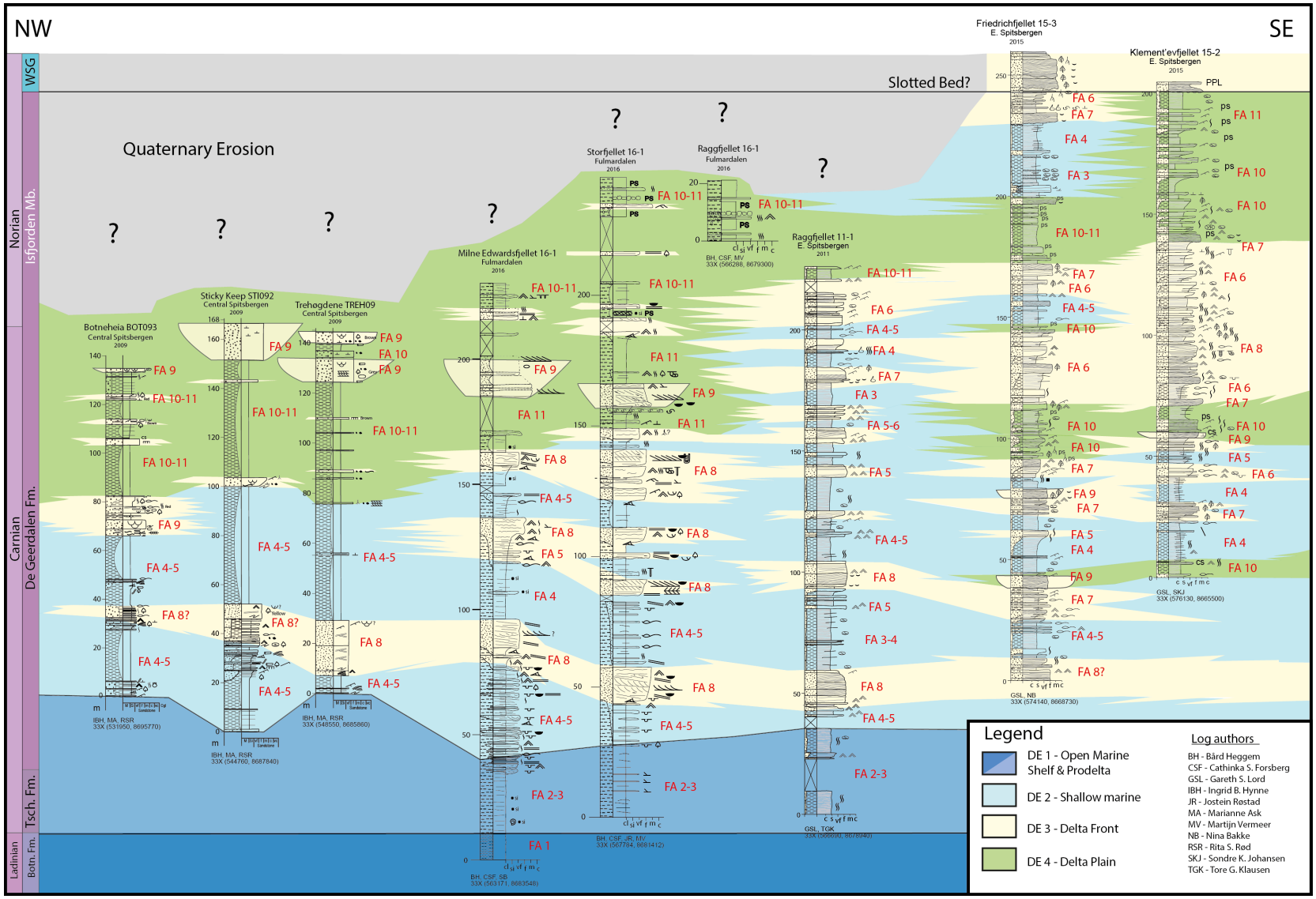

Figure 7.6 *Extended correlation panel including sections measured in central Spitsbergen (Rød et al., 2014), Fulmardalen and Agardhdalen (Lord et al., 2017a). Positions of the logs are shown in Figure 7.7. Depositional environments have been suggested based on facies and the interpreted facies associations.*

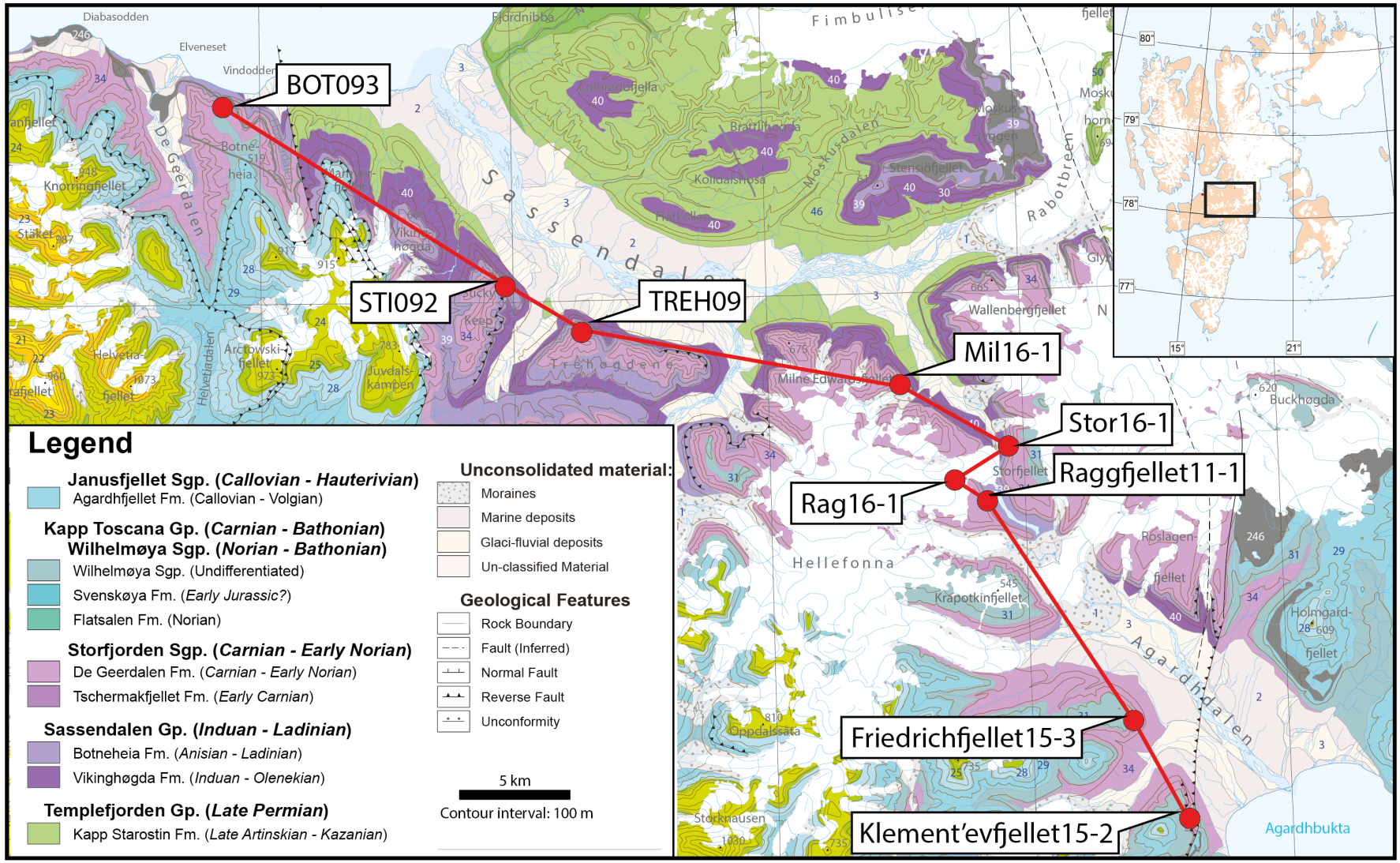

Figure 7.7 *Transect across Spitsbergen through Agardhdalen, Fulmardalen and Sassendalen. The position of the logs from the correlation panel in Figure 7.6 have been marked. Geological map retrieved from Dallmann (2015).*

thickness comparisons controversial and highly speculative at best, and other parameters, such as facies analysis, are necessary to understand the deltaic evolution of the De Geerdalen Formation across Spitsbergen.

The Isfjorden Member is exposed both in Agardhdalen and in Fulmardalen, but has not been described from central Spitsbergen where it may have been eroded or not recognized (Rød et al., 2014). Lord et al. (2017a) recognise facies that indicate a marine incursion in the upper parts of the De Geerdalen Formation in Agardhdalen. This marine interval is not recognised in Fulmardalen, where it may have been subjected to Quaternary erosion. Alternatively, the incursion may represent a local phenomenon such an interdistributary lobe bay area.

7.3.2 Edgeøya, Barentsøya, Wilhelmøya and Hopen

The De Geerdalen Formation on the islands Edgeøya, Wilhelmøya and Hopen, reflects a paralic deltaic environment, generally with a stronger fluvial signature compared to observations from Fulmardalen and elsewhere on Spitsbergen (Klausen and Mørk, 2014; Lord et al., 2014a,b, 2017; Rød et al., 2014)

Rød et al. (2014) describes thick ellipsoid shaped sandstone bodies at Blanknuten on Edgeøya (see locations in Figure 7.2), typical for fluvial dominated delta fronts. Similar deposits are described from Svartnosa at Barentsøya (Lord et al., 2017a). The relatively thick sandstones are interpreted as being amalgamated mouth bars deposited in a delta lobe and may represent the eastern and more proximal equivalent to the relatively thin and laterally extensive shoreface deposits observed in Agardhdalen, Fulmardalen and on central Spitsbergen (Rød et al., 2014; Lord et al., 2017a). Available accommodation space has been suggested as being the most likely reason for the geometrical differences, with the formation of thick and thin sandstone bodies forming in areas of high and low accommodation space, respectively. The fluvial signatures on the deposits are thought to decrease with less accommodation space, which allows basinal processes, such as wave activity, to rework and redistribute the sediment (Rød et al., 2014; Lord et al., 2017a). Furthermore, growth faults are described from the western side of Edgeøya (Edwards, 1976; Anell et al., 2013; Osmundsen et al., 2014; Rød et al., 2014). Such faults are typically associated with deltaic progradations that are characterized by high depositon rates (Edwards, 1976).

The northernmost log-localities presented in Lord et al. (2017a) are located on Wilhelmøya. Here, a complete succession of the De Geerdalen Formation is exposed, and is characterized by units of paralic delta front and delta plain deposits with abundant coal layers in the lower part (Haugen, 2016; Lord et al., 2017a). The upper part consists of delta plain

deposits with well-developed paleosols, interpreted to belong to the Isfjorden Member (Haugen, 2016; Lord et al., 2017a). The lower part has been interpreted as being deposited in a minor delta lobe system with fluvial distributary channels flowing in a coastal setting (Lord et al., 2017a). Both the paleosols and the coal deposits are better developed here compared to on Spitsbergen. The paleosols in the Isfjorden Member may have developed as a result of a delta lobe abandonment resulting in local subaerial unconformities and a change to a more stable environment with lower volumes of deltaic deposits (Lord et al., 2017a). (Haugen, 2016) suggests a slightly more proximal and terrestrial setting for the Isfjorden Member on Wilhelmøya compared to elsewhere in Svalbard.

The island of Hopen in south eastern Svalbard is the most proximal locality, with respect to the proposed Uralian source areas, where outcrops of the De Geerdalen Formation can be studied. Here, only the upper part of the formation is exposed, and the formation is composed of paralic delta plain sediments with minor marine incursions (Klausen and Mørk, 2014; Lord et al., 2014a,b) and is of late Carnian age (Paterson and Mangerud, 2015; Paterson et al., 2016). The island holds exposures of multiple fluvial trunk and distributary channel deposits (Klausen and Mørk, 2014; Lord et al., 2014b). Channel bodies occur frequently on Hopen, and are significantly larger in size compared to the channels observed in Spitsbergen. Evidence of coal formation (Klausen and Mørk, 2014; Lord et al., 2014b) indicates an environment which allowed for peat formation and were organic material was allowed to accumulate and be preserved. Paterson et al. (2016) suggest wet and humid conditions to have prevailed at that time. Presence of large tree remains in addition to large volumes of plant materials in the sandstone units, witness of a vegetated landscape in the late Carnian (Lord et al., 2014b, 2017).

The Late Triassic succession across Svalbard display a significant thinning from southeast to northwest (Anell et al., 2014a,b; Lord et al., 2017a,b). A well from Hopen shows the composite thickness of the Tschermakfjellet and the De Geerdalen Formation to be 1100 m (Anell et al., 2014a), whereas in Spitsbergen the equivalent thickness is approximately 300 m (Vigran et al., 2014). At Wilhelmøya, the De Geerdalen Formation alone is some 350-400 m (Lord et al., 2017a). The equivalent Snadd Formation in the Barents Sea reaches a thickness up to 1500 m (Klausen et al., 2014). This northwestward thinning is according to Anell et al. (2014a,b) related to the progression of the Carnian deltaic system on to the Svalbard Platform and an associated decreased accommodation space, similar to the interpretations of Rød et al. (2014). As shown in Figure 9.8, Svalbard was located in a proximal position to paleo-Greenland in the Triassic, and it could speculated if the thinning of the succession may have been related

to shallowing of the basin morphology as the delta system approached the shorelines of paleo-Greenland in the west. The overall paralic deltaic setting of the De Geerdalen Formation, with laterally discontinuous facies and depositional environments, also reflect upon a low progradation angle of the deltaic system, easily affected by changes in the delta or sea level (Lord et al., 2017a). The new dataset from Fulmardalen is, as discussed above, in accordance with and extends the understanding of this existing model.

8 Provenance of the Triassic succession at Festningen

There are several reasons for why Festningen was chosen as a locality for investigating provenance of the Triassic succession on Svalbard. First of all, the Festningen section represents a standard geological reference-section for the Mesozoic deposits on Svalbard, and it has been visited by geologists since the early 1900's (Mørk and Worsley, 2006). Detailed sedimentological and stratigraphical data from the section have been presented and discussed in several publications (e.g. Hoel and Orvin, 1937; Mørk et al., 1982; Steel and Worsley, 1984; Mørk et al., 1999a; Mørk and Worsley, 2006; Vigran et al., 2014). Thorough sedimentological and biostratigraphic investigations of the section at Festningen have enabled a precise stratigraphic control, which was crucial to have in hand when choosing the specific intervals for sampling. The western coast of Spitsbergen, has been heavily affected by Cenozoic faulting and folding. As a consequence, the Festningen section has been steeply tilted and folded (see Figure 8.4). The tectonic influence has ensured that a stratigraphic succession stretching from the Precambrian to the Cenozoic is exposed along the 8 km long coastline section at Festningen (Mørk and Worsley, 2006). This makes it a convenient location for studies of the entire Triassic succession on Svalbard. Previous sedimentological studies of the Triassic succession from various localities across Svalbard has shown that the Lower and Middle Triassic succession is more sand-rich in the western areas than it is in areas further east (Vigran et al., 2014). The westernmost exposure of Triassic strata on Svalbard is found at the Festningen section, and as it also is a relatively easy accessible locality, it is a logical location for collecting coarser grained sediments for detrital zircon analysis.

8.1 Purpose of study and sample material

Samples were collected during fieldwork at the Festningen section in August 2016, which were organized by the University Centre in Svalbard (UNIS) and financed by the Norwegian Petroleum Directorate (NPD). Applying detrital zircon (DZ) geochronology to investigate provenance for the Triassic succession at Festningen has previouly been done by Bue and Andresen (2014). Amongst the findings from this study were indications a significant provenance shift between the Lower and Upper Triassic successions. When designing a sample strategy for this study, it was decided to further investigate the DZ age signatures of the Triassic succession at Festningen, with special focus on pinning down a more exact stratigraphic position for the aforementioned provenance shift. An overview of the stratigraphic sub-division of the Festningen section has been given in Figure 8.1, where the location of each sample that

were collected are marked. A total of 11 samples were collected, and a table with coordinates and the current analytical status for each sample can be found in Appendix E.

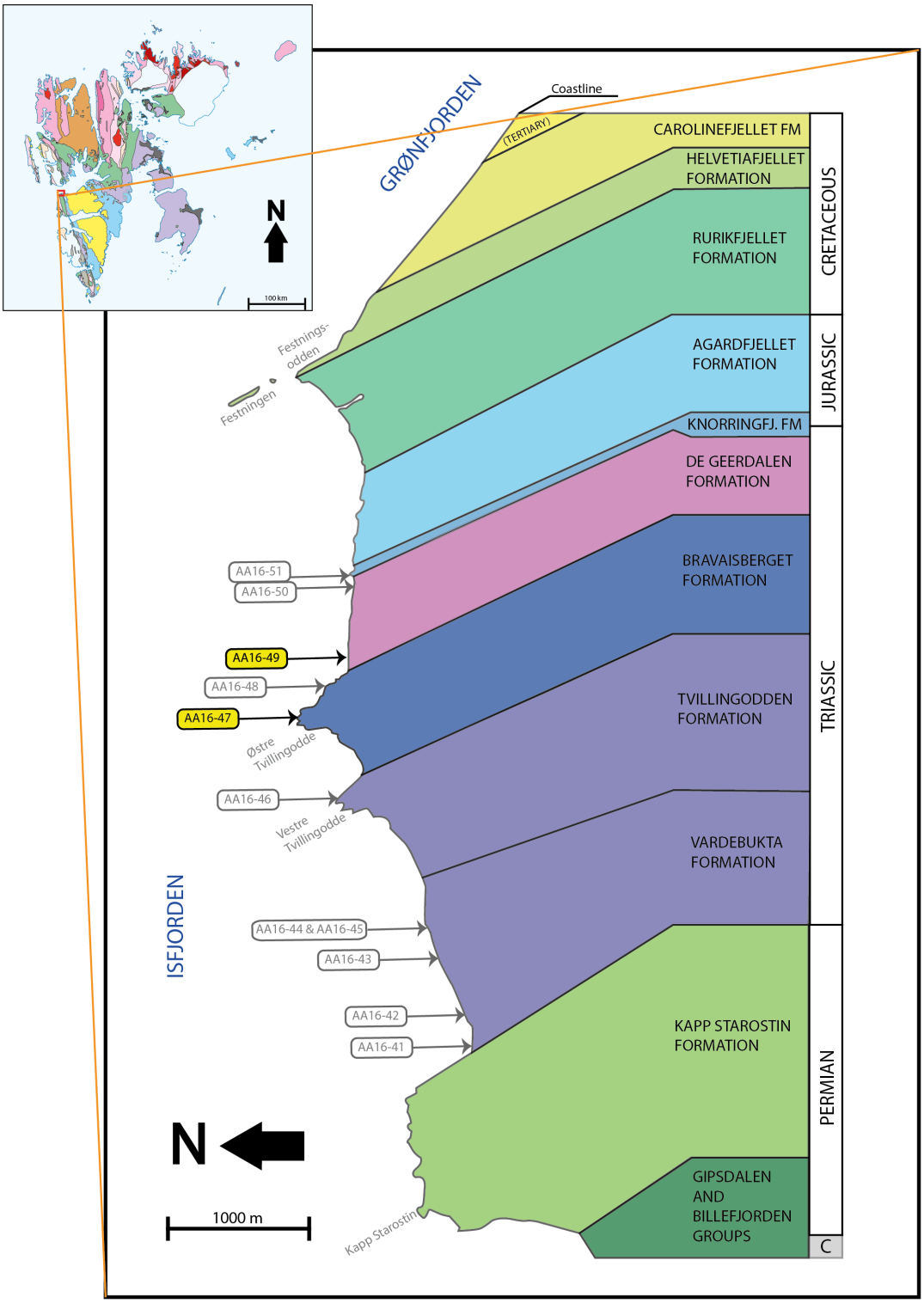

Figure 8.1 *Stratigraphic overview of the Festningen section. The position of each sample-location are indicated. Samples marked in yellow show the postion of the two samples that were fully analysed for detrital zircon age signatures. Modified from Hoel and Orvin (1937).*

8.2 Analytical results

Due to time limitations and restricted instrument availability at the Department of Geosciences at the University of Oslo, it was decided to analyse 3 of the 11 samples that were collected. The chosen samples were samples AA16-46, AA16-47 and AA16-49, collected from the Tvillingodden, Bravaisberget and the De Geerdalen formations, respectively (Figure 8.1). However, as sample AA16-46 did not yield any zircons, only two of the samples were fully analysed. Statistical analysis of concordant detrital zircon (DZ) ages of samples AA16-47 and AA16-49 has been interpreted to display two highly disparate age signatures, both shown with the use of histograms and Kernel density estimates (KDE) plots in Figure. 8.2.

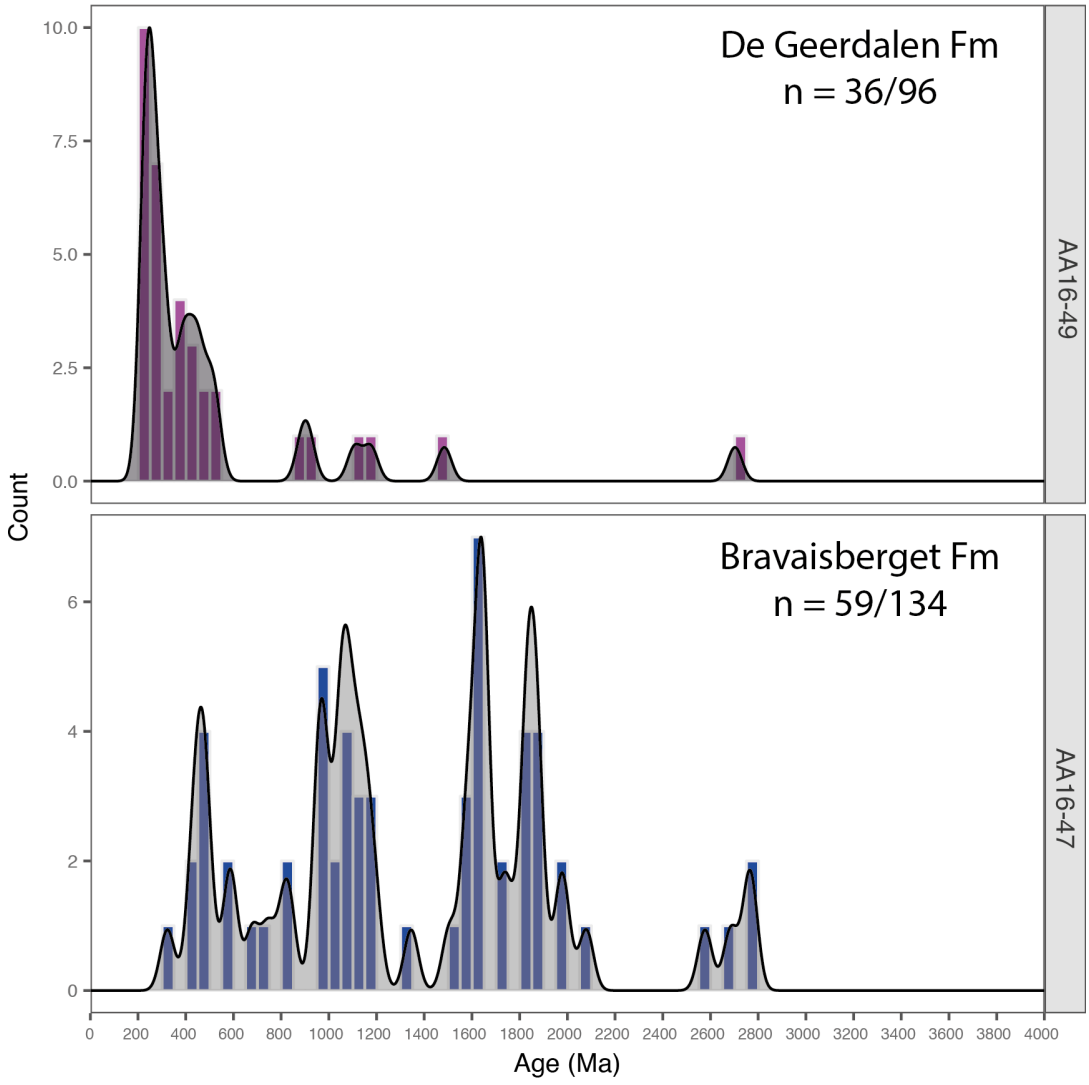

Figure 8.2 *Combined histogram and Kernel density estimate (KDE) plots of the two analysed samples. Ages are based on the lowest degree of uncertainty. Note that the two panels use different y-axis scaling. The histogram is produced with a bin width of 50 Ma while the continuous line is a Gaussian KDE curve given with a bandwidth of 30 Ma.*

Both of the analysed samples also yielded a high amount of discordant U-Pb ages (see Concordia diagrams in Figure 9.10), which are not included in the results of the analysis. If treated and interpreted correctly, discordant ages may provide valuable information regarding any deformation, alteration and metamorphism a zircon population has experienced (Reimink et al., 2016), but this aspect is considered to be beyond the scope of this thesis. Unfiltered results from both sample analyses are presented in Appendix F.

8.2.1 Sample AA16-47 – The Bravaisberget Formation

Sample AA16-47 was collected from the upper part of the Middle Triassic Bravaisberget Formation (Vigran et al., 2014). Out of 134 analysed zircons, 59 grains yielded ages with a level of discordance that falls within the ± 10% of the central discordance criteria and are included in the results. The analysis shows a wide span of age-populations, ranging from the Neoarchean to the Carboniferous. The oldest age population dates to the Neoarchean (2800 Ma – 2500 Ma), constituting approximately 7 % of the concordant grains. A large portion of the zircons ages falls within the Paleoproterozoic part (2500 Ma – 1600 Ma) of the age spectra, making up approximately 41 % of the concordant zircons. Another population with approximately 41 % of the concordant zircon ages belongs to the Meso- and Neoproterozoic Era (1600 Ma – 541 Ma) on the geological timescale. Zircon ages from 500 Ma to 400 Ma roughly correspond to the age of the Caledonian orogeny. This age population constitutes approximately 10 % of the analysed zircons of sample AA16-47. Concordant ages younger than 400 Ma are not present in the sample, except from one grain that yielded a Carboniferous age. The most dominant age-populations are found between 1900 and 1800 Ma, 1700 and 1500 Ma, and between 1200 and 1000 Ma. DZ ages in the intervals between 2500 to 2200 Ma and 1500 to 1300 Ma are rare, and the lack of these age-populations create significant gaps in the histograms (Figure 8.2).

8.2.2 Sample AA16-49 – The De Geerdalen Formation

Sample AA16-49 was collected from the lowermost sandstone unit in the Upper Triassic De Geerdalen Formation. Out of 96 analysed zircons, only 36 grains yielded ages with a level of discordance that falls within the ± 10% central discordance criteria. The sample yielded a very limited amount of Precambrian ages. Only one grain (approx. 3 % of the concordant grains) gave an Archean age. None of the analysed DZs gave Paleoproterozoic ages. Approximately 14 % of the zircon ages falls within the Meso- and Neoproterozoic Era of the age spectra. The DZ age distribution in sample AA16-49 is dominated by Cambrian to Triassic age-populations.

Cambrian to early Permian (ca. 540 – 270 Ma) ages makes up approximately 47 % of the age signature. DZ ages falling within the relatively short interval between the Late Permian and the Late Triassic makes up the most densely populated part of the age spectra, characterized by a very distinct population at around 233 Ma. About 28 % of the zircon ages falls within this interval. In Figure 8.3, the Paleozoic and Early Mesozoic part of the age spectra has been highlighted.

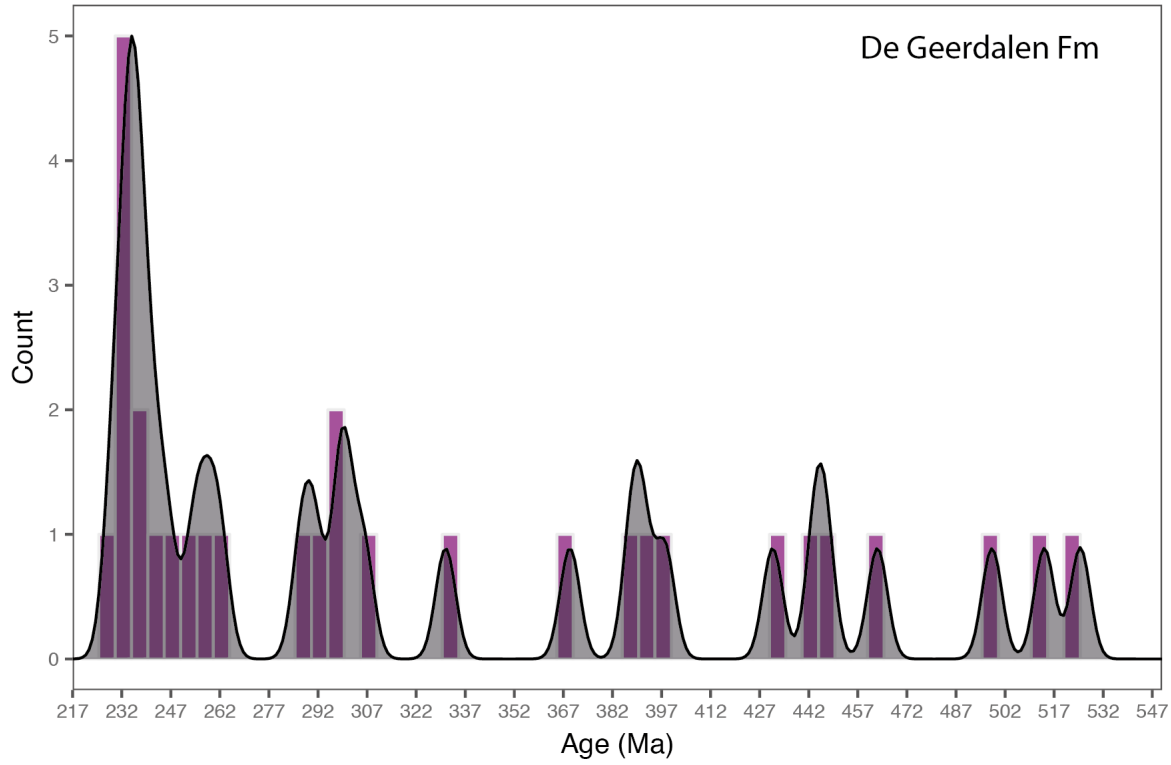

Figure 8.3 *Combined histogram and Kernel density estimate plot of sample AA16-49, displaying the Paleozoic and Early Mesozoic part of the age-spectra. Notice the very distinct peak at approximately 233 Ma. The histogram was produced with a bin width of 5 Ma, while the KDE curve has a bandwidth of 3 Ma.*

8.2.3 Comparison of the detrital zircon age-populations

The detrital zircon (DZ) age-populations in the two samples appear to represent two significantly different and distinct DZ age signatures. The data compares well to the findings of Bue and Andresen (2014), and supports the suggestion of a major shift in the dominating source area at the transition between the Middle and Late Triassic (see Figure 8.4), and indicates sediment input from at least two distinctly different source areas.

DZ U-Pb geochronology is a rapidly expanding and useful technique for interpretations in provenance research. In order to compare age distribution datasets from different samples in a sophisticated and quantitative way, several methods have been proposed. Satkoski et al.

(2013) presents a likeness parameter that utilize a pairwise comparison of samples. The method examines the degree of sameness among DZ age-populations by applying a likeness metric that quantify the degree of overlap between the probability density plots (PDP). It should be noted that PDPs are mathematically equivalent to the Kernel density estimates (KDEs) that have been used to present the DZ age data in this thesis, and the likeness test is thus also valid when applied for KDEs. The difference between KDEs and PDPs is that KDEs applies a constant bandwidth, while PDP bandwidth varies locally based on the uncertainty in the given ages (Sircombe, 2004; Andersen et al., 2017). In order to compare the datasets from the Bravaisberget and the De Geerdalen Formation, a pairwise 1D likeness test with a constant age-bandwidth of 30 Ma has been carried out. The test gives a likeness-value of 0.26 (see Table 8.1), and supports the interpretation of two significantly different parent zircon age-populations. Samples drawn from a single parent population should yield a likeness value around 0.61 (0.61±0.09 for n≈50; Satkoski et al., 2013).

The DZ age signature of the Middle Triassic Bravaisberget Formation is dominated by Proterozoic ages, with a few Archean ages. No Mesozoic ages are found, which is quite the opposite from what has been found in the Late Triassic sample of the De Geerdalen Formation. The De Geerdalen Formation sample yielded a very limited amount of ages older than the Paleozoic, and is characterized by a significant zircon age population situated between 242 – 228 Ma, with a distinct peak at around 233 Ma. Similar peaks are also present in all samples from the De Geerdalen Formation that was presented in Bue and Andresen (2014).

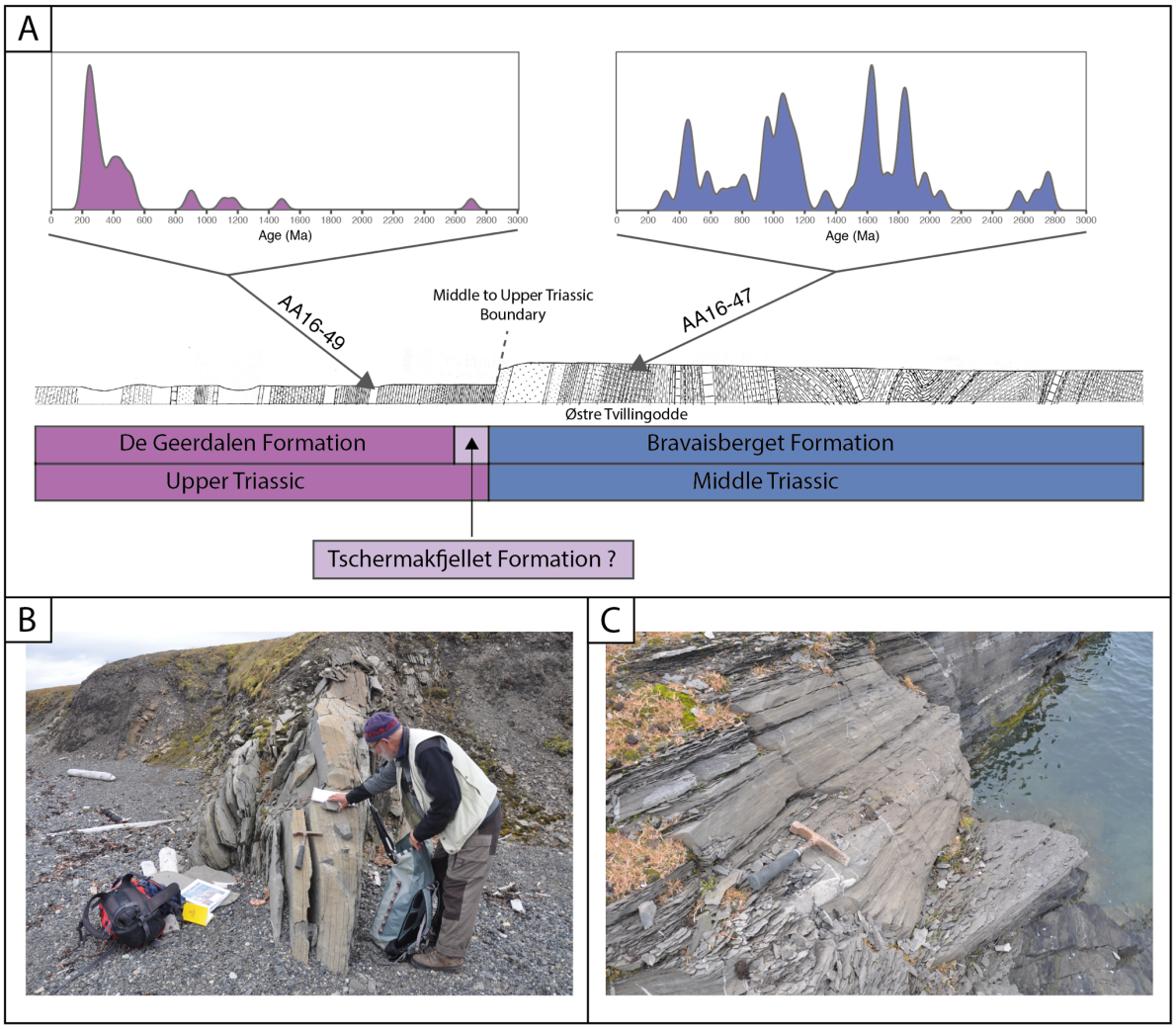

Figure 8.4 *Figure illustrating a shift in provenance at the Festningen section.* ***(A)*** *Kernel Density estimates for samples AA16-49 and AA16-47 display significant differences between the DZ age-populations in the Middle Triassic and the Upper Triassic, and indicate a significant change in provenance over the Middle to Upper Triassic boundary. The approximate position of which each of the samples were collected from has been indicated on the geological sketch (from Hoel and Orvin, 1937). The sketch also illustrate how tectonic forces has influenced the succession at Festningen.* ***(B)*** *Sample location for sample AA16-49, taken from the first prominent sandstone unit in the De Geerdalen Formation.* ***(C)*** *Sample location for sample AA16-47, taken from dark sandstones in the Bravaisberget Formation, at the tip of Østre Tvillingodde.*

9 Discussion – provenance for the Triassic succession

Before comparing and correlating the detrital zircon (DZ) U-Pb age data presented in this thesis with those presented from the Festningen section in Bue and Andresen (2014), it is necessary to point out two small, but significant errors regarding the location of two of the samples that were analysed by Bue and Andresen (2014). The first mis-location concerns sample S5, which in the paper is described as a sample collected from the Middle Triassic Bravaisberget Formation. Plotting of the coordinates given in Bue and Andresen (2014) show that this sample was collected from Vestre Tvillingodde, in the uppermost part of the Lower Triassic Tvillingodden Formation, and not from the Bravaisberget Formation as it has been stated in the paper. Essentially this means that no samples from Middle Triassic sands were analysed by Bue and Andresen (2014), and that sample AA16-47 is the first sample from the Middle Triassic succession on Svalbard to be analysed for DZ age-populations.

The second mis-location is concerning sample P-09-34 that is presented by Bue and Andresen (2014). The sample has been presented as a sample collected from the De Geerdalen Formation at Festningen. However, plotting of the given sample coordinates yielded a sample location in the uppermost part of the Middle Triassic Bravaisberget Formation. Investigations of this error have shown that the coordinates given in the paper are incorrect, and the sample was indeed collected somewhere in the lower part of the De Geerdalen Formation, most probably collected from within a meter or so from sample AA16-49 of this thesis (Arild Andresen, pers. comm., 2017).

With this information and the addition of new data from this study, it is confirmed that sands from all the Triassic formations at the Festningen section has been analysed for DZ age signatures. A new analysis of sand from the De Geerdalen Formation was also necessary due to discrepancies between the coordinates and the given stratigraphic position of sample P-09-34 from Bue and Andresen (2014).

9.1 Comparison to the Bue and Andresen (2014) study

The main aim for the DZ age analysis of samples from the Festningen section was to investigate a proposed provenance shift happening at the transition from the Middle Triassic to the Upper Triassic succession. Based on sedimentological and stratigraphic evidence, a change in the dominating sediment source in this part of the succession has for long been established as an accepted model (Mørk et al., 1982, 1999a; Worsley, 2008; Lord et al., 2017a,b). The main goal

for the study presented by Bue and Andresen (2014) was to test and to constrain such sedimetologically induced models by using DZ geochronological data from Svalbard, and for this purpose, samples from the Festningen section played a key role.

Based on DZ age signatures of Triassic samples collected across the Svalbard archipelago, Bue and Andresen (2014) suggest a provenance subdivision into three DZ age-population endmembers. The first endmember are found in the Lower Triassic Vardebukta Formation and Tvillingodden Formation (incorrectly described as the Bravaisberget Formation in the paper). The DZ populations in this endmember are dominated by Paleo- and Mesoproterozoic ages, with minor populations of Neoproterozoic, Paleozoic, Caledonian and Mesozoic ages. Archean grains also make up a significant portion of these age signatures. The resulting age-populations from sample AA16-47 of the Middle Triassic Bravaisberget Formation presented in this thesis, strongly resemble the populations found in the Lower Triassic, especially to the sample from the Tvillingodden Formation. Thus, the DZ data indicate that the sediments of the Bravaisberget Formation most likely were derived from the same parent zircon age population as the sediments in the Tvillingodden Formation and probably the Vardebukta Formation. A single common provenance area thus seems to have been sourcing sediments to Svalbard from the Early Triassic to the end of the Middle Triassic.

The second DZ age-population endmember presented in Bue and Andresen (2014) are defined from three samples from the Upper Triassic De Geerdalen Formation. The endmember is characterized by very few Archean ages, a considerable amount of zircon grains dated to the younger parts of the Proterozoic, but with a clear domination of Ordovician-Silurian and Mesozoic ages. This age population pattern is consistent with the observations made from the sample of the De Geerdalen Formation that has been analysed for this thesis, and supports the interpretation of a significant provenance shift at the transition from the Middle to the Upper Triassic. In Figure 9.1, Kernel density estimates (KDEs) for the Vardebukta, Tvillingodden, Bravaisberget and De Geerdalen formation has been correlated to their stratigraphic position on a sedimentological log from the Festnigen section (from Vigran et al., 2014) and illustrates changes in DZ age signature with time through the Triassic succession. The figure clearly illustrates the provenance shift at the transition between the Middle and Upper Triassic. This shift can also be identified from the empirical cumulative density plots in Figure 8.2.

The third endmember that were presented in Bue and Andresen (2014) are found in the Uppermost Triassic to Lower Jurassic Wilhelmøya Subgroup, and are suggested to represent mixing of the latter two endmembers, potentially due to reworking of older sediments, and/or with renewed influx from the same source area that dominated in the Early to Middle Triassic.

Table 9.1 presents a likeness tests of samples both analysed by Bue and Andresen (2014) and of those presented in this thesis. As described in Section 8.2.3, the likeness test represents a quantitative way of testing the degree of overlap between probability density plots (PDPs) or Kernel density estimates (KDEs), essentially meaning that it is a measure of probability of two samples being derived from the same parent zircon population/source area. The table is based on a metric developed by Satkoski et al. (2013).

Table 9.1 *Result of 1D likeness tests comparing detrital zircon (DZ) age-populations from all the Triassic formations at the Festningen section. Likeness values are highly dependent on the number of sample ages obtained from the analysis, and the average likeness value will increase with the number of ages. For samples sourced from the same parent population, the average likeness value should be 0.61±0.09 for n≈50, 0.72±0.06 for n≈100, and 0.79±0.04 for n≈150 (Satkoski et al., 2013). The number of valid ages n from each analysis are given in Figure 8.5.*

	Vardebukta Fm. (P-09-33)	*Tvillingodden Fm. (S5)*	*Bravaisberget Fm. (AA16-47)*	*De Geerdalen Fm. (AA16-49)*	*De Geerdalen Fm. (P-09-34)*
Vardebukta Fm. (P-09-33)		0.53	0.51	0.21	0.20
Tvillingodden Fm. (S5)	0.53		0.66	0.17	0.15
Bravaisberget Fm. (AA16-47)	0.51	0.66		0.26	0.27
De Geerdalen Fm. (AA16-49)	0.21	0.17	0.26		0.73
De Geerdalen Fm. (P-09-34)	0.20	0.15	0.27	0.73	

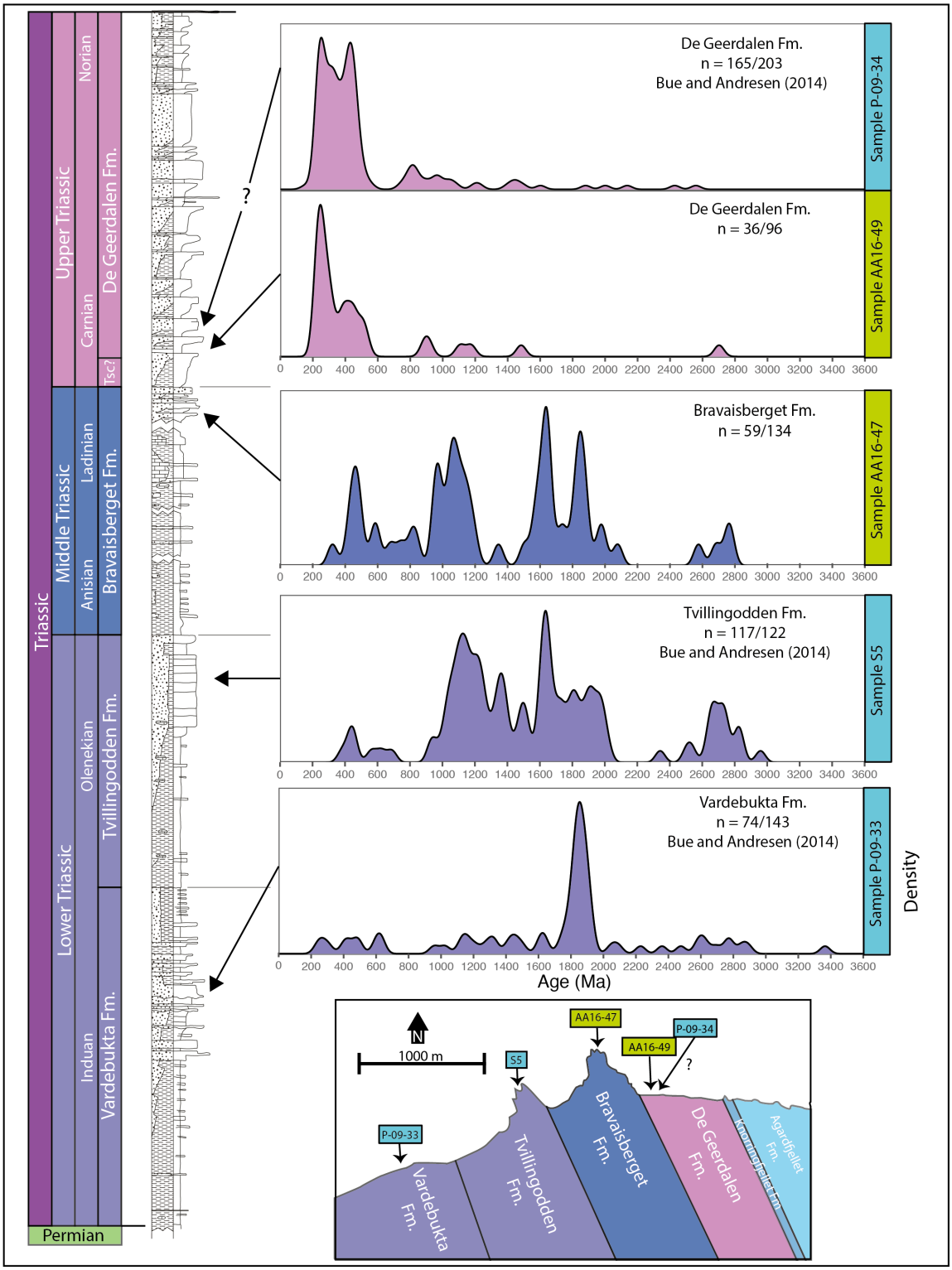

Figure 9.1 *Graphic presentation of changes in the detrital zircon (DZ) age signatures in relation to the stratigraphic position of each sample. Approximate stratigraphic positions of each sample are indicated with black arrows. Note the significant changes in the DZ age-population signature at the transition between the Middle and Upper Triassic. The geographic location of each sample is indicated at the map of the Festningen profile at the bottom of the figure. Continuous curves are Gaussian Kernel density estimate plots, produced with a bandwidth of 30 Ma. The log is retrieved from Vigran et al. (2014).*

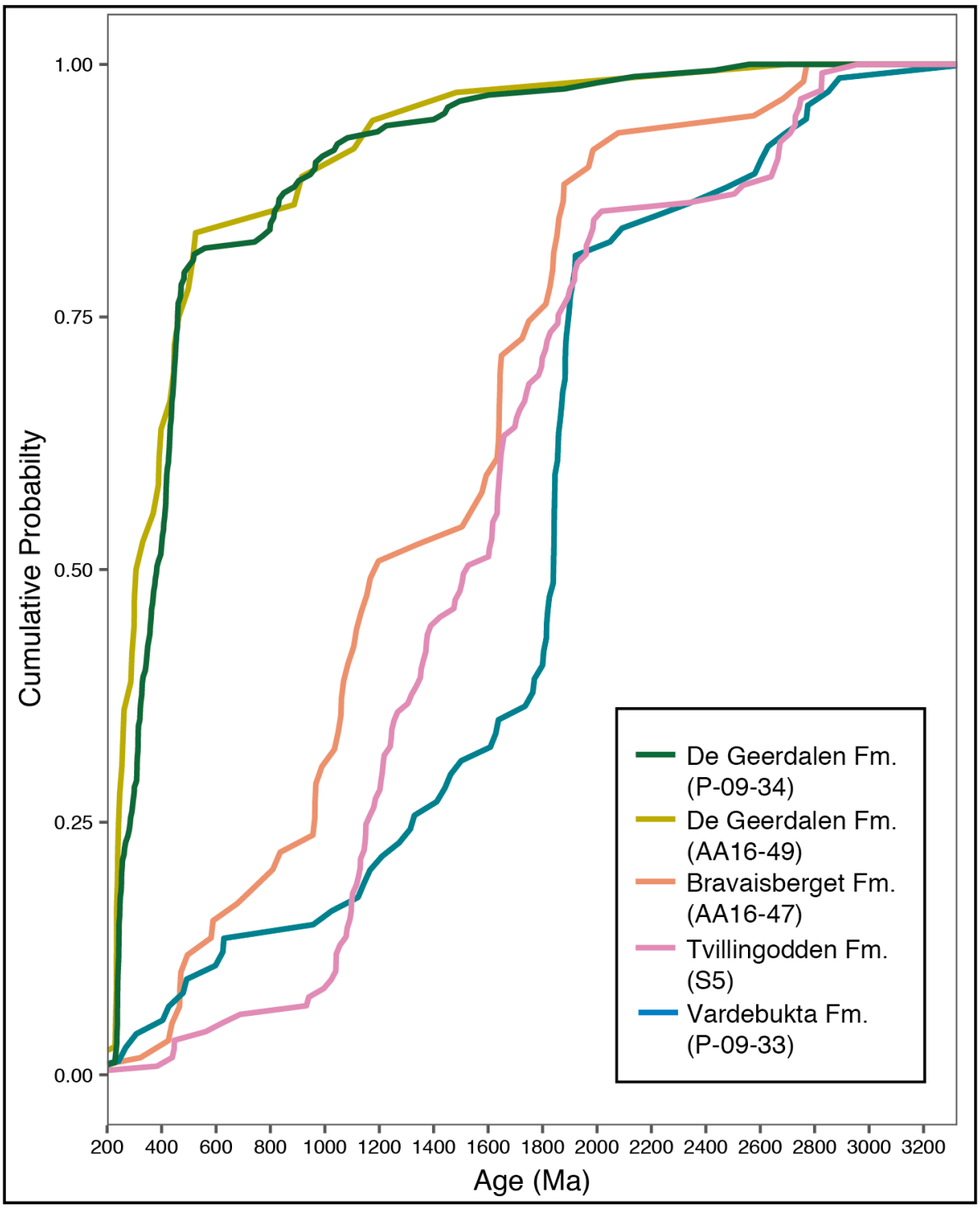

Figure 9.2 *Empirical cumulative distribution function (ECDF) plots for the Triassic samples from the Festningen section. Samples AA16-47 and AA16-49 have been analysed as part of this thesis, while the other three samples were analysed by Bue and Andresen (2014). The figure displays a similar distribution function for the Lower and Middle Triassic samples, which is significantly different from the distribution function of the Late Triassic samples from the De Geerdalen Formation.*

9.2 Triassic paleogeography

9.2.1 Sedimentological, stratigraphic and offshore evidence

Sedimentological and stratigraphic data from Lower and Middle Triassic deposits on Svalbard shows a significantly different development in areas along western Spitsbergen compared to areas on Central and Eastern Spitsbergen, and on the eastern islands (Mørk et al., 1999a; Krajewski and Weitschat, 2015). The deltaic facies that are present in upwards coarsening units of the Lower Triassic Vardebukta and Tvillingodden formations on western Spitsbergen, are replaced by more distal open marine facies in the Vikinghøgda Formation in Central Spitsbergen and on Eastern Svalbard (Mørk et al., 1982, 1999a,b). The lateral facies variations have been interpreted as indications of deltaic progradations from a westerly located source in the Early and Middle Triassic. Structural highs and platform areas, which emerged as a result of tectonic movements in the latest half of the Paleozoic, were progressively flooded through the Early Triassic (Mørk et al., 1982; Worsley, 2008; Vigran et al., 2014). On the Sørkapp-Hornsund High in southern Spitsbergen, sedimentation did not start until the mid-Induan (Nakrem and Mørk, 1991), and the Triassic sediments lie directly upon pre-Caledonian basement rocks (Worsley and Mørk, 1978). Such local positive highs and platforms are worth noticing, as they may have represented potential source areas for the Lower Triassic Vardebukta Formation.

Sedimentological data suggests that the Middle Triassic evolution in the Svalbard area was similar to in how it was in the Early Triassic (Mørk et al., 1999a). The Middle Triassic succession is represented by the Bravaisberget Formation on western Spitsbergen, where it shows a more proximal facies development than displayed in the age equivalent Botneheia Formation on Central Spitsbergen and on eastern Svalbard (Mørk et al., 1982, 1999a). During the Cenozoic, compressional tectonics resulted in approximately 20-40 km crustal shortening on western Svalbard (Bergh et al., 1997; Leever et al., 2011; Dallmann et al., 2015). This is an important factor to take under consideration as it suggests that the Triassic succession found on western Spitsbergen today, was originally deposited in a different, probably more westerly located, position. The combination of facies observations and thickness data has been interpreted to suggest a westerly located source dominating the basin fill pattern in the Svalbard area during both the Early and Middle Triassic (e.g. isopach maps in Figure 9.3). Recently, a conceptual study by Lord et al. (2017b) quantifies and interprets stratigraphic sequence patterns in the Triassic succession across Svalbard and the Northern Barents Sea. The study supports previously suggested theories of a dominating source area located to the west of Svalbard in the Early and Middle Triassic. The interpretation is based on observations of a significantly

high number of parasequences along the western parts of Spitsbergen, a number that decreases in a north-easterly and south-easterly direction.

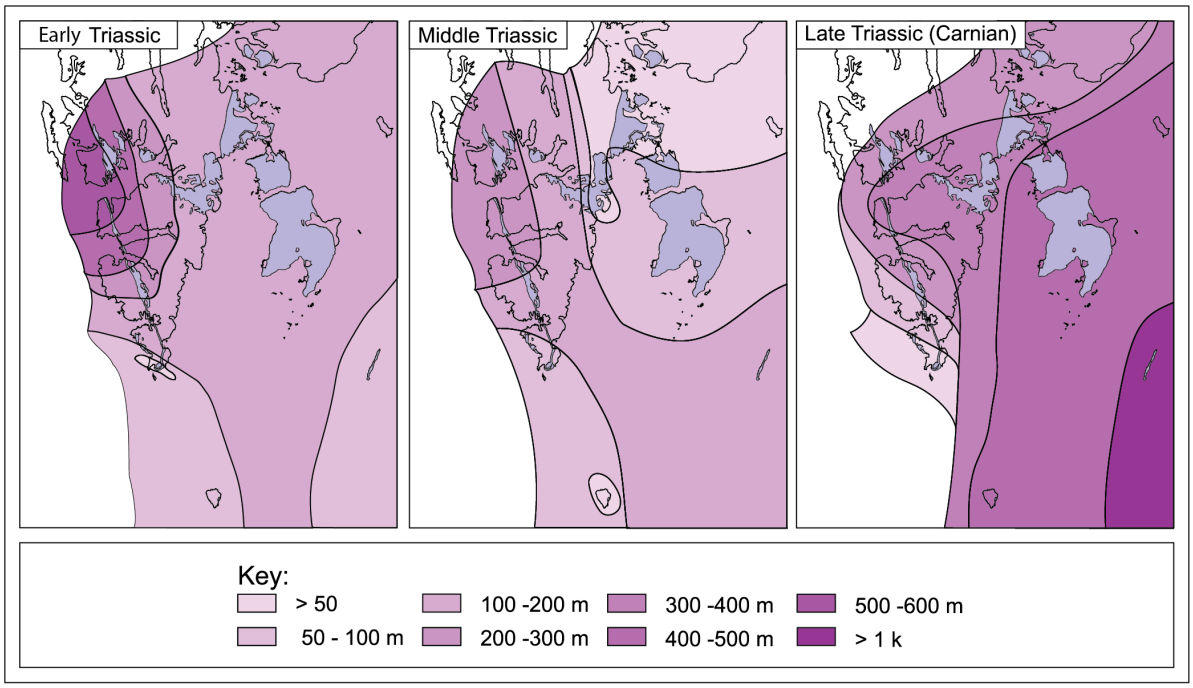

Figure 9.3 *Isopach maps of the Triassic succession in Svalbard and the NE Barents Sea based on measured sections across Svalbard. From Lord et al. (2017b).*

Lord et al. (2017b) presents an opposite trend for the Late Triassic, where the parasequence pattern shows evidence of thickening and increasing numbers towards the north-east and south-east. This trend is consistent with sedimentological studies (described in more detail in Section 7.3.2), where more proximal facies have been found in Upper Triassic succession of the eastern areas on Svalbard, compared to more distal facies displayed in more westerly located exposures (Knarud, 1980; Mørk et al., 1999a; Rød et al., 2014; Vigran et al., 2014; Lord et al., 2017a). Even more proximal deposits have also been reported from Hopen, where well-developed delta plain facies and major channel bodies have been reported from the Upper Triassic succession (Klausen and Mørk, 2014; Lord et al., 2014b).

Seismic studies carried out on the Triassic succession on the Barents Sea Shelf have shown the existence of large clinoform sequences prograding from the SE and across the Barents Sea Shelf (Riis et al., 2008; Glørstad-Clark et al., 2010; Høy and Lundschien, 2011; Klausen et al., 2014, 2015; Lundschien et al., 2014) The resulting deposits from this system belongs to the Snadd Formation, which represents the offshore equivalent to the De Geerdalen Formation on Svalbard (Klausen and Mørk, 2014; Lord et al., 2014b; Klausen et al., 2015).

Based on correlations between seismic data and outcrop data from Svalbard, it is suggested that both the Snadd and the De Geerdalen Formation were mainly sourced from the SE, with erosional products being shed from the Uralian Orogeny (Glørstad-Clark et al., 2010; Henriksen et al., 2011; Lundschien et al., 2014; Klausen et al., 2015). In Figure 9.4, evidence of clinoform progradation detected from break-points in the clinoform sequences are shown.

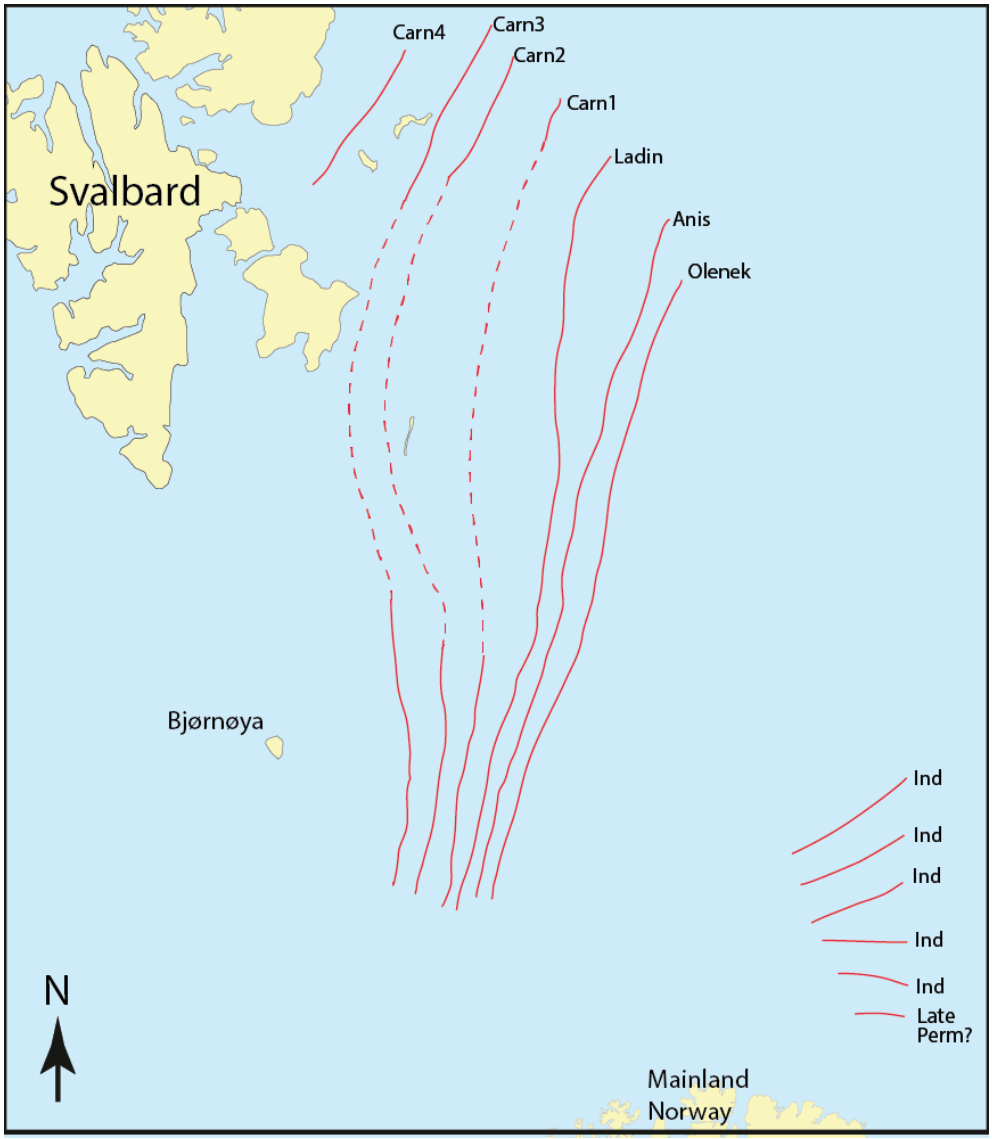

Figure 9.4 *Seismically detectable breaks of prograding clinoforms in the western Barents Sea. The uppermost Permian and lowermost Triassic clinoforms prograde NNE from the Fennoscandian Shield, but are progressively younger further out in the basin, where they merge with more dominant clinoform successions interpreted to be fed from the building Uralian Orogeny. The clinofroms are interpreted to have reached Svalbard in the Carnian Stage of the Late Triassic. From Lundschien et al. (2014).*

The application of DZ age-population signatures in provenance research represents a direct way of testing and constraining regional depositional models that may be inferred from

sedimentological and stratigraphic studies, as well as from seismic surveys. In the following section, proposed depositional models for the Triassic on Svalbard will be discussed in the light of the observed DZ age-populations from the Festningen section and from other published DZ age-population signatures from relevant areas.

9.2.2 The Early and Middle Triassic

As previously mentioned, sedimentological and stratigraphic data suggest a dominance of a westerly located source for the Lower and Middle Triassic succession on Svalbard. When this data has been combined with the understanding of the Triassic paleogeography (e.g. Torsvik et al., 2002; Gee and Teben'kov, 2004; Gee et al., 2006; Riis et al., 2008; Smelror et al., 2009) (Figure 9.6), it has been proposed that Laurentia, or more specifically Greenland and northern Canada, are the most likely candidates for the western source area (e.g. Mørk et al., 1982, 1999a; Vigran et al., 2014). To test this model, detrital age signatures of the Lower and Middle Triassic formations at the Festningen section may be compared to DZ provenance studies from sedimentary successions that are exposed on northern Greenland today (Figure 9.5). Røhr et al. (2008) present DZ age signatures from Lower Cretaceous sediments from the Wandel Sea Basin, which is located at the eastern corner of Northern Greenland. Their data shows a wide range of age-populations dating from to the late Archean (3000 Ma) to Caledonian ages (400 Ma), but are generally clustered in three main populations. One of these population displays ages between 1900 and 1800 Ga, another between 1700 and 1600 Ma, and a third population between 1100 and 1000 Ma. Zircon ages falling in the intervals between 2400 to 2100 Ma, 1580 to 1510 Ma and 910 to 480 Ma are found to be rare, leaving gaps in the histograms. A similar pattern are also found in Lower Cretaceous sediments in the Sverdrup Basin (Røhr et al., 2010) and Svalbard (Røhr and Andersen, 2009), from which Greenland also was interpreted to be the main source area. In Figure 9.5, the data from Lower and Middle Triassic samples from the Festningen section is correlated to the main age population-patterns found by Røhr et al. (2008, 2010). The correlation display very similar population patterns, and is interpreted to suggest that similar geological domains on Greenland may have sourced sediments to both Svalbard, the Wandel Sea Basin and the Sverdrup basin.

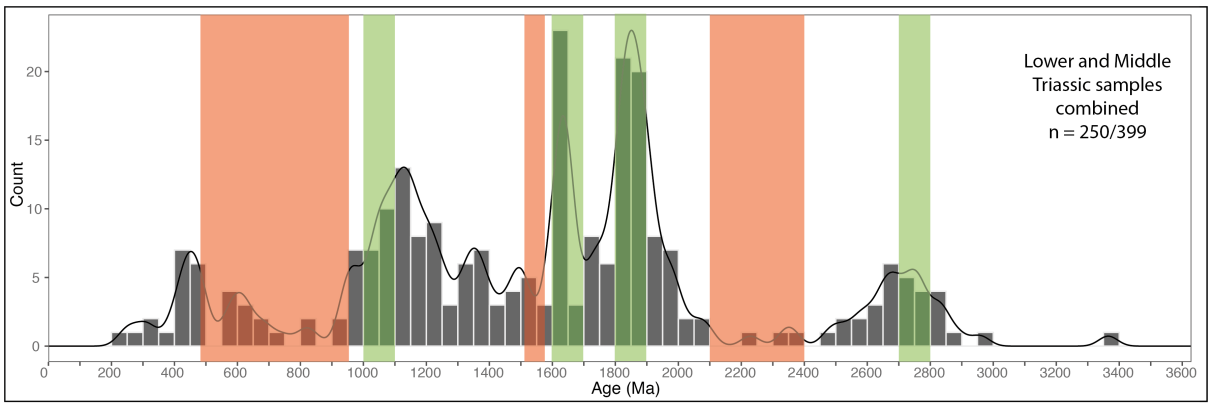

Figure 9.5 *Correlation between data from Svalbard and Greenland. The correlation is based on Lower and Middle Triassic DZ age signatures from Festningen and the findings of Røhr et al. (2008) and Røhr et al. (2010) from the Wandel Sea Basin and the Sverdrup Basin, respectively. Both of the aforementioned studies found Greenland to be the most likely source. The combined histogram and KDE plot is produced using data from all three Lower and Middle Triassic formations at the Festningen section combined (with data from Bue and Andresen (2014)), produced with a histogram binwidth of 50 Ma and a KDE bandwidth of 30 Ma. The coloured sections represent age-intervals that Røhr et al. (2008, 2010) reports as typical for large zircon age-populations (green intervals) or intervals represented by very few zircon ages (orange intervals) in sediments from Greenland. .*

While the likeness-values from the samples of the Tvillingodden and Bravaisberget formations suggest that they stem from same parent zircon population, the Vardebukta Formation has a lower degree of "sameness" when compared the other Lower and Middle Triassic formations at Festningen. A very distinct peak population of Paleoproterozoic grains dating between 1920 and 1820 is the main characteristic for the sample from the Vardebukta Formation. Similar age-populations are also present in the Tvillingodden and Bravaisberget formations, but are not as dominant. Sedimentological and stratigraphic studies have shown that positive highs, such as the Sørkapp-Hornsund High, were still sub-aerially exposed in early Induan times of the Lowermost Triassic (Worsley, 2008; Vigran et al., 2014). This stage corresponds to the interpreted depositional age of the Vardebukta Formation (Mørk et al., 1999a; Egorov and Mørk, 2000; Vigran et al., 2014). Evidence of the emergence of the Sørkapp-Hornsund High is found from the presence of Lower Triassic basal conglomerates and sandstones that rests directly upon folded metamorphic basement rocks in this area (Worsley and Mørk, 1978). Although the DZ age-population signature from the Vardebukta Formation are slightly different from the other Lower and Middle Triassic samples, one cannot exclude the possibility of a common parent population for all three Lower and Middle Triassic formations. A large population of grains dating between 1900 and 1800 Ma was for an example present in samples in the Wandel Sea Basin (Røhr et al., 2008). However, the basement rocks on Svalbard has been interpreted to represent a direct northerly continuation of the Caledonides

on Greenland (Gee et al., 2006), and could thus naturally yield similar DZ age-populations as those found on Greenland. Sedimentation on the Sørkapp-Hornsund High did not start until the mid-Induan (Nakrem and Mørk, 1991), such could potentially, together with other structural highs, have acted as local source areas for the lowermost Triassic deposits on Svalbard, before the highs were progressively flooded and lost their source area potential during the Early Triassic. This hypothesis could be further tested by analysing DZ signatures in the basal conglomerates and sandstones that rests unconformably on top of the basement at the Sørkapp-Hornsund High, and compare the resulting DZ age signatures to the signature of the Vardebukta Formation from the Festningen section.

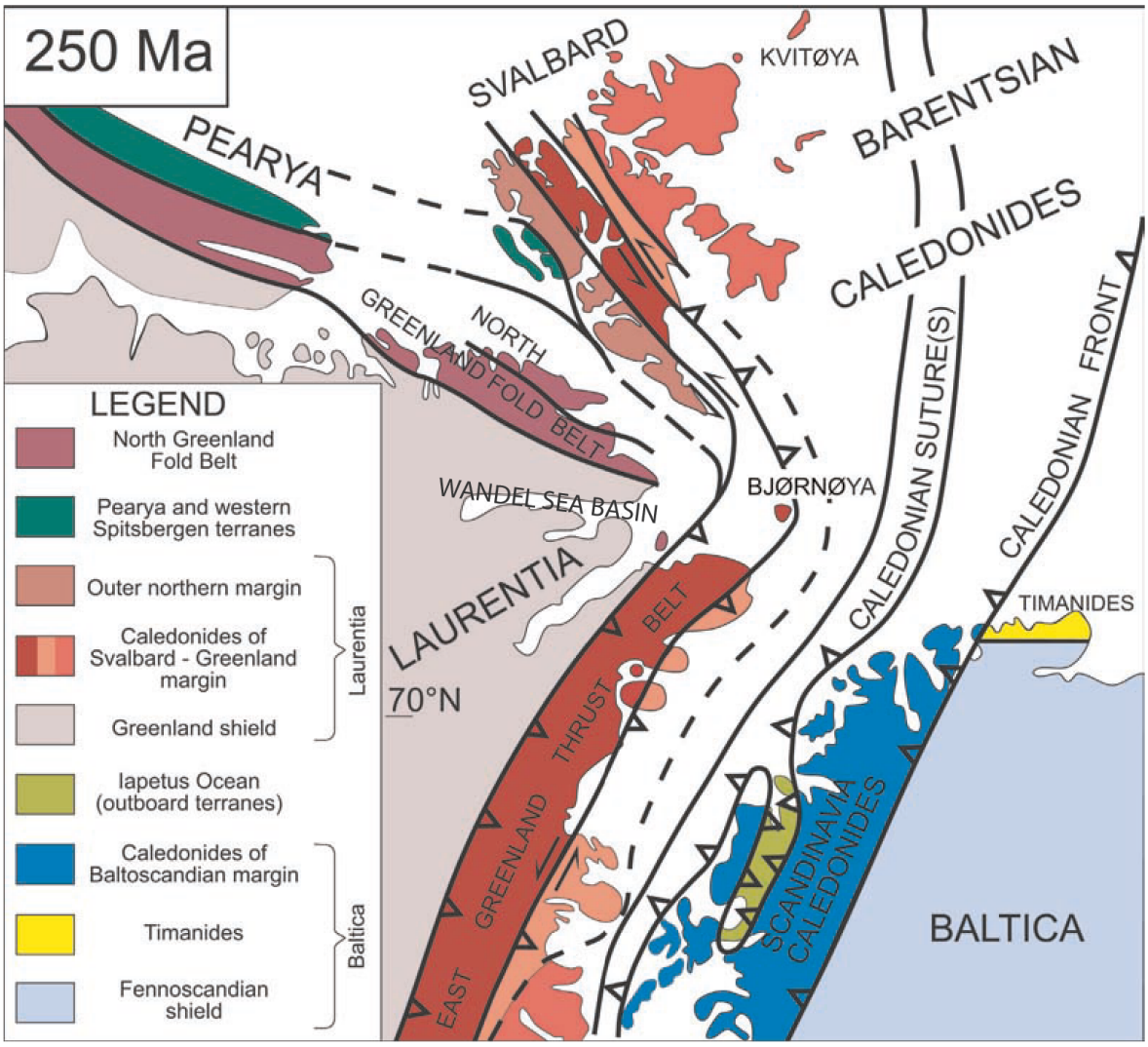

Figure 9.6 *Early Mesozoic paleogeographical reconstruction of the tectonic setting for Svalbard, Laurentia and Baltica. Svalbard was at the time located in a relatively proximal position to the northern parts of Laurentia (Greenland). From Gee and Teben'kov (2004).*

The DZ age signatures for the Lower and Middle Triassic deposits on Svalbard show strong affinities to Greenland. With a dataset that covers a very wide age-span, many of the ages present in the samples will naturally also be present in several source areas surrounding the Barents Sea (presented in Section 2.5). Based on zircon age data alone, it is not possible to fully exclude sediment input from any alternative source areas. However, combined with paleogeographic reconstructions and sedimentological data, the interpretation of a dominant provenance area located to the west, probably represented by the northern parts of Greenland and/or Canada, seems like the most plausible model. This scenario thus stand out as an example of how DZ geochronology as a method in provenance research is best understood when it is combined with other types of data.

9.2.3 The Late Triassic

The DZ U-Pb age data from the Festningen section demonstrates a significant change in provenance signature at the transition from the Middle Triassic to the Upper Triassic succession. The age-populations from the Late Archean to Caledonian age spectrum that characterize the Lower and Middle Triassic succession, are replaced by a more restricted age-population spectrum with a clear dominance of Paleozoic to Early Mesozoic ages in the Upper Triassic succession. As previously mentioned in Section 9.2.1, sedimentological data have suggested a dominance of easterly located sources in the Late Triassic, and based on seismic data from the Barents Sea Shelf it has been suggested that the sediments are dominated erosional products from the Uralian orogeny in the south-east. The data presented in this thesis does not necessarily contradict this model, but may help to refine the definition of an easterly located source.

Bue and Andresen (2014) interpreted domains within the Uralides and possibly Taimyr to be the main provenance areas for the Upper Triassic on Svalbard, accompanied by minor sediment input from Caledonian (Baltica) and possibly Timanide related domains. Uralide granitoids formed almost at a constant rate between 370 Ma to 250 Ma (Vernikovskij et al., 1995; Bea et al., 2002). A large portion of the zircon ages from the samples of the Upper Triassic De Geerdalen Formation on Festningen are placed within this time-interval. However, the most distinct DZ age population is situated within the time-interval between 245 and 235 Ma (Figure 9.7). Zircon-producing events related to the formation of the Uralide Orogeny had to a large extent ceased with the onset of Sibirian Traps related magmatism, which had its main stage around 251-249 Ma (Dalrymple et al., 1995; Czamanske et al., 2000). Early Mesozoic ages that post-date the main stage of the Sibirian Traps magmatic events are common in the

Taimyr region (Czamanske et al., 2000; Vernikovskij et al., 2003; Walderhaug et al., 2005), which is located to the east-northeast of Svalbard at present. Comparing data from published literature and data from sandstones in southern Taimyr, Zhang et al. (2016) found it likely that deposits from several areas surrounding the Taimyr region, including Svalbard and Franz Josef Land, shared common sediment sources from Taimyr, the Siberian Traps and the Polar Urals in the Triassic. Such an interpretation would indicate that there would have been no geographic barriers between Taimyr and Svalbard at the time, which allowed for a direct sediment transportation-route between the two areas. Based on the presence of sediment components that seem to have been eroded of relatively young felsic volcanics or shallow intrusive rocks and deposited in the Barents Sea during the Triassic, Mørk (1999) suggested a north-easterly located source area as a potential provenance area. The influence of a north-easterly located source has later also been proposed by Fleming et al. (2016) and Harstad (2016), working on sample data from the Barents Sea and Svalbard, respectively. In contrast to the north-eastern source area in Taimyr, parts of the potential source areas south of present day Taimyr were probably located east of mountainous and dry land areas where Novaya Zemlya is located today (Preobrazhenskaya et al., 1984; Ulmishek, 1985). For these areas, Novaya Zemlya could have acted as a physical barrier that prevented a direct sediment transportation-route to Svalbard, potentially suggesting that parts of the eastern areas would be less likely to have been dominant source areas. Alternatively, sediments could have been transported around this obstacle. As a potential source area, the Novaya Zemlya Fold Belt has been suggested to have been an important sediment source for the Barents Sea in the Middle Triassic (Milanovsky, 1987).

Based on investigations of the Triassic succession on the Franz Josef Land archipelago, which is located between Svalbard and the Taimyr peninsula, Dypvik et al. (1998) point out several mutual facies relationships between to Triassic succession Svalbard. The sedimentological evidence suggests that the Franz Josef Land area received a considerable amount of sediment from a source located to the east of this archipelago during the Triassic (Preobrazhenskaya et al., 1984; Dypvik et al., 1998), implying that the Taimyr region was an important source area. From samples collected from drillholes in Upper Triassic strata on Franz Josef Land, Soloviev et al. (2015) present large DZ age-populations in the time-intervals between 245-220 Ma and 490-250 Ma. Similar to observations from the Upper Triassic samples at Festningen, the detrital zircon age signature showed a clearly expressed peak at around 233 Ma. Comparison of the signatures from Upper Triassic deposits on Svalbard and Franz Josef Land could indicate an environmental and evolutionary relationship between the deposits from

the two archipelagos, and may support the hypothesis of a similar provenance development on Svalbard and Franz Josef Land (Zhang et al., 2016). In correspondence with models interpreted from seismic data (e.g. Glørstad-Clark et al., 2010; Lundschien et al., 2014), sediments derived from areas along the eastern margin of the Barents Sea reached Franz Josef Land in the Middle Traissic, at an earlier stage than on Svalbard. Soloviev et al. (2015) suggest that the main sediment sources for the Northern Barents Sea in the Middle to Late Triassic were domains located within Uralian orogeny in the south and southeast, but also with input from Baltica, the Timanides, the Taimyr region with rocks related to the Siberian Traps event. In Svalbard, these sources would not have influenced the deposition before the Carnian period of the Late Triassic.

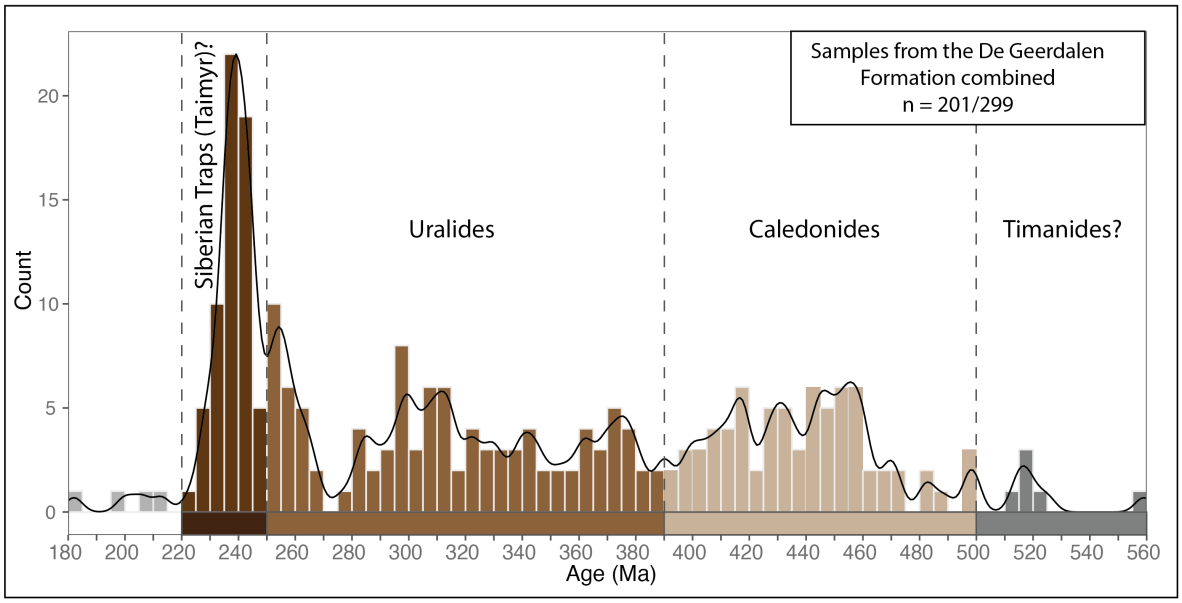

Figure 9.7 *Histogram and KDE of the Paleozoic and Mesozoic part of DZ age signatures, from the two Upper Triassic De Geerdalen Formation samples AA16-49 and P-09-34 from the Festningen section combined. The most likely source domain for the detrital zircon age intervals are indicated. The histogram is produced with a bin width of 5 Ma, and the KDE bandwidth was set at 3 Ma.*

Fleming et al. (2016) pointed out discrepancies between DZ age-population signatures in the Snadd Formation in the southwestern Barents Sea and the De Geerdalen Formation on Svalbard. The characteristic large zircon age-populations of Middle Triassic aged zircons (ca. 245-235 Ma, peak at 237 Ma; Bue and Andresen, 2014) that is observed from the Upper Triassic deposits on Svalbard, is not dominating in the same way in samples from the Snadd Formation. The deposits of the Snadd Formation in the southwestern Barents Sea are to a large degree dominated by DZ ages between 400 and 280 Ma, which correspond to sediments derived from granitoid rocks within the Uralian orogeny (Fleming et al., 2016). The fact that the samples from Festningen are dominated by younger DZ ages does not exclude the possibility of south-

easterly located source areas feeding sediment to Svalbard in the Late Triassic, but it may suggest that Svalbard also received a considerable amount from other sources that yield younger ages (e.g. domains in Taimyr).

The De Geerdalen Formation on Svalbard has been interpreted to have been deposited between the Carnian and Early Norian (Mørk et al., 1999a; Vigran et al., 2014). The Upper Triassic samples that were collected from the Festningen section were taken from the lowermost part of the De Geerdalen Formation, suggesting a depositional age well within the early Carnian Stage for this sample. According to the International Commission on Stratigraphy, the Carnian period lasted from approximately 237 to 227 Ma (Cohen et al., 2013). From shallow stratigraphic cores east of Kong Karls Land, the Ladinian-Carnian stage boundary close to the base of the De Geerdalen Formation has been dated to 236.6-237.5 Ma, based on Re-Os isochron ages (Xu et al., 2014). A Carnian age for the lower part of the De Geerdalen Formation on Hopen has also been suggested on the basis of magnetostratigraphy (Lord et al., 2014a), palynology (Paterson and Mangerud, 2015) and paleoflora studies (Launis et al., 2014). Considering the large DZ age population that falls within the 235-245 Ma age spectra, it is striking how similar these DZ ages are to the depositional age of the De Geerdalen Formation. With the most significant peak at 237 Ma (233 Ma for sample AA16-49), these zircons are found to display a near-syn-depositional age. Given that the zircons were transported from Taimyr or any other easterly located sources, this process would have required a relatively rapid sediment transportation rate. The zircons would have to form, be eroded and transported across the Barents Sea Shelf over the course of only a couple million years. While such a scenario may not be unachievable, other models or processes for bringing the zircons from "source to sink" should at least also be considered.

One process that may be considered is the possibility of zircons being transported and deposited from the air as volcanic ash. Through this process, zircons may be transported over long distances from a eruption centre shortly after formation, and could explain the near-syn-depositional zircon-ages. While volcanic ash beds are not common in the De Geerdalen Formation, Mørk (2013) presents evidence of volcanoclastic components in samples from Late Triassic deposits. As described in Chapter 7, the depositional environment of the De Geerdalen Formation was highly dynamic, with basinal processes like waves and tides that reworked and redistributed the deposits. It is reasonable that potential volcanic ash layers could have been eroded and redistributed within the paralic sediments of the formation after depositon. Given that the near-syn-depositional zircon ages was derived from airborne volcanic ash, the next

question to address would be where to find volcanic centres and the origins of the hypothetical volcanic ash layers.

Today, evidence of granitic and syenetic magmatism and related to the formation of the Sibrian Traps are known from Taimyr (Vernikovskij et al., 1995; Zhang et al., 2016). If this magmetism also had extrusive equivalents, the Taimyr region could represent a candidate for volcanic ash layers to originate from. Volcanic ash beds have also recently been reported to be present in the Triassic succession on Axel Heiberg Island in the Sverdrup Basin (Midwinter et al., 2016). Based on the occurrence of these volcanic ash beds, together with evidence of near-syn-depositional DZ ages and εHf isotope values, Midwinter et al. (2016) argue that the Sverdrup Basin was located proximal to a hypothetical tectonically and magmatically active convergent margin located between the north-western rim of Laurentia and Arctic Alaska Chukotka microplate. Midwinter et al. (2016) interprets the volcanic ash-layers to have been deposited as a result of volcanic activity that prevailed along this margin for approximately 50 Myr during the Late Permian and Triassic. Omma et al. (2011) attributes the near-syn-depositional detrital zircon age signatures of Triassic strata in the Sverdrup Basin to sources in western Siberia (Taimyr, Urals, and Siberian Traps), similar to what is suggested for age-equivalent deposits on Svalbard (Bue and Andresen, 2014; Fleming et al., 2016) and Franz Josef Land (Soloviev et al., 2015). Lithic volcanic clasts that are present in samples from Franz Josef Land, are suggested to have originated from Siberian Plume magmatism (Soloviev et al., 2015). The study of Midwinter et al. (2016) presents an alternative model, where volcanic sediments could have been derived from the active margin area to the north of the Sverdrup Basin. The challenge with this theory is that there are no known remnants of an active margin north of the Sverdrup Basin at present. However, the fact that near-syn-depositional detrital zircon ages also are present in the Upper Triassic samples from the Festningen section could support the theory of Midwinter et al. (2016). It is thought that Svalbard was located in a more proximal position to the Greenland and the Sverdrup Basin in the Triassic (Torsvik et al., 2002). Given the existence of an active margin north of the Svalbard and the Sverdrup Basin, near-syn-depositional aged DZs could have been received from this margin area, either transported southwards through a drainage system or as volcanic ash.

Cawood et al. (2012) shows that multiple DZ ages that fall close to the age of sediment deposition typically characterize the DZ age-populations in basins that receive sediments from an active tectonic margin. From studies of Upper Triassic and Lower Jurassic formations in the Southwestern Barents Sea, Klausen et al. (2016) present DZ age populations with near-syn-depositional DZ ages. In their model, it is proposed that a tectonically and magmatically active

area were located somewhere along the eastern margin of the Barents Sea. It is suggested that this area must have been active at least until the Sinemurian stage of the Early Jurassic. Although no source areas that could have produced Latest Triassic and Early Jurassic zircon ages are known from the areas surrounding the Barents Sea at present, Klausen et al. (2016) suggest that the Novaya Zemlya protrusion of the Northern Uralian Orogeny is a likely candidate. The suggestion is based on evalutions of the regional tectonic setting and paleogeography. The study of Klausen et al. (2016) focus on the Uppermost Triassic to the Lower Jurassic deposits, but it also is pointed out that near-syn-depositional ages exist in the Snadd Formation and its equivalents as well. The formation of the Novaya Zemlya protrution has been dated to Late Triassic/Early Jurassic (Zonenshain et al., 1990; Ritzmann and Faleide, 2009), so it may be reasonable to speculate if it also could have been tectonically and magmatically active during the deposition of the De Geerdalen Formation in the Carnian. If so, the Novaya Zemlya protrusion may represent an additional source area candidate for the near-syn-depositional zircon ages that are displayed in samples from the De Geerdalen Formation.

9.2.4 Summary

Figure 9.8 illustrates an interpreted paleogeographical and paleoenvironmental evolution for Svalbard and the Barents Sea during the Middle and Late Triassic. Figure 9.8A tries to sum up what was discussed in Section 9.2.2, and shows how Svalbard and the area around the Festningen section mainly received sediments from deltaic progradations from the shorelines of Greenland. The deposits from this stage belongs to the Bravaisberget Formation in the areas most proximal to Greenland, while the Botneheia Formation were deposited further out in the basin, under more open marine conditions. The large deltaic system in the eastern Barents Sea had prograded out on the Barents Sea Shelf and filled large areas with sediments, mainly from the Uralides and the Timanides. Figure 9.8B summerizes what was discussed in Section 9.2.3, and shows the evolution during the Early Carnian Stage of the Late Triassic, when the eastern deltaic system reached the Svalbard platform and deposited the De Geerdalen Formation. At this stage, the Festningen area experienced sedimentation in a shallow shelf to shoreface environment. The figure also shows how Late Triassic sediments may have been transported to the Svalbard area through deltaic progradations from the north-east located Taimyr region. Potential transport-routes for the near-syn-depositional DZ ages are also indicated. The landmass called Crockerland (Embry, 1993), situated in the north-western corner on the figure, refers to the hypothetical landmass which has been described in Section 2.5.6, but it may also represent the active margin that has been proposed by Midwinter et al. (2016).

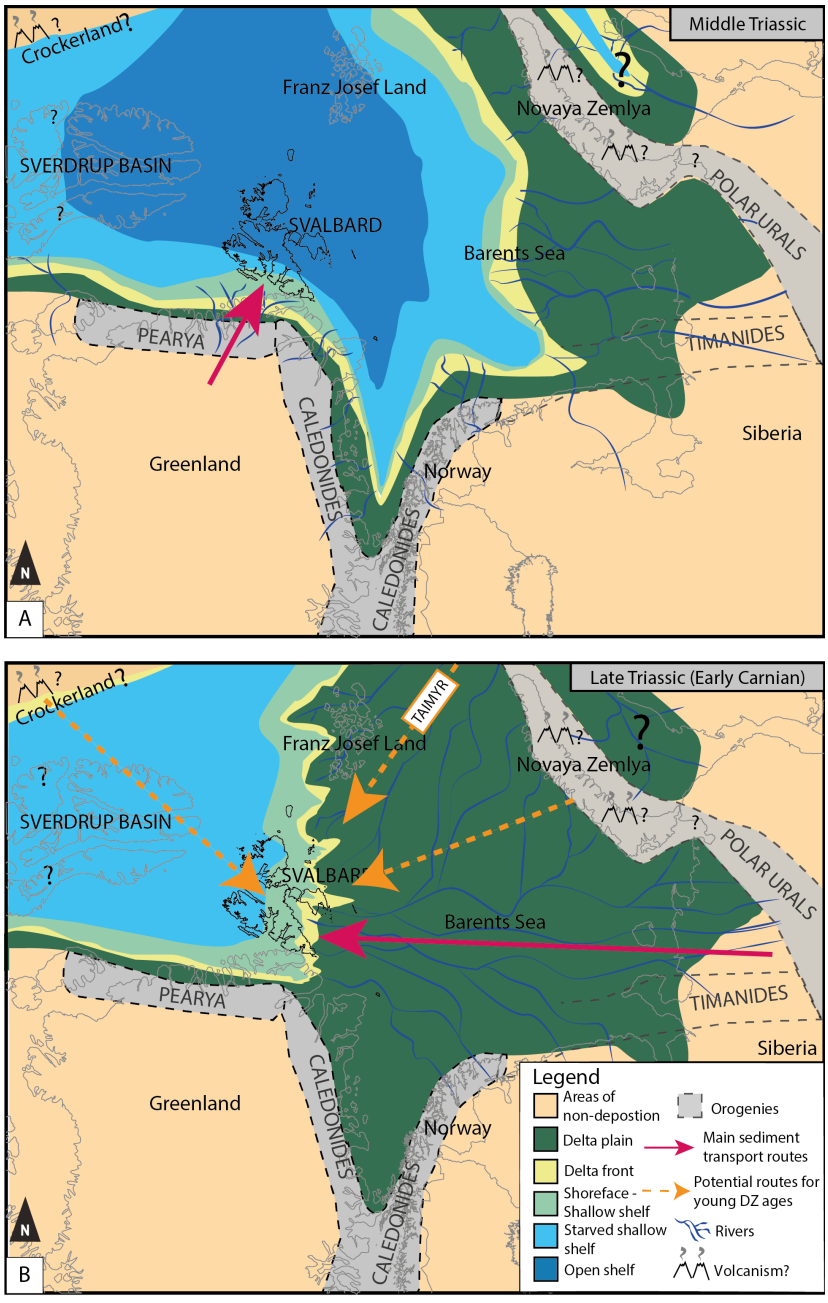

Figure 9.8 *Paleogeographical and -environmental evolution in the Triassic.* ***(A)*** *Middle Triassic evolution. The figure illustrates how Svalbard and the Festningen area received most sediments from deltaic progradations from Greenland. A major delta-system had developed in the east and started to prograde across the Barents Sea Shelf.* ***(B)*** *In the Late Triassic, the eastern deltaic system reached Svalbard. Shoreface and shallow shelf sediments are deposited in front of the system at Festningen.*

Detrital zircon (DZ) geochronology represents a way of testing and constraining depositional models that are proposed based on sedimentological data. Mørk et al. (1982) propose a depositional model for the Upper Triassic on southern half of Spitsbergen and the eastern islands of Svalbard (Figure 9.9), which are based on sedimentological data from various

localities on Svalbard. Since the publication of Mørk et al. (1982), quite a lot of new data has been collected from the Upper Triassic part of the succession on Svalbard, especially in the project of which this thesis is a part of. Mørk et al. (1982) suggest that deltaic progradations from Greenland also dominated the depositional environment on western Spitsbergen in the Late Triassic. In their model, which is shown in Figure 9.9A, fluvial and wave dominated deltaic lobes are protruding around the Festningen and Hornsund-Sørkapp areas. In Figure 9.9B, more recent sedimentological data from Vigran et al. (2014), Rød et al. (2014), Lord et al. (2017a), as well as from this thesis, has been combined with the DZ age data presented herein to construct a new depositional model. As described in Section 9.2.3, the DZ age-populations from Upper Triassic succession at Festningen suggest that sediments were received from easterly located sources, and thus contradict the model from Mørk et al. (1982). Although the sedimentological data may indicate that deltaic sediments were received from the west, the DZ age data suggests the opposite, and the model in Figure 9.9B seems to represent a more likely scenario.

In Figure 9.9B, the westerly derived deltaic lobe in the Sørkapp-Hornsund area (proposed by Mørk et al. (1982), shown in Figure 9.9A) has been replaced by a deltaic lobe that are prograding from the east. The De Geerdalen Formation has its thinnest development on Svalbard in the Sørkapp-Hornsund area, with channel deposits that indicate proximity to a delta (Vigran et al., 2014). The sedimentological development of the De Geerdalen Formation in the Sørkapp-Hornsund area is complex and not fully understood. The models in both Figure 9.9A and Figure 9.9B are both reasonable alternatives, and the scenario is an excellent example of where DZ geochronology may be used to constrain such depositional models.

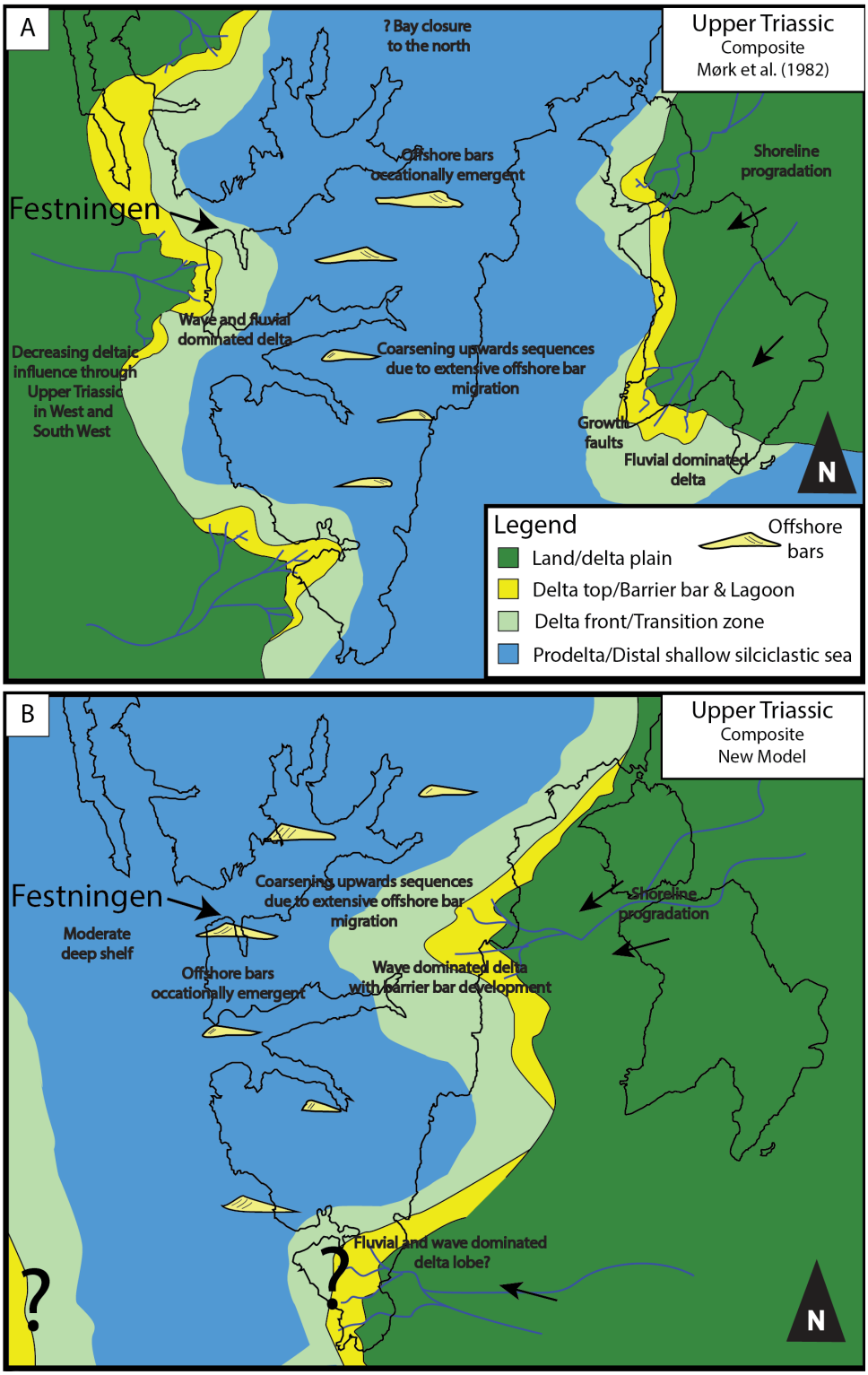

Figure 9.9 *Depositional models for the Upper Triassic on Spitsbergen, Edgeøya and Barentsøya.* ***(A)*** *Model from Mørk et al. (1982). In this model, the western coast of Spitsbergen, including the Festningen area, received deltaic sediments from the west.* ***(B)*** *Model based on sedimentological data from more recent publications and from this thesis, combined with the DZ age data presented herein. In this model, deltaic sediments in the Festningen area come from the east. The evolution in the Sørkapp-Hornsund area in southern Spitsbergen remains uncertain, and are an objective for future DZ age-population analysis.*

9.3 Detrital zircon geochronology in provenance research

U-Pb age analysis of detrital zircon (DZ) is a powerful method which allows for concrete testing and constraining of depositional models that are based on other types of data, such as facies- or seismic data. In this thesis, the application of DZ age analysis has been tested as a technique for investigating provenance in ancient sedimentary systems. The method represents a direct and quantitative way of investigating sedimentation patterns from "sink to source". Recent developments of more advanced and efficient methodology have allowed for rapid collection of large amounts of DZ U-Pb age data. The popularity of the method among geoscientists has grown rapidly, something that is shown by the large number of publications that are dealing with detrital zircon age datasets that have been released over the past decade. However, the method also has its limitations, some of which has been experienced when working with this thesis.

The most common challenges when working with DZ age signatures in provenance research are related to the statistical aspect of the analytical age data. The availability of large amounts of DZ age data has revealed major challenges with regards to the presentation, quantitative interpretation and analysis of the results. Numerous papers dealing with such issues have been published (e.g. Satkoski et al., 2013; Andersen et al., 2016; Andersen et al., 2017), and studying the statistics behind the analysis itself has become a comprehensive branch of the DZ provenance research. The statistical aspects of the analytical DZ data presented in this thesis have not been the main focus, but the data have been treated in a way that are considered sufficient for answering the main research-questions presented herein.

When collecting samples for detrital zircon age analysis, there are always a risk of sampling zircon-free material. This risk may be reduced by collecting several and larger samples, but the risk cannot be fully discarded, as some sedimentary units may not contain any zircons. This challenge was experienced when analysing sample AA16-46. This sample was crushed and washed, and the heavy fraction of the sample was separated with heavy liquid, but the sample proved to be completely dominated by quartz, and no zircons could be found with use of binocular microscopes. Handpicking and recognition of zircons with the help of binocular microscopy is also a process that requires experience, a challenge that was also recognized by the author of this thesis. In the two analysed samples, a relatively high amount of the grains that were picked turned out to be apatite and titanite, and not zircon. It could have been possible to go back and look for more zircons in the samples, but this was not done due to time restrictions and instrument availability.

Another potential source of error is related to the crushing and preparing of samples for analysis. In order to avoid sample contamination, it is important to follow strict cleaning procedures on the lab. Sample contamination potentially presents a major source of error, and such analysis-bias may be hard to reveal. The samples that have been analysed as part of this thesis were treated with caution, following strict procedures used at the Department of Geoscience at the University of Oslo (described in Andersen et al. (2011)), and contamination is not considered as a major source of error for this dataset.

Zircon U-Pb geochronology relies on the presence of two independent isotopic systems, $^{206}Pb/U^{238}$ and $^{207}Pb/U^{235}$. If the ages calculated from the two systems agree, the analysis are regarded as concordant, otherwise the ages are said to be discordant. Discordance occur when the isotopic systems are in some way disturbed. The most common reasons for discordance are related to removal of radiogenic Pb from the crystal structure of zircon by fluid alteration or metamorphism (Pb-loss) or mixing of zircon components with different ages during the analysis (e.g. cores and rims) (Reimink et al., 2016). Analysis of both sample AA16-47 and AA16-49 yielded a significant portion of ages falling outside the ±10% central discordance criteria (Figure 9.10), and these age were therefore not included in the statistical analysis. Bue and Andresen (2014) analysed a sample collected close to sample AA16-49, but got a dataset with a significantly lower portion of discordant analyses. It is not easy to point out a reason for this discrepancy, but it could be a random result of differences occurring in the picking process, where more metamict grains where unconsciously picked from sample AA16-49 compared to sample P-09-34. The analysed zircons found in both samples presented in this thesis, however, were relatively small, and it was noted that the smaller zircons had a tendency of being fractured, which again could have influenced the U-Pb measurements. Reimink et al. (2016) argue that filtering of discordant data may impose biases onto to the final age distributions, where distinct populations of zircons may be selectively removed. Thus, quantitative comparisons of age distributions within and between samples (e.g. 1D likeness tests; Table 9.1), may carry biases already derived from the discordance filtering.

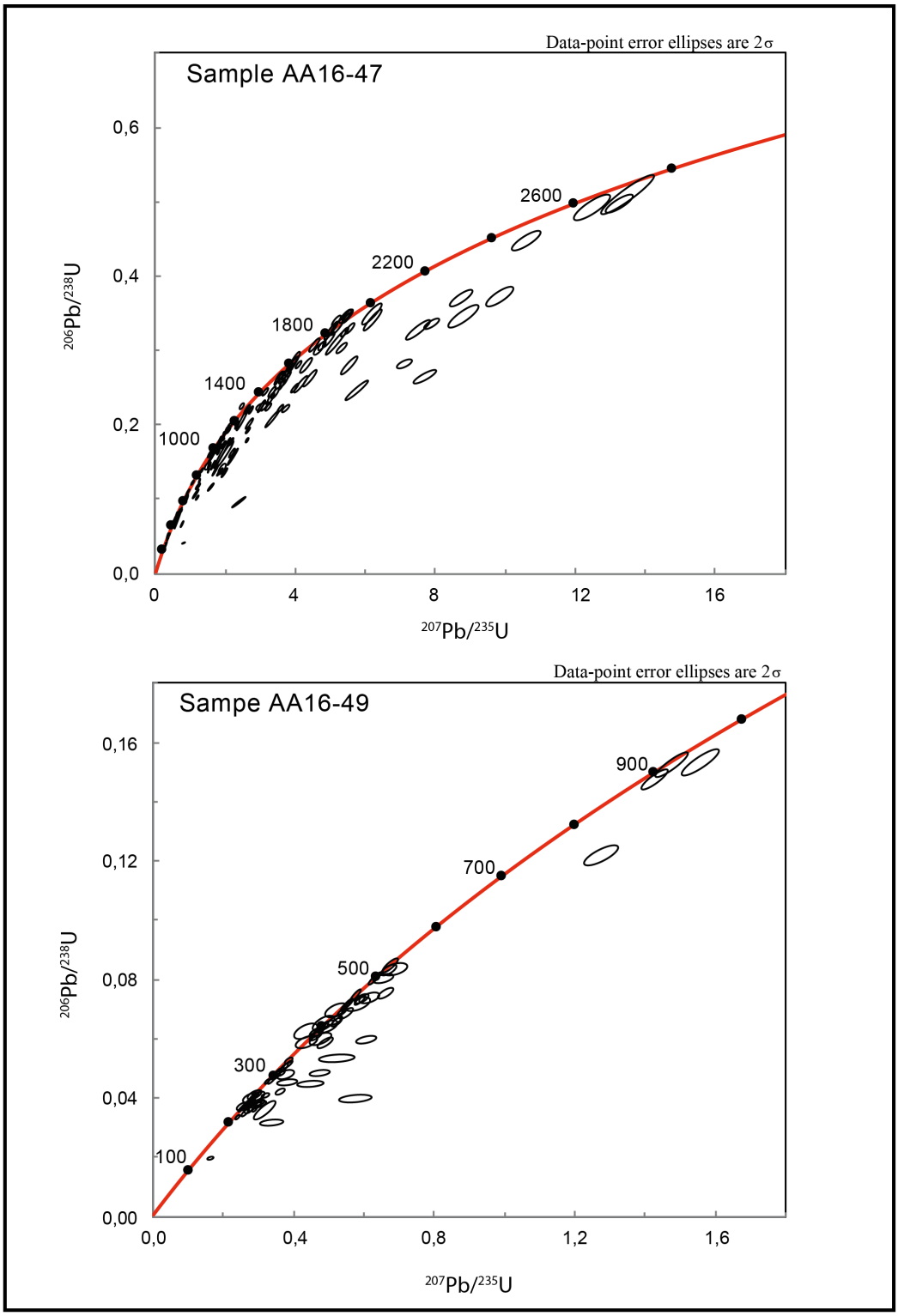

Figure 9.10 *Concordia diagrams for detrital zircon analysis of sample AA16-47 and AA16-49, displaying a high level of discordance. Concordia diagrams are plots of isotope ratios $^{206}Pb^*/^{238}U$ vs. $^{207}Pb^*/^{235}U$, both of which are regarded as being proportional with time. Along the Concordia curve the ^{238}U-^{206}Pb age equals the ^{235}U-^{207}Pb age, and ages that plot on this line are considered 'concordant'. Ages highlighted along the curve on the figure represent reference ages. The figure was produced using Isoplot (Ludwig, 2008).*

When applying the DZ age population analysis for interpreting sediment provenance, it is critical to have a solid control on the crystalline geology of potential source areas. In some cases, several of the potential source areas may share many of the characteristic parent zircon age-populations, and it is therefore not possible to distinguish between the provenance areas solely based on detrital zircon data. Especially with samples that hold a wide range of zircon age-populations this may be a challenge. In such cases it is necessary to combine DZ age-population signatures with other datatypes, such as sedimentological data, to better understand the provenance of the deposits. Sample AA16-47 from this thesis has been interpreted to have been composed of sediments derived from domains within the northern parts of Greenland and Canada. As described in Section 2.5, several of the zircon age-populations from this sample are present in more than one of the potential source areas surrounding the Barents Sea. The interpretation of Greenland and northern Canada as the most likely source area is therefore based several datatypes combined (e.g. facies data and paleogeographic reconstructions). The scenario with sample AA16-47 is another example of how provenance models are most solid when several approaches are combined. Models that are based on DZ geochronology may be constrained themselves when seen in combination with other types of data. An example of such an alternative dataset from Svalbard and the Barents Sea are the petrographic observations presented in Mørk (1999). Based on this dataset, Mørk (1999) interprets basin fill patterns and sediment sources which are consistent with the DZ data presented in this thesis, and suggests Greenland as a likely source for the Lower and Middle Triassic on Svalbard.

Another aspect that should be considered when interpreting DZ age data is the possibility of sedimentary recycling. Zircon is an extremely robust mineral with great abilities to withstand physical abrasion and chemical alteration. In most DZ provenance studies, the DZ age data are thought to reflect protosources in the provenance areas. However, Andersen et al. (2016) point out that recycling of older sedimentary rocks may occur in multiple events in geological time. Extensive recycling may influence the sediments in a way that ensures that zircon signatures may no longer be assigned to a distinct protosource from the present day geological setting. Over long cycles, DZs may be part of sediments that are reworked and redeposited several times, resulting in transportation far away from place the zircons first crystallized. In such cases, the maturity of sandstone deposits may an important indicator for the understanding the degree of recycling, transport length and transport mechanism. One should expect that recycled sediments have a more mature character than sediments that travel more directly from “source to sink”.

Sample AA16-47 was collected from the Bravaisberget Formation. This formation contains sub-mature to mature sandstones (Krajewski et al., 2007), and the units of may have experienced extensive recycling. Røhr et al. (2010) suggests that the Lower Cretaceous sediments from both the Wandel Sea Basin and the Sverdrup Basin were to a large degree eroded and redeposited from metamorphosed sediments within Caledonian Thrust Sheets. This may well also be the case for the sediments in the Bravaisberget Formation on Svalbard. Nevertheless, Caledonian Thrust Sheets are present on Greenland, and sediment recycling would therefore not change the provenance model presented in this thesis.

Sample AA16-49 however, were collected from the more immature sands of the De Geerdalen Formation, which are not believed to have subjected to sediment recycling. Further up in the stratigraphy, the DZ age population of the overlying Wilhelmøya Subgroup seem to represent a mixture of the zircon populations that are present in the Lower Triassic and the Upper Triassic (Bue and Andresen, 2014), which could indicate sediment recycling as a result of reworking of the older formations. This theory is supported by the mineralogical maturity of the sandstones in the Wilhelmøya Subgroup, which are significantly more mature than sandstones in the De Geerdalen Formation (Vigran et al., 2014).

In summary, the application of detrital zircon geochronology represents an indispensable tool for investigating the provenance of sedimentary successions. However, as highlighted in this section, several aspects of the analysis should be considered fully understand and interpret the data that are retrieved from it correctly.

10 Conclusions

- Facies observations from the De Geerdalen Formation in Fulmardalen are consistent with the previous studies of Knarud (1980), Mørk et al. (1982), Rød et al. (2014) and Lord et al. (2017a), and suggests that the formation was deposited in a paralic delta environment.
- The vertical evolution through the formation records a transition from distal to a more proximal depositional environment. Shale dominated, shallow marine facies that occur at base of the formation are gradually replaced by more sand-rich delta front facies. The upper part of the formation displays delta plain facies, with characteristic features for the Isfjorden Member.
- Data from Fulmardalen highlights the paralic nature of the De Geerdalen Formation, with significant facies variations over relatively short distances in both vertical and lateral directions. The number of stacked upwards coarsening sequences, interpreted as parasequences, varies between the localities in Fulmardalen. The stacking pattern is interpreted to be a result of delta lobe switching and repeated shoreline progradations.
- The sediments of the De Geerdalen Formation in Fulmardalen represent a relatively fine grained system, deposited with a relatively flat gradient and restricted accommodation space, where the sediments have experienced significant modulation from basinal processes such as wave- and tidal energy.
- Sandstone thickness and geometry varies vertically through the formation. The largest sandstone bodies are found in the lower parts of the formation, and can be described as laterally continuous with a relatively homogenous thickness, and have been interpreted as barrier bar complexes. The barrier bar complexes can be traced across the whole study area. Sandstones higher up in the formation are generally thinner and less continuous, and have been interpreted as smaller barrier complexes, subaqueous banks, distributary and tidal channels, crevasse splay deposits etc.
- Regional facies correlations across Spitsbergen shows a gradual trend from a more proximal to a more distal facies expression from the SE towards the NW. On a larger scale, the wave and tidally influenced facies expression on

Spitsbergen has a more distal character than the more fluvial influenced facies expression from the eastern islands of Svalbard.

- The results from detrital zircon (DZ) age analysis of samples from the Festningen section display two significantly different age-population signatures. While analysis of the Middle Traissic Bravaisberget Formation yielded a wide span of age-populations from the Archean to the Paleozoic, the sample from the Upper Triassic De Geerdalen Formation is clearly dominated by Paleozoic and Early Mesozoic detrital zircon ages.
- The discrepancies between the DZ age signatures indicate a major shift in provenance happening at the transition between the Middle Triassic and Upper Triassic at the Festningen section. This shift has previously also been proposed based on sedimentological evidence (Mørk et al., 1999a; Vigran et al., 2014).
- The DZ age signature from the Bravaisberget Formation resembles the signature from the underlying Vardebukta and Tvillingodden formations, presented in Bue and Andresen (2014). Comparisons with published DZ age data suggest that geological domains on Greenland are the most likely sediment sources for this part of the succession, potentially with contribution from local positive highs and structures for the Vardebukta Formation.
- The DZ age signature from the De Geerdalen Formation strongly resemble the age signatures obtained from samples of the same formation that were tested by Bue and Andresen (2014). The most likely source domains for this part of the succession has been interpreted to have been located within the Uralides and the Taimyr region, with additional input from the Caledonian and Timanide domains.
- Near-syn-depositonal DZ ages in the samples from the De Geerdalen Formation may suggest a rapid transportation rate from source to sink. Alternatively, the DZ ages indicate the presence of a proximal, unidentified tectonically and magmatically active margin from the Triassic, or they reflect deposition of zircons from airborne volcanic ash.

11 Suggestions for further work

- Triassic outcrops at Oscar II Land, which is directly north of the Festningen section at western Spitsbergen, are heavily tectonized and therefore not fully understood. The area will be investigated by NTNU students during fieldwork in 2017, and the results from this work may provide valuable information to the facies and structural development for the Traissic succession on western Spitsbergen.
- The Tschermakfjellet Formation is very thin or absent at the Festningen profile. This formation has been suggested to have been deposited in a prodeltaic environment in front of the deltaic deposits from the overlying De Geerdalen Formation. By dating detrital zircons (DZ) from siltstone (or sandstone if present) benches within this unit, it may be possible to test this hypothesis.
- *In situ* Hf-isotope analysis is often combined with U-Pb dating of DZ, but such an analysis was not carried out in this study. While the U-Pb systems mainly records the crystallization-age of a zircon, the Hf-isotope system offers information on the evolution of the (proto)source rock (magma from juvenile mantle vs. recycled crust). To get a better understanding and constraint on the DZ sources of the De Geerdalen Formation, any future analysis could additionally investigate the Hf-signature of the zircons.
- The Sørkapp-Hornsund area are thought to have been an emerged platform high during the early stages of the Triassic, and could represent a local source for sediments of the Vardebukta Formation on Svalbard. This theory could be tested by conducting a DZ analysis of the basal sandstones and conglomerates that are present on the Sørkapp-Hornsund High, and compare it to DZ data from the Vardebukta Formation in the Festningen section.
- The De Geerdalen Formation on the Sørkapp-Hornsund High has the thinnest development on Svalbard and are not fully understood. Mørk et al. (1982) has suggest that the deltaic sediments were derived from the west. This model could be tested by applying DZ age analysis on samples from De Geerdalen Formation in this area.

References

Alonso-Zarza, A. M. and Wright, V. (2010) Calcretes, *Developments in Sedimentology*, 61, pp. 225-267.

Andersen, T., Andresen, A. and Sylvester, A. (2002) Timing of late-to post-tectonic Sveconorwegian granitic magmatism in South Norway, *Norges Geologiske Undersøkelse Bulletin*, 440, pp. 5-18.

Andersen, T., Andersson, U. B., Graham, S., Åberg, G. and Simonsen, S. L. (2009) Granitic magmatism by melting of juvenile continental crust: new constraints on the source of Palaeoproterozoic granitoids in Fennoscandia from Hf isotopes in zircon, *Journal of the Geological Society*, 166(2), pp. 233-247.

Andersen, T., Saeed, A., Gabrielsen, R. H. and Olaussen, S. (2011) Provenance characteristics of the Brumunddal sandstone in the Oslo Rift derived from U-Pb, Lu-Hf and trace element analyses of detrital zircons by laser ablation ICMPS, *Norwegian Journal of Geology*, 91, pp. 1-19.

Andersen, T., Kristoffersen, M. and Elburg, M. A. (2016) How far can we trust provenance and crustal evolution information from detrital zircons? A South African case study, *Gondwana Research*, 34, pp. 129-148.

Andersen, T., Kristoffersen, M. and Elburg, M. A. (2017) Visualizing, interpreting and comparing detrital zircon age and Hf isotope data in basin analysis - a graphical approach., *Basin Research*, pp. 39. doi: 10.1111/bre.12245.

Andresen, A., Haremo, P., Swensson, E. and Bergh, S. G. (1992) Structural geology around the southern termination of the Lomfjorden Fault Complex, Agardhdalen, east Spitsbergen, *Norsk Geologisk Tidsskrift*, 72(1), pp. 83-91.

Andresen, A., Rehnström, E. and Holte, M. (2007) Evidence for simultaneous contraction and extension at different crustal levels during the Caledonian orogeny in NE Greenland, *Journal of the Geological Society*, 164(4), pp. 869-880.

Anell, I., Braathen, A., Olaussen, S. and Osmundsen, P. (2013) Evidence of faulting contradicts a quiescent northern Barents Shelf during the Triassic, *First Break*, 31(6), pp. 67-76.

Anell, I., Braathen, A. and Olaussen, S. (2014a) The Triassic--Early Jurassic of the northern Barents Shelf: a regional understanding of the Longyearbyen CO 2 reservoir, *Norwegian Journal of Geology/Norsk Geologisk Forening*, 94, pp. 83-98.

Anell, I., Midtkandal, I. and Braathen, A. (2014b) Trajectory analysis and inferences on geometric relationships of an Early Triassic prograding clinoform succession on the northern Barents Shelf, *Marine and Petroleum Geology*, 54, pp. 167-179.

Anfinson, O. A., Embry, A. F. and Stockli, D. F. (2016) Geochronologic constraints on the Permian–Triassic northern source region of the Sverdrup basin, Canadian Arctic Islands, *Tectonophysics*, 691, pp. 206-219.

Bea, F., Fershtater, G. and Montero, P. (2002) Granitoids of the Uralides: Implications for the evolution of the orogen, *Mountain Building in the Uralides: Pangea to the Present*, pp. 211-232.

Bergan, M. and Knarud, R. (1993) Apparent changes in clastic mineralogy of the Triassic–Jurassic succession, Norwegian Barents Sea: possible implications for palaeodrainage and subsidence, *Arctic Geology and Petroleum Potential, Norwegian Petroleum Society (NPF), Special Publication*, 2, pp. 481-493.

Bergh, S. G., Braathen, A. and Andresen, A. (1997) Interaction of basement-involved and thin-skinned tectonism in the Tertiary fold-thrust belt of central Spitsbergen, Svalbard, *AAPG bulletin*, 81(4), pp. 637-661.

Bhattacharya, H., Bhattacharya, B., Chakraborty, I. and Chakraborty, A. (2004) Sole marks in storm event beds in the Permo-Carboniferous Talchir Formation, Raniganj basin, India, *Sedimentary Geology*, 166(3), pp. 209-222.

Bhattacharya, J. P. (1992) Deltas, in Walker, R. and James, N. (ed.) *Facies Models.* Geological Association of Canada, pp. 157-177.

Bhattacharya, J. P. and Giosan, L. (2003) Wave-influenced deltas: Geomorphological implications for facies reconstruction, *Sedimentology*, 50(1), pp. 187-210.

Bhattacharya, J. P. (2006) Deltas, *Special Publication-SEPM*, 84, pp. 237.

Bhattacharya, J. P. and MacEachern, J. A. (2009) Hyperpycnal rivers and prodeltaic shelves in the Cretaceous seaway of North America, *Journal of Sedimentary Research*, 79(4), pp. 184-209.

Blomeier, D. (2015) Historical Geology - Permian, in Dallmann, W. (ed.) *Geoscience Atlas of Svalbard.* Norsk Polarinstitutt, pp. 110-113.

Boggs, S. (2009) *Petrology of sedimentary rocks*. Second edn. Cambridge University Press.

Boggs, S. (2011) *Principles of sedimentology and stratigraphy*. Fifth edn. Pearson Prentice Hall.

Boyd, R. and Penland, S. (1988) A geomorphologic model for Mississippi Delta evolution, *Gulf Coast Association of Geological Societies Transactions*, 38, pp. 443-452.

Braathen, A., Bergh, S. G. and Maher, H. D. (1999) Application of a critical wedge taper model to the Tertiary transpressional fold-thrust belt on Spitsbergen, Svalbard, *Geological Society of America Bulletin*, 111(10), pp. 1468-1485.

Buchan, S., Challinor, A., Harland, W. and Parker, J. (1965) The Triassic stratigraphy of Svalbard, *Norsk Polarinstitutt Skrifter*, 35, pp. 93.

Bue, E. P. and Andresen, A. (2014) Constraining depositional models in the Barents Sea region using detrital zircon U–Pb data from Mesozoic sediments in Svalbard, *Geological Society, London, Special Publications*, 386(1), pp. 261-279.

Bugge, T., Elvebakk, G., Fanavoll, S., Mangerud, G., Smelror, M., Weiss, H. M., Gjelberg, J., Kristensen, S. E. and Nilsen, K. (2002) Shallow stratigraphic drilling applied in hydrocarbon exploration of the Nordkapp Basin, Barents Sea, *Marine and Petroleum Geology*, 19(1), pp. 13-37.

Buiter, S. J. and Torsvik, T. H. (2007) Horizontal movements in the eastern Barents Sea constrained by numerical models and plate reconstructions, *Geophysical Journal International*, 171(3), pp. 1376-1389.

Cawood, P. A., Hawkesworth, C. and Dhuime, B. (2012) Detrital zircon record and tectonic setting, *Geology*, 40(10), pp. 875-878.

Clifton, H. (2006) A reexamination of facies models for clastic shorelines, *Special Publication-SEPM*, 84, pp. 293.

Cohen, K., Finney, S., Gibbard, P. and Fan, J.-X. (2013) The ICS international chronostratigraphic chart, *Episodes*, 36(3), pp. 199-204.

Collinson, J. (1996) Alluvial sediments, *Sedimentary environments: processes, facies and stratigraphy*, 3, pp. 37-82.

Collinson, J. D., Mountney, N. and Thompson, D. (2006) *Sedimentary Structures*. Third edn. Terra Publishing.

Corfu, F., Polteau, S., Planke, S., Faleide, J. I., Svensen, H., Zayoncheck, A. and Stolbov, N. (2013) U–Pb geochronology of Cretaceous magmatism on Svalbard and Franz Josef Land, Barents Sea large igneous province, *Geological Magazine*, 150(06), pp. 1127-1135.

Czamanske, G. K., Wooden, J. L., Walker, R. J., Fedorenko, V. A., Simonov, O. N., Budahn, J. R. and Siems, D. F. (2000) Geochemical, isotopic, and SHRIMP age data for Precambrian basement rocks, Permian volcanic rocks, and sedimentary host rocks to the

ore-bearing intrusions, Noril'sk-Talnakh District, Siberian Russia, *International Geology Review*, 42(10), pp. 895-927.
Dallmann, W. K. (2015) *Geoscience Atlas of Svalbard*. Norwegian Polar Institute
Dallmann, W. K., Elvevold, S., Majka, J. and Piepjohn, K. (2015) Tectonics and tectonothermal events, in Dallmann, W. (ed.) *Geoscience Atlas of Svalbard.* Norwegian Polar Institute, pp. 175-217.
Dalrymple, G. B., Czamanske, G. K., Fedorenko, V. A., Simonov, O. N., Lanphere, M. A. and Likhachev, A. P. (1995) A reconnaissance 40Ar39Ar geochronologic study of ore-bearing and related rocks, Siberian Russia, *Geochimica et Cosmochimica Acta*, 59(10), pp. 2071-2083.
Dalrymple, R. (1999) Tide-dominated deltas: do they exist or are they all estuaries, *American Association of Petroleum Geologists Annual Meeting, Official Program, San Antonio*. pp. A29-A30.
Dalrymple, R. (2010) Interpreting sedimentary successions: facies, facies analysis and facies models, *Facies models*, 4(2), pp. 3-18.
Dalrymple, R. W. and Choi, K. (2007) Morphologic and facies trends through the fluvial–marine transition in tide-dominated depositional systems: a schematic framework for environmental and sequence-stratigraphic interpretation, *Earth-Science Reviews*, 81(3), pp. 135-174.
Davis Jr, R. A. (2012) Tidal signatures and their preservation potential in stratigraphic sequences, in Davis Jr, R. and Dalrymple, R. (ed.) *Principles of tidal sedimentology.* Springer Sciene+Business Media B.V, pp. 35-55.
De Raaf, J. and Boersma, J. (2007) Tidal deposits and their sedimentary structures (seven examples from Western Europe), *Netherlands Journal of Geosciences/Geologie en Mijnbouw*, 50, pp. 479-504.
Doré, A. (1995) Barents Sea geology, petroleum resources and commercial potential, *Arctic*, pp. 207-221.
Dumas, S. and Arnott, R. (2006) Origin of hummocky and swaley cross-stratification—the controlling influence of unidirectional current strength and aggradation rate, *Geology*, 34(12), pp. 1073-1076.
Dypvik, H., Sokolov, A., Pcelina, T., Fjellså, B., Bjærke, T., Korchinskaja, M. and Nagy, J. (1998) The Triassic successions of Franz Josef Land, stratigraphy and sedimentology of three wells from Alexandra, Hayes and Graham-Bell islands, *Geological aspects of Franz Josef Land and the northernmost Barents Sea—the Northern Barents Sea Geotraverse. Norsk Polarinstitutt Meddelelser*, 151, pp. 50-82.
Edwards, M. B. (1976) Growth faults in Upper Triassic deltaic sediments, Svalbard, *AAPG Bulletin*, 60(3), pp. 341-355.
Egorov, A. Y. and Mørk, A. (2000) The East Siberian and Svalbard Triassic successions and their sequence stratigraphical relationships, *Zentralblatt für Geologie und Paläontologie, Teil*, 1, pp. 1377-1430.
Elliott, T. (1986) Deltas, *Sedimentary environments and facies*, 2, pp. 113-154.
Elvevold, S., Dallmann, W. and Blomeier, D. (2007) *Geology of Svalbard*. Norwegian Polar Institute.
Elvevold, S. and Dallmann, W. (2015a) Historical Geology - Pre-Caledonian Era, in Dallmann, W. (ed.) *Geoscience Atlas of Svalbard.* Norwegian Polar Institute, pp. 94-97.
Elvevold, S. and Dallmann, W. (2015b) Historical Geology - Caledonian period, in Dallmann, W. (ed.) *Geoscience Atlas of Svalbard.* Norwegian Polar Institute, pp. 98-101.

Embry, A. (1993) Transgressive–regressive (T–R) sequence analysis of the Jurassic succession of the Sverdrup Basin, Canadian Arctic Archipelago, *Canadian Journal of Earth Sciences*, 30(2), pp. 301-320.

Embry, A. (2009) Crockerland–The Source Area for the Triassic to Middle Jurassic Strata of Northern Axel Heiberg Island, Canadian Arctic Islands, *Bulletin of Canadian Petroleum Geology*, 57(2), pp. 129-140.

Enga, J. (2015) *Paleosols in the Triassic De Geerdalen and Snadd formations*. Master's Thesis, Norwegian University of Science and Technology, 127pp.

Eyles, N. and Lagoe, M. B. (1989) Sedimentology of shell-rich deposits (coquinas) in the glaciomarine upper Cenozoic Yakataga Formation, Middleton Island, Alaska, *Geological Society of America Bulletin*, 101(1), pp. 129-142.

Faleide, J. I., Gudlaugsson, S. T. and Jacquart, G. (1984) Evolution of the western Barents Sea, *Marine and Petroleum Geology*, 1(2), pp. 123-150.

Faleide, J. I., Tsikalas, F., Breivik, A. J., Mjelde, R., Ritzmann, O., Engen, O., Wilson, J. and Eldholm, O. (2008) Structure and evolution of the continental margin off Norway and the Barents Sea, *Episodes*, 31(1), pp. 82-91.

Fleming, E. J., Flowerdew, M. J., Smyth, H. R., Scott, R. A., Morton, A. C., Omma, J. E., Frei, D. and Whitehouse, M. J. (2016) Provenance of Triassic sandstones on the southwest Barents Shelf and the implication for sediment dispersal patterns in northwest Pangaea, *Marine and petroleum geology*, 78, pp. 516-535.

Flood, B., Nagy, J. and Winsnes, T. S. (1971) The Triassic succession of Barentsøya, Edgeøya, and Hopen (Svalbard), *Norsk Polarinstitutt Meddelelser*, 100, pp. 20.

Gabrielsen, R. H., Faerseth, R. B. and Jensen, L. N. (1990) *Structural Elements of the Norwegian Continental Shelf. Pt. 1. The Barents Sea Region*. Norwegian Petroleum Directorate.

Galloway, W. E. (1975) Process framework for describing the morphologic and stratigraphic evolution of deltaic depositional systems, *Deltas: Models for Exploration*, pp. 87-98.

Gee, D., Bogolepova, O. and Lorenz, H. (2006) The Timanide, Caledonide and Uralide orogens in the Eurasian high Arctic, and relationships to the palaeo-continents Laurentia, Baltica and Siberia, *Geological Society, London, Memoirs*, 32(1), pp. 507-520.

Gee, D. G. and Teben'kov, A. (2004) Svalbard: a fragment of the Laurentian margin, *Geological Society, London, Memoirs*, 30(1), pp. 191-206.

Glørstad-Clark, E., Faleide, J. I., Lundschien, B. A. and Nystuen, J. P. (2010) Triassic seismic sequence stratigraphy and paleogeography of the western Barents Sea area, *Marine and Petroleum Geology*, 27(7), pp. 1448-1475.

Glørstad-Clark, E. (2011) *Basin analysis in the western Barents Sea area: the interplay between accommodation space and depositional systems*. PhD Thesis, University of Oslo, 252pp.

Glørstad-Clark, E., Birkeland, E., Nystuen, J., Faleide, J. and Midtkandal, I. (2011) Triassic platform-margin deltas in the western Barents Sea, *Marine and Petroleum Geology*, 28(7), pp. 1294-1314.

Gower, C., Ryan, A. and Rivers, T. (1990) Mid-Proterozoic Laurentia–Baltica: an overview of its geological evolution and a summary of the contributions made by this volume, *Mid-Proterozoic Laurentia-Baltica*, 38, pp. 1-20.

Gower, C. F. and Krogh, T. E. (2002) AU–Pb geochronological review of the Proterozoic history of the eastern Grenville Province, *Canadian Journal of Earth Sciences*, 39(5), pp. 795-829.

Gressly, A. (1838) Observations géologiques sur le Jura soleurois, *Neuchâtel: Nouveaux mémoires de la Société Helvétique des Sciences Naturelles*, 2.

Grundvåg, S.-A. (2015) Historical Geology - Cretaceous, in Dallmann, W. (ed.) *Geoscience Atlas of Svalbard.* Norwegian Polar Institute, pp. 122-125.

Harstad, T. (2016) *Sandstone Provenance of the De Geerdalen Formation, Svalbard. Emphasis on Petrography and Chromium Spinel Compostitions*. Master Thesis, Norwegian Unversity of Science and Technology, 98pp.

Haugen, T. (2016) *A Sedimentologicalal Study of the De Geerdalen Formation with Focus on the Isfjorden Member and Palaeosols*, Norwegian University of Science and Technology, 155pp.

Hellman, F. J., Gee, D. G. and Witt-Nilsson, P. (2001) Late archean basement in the bangenhuken complex of the Nordbreen Nappe, western Ny-Friesland, Svalbard, *Polar Research*, 20(1), pp. 49-59.

Henriksen, E., Ryseth, A., Larssen, G., Heide, T., Rønning, K., Sollid, K. and Stoupakova, A. (2011) Chapter 10 Tectonostratigraphy of the greater Barents Sea: implications for petroleum systems: Geological Society, *London, Memoirs*, 32, pp. 163-195.

Higgins, A. and Leslie, A. (2000) Restoring thrusting in the East Greenland Caledonides, *Geology*, 28(11), pp. 1019-1022.

Hoel, A. and Orvin, A. K. (1937) Das Festungsprofil auf Spitzbergen. Karbon-Kreide I: Vermessungsresultate, *Norges Svalbard- og Ishavs Undersøkelser Skrifter*, 18, pp. 59.

Hofmann, H. (1973) Stromatolites: characteristics and utility, *Earth-Science Reviews*, 9(4), pp. 339-373.

Hori, K., Saito, Y., Zhao, Q. and Wang, P. (2002) Evolution of the coastal depositional systems of the Changjiang (Yangtze) River in response to late Pleistocene-Holocene sea-level changes, *Journal of Sedimentary Research*, 72(6), pp. 884-897.

Hormes, A. and Dallmann, W. K. (2015) Neogene and Quaternary, in Dallmann, W. K. (ed.) *Geoscience Atlas of Svalbard.* Norwegian Polar Institute, pp. 130-131.

Howell, J. A., Skorstad, A., MacDonald, A., Fordham, A., Flint, S., Fjellvoll, B. and Manzocchi, T. (2008) Sedimentological parameterization of shallow-marine reservoirs, *Petroleum Geoscience*, 14(1), pp. 17-34.

Huhma, H., Mänttäri, I., Peltonen, P., Kontinen, A., Halkoaho, T., Hanski, E., Hokkanen, T., Hölttä, P., Juopperi, H. and Konnunaho, J. (2012) The age of the Archaean greenstone belts in Finland, *Geological Survey of Finland, Special Paper*, 54, pp. 74-175.

Hynne, I. (2010) *Depositional environment on eastern Svalbard and central Spitsbergen during Carnian time (Late Triassic)*, Master thesis, Norwegian University of Science and Technology, Trondheim, Norway.

Høy, T. and Lundschien, B. (2011) Triassic deltaic sequences in the northern Barents Sea, *Geological Society, London, Memoirs*, 35(1), pp. 249-260.

Jackson, S. E., Pearson, N. J., Griffin, W. L. and Belousova, E. A. (2004) The application of laser ablation-inductively coupled plasma-mass spectrometry to in situ U–Pb zircon geochronology, *Chemical Geology*, 211(1), pp. 47-69.

Johansen, S. K. (2016) *Sedimentology and facies distribution of the Upper Triassic De Geerdalen Formation in the Storfjorden area and Wilhelmøya, eastern Svalbard*. Master's Thesis, Norwegian University of Science and Technology, 179pp.

Johnson, H. and Baldwin, C. (1996) Shallow clastic seas, *Sedimentary environments: processes, facies and stratigraphy*, pp. 232-280.

Kalsbeek, F., Nutman, A. P. and Taylor, P. N. (1993) Palaeoproterozoic basement province in the Caledonian fold belt of North-East Greenland, *Precambrian Research*, 63(1-2), pp. 163-178.

Kalsbeek, F., Thrane, K., Nutman, A. P. and Jepsen, H. F. (2000) Late Mesoproterozoic to early Neoproterozoic history of the East Greenland Caledonides: evidence for Grenvillian orogenesis?, *Journal of the Geological Society*, 157(6), pp. 1215-1225.

Kalsbeek, F., Jepsen, H. F. and Nutman, A. P. (2001) From source migmatites to plutons: tracking the origin of ca. 435 Ma S-type granites in the East Greenland Caledonian orogen, *Lithos*, 57(1), pp. 1-21.

Ketzer, J. M., Holz, M., Morad, S. and Al-Aasm, I. (2003) Sequence stratigraphic distribution of diagenetic alterations in coal-bearing, paralic sandstones: evidence from the Rio Bonito Formation (early Permian), southern Brazil, *Sedimentology*, 50(5), pp. 855-877.

Klausen, T. and Mørk, A. (2014) The Upper Triassic paralic deposits of the De Geerdalen Formation on Hopen: outcrop analog to the subsurface Snadd Formation in the Barents Sea, *AAPG Bulletin*, 98(10), pp. 1911-1941.

Klausen, T. G., Ryseth, A. E., Helland-Hansen, W., Gawthorpe, R. and Laursen, I. (2014) Spatial and temporal changes in geometries of fluvial channel bodies from the Triassic Snadd Formation of offshore Norway, *Journal of Sedimentary Research*, 84(7), pp. 567-585.

Klausen, T. G., Ryseth, A. E., Helland-Hansen, W., Gawthorpe, R. and Laursen, I. (2015) Regional development and sequence stratigraphy of the Middle to Late Triassic Snadd formation, Norwegian Barents Sea, *Marine and Petroleum Geology*, 62, pp. 102-122.

Klausen, T. G., Müller, R., Slama, J. and Helland-Hansen, W. (2016) Evidence for Late Triassic provenance areas and Early Jurassic sediment supply turnover in the Barents Sea Basin of northern Pangea, *Lithosphere*, pp. 15.

Knarud, R. (1980) En sedimentologisk og diagenetisk undersøkelse av Kapp Toscana Formasjonens sedimenter på Svalbard.(A sedimentological and diagenetic study of the sediments of the Kapp Toscana Formation in Svalbard), *University of Oslo*.

Korčinskaja, M. (1980) Rannenoriskaja fauna Arhipelaga Svalbard, *Early Norian fauna of the Svalbard Archipelago.) In DV Semevskij (ed.): Geologija osadocnogo cehla arhipelaga Sval'bard.(Geology of the sedimentary cover of Svalbard.)*, pp. 30-43.

Korčinskaja, M. (1982) Ob''jasnitel'naja zapiska k stratigraficeskoj sheme mezozoja (trias) Sval'barda, *An explanatory note to the stratigraphic scheme of the Mesozoic [Triassic] of Svalbard*.

Krajewski, K. P., Karcz, P., Wozny, E. and Mørk, A. (2007) Type section of the Bravaisberget Formation (Middle Triassic) at Bravaisberget, western Nathorst Land, Spitsbergen, Svalbard, *Polish Polar Research*, 28(2), pp. 79-122.

Krajewski, K. P. (2008) The Botneheia Formation (Middle Triassic) in Edgeøya and Barentsøya, Svalbard: lithostratigraphy, facies, phosphogenesis, paleoenvironment, *Polish Polar Research*, 29(4), pp. 319-364.

Krajewski, K. P. and Weitschat, W. (2015) Depositional history of the youngest strata of the Sassendalen Group (Bravaisberget Formation, Middle Triassic–Carnian) in southern Spitsbergen, Svalbard, *Annales Societatis Geologorum Poloniae*. pp. 151-175, doi: 110.14241/asgp. 12014.14005.

Kraus, M. J. (1999) Paleosols in clastic sedimentary rocks: their geologic applications, *Earth-Science Reviews*, 47(1), pp. 41-70.

Kristoffersen, M., Andersen, T. and Andresen, A. (2014) U–Pb age and Lu–Hf signatures of detrital zircon from Palaeozoic sandstones in the Oslo Rift, Norway, *Geological Magazine*, 151(05), pp. 816-829.

Kristoffersen, M., Andersen, T., Elburg, M. A. and Watkeys, M. K. (2016) Detrital zircon in a supercontinental setting: locally derived and far-transported components in the Ordovician Natal Group, South Africa, *Journal of the Geological Society*, 173(1), pp. 203-215.

Kuznetsov, N., Soboleva, A., Udoratina, O., Hertseva, M. and Andreichev, V. (2007) Pre-Ordovician tectonic evolution and volcano–plutonic associations of the Timanides and northern Pre-Uralides, northeast part of the East European Craton, *Gondwana Research*, 12(3), pp. 305-323.

Lander, R., Bloch, S., Mehta, S. and Atkinson, C. (1991) Burial diagenesis of paleosols in the Giant Yacheng gas field, People's Republic of China: bearing on Illite reaction pathways, *Journal of Sedimentary Research*, 61(2).

Langford, F. and Blanc-Valleron, M.-M. (1990) Interpreting Rock-Eval pyrolysis data using graphs of pyrolizable hydrocarbons vs. total organic carbon (1), *AAPG Bulletin*, 74(6), pp. 799-804.

Larionov, A. N., Andreichev, V. and Gee, D. G. (2004) The Vendian alkaline igneous suite of northern Timan: ion microprobe U-Pb zircon ages of gabbros and syenite, *Geological Society, London, Memoirs*, 30(1), pp. 69-74.

Launis, A., Pott, C. and Mørk, A. (2014) A glimpse into the Carnian: Late Triassic plant fossils from Hopen, Svalbard, *Norwegian Petroleum Directorate Bulletin*, 11, pp. 129-136.

Lauri, L. S., Andersen, T., Hölttä, P., Huhma, H. and Graham, S. (2011) Evolution of the Archaean Karelian Province in the Fennoscandian Shield in the light of U–Pb zircon ages and Sm–Nd and Lu–Hf isotope systematics, *Journal of the Geological Society*, 168(1), pp. 201-218.

Leever, K. A., Gabrielsen, R. H., Faleide, J. I. and Braathen, A. (2011) A transpressional origin for the West Spitsbergen fold-and-thrust belt: Insight from analog modeling, *Tectonics*, 30(2), pp. 24.

Leith, T., Weiss, H., Mørk, A., Århus, N., Elvebakk, G., Embry, A., Brooks, P., Stewart, K., Pchelina, T. and Bro, E. (1992) Mesozoic hydrocarbon sourcerocks of the Arctic region, *Arctic Geology and Petroleum Potential, Norw. Petrol. Soc. Spec. Publ*, 2, pp. 1-25.

Lock, B., Pickton, C., Smith, D., Batten, D. and Harland, W. (1978) The geology of Edgeøya and Barentsøya, Svalbard, *Norsk Polarinstitutt Skrifter*, 168, pp. 64.

López, G. I. (2015) Walther's Law of Facies, *Encyclopedia of Scientific Dating Methods*, pp. 957-958.

Lord, G. S., Solvi, K. H., Ask, M., Mørk, A., Hounslow, M. W. and Paterson, N. W. (2014a) The Hopen Member: A new member of the Triassic De Geerdalen Formation, Svalbard, *Norwegian Petroleum Directorate Bulletin*, 11(1), pp. 81-96.

Lord, G. S., Solvi, K. H., Klausen, T. G. and Mørk, A. (2014b) Triassic channel bodies on Hopen, Svalbard: Their facies, stratigraphical significance and spatial distribution, *Norwegian Petroleum Directorate Bulletin*, 11, pp. 41-59.

Lord, G. S., Krogh Johansen, S., Støen Jenvin, S. and Mørk, A. (2017a) Facies development of the Upper Triassic succession on Barentsøya, Wilhelmøya and NE Spitsbergen, Svalbard *Norwegian Journal of Geology*, 97(1), pp. 33-62. doi: https://dx.doi.org/10.17850/njg97-1-03.

Lord, G. S., Mørk, A. and Høy, T. (2017b) Sequence patterns in the Triassic succession of Svalbard and the northern Barents Sea, *In Lord, G.S: Sequence stratigraphy and facies development of the Triassic succession in Svalbard and the Northern Barents Sea. PhD Thesis, Norwegian University of Science and Technology*, pp. 200p.

Lord, G. S., Mørk, M. B. E., Mørk, A. and Olaussen, S. (2017c) The Svenskøya Formation on Hopen: An analogue to sandstone reservoirs in the Realgrunnen Subgroup, *In Lord, G.S: Sequence stratigraphy and facies development of the Triassic succession in Svalbard and the Northern Barents Sea. PhD Thesis, Norwegian University of Science and Technology*, pp. 200p.

Ludwig, K. (2008) User's Manual for Isoplot 3.70. Berkeley Geochronology Center, Special Pub. 4.
Lundschien, B. A., Høy, T. and Mørk, A. (2014) Triassic hydrocarbon potential in the Northern Barents Sea; integrating Svalbard and stratigraphic core data, *Norwegian Petroleum Directorate Bulletin*, 11, pp. 3-20.
Maher, J., Harmon D (2001) Manifestations of the Cretaceous High Arctic large igneous province in Svalbard, *The Journal of Geology*, 109(1), pp. 91-104.
Martinius, A. W., Howell, J., Steel, R. and Wonham, J. (2014) *From Depositional Systems to Sedimentary Successions on the Norwegian Continental Margin (Special Publication 46 of the IAS)*. John Wiley & Sons.
Miall, A. D. (2016) Facies Analysis *Stratigraphy: A Modern Synthesis.* Springer, pp. 77-151.
Middleton, G. V. (1973) Johannes Walther's law of the correlation of facies, *Geological Society of America Bulletin*, 84(3), pp. 979-988.
Midtgaard, H. H. (1996) Inner-shelf to lower-shoreface hummocky sandstone bodies with evidence for geostrophic influenced combined flow, Lower Cretaceous, West Greenland, *Journal of Sedimentary Research*, 66(2).
Midwinter, D., Hadlari, T., Davis, W., Dewing, K. and Arnott, R. (2016) Dual provenance signatures of the Triassic northern Laurentian margin from detrital-zircon U-Pb and Hf-isotope analysis of Triassic–Jurassic strata in the Sverdrup Basin, *Lithosphere*, 8(6), pp. 668-683.
Milanovsky, E. (1987) Geology of the USSR, *Izdatelstvo of Moscow University*, 1, pp. 416.
Miller, E. L., Toro, J., Gehrels, G., Amato, J. M., Prokopiev, A., Tuchkova, M. I., Akinin, V. V., Dumitru, T. A., Moore, T. E. and Cecile, M. P. (2006) New insights into Arctic paleogeography and tectonics from U-Pb detrital zircon geochronology, *Tectonics*, 25(3).
Miller, E. L., Soloviev, A. V., Prokopiev, A. V., Toro, J., Harris, D., Kuzmichev, A. B. and Gehrels, G. E. (2013) Triassic river systems and the paleo-Pacific margin of northwestern Pangea, *Gondwana Research*, 23(4), pp. 1631-1645.
Mills, P. C. (1983) Genesis and diagnostic value of soft-sediment deformation structures—a review, *Sedimentary Geology*, 35(2), pp. 83-104.
Morad, S. (1998) Carbonate cementation in sandstones: distribution patterns and geochemical evolution. , in Morad, S. (ed.) *Carbonate cementation in sandstones.* International Association of Sedimentologists Special Publication, pp. 1-26.
Müller, R., Nystuen, J. P. and Wright, V. P. (2004) Pedogenic mud aggregates and paleosol development in ancient dryland river systems: criteria for interpreting alluvial mudrock origin and floodplain dynamics, *Journal of Sedimentary Research*, 74(4), pp. 537-551.
Müller, R. D. and Spielhagen, R. F. (1990) Evolution of the Central Tertiary Basin of Spitsbergen: towards a synthesis of sediment and plate tectonic history, *Palaeogeography, Palaeoclimatology, Palaeoecology*, 80(2), pp. 153-172.
Myskova, T., Berezhnaya, N., Glebovitsky, V., Mil'kevich, R., Lepekhina, E., Matukov, D., Antonov, A., Sergeev, S. and Shuleshko, I. (2005) Findings of the oldest (3600 Ma) zircons in gneisses of the Kola Group, Central Kola Block, Baltic Shield: evidence from U-Pb (SHRIMP-II) data, *Doklady earth sciences*. Springer, pp. 547-550.
Mørk, A., Knarud, R. and Worsley, D. (1982) Depositional and diagenetic environments of the Triassic and Lower Jurassic succession of Svalbard, *Arctic Geology and Geophysics. Canadian Society of Petroleum Geologists Memoir*, 8, pp. 371-398.
Mørk, A. and Bjorøy, M. (1984) Mesozoic source rocks on Svalbard *Petroleum geology of the North European margin, pp 371-382.* Springer, pp. 371-382.

Mørk, A., Embry, A. F. and Weitschat, W. (1989) Triassic transgressive-regressive cycles in the Sverdrup Basin, Svalbard and the Barents Shelf *Correlation in hydrocarbon exploration.* Springer, pp. 113-130.
Mørk, A., Vigran, J., Korchinskaya, M., Pchelina, T., Fefilova, L., Vavilov, M. and Weitschat, W. (1993) Triassic rocks in Svalbard, the Arctic Soviet islands and the Barents Shelf: bearing on their correlations, *Arctic geology and petroleum potential*, Special Publication 2, pp. 457-479.
Mørk, A., Dallmann, W., Dypvik, H., Johannessen, E., Larssen, G., Nagy, J., Nøttvedt, A., Olaussen, S., Pchelina, T. and Worsley, D. (1999a) Mesozoic lithostratigraphy, *Lithostratigraphic lexicon of Svalbard. Upper Palaeozoic to Quaternary bedrock. Review and recommendations for nomenclature use*, pp. 127-214.
Mørk, A. and Elvebakk, G. (1999) Lithological description of subcropping Lower and Middle Triasic rocks from the Svalis Dome, Barents Sea, *Polar Research*, 18(1), pp. 83-104.
Mørk, A., Elvebakk, G., Forsberg, A. W., VIGRAN, J. O. and WEITSCHAT, W. (1999b) The type section of the Vikinghogda Formation: a new Lower Triassic unit in central and eastern Svalbard, *Polar Research*, 18(1), pp. 51-82.
Mørk, A. and Smelror, M. (2001) Correlation and non-correlation of high order circum-Arctic Mesozoic sequences, *Polarforschung*, 69, pp. 65-72.
Mørk, A. and Worsley, D. (2006) The Festningen section, *Norsk Geologisk Forening (NGF) Abstracts and Proceedings*, 3, pp. 31-35.
Mørk, A. and Bromley, R. G. (2008) Ichnology of a marine regressive systems tract: the Middle Triassic of Svalbard, *Polar Research*, 27(3), pp. 339-359.
Mørk, A., Lord, G., Solvi, K. and Dallmann, W. (2013) Geological map of Svalbard 1: 100 000, sheet G14G Hopen, *Norsk Polarinstitutt Temakart No*, 50.
Mørk, A. (2015) Historical Geology - Triassic, in Dallmann, W. K. (ed.) *Geoscience Atlas of Svalbard.* Norwegian Polar Institute, pp. 114-117.
Mørk, M. B. E. (1999) Compositional variations and provenance of Triassic sandstones from the Barents Shelf, *Journal of Sedimentary Research*, 69(3), pp. 690-710.
Nakrem, H. A. and Mørk, A. (1991) New Early Triassic Bryozoa (Trepostomata) from Spitsbergen, with some remarks on the stratigraphy of the investigated horizons, *Geological Magazine*, 128(02), pp. 129-140.
Nathorst, A. G. (1910) *Beiträge zur Geologie der Bären-Insel, Spitzbergens und des König-Karl-Landes*. Almquist & Wiksells boktryckeri-a.-b.
Nichols, G. (2009) *Sedimentology and stratigraphy*. John Wiley & Sons.
Nøttvedt, A. and Kreisa, R. (1987) Model for the combined-flow origin of hummocky cross-stratification, *Geology*, 15(4), pp. 357-361.
Olariu, C. (2014) Autogenic process change in modern deltas, *From Depositional Systems to Sedimentary Successions on the Norwegian Continental Margin*, pp. 149-166.
Oliveira, C. M., Hodgson, D. M. and Flint, S. S. (2011) Distribution of soft-sediment deformation structures in clinoform successions of the Permian Ecca Group, Karoo Basin, South Africa, *Sedimentary Geology*, 235(3), pp. 314-330.
Omma, J., Pease, V. and Scott, R. (2011) U–Pb SIMS zircon geochronology of Triassic and Jurassic sandstones on northwestern Axel Heiberg Island, northern Sverdrup Basin, Arctic Canada, *Geological Society, London, Memoirs*, 35(1), pp. 559-566.
Orton, G. and Reading, H. (1993) Variability of deltaic processes in terms of sediment supply, with particular emphasis on grain size, *Sedimentology*, 40(3), pp. 475-512.
Osmundsen, P. T., Braathen, A., Rød, R. S. and Hynne, I. B. (2014) Styles of normal faulting and fault-controlled sedimentation in the Triassic deposits of Eastern Svalbard, *Norwegian Petroleum Directorate Bulletin*, 11, pp. 61-79.

Paterson, N. W. and Mangerud, G. (2015) Late Triassic (Carnian–Rhaetian) palynology of Hopen, Svalbard, *Review of Palaeobotany and Palynology*, 220, pp. 98-119.
Paterson, N. W., Mangerud, G., Cetean, C. G., Mørk, A., Lord, G. S., Klausen, T. G. and Mørkved, P. T. (2016) A multidisciplinary biofacies characterisation of the Late Triassic (late Carnian–Rhaetian) Kapp Toscana Group on Hopen, Arctic Norway, *Palaeogeography, Palaeoclimatology, Palaeoecology*, 464, pp. 16-42.
Pčelina, T. (1972) K voprosu o vozraste osadočnoj tolšči ostrova Nadeždy (Sval'bard).(On the age of the sedimentary succession of the island of Hopen (Svalbard)), *Mezozoiskie otloženija Sval'barda (Mesozoic deposits of Svalbard), NIIGA, Leningrad*, pp. 75-81.
Pčelina, T. (1983) Novye dannye po stratigrafi mezozoja archipelago Špicbergena, *New data on the Mesozoic Stratigraphy of the archipelago of Spitsbergen.) In: Geologija Špichergena.(Geology of Spitsbergen.) Pp*, pp. 121-141.
Pease, V. (2011) Eurasian orogens and Arctic tectonics: an overview, *Geological Society, London, Memoirs*, 35(1), pp. 311-324.
Pedersen, S. A., Craig, L. E., Upton, B. G., Rämö, O. T., Jepsen, H. F. and Kalsbeek, F. (2002) Palaeoproterozoic (1740 Ma) rift-related volcanism in the Hekla Sund region, eastern North Greenland: field occurrence, geochemistry and tectonic setting, *Precambrian Research*, 114(3), pp. 327-346.
Petersen, T. G., Thomsen, T., Olaussen, S. and Stemmerik, L. (2016) Provenance shifts in an evolving Eurekan foreland basin: the Tertiary Central Basin, Spitsbergen, *Journal of the Geological Society*, 173(4), pp. 634-648.
Pettijohn, F., Potter, P. and Siever, R. (1987) *Sand and Sandstone*. Berlin, Heidelberg, New York: Springer.
Preobrazhenskaya, E., Skola, I. and KORCINSKAYA, M. (1984) Stratigraphy of Triassic deposits of the archipelago of Franz Josef Land (on materials of a parametric drilling), *Stratigraphy and Paleontology of Mesozoic Sedimentary Basins of the North of the USSR: Collection of Scientific papers, Leningrad*, pp. 5-15.
Puchkov, V. N. (2009) The evolution of the Uralian orogen, *Geological Society, London, Special Publications*, 327(1), pp. 161-195.
R Development Core Team (2015) R: A Language and Environment for Statistical Computing. Available at: http://www.r-project.org/.
Reading, H. and Collinson, J. (1996) Clastic coasts, *Sedimentary environments: processes, facies and stratigraphy*, pp. 154-231.
Reading, H. and Levell, B. (1996) Controls on the sedimentary rock record *Sedimentary environments: processes, facies and stratigraphy.* Third edn., pp. 5-36.
Reimink, J., Davies, J., Waldron, J. and Rojas, X. (2016) Dealing with discordance: a novel approach for analysing U–Pb detrital zircon datasets, *Journal of the Geological Society*, 173(4), pp. 577-585.
Reineck, H.-E. and Singh, I. B. (1980) *Depositional sedimentary environments: with reference to terrigenous clastics*. Second Edition edn. Springer Science & Business Media.
Reinson, G. (1984) Barrier island and associated strandplain systems, in Walker, R. (ed.) *Facies models.* Geoscience Canada, pp. 119-140.
Reinson, G. E. (1992) Transgressive barrier island and estuarine systems, *Facies models: response to sea level change: Geological Association of Canada*, pp. 179-194.
Renne, P. R. and Basu, A. R. (1991) Rapid eruption of the Siberian Traps flood basalts at the Permo-Triassic boundary, *Science*, 253(5016), pp. 176-180.
Retallack, G. (1991) Untangling the effects of burial alteration and ancient soil formation, *Annual Review of Earth and Planetary Sciences*, 19(1), pp. 183-206.
Riis, F., Lundschien, B. A., Høy, T., Mørk, A. and Mørk, M. B. E. (2008) Evolution of the Triassic shelf in the northern Barents Sea region, *Polar Research*, 27(3), pp. 318-338.

Ritzmann, O. and Faleide, J. I. (2009) The crust and mantle lithosphere in the Barents Sea/Kara Sea region, *Tectonophysics*, 470(1), pp. 89-104.

Roberts, D. (2003) The Scandinavian Caledonides: event chronology, palaeogeographic settings and likely modern analogues, *Tectonophysics*, 365(1), pp. 283-299.

Rød, R. (2011) Spatial occurrences of selected sandstone bodies in the De Geerdalen Formation, *Svalbard, and their relation to depositional facies: Master's Thesis, Norwegian University of Science and Technology, Trondheim, Norway*.

Rød, R. S., Hynne, I. B. and Mørk, A. (2014) Depositional environment of the Upper Triassic De Geerdalen Formation—an EW transect from Edgeøya to Central Spitsbergen, Svalbard, *Norwegian Petroleum Directorate Bulletin*, 11, pp. 21-40.

Røhr, T., Andersen, T. and Dypvik, H. (2008) Provenance of Lower Cretaceous sediments in the Wandel Sea Basin, North Greenland, *Journal of the Geological Society*, 165(3), pp. 755-767.

Røhr, T. and Andersen, T. (2009) Detrital zircons from the high Arctic; evidence of extensive recycling of sediment from Devonian through Mesozoic times., *In: Røhr, T.S. (ed) Sedimentary Provenance analysis of Lower Cretaceous Sedimentary Successions in the Arctic; Constraints from Detrital Zircon data. PhD thesis, University of Oslo*.

Røhr, T. S., Andersen, T., Dypvik, H. and Embry, A. F. (2010) Detrital zircon characteristics of the Lower Cretaceous Isachsen Formation, Sverdrup Basin: source constraints from age and Hf isotope data, *Canadian Journal of Earth Sciences*, 47(3), pp. 255-271.

Satkoski, A. M., Wilkinson, B. H., Hietpas, J. and Samson, S. D. (2013) Likeness among detrital zircon populations—An approach to the comparison of age frequency data in time and space, *Geological Society of America Bulletin*, 125(11-12), pp. 1783-1799.

Senger, K., Tveranger, J., Ogata, K., Braathen, A. and Planke, S. (2014) Late Mesozoic magmatism in Svalbard: A review, *Earth-Science Reviews*, 139, pp. 123-144.

Sircombe, K. N. and Stern, R. A. (2002) An investigation of artificial biasing in detrital zircon U-Pb geochronology due to magnetic separation in sample preparation, *Geochimica et Cosmochimica Acta*, 66(13), pp. 2379-2397.

Sircombe, K. N. (2004) AgeDisplay: an EXCEL workbook to evaluate and display univariate geochronological data using binned frequency histograms and probability density distributions, *Computers & Geosciences*, 30(1), pp. 21-31.

Smelror, M., Petrov, O., Larssen, G. B. and Werner, S. (2009) Geological history of the Barents Sea, *Norges Geol. undersøkelse*, pp. 1-135.

Smith, D. G., Harland, W. and Hughes, N. (1975) Geology of Hopen, Svalbard, *Geological Magazine*, 112(1), pp. 1-23.

Soloviev, A., Zaionchek, A., Suprunenko, O., Brekke, H., Faleide, J., Rozhkova, D., Khisamutdinova, A., Stolbov, N. and Hourigan, J. (2015) Evolution of the provenances of Triassic rocks in Franz Josef Land: U/Pb LA-ICP-MS dating of the detrital zircon from Well Severnaya, *Lithology and Mineral Resources*, 50(2), pp. 102-116.

Spearing, D. R. (1976) Upper Cretaceous Shannon Sandstone: an offshore, shallow-marine sand body, *Geology and Energy Resources of the Powder River, 28th Annual Field Conference Guidebook*.

Steel, R., Dalland, A., Kalgraff, K. and Larsen, V. (1981) The Central Tertiary Basin of Spitsbergen: sedimentary development of a sheared-margin basin, *Geology of the North Atlantic Borderlands - Memoir 7*, pp. 647-664.

Steel, R. J. and Worsley, D. (1984) Svalbard's post-Caledonian strata—an atlas of sedimentational patterns and palaeogeographic evolution *Petroleum geology of the North European margin.* Springer, pp. 109-135.

Steiger, R. H. and Jäger, E. (1977) Subcommission on geochronology: convention on the use of decay constants in geo-and cosmochronology, *Earth and planetary science letters*, 36(3), pp. 359-362.
Steno, N. (1669) *De Solido intra Solidum naturaliter contento dissertationis prodromus*. Florence.
Støen, S. J. (2016) *Late Triassic sedimentology and diagenesis of Barentsøya, Wilhelmøya and eastern Spitsbergen*. Master's Thesis, Norwegian University of Science and Technology, 151pp.
Teichert, C. (1958) Concepts of facies, *AAPG Bulletin*, 42(11), pp. 2718-2744.
Torsvik, T. H., Carlos, D., Mosar, J., Cocks, L. R. M. and Malme, T. N. (2002) Global reconstructions and North Atlantic paleogeography 440 Ma to recent, *BATLAS—Mid Norway plate reconstruction atlas with global and Atlantic perspectives*, pp. 18-39.
Tozer, E. and Parker, J. (1968) Notes on the Triassic biostratigraphy of Svalbard, *Geological Magazine*, 105(06), pp. 526-542.
Tucker, M. E. (2011) *Sedimentary rocks in the field: A practical guide*. John Wiley & Sons.
Tugarova, M. A. and Fedyaevsky, A. G. (2014) Calcareous microbialites in the Upper Triassic succession of Eastern Svalbard, *Norwegian Petroleum Directorate Bulletin*, 11, pp. 137-152.
Ulmishek, G. (1985) *Geology and petroleum resources of the Barents-Northern Kara Shelf in light of new geologic data*. Argonne National Lab., IL (USA).
Van Wagoner, J., Posamentier, H., Mitchum, R., Vail, P., Sarg, J., Loutit, T. and Hardenbol, J. (1988) An overview of the fundamentals of sequence stratigraphy and key definitions.
Van Wagoner, J. C., Mitchum, R., Campion, K. and Rahmanian, V. (1990) Siliciclastic sequence stratigraphy in well logs, cores, and outcrops: concepts for high-resolution correlation of time and facies.
Vernikovskij, V., Ponomarchuk, V., Vernikovskaya, A., Kireev, A., Kuz'min, D. and Nejmark, L. (1995) Geochemistry and age of collisional granitoids and metamorphites of the Kara microcontinent (North Taimyr), *Geologiya i Geofizika*, 36(12), pp. 50-64.
Vernikovskij, V. A., Pease, V. L., Vernikovskaya, A. E., Romanov, A. P., Gee, D. G. and Travin, A. V. (2003) First report of early Triassic A-type granite and syenite intrusions from Taimyr: product of the northern Eurasian superplume?, *Lithos*, 66(1), pp. 23-36.
Vigran, J. O., Mangerud, G., Mørk, A., Bugge, T. and Weitschat, W. (1998) Biostratigraphy and sequence stratigraphy of the Lower and Middle Triassic deposits from the Svalis Dome, central Barents Sea, Norway, *Palynology*, 22(1), pp. 89-141.
Vigran, J. O., Mangerud, G., Mørk, A., Worsley, D. and Hochuli, P. A. (2014) *Palynology and geology of the Triassic succession of Svalbard and the Barents Sea*. Geological Society of Norway Special Publication, 270pp.
Walderhaug, H., Eide, E., Scott, R., Inger, S. and Golionko, E. (2005) Palaeomagnetism and 40Ar/39Ar geochronology from the South Taimyr igneous complex, Arctic Russia: a Middle-Late Triassic magmatic pulse after Siberian flood-basalt volcanism, *Geophysical Journal International*, 163(2), pp. 501-517.
Walker, R. (2006) Facies models revisited: Introduction, *Special Publication-SEPM*, 84, pp. 1.
Walther, J. (1894) *Einleitung in die Geologie als historische Wissenschaft: Beobachtungen über die Bildung der Gesteine und ihrer organischen Einschlüsse*. G. Fischer.
Watt, G., Kinny, P. and Friderichsen, J. (2000) U–Pb geochronology of Neoproterozoic and Caledonian tectonothermal events in the East Greenland Caledonides, *Journal of the Geological Society*, 157(5), pp. 1031-1048.
Watt, G. and Thrane, K. (2001) Early Neoproterozoic events in east Greenland, *Precambrian Research*, 110(1), pp. 165-184.

Webb, G. E. (1994) Paleokarst, paleosol, and rocky-shore deposits at the Mississippian-Pennsylvanian unconformity, northwestern Arkansas, *Geological Society of America Bulletin*, 106(5), pp. 634-648.

Whitehouse, M. J. and Kamber, B. S. (2005) Assigning dates to thin gneissic veins in high-grade metamorphic terranes: a cautionary tale from Akilia, southwest Greenland, *Journal of Petrology*, 46(2), pp. 291-318.

Wiedenbeck, M., Alle, P., Corfu, F., Griffin, W., Meier, M., Oberli, F., Quadt, A. v., Roddick, J. and Spiegel, W. (1995) Three natural zircon standards for U-Th-Pb, Lu-Hf, trace element and REE analyses, *Geostandards newsletter*, 19(1), pp. 1-23.

Winsnes, T. and Worsley, D. (1981) *Geological Map of Svalbard 1: 500,000: Sheet 2G, Edgeøya*. Norsk Polarinstitutt.

Worsley, D. (1973) The Wilhelmøya Formation–a new lithostratigraphical unit from the Mesozoic of eastern Svalbard, *Arb. norsk Polarinst*, 1971, pp. 7-16.

Worsley, D. and Mørk, A. (1978) The Triassic stratigraphy of southern Spitsbergen, *Norsk Polar− institutt Årbok 1977*, pp. 43-60.

Worsley, D., Johansen, R. and Kristensen, S. (1988) The Mesozoic and Cenozoic succession of Tromsøflaket, *A lithostratigraphic scheme for the Mesozoic and Cenozoic succession offshore mid-and northern Norway. Norwegian Petroleum Directorate Bulletin*, 4, pp. 42-65.

Worsley, D. (2008) The post-Caledonian development of Svalbard and the western Barents Sea, *Polar Research*, 27(3), pp. 298-317.

Wright, V. and Tucker, M. (1991) Calcretes. The international association of Sedimentologists, *Blackwell Scientific Publications, Oxford), Reprint Ser*, 2, pp. 380.

Wright, V. P. (1994) Paleosols in shallow marine carbonate sequences, *Earth-Science Reviews*, 35(4), pp. 367-395.

Xu, G., Hannah, J. L., Stein, H. J., Mørk, A., Vigran, J. O., Bingen, B., Schutt, D. L. and Lundschien, B. A. (2014) Cause of Upper Triassic climate crisis revealed by Re–Os geochemistry of Boreal black shales, *Palaeogeography, Palaeoclimatology, Palaeoecology*, 395, pp. 222-232.

Yang, B., Dalrymple, R. W. and Chun, S. (2006) The significance of hummocky cross-stratification (HCS) wavelengths: evidence from an open-coast tidal flat, South Korea, *Journal of Sedimentary Research*, 76(1), pp. 2-8.

Young, F. and Reinson, G. (1975) Sedimentology of Blood Reserve and adjacent formations (Upper Cretaceous), St. Mary River, southern Alberta, *Guidebook to selected sedimentary environments In southwestern Alberta, Canada: Canadian Society of Petroleum Geologists, Field Conference*. pp. 10-20.

Zhang, X., Pease, V., Skogseid, J. and Wohlgemuth-Ueberwasser, C. (2016) Reconstruction of tectonic events on the northern Eurasia margin of the Arctic, from U-Pb detrital zircon provenance investigations of late Paleozoic to Mesozoic sandstones in southern Taimyr Peninsula, *Geological Society of America Bulletin*, 128(1-2), pp. 29-46.

Zonenshain, L. P., Kuzmin, M. I., Natapov, L. M. and Page, B. M. (1990) Uralian foldbelt, *Geology of the USSR: a plate-tectonic synthesis*, pp. 27-54.

Appendices

Appendix A: UTM Coordinates Fulmardalen

Locality	Log name	UTM Start (Zone, E, N)	UTM End (Zone, E, N)
Wallenbergfjellet	Wal 16-1	33X, 0565413, 8685660	33X, 0565693, 8685796
Dyrhø	Dyr 16-1	33X, 0564923, 8681912	33X, 0564813, 8681730
Ryssen	Rys 16-1	33X, 0567299, 8682728	33X, 0568800, 8683050
Milne Edwardsfjellet	Mil 16-1	33X, 0563171, 8683548	33X, 0562392, 8683776
Storfjellet	Stor 16-1	33X, 0567784, 8681412	33X, 0568321, 8681562
Raggfjellet	Rag 16-1	33X, 0565288, 8679300	33X, 0565286, 8679272

Appendix B: Legend for measured sections

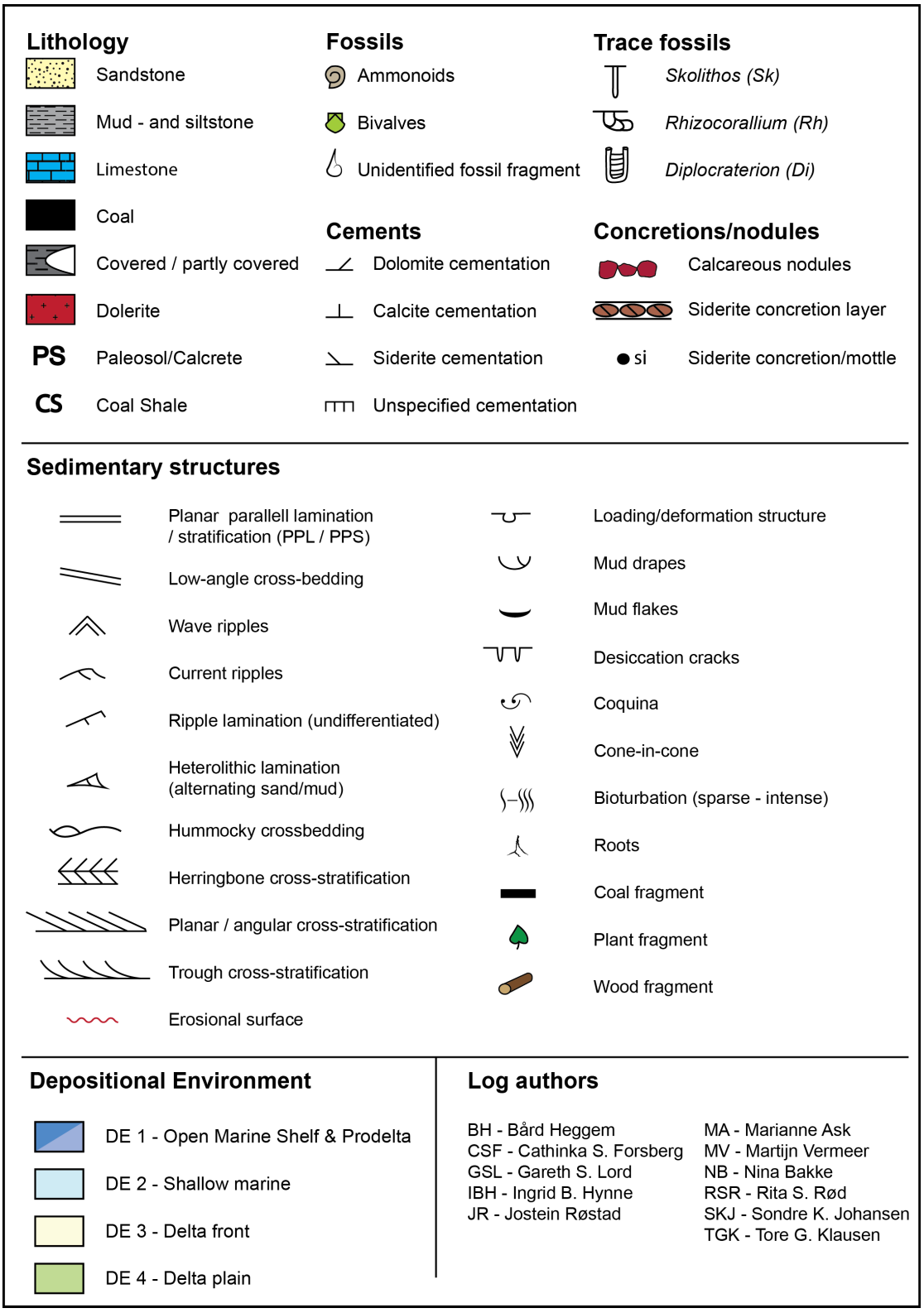

Appendix C: Storfjellet Knarud (1980) correlated to Stor 16-1

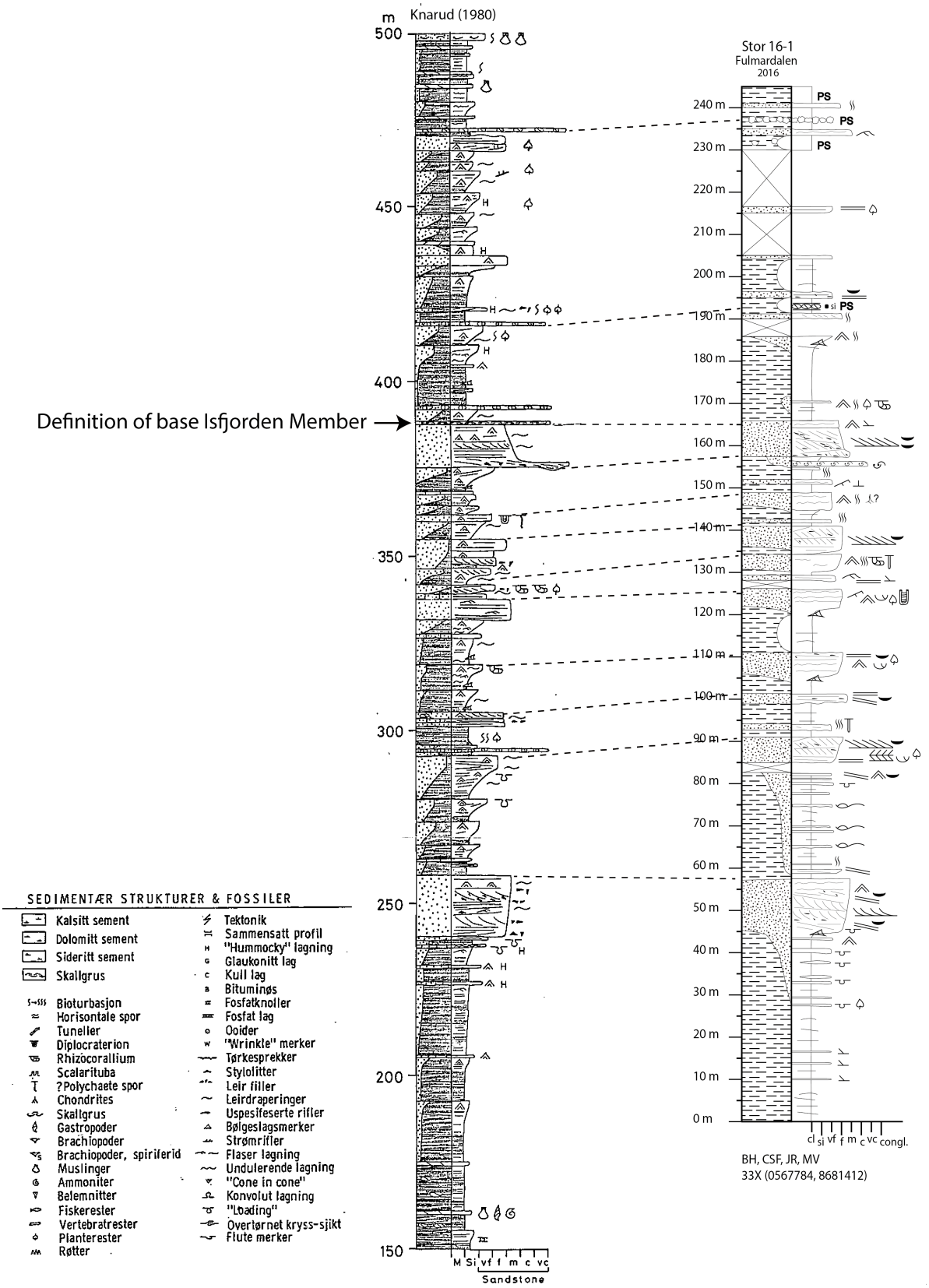

Appendix D: Rock-Eval Analysis

Table D.1 *Measured values from Rock-Eval analysis*

	Dyr16-1.19B	**Rys16-1.28B**
S1 (mg/g)	0.13	0.01
S2 (mg/g)	2.55	0.47
S3 (mg/g)	0.26	0.32
Tmax (C)	446	449
HI (mg HC/g TOC)	109	51
OI (mg CO_2/g TOC)	11	35
TOC (%)	2.35	0.92

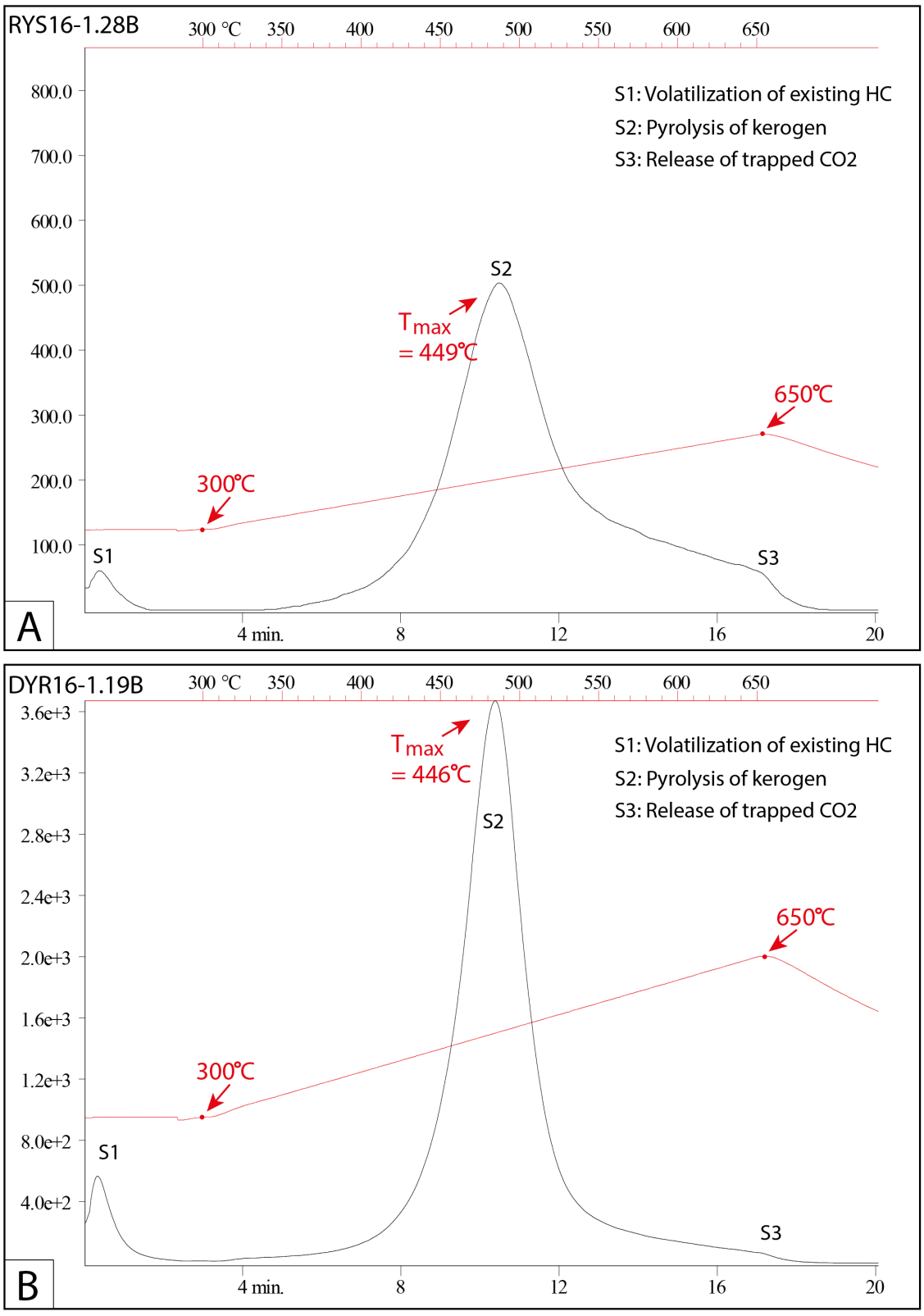

Figure D.1 *Resulting chromatograms from pyrolysis of* ***(A)*** *Rys16-1.28B and* ***(B)*** *Dyr16-1.19B.*

Appendix E: Sample table from the Festningen section

Sample	Coordinates (Degrees and Decimal Minutes)	Depositional age	Group	Formation	Status
AA16-41	78° 05,625 N 13° 50,095 E	Lower Triassic (Induan)	Sassendalen	Vardebukta	Not analysed. Potential bentonite layer close to P-T boundary.
AA16-42	78° 05,641 N 13° 50,596 E	Lower Triassic (Induan)	Sassendalen	Vardebukta	Not analysed.
AA16-43	78° 05,706 N 13° 51,011 E	Lower Triassic (Induan)	Sassendalen	Vardebukta	Not analysed.
AA16-44	78° 05,733 N 13° 51,356 E	Lower Triassic (Induan)	Sassendalen	Vardebukta	Not analysed.
AA16-45	78° 05,733 N 13° 51,356 E	Lower Triassic (Induan)	Sassendalen	Vardebukta	Not analysed. Sampled for mica-analysis.
AA16-46	78° 05,919 N 13° 52,523 E	Lower Triassic (Olenekian)	Sassendalen	Tvillingodden	Crushed, washed, and heavy liquid separated. Did not yield any zircons.
AA16-47	78° 06,007 N 13° 53,351 E	Middle Triassic (Ladinian)	Sassendalen	Bravaisberget	Fully analysed.
AA16-48	78° 05,952 N 13° 53,663 E	Middle Triassic (Ladinian)	Sassendalen	Bravaisberget	Crushed, but not analysed.
AA16-49	78° 05,911 N 13° 53,947 E	Upper Triassic (Carnian)	Kapp Toscana	De Geerdalen	Fully analysed.
AA16-50	78° 05,903 N 13° 54,595 E	Upper Triassic (Norian)	Kapp Toscana	De Geerdalen	Not analysed.
AA16-51	78° 05,912 N 13° 54,772 E	Upper Triassic – Lower Jurassic (Norian - Bathonian)	Kapp Toscana (Wilhelmøya Subgroup)	Knorringfjellet	Not analysed.

Appendix F: Results from zircon U-Pb age analysis

Sample AA16-47

Sample	ppm				Ratios							Discordance		Ages					
Name	U	^{206}Pb	$^{206}Pb_c$(%)	206/204	$^{207}Pb/^{206}Pb^*$	1SE	$^{207}Pb/^{235}U^*$	1SE	$^{206}Pb/^{238}U^*$	1SE	Rho	Central (%)	Minimum rim (%)	207/206	1σ	207/235	1σ	206/238	1σ
A47-01	162	11,2	0,00E+00	1190	0,05569	0,00033	0,52366	0,00758	0,068198	0,0009	0,911	-3,5	.	440	12	428	5	425	5
A47-02	157	33,3	0,00E+00	4694	0,08748	0,00061	2,49699	0,0757	0,207025	0,006109	0,973	-12,6	-9,8	1371	12	1271	22	1213	33
A47-03	94	32	0,00E+00	11577	0,11166	0,00065	5,0246	0,0843	0,326354	0,005132	0,937	-0,4	.	1827	10	1823	14	1821	25
A47-04	368	117,6	0,00E+00	32479	0,12032	0,00071	5,17053	0,11939	0,311659	0,006954	0,966	-12,3	-10,4	1961	10	1848	20	1749	34
A47-05	126	9,1	0,00E+00	2682	0,05883	0,001	0,58633	0,01197	0,072279	0,00081	0,549	-20,5	-6,1	561	35	469	8	450	5
A47-06	737	82,2	0,00E+00	57803	0,06165	0,00028	0,94325	0,01155	0,110968	0,001264	0,930	2,6	.	662	9	675	6	678	7
A47-07	193	44,1	0,00E+00	8145	0,09802	0,00053	3,03341	0,0478	0,224451	0,003321	0,939	-19,6	-17,7	1587	10	1416	12	1305	17
A47-08	151	80,9	0,00E+00	44922	0,19192	0,00155	13,50278	0,30372	0,510275	0,010707	0,933	-4,5	-2,1	2759	13	2715	21	2658	46
A47-09	153	53,7	0,00E+00	23662	0,13222	0,00086	6,22045	0,11175	0,341199	0,005714	0,932	-12,7	-10,8	2128	11	2007	16	1892	27
A47-10	641	88,4	0,00E+00	1166	0,09837	0,00175	1,906	0,04887	0,140526	0,0026	0,722	-49,9	-46,8	1593	31	1083	17	848	15
A47-11	296	29,7	0,00E+00	3259	0,06575	0,00033	0,9	0,01189	0,101239	0,001208	0,921	-23,2	-20,5	799	10	661	6	622	7
A47-12	231	17,1	0,00E+00	3685	0,05646	0,00031	0,58329	0,00714	0,074927	0,000822	0,897	-1	.	471	12	467	5	466	5
A47-13	608	171,3	0,00E+00	19812	0,1433	0,00107	5,5395	0,10414	0,280365	0,004841	0,919	-33,5	-31,8	2267	12	1907	16	1593	24
A47-16	62	8,8	0,00E+00	4686	0,06626	0,00069	1,22099	0,02082	0,13365	0,001813	0,795	-0,8	.	815	21	810	10	809	10
A47-17	280	22,5	0,00E+00	8148	0,05654	0,00041	0,62198	0,0085	0,079782	0,000927	0,85	4,6	.	474	15	491	5	495	6
A47-18	131	38,5	0,00E+00	9021	0,10077	0,00075	3,98964	0,06696	0,287142	0,004315	0,895	-0,8	.	1638	13	1632	14	1627	22
A47-19	161	18,9	0,00E+00	17168	0,07613	0,00064	1,22928	0,02127	0,117107	0,001771	0,874	-37	-34,2	1099	16	814	10	714	10
A47-20	316	38,8	0,00E+00	13173	0,06325	0,00041	1,1	0,01453	0,122306	0,001467	0,88	4	.	717	13	737	7	744	8
A47-21	635	225	0,00E+00	11158	0,18449	0,00195	8,80308	0,17608	0,34606	0,005881	0,85	-33,3	-31,2	2694	17	2318	18	1916	28
A47-22	269	76,2	0,00E+00	33375	0,10106	0,00075	3,87811	0,07329	0,278325	0,004842	0,921	-4,2	-1,3	1644	13	1609	15	1583	24
A47-23	287	81,7	0,00E+00	20733	0,11169	0,00086	4,31409	0,07389	0,280133	0,004288	0,894	-14,5	-12,1	1827	14	1696	14	1592	22
A47-24	188	66,9	0,00E+00	15695	0,12855	0,00103	6,18116	0,11412	0,348724	0,005798	0,901	-8,3	-5,8	2078	14	2002	16	1929	28
A47-25	345	55,5	0,00E+00	4622	0,09883	0,0007	2,20412	0,03816	0,161756	0,002554	0,912	-42,7	-41	1602	13	1182	12	967	14
A47-14	236	18	0,00E+00	6719	0,05649	0,00039	0,58514	0,00805	0,075121	0,000891	0,863	-1,1	.	472	15	468	5	467	5
A47-15	432	71,1	0,00E+00	23631	0,0708	0,00044	1,5738	0,02231	0,161218	0,002058	0,900	1,3	.	952	12	960	9	964	11
A47-26	132	13,4	0,00E+00	5170	0,06295	0,00104	0,87309	0,02494	0,100585	0,002343	0,816	-13,2	-2,1	707	35	637	14	618	14
A47-27	143	39,2	0,00E+00	13307	0,10087	0,00079	3,90548	0,06082	0,280818	0,003773	0,863	-3,1	-0,1	1640	14	1615	13	1595	19
A47-28	107	18,8	0,00E+00	9259	0,07637	0,00043	1,92957	0,02065	0,183258	0,001668	0,850	-2	.	1105	11	1091	7	1085	9
A47-29	345	24,6	0,00E+00	9351	0,05598	0,00028	0,58469	0,00453	0,075756	0,000445	0,759	4,4	.	451	11	467	3	471	3
A47-30	120	10,8	0,00E+00	2440	0,05931	0,00035	0,78309	0,00686	0,095755	0,000617	0,735	2	.	579	13	587	4	589	4
A47-31	156	26,5	0,00E+00	6957	0,07465	0,00037	1,8244	0,03363	0,177242	0,003145	0,963	-0,7	.	1059	10	1054	12	1052	17
A47-32	180	29	0,00E+00	4607	0,07473	0,00042	1,7004	0,05011	0,165033	0,004774	0,982	-7,8	-4,8	1061	11	1009	19	985	26
A47-33	105	18,1	0,00E+00	3474	0,07805	0,00044	1,94059	0,01686	0,180334	0,001193	0,762	-7,5	-5,1	1148	10	1095	6	1069	7
A47-34	371	71	0,00E+00	126012	0,07843	0,00066	2,14623	0,02812	0,198461	0,001985	0,763	0,9	.	1158	16	1164	9	1167	11
A47-35	391	52,1	0,00E+00	3049	0,08916	0,00044	1,71226	0,03661	0,139277	0,002896	0,973	-42,9	-41,6	1408	9	1013	14	841	16
A47-36	255	51,4	0,00E+00	5575	0,11682	0,00062	3,33822	0,07347	0,207249	0,004427	0,97	-39,8	-38,6	1908	9	1490	17	1214	24

Sample	*ppm*				Ratios							Discordance		Ages					
Name	U	^{206}Pb	$^{206}Pb_c$(%)	206/204	$^{207}Pb/^{206}Pb$*	1SE	$^{207}Pb/^{235}U$*	1SE	$^{206}Pb/^{238}U$*	1SE	Rho	Central (%)	Minimum rim (%)	207/206	1σ	207/235	1σ	206/238	1σ
A47-37	176	45,6	0,00E+00	21219	0,09832	0,00048	3,6	0,03375	0,266123	0,002121	0,852	-5	-3,2	1593	9	1551	7	1521	11
A47-38	806	22,1	0,00E+00	2998	0,05973	0,00039	0,24119	0,00656	0,029289	0,000773	0,970	-69,6	-67,8	594	15	219	5	186	5
A47-39	459	70,7	0,00E+00	17091	0,07067	0,0003	1,56946	0,0123	0,161074	0,001058	0,839	1,7	.	948	9	958	5	963	6
A47-40	207	52	0,00E+00	17093	0,09752	0,00048	3,47337	0,03249	0,258319	0,002054	0,85	-6,8	-5	1577	9	1521	7	1481	11
A47-41	109	36,6	0,00E+00	25041	0,11076	0,00059	5,18312	0,05003	0,339409	0,002733	0,834	4,6	2,5	1812	9	1850	8	1884	13
A47-42	72	21,4	0,00E+00	5766	0,12775	0,00076	5,34192	0,06038	0,303283	0,002915	0,85	-19,8	-18,2	2067	10	1876	10	1708	14
A47-43	140	25,7	0,00E+00	11120	0,07681	0,00039	2,02158	0,02562	0,190882	0,00222	0,918	1	.	1116	10	1123	9	1126	12
A47-44	371	14,4	0,00E+00	5120	0,05499	0,00038	0,31434	0,00364	0,041458	0,000383	0,798	-37,2	-31,7	412	15	278	3	262	2
A47-45	289	96,4	4,40E-01	3909	0,17066	0,00119	7,9	0,08825	0,335249	0,002933	0,782	-31,4	-30	2564	11	2218	10	1864	14
A47-46	342	45,1	0,00E+00	20002	0,06948	0,00034	1,32701	0,01325	0,138521	0,001206	0,872	-9	-6,3	913	10	858	6	836	7
A47-47	60	15,5	0,00E+00	9255	0,10048	0,00061	3,71865	0,08185	0,26842	0,005682	0,962	-6,9	-4,6	1633	11	1575	18	1533	29
A47-48	99	13,7	0,00E+00	3649	0,08209	0,00045	1,65096	0,03315	0,145855	0,002816	0,962	-31,7	-29,8	1248	10	990	13	878	16
A47-49	640	136,9	0,00E+00	40613	0,11703	0,00064	3,58172	0,04	0,22196	0,002162	0,872	-35,7	-34,4	1911	10	1545	9	1292	11
A47-50	494	91,2	0,00E+00	27156	0,10042	0,00047	2,66049	0,02728	0,192149	0,001752	0,889	-33,3	-32,1	1632	9	1318	8	1133	9
A47-51	180	42,7	0,00E+00	15630	0,09379	0,00047	3,15287	0,03037	0,243807	0,002011	0,856	-7,2	-5,3	1504	9	1446	7	1406	10
A47-52	619	131,5	0,00E+00	34399	0,09024	0,0004	2,73585	0,02459	0,219882	0,001718	0,869	-11,5	-9,8	1431	8	1338	7	1281	9
A47-53	811	104,5	0,00E+00	14577	0,098	0,00052	1,84408	0,03231	0,136471	0,002281	0,954	-51,1	-50	1586	9	1061	12	825	13
A47-54	102	26,5	0,00E+00	10599	0,10091	0,00054	3,72346	0,04911	0,267612	0,003231	0,915	-7,7	-5,7	1641	10	1576	11	1529	16
A47-55	964	229,9	0,00E+00	3502	0,16906	0,00115	5,75449	0,13402	0,246873	0,005497	0,956	-49,1	-48	2548	11	1940	20	1422	28
A47-56	327	89,7	0,00E+00	74813	0,11231	0,00092	4,67923	0,06312	0,302176	0,003245	0,796	-8,4	-5,8	1837	14	1764	11	1702	16
A47-57	88	7,8	0,00E+00	2099	0,05954	0,00047	0,77525	0,00788	0,094433	0,000613	0,639	-0,9	.	587	16	583	5	582	4
A47-58	214	108,6	0,00E+00	120291	0,19336	0,00132	13,25598	0,16217	0,497202	0,005051	0,83	-7,4	-5,6	2771	11	2698	12	2602	22
A47-59	148	41,2	0,00E+00	13965	0,10101	0,00051	3,97543	0,03704	0,285456	0,002244	0,844	-1,6	.	1643	9	1629	8	1619	11
A47-60	147	36,2	0,00E+00	10471	0,10305	0,00055	3,61852	0,0435	0,254679	0,002746	0,897	-14,4	-12,6	1680	9	1554	10	1463	14
A47-61	314	53	0,00E+00	15998	0,07651	0,00044	1,86339	0,01813	0,176633	0,001387	0,807	-5,9	-3,2	1109	11	1068	6	1049	8
A47-62	310	47,9	0,00E+00	15108	0,07177	0,00032	1,60138	0,01242	0,161826	0,001026	0,817	-1,4	.	979	9	971	5	967	6
A47-63	367	53,3	0,00E+00	21221	0,07492	0,00035	1,65406	0,0536	0,160115	0,005134	0,990	-11	-8,7	1066	9	991	21	957	29
A47-64	262	50,1	0,00E+00	11705	0,08574	0,00044	2,35541	0,02942	0,199249	0,002272	0,913	-13,2	-11,1	1332	10	1229	9	1171	12
A47-65	1152	196,8	0,00E+00	5781	0,10666	0,00053	2,62991	0,02141	0,178836	0,001149	0,789	-42,4	-41,4	1743	9	1309	6	1061	6
A47-66	67	9,9	0,00E+00	4184	0,08486	0,0007	1,8952	0,09795	0,161975	0,008263	0,987	-28,3	-25,5	1312	15	1079	34	968	46
A47-67	454	116,2	0,00E+00	15544	0,10383	0,00051	3,79077	0,04403	0,264793	0,002792	0,908	-11,9	-10,2	1694	9	1591	9	1514	14
A47-68	2054	77,6	0,00E+00	2693	0,14302	0,00111	0,80191	0,01276	0,040666	0,000565	0,873	-90,3	-90,1	2264	13	598	7	257	3
A47-69	434	28,5	0,00E+00	15639	0,05513	0,00026	0,53458	0,00464	0,070329	0,000509	0,835	5,1	.	417	10	435	3	438	3
A47-70	731	32	0,00E+00	9224	0,05641	0,00032	0,36956	0,00874	0,047518	0,001092	0,971	-36,9	-32,8	468	12	319	6	299	7
A47-71	241	68,4	0,00E+00	17301	0,18261	0,00171	7,11214	0,09162	0,282472	0,0025	0,687	-45,1	-43,9	2677	15	2126	11	1604	13
A47-72	238	83,7	0,00E+00	28562	0,11491	0,0008	5,49997	0,06623	0,347132	0,003415	0,817	2,6	0,1	1879	12	1901	10	1921	16

Sample	*ppm*				Ratios							Discordance		Ages					
Name	U	^{206}Pb	$^{206}Pb_c$(%)	206/204	$^{207}Pb/^{206}Pb$*	1SE	$^{207}Pb/^{235}U$*	1SE	$^{206}Pb/^{238}U$*	1SE	Rho	Central (%)	Minimum rim (%)	207/206	1σ	207/235	1σ	206/238	1σ
A47-73	422	130,3	0,00E+00	40763	0,11257	0,00077	4,76707	0,05136	0,307137	0,002551	0,771	-7,1	-5	1841	12	1779	9	1727	13
A47-74	470	76	0,00E+00	17144	0,07945	0,00049	1,7986	0,01987	0,164194	0,001507	0,831	-18,5	-16,1	1183	12	1045	7	980	8
A47-75	162	23,9	0,00E+00	5078	0,10241	0,00058	2,20646	0,06456	0,156267	0,004484	0,981	-47,1	-45,9	1668	10	1183	20	936	25
A47-76	1233	38	0,00E+00	4586	0,05906	0,00052	0,30187	0,01514	0,037068	0,00183	0,984	-59,9	-56,3	569	18	268	12	235	11
A47-77	63	14	0,00E+00	4078	0,07958	0,00054	2,46123	0,02374	0,22432	0,00154	0,712	11	8,1	1186	13	1261	7	1305	8
A47-78	262	72,8	0,00E+00	20986	0,10561	0,00051	4,08386	0,03725	0,280463	0,002166	0,847	-8,6	-6,9	1725	9	1651	7	1594	11
A47-80	251	45,9	0,00E+00	20239	0,07572	0,00034	1,9545	0,01476	0,187208	0,001137	0,804	1,9	.	1088	9	1100	5	1106	6
A47-81	787	105,2	0,00E+00	6544	0,07984	0,00034	1,51965	0,01594	0,138038	0,001322	0,913	-32,1	-30,6	1193	8	938	6	834	7
A47-82	763	187,3	0,00E+00	30358	0,11564	0,00054	3,98555	0,04365	0,249969	0,002473	0,903	-26,6	-25,4	1890	8	1631	9	1438	13
A47-83	136	25,9	0,00E+00	7465	0,07793	0,0004	2,10731	0,01727	0,196121	0,001256	0,781	0,9	.	1145	10	1151	6	1154	7
A47-84	202	32,5	0,00E+00	10329	0,07108	0,00032	1,62515	0,0128	0,165818	0,001073	0,822	3,3	0,8	960	9	980	5	989	6
A47-85	156	50,6	0,00E+00	35615	0,12086	0,00062	5,41847	0,04964	0,325169	0,002465	0,827	-9	-7,4	1969	9	1888	8	1815	12
A47-86	203	66,8	0,00E+00	19135	0,12197	0,00062	5,54861	0,05332	0,329929	0,002692	0,849	-8,5	-6,9	1985	9	1908	8	1838	13
A47-87	652	59,5	0,00E+00	15936	0,181	0,00111	2,40017	0,07602	0,096172	0,002988	0,981	-81,2	-80,8	2662	10	1243	23	592	18
A47-89	171	71,6	0,00E+00	11129	0,17183	0,00147	10,60117	0,16385	0,44747	0,005752	0,832	-8,9	-6,6	2576	14	2489	14	2384	26
A47-90	446	92,7	0,00E+00	1109	0,09825	0,00166	3,04385	0,05881	0,224685	0,002113	0,487	-19,7	-15,7	1591	30	1419	15	1307	11
A47-91	152	7,2	0,00E+00	4098	0,0577	0,00059	0,41401	0,00783	0,052039	0,00083	0,843	-37,9	-31,4	518	21	352	6	327	5
A47-92	501	92,5	0,00E+00	21474	0,09637	0,00062	2,67234	0,04442	0,201109	0,003082	0,922	-26,3	-24,3	1555	12	1321	12	1181	17
A47-93	557	191,9	0,00E+00	12362	0,17112	0,00147	8,73492	0,13681	0,370219	0,004855	0,837	-24,4	-22,5	2569	14	2311	14	2030	23
A47-94	1148	184,6	0,00E+00	206823	0,07695	0,00044	1,84699	0,02219	0,174089	0,001843	0,881	-8,2	-5,5	1120	11	1062	8	1035	10
A47-96	183	8,6	9,80E-01	1251	0,05328	0,00051	0,37643	0,00855	0,051238	0,001058	0,909	-5,6	.	341	20	324	6	322	6
A47-95	406	130,7	0,00E+00	37865	0,11376	0,00076	5,42572	0,06725	0,34592	0,003609	0,842	3,4	0,8	1860	11	1889	11	1915	17
A47-97	553	104,1	0,00E+00	27001	0,08257	0,00048	2,3	0,02479	0,203962	0,001824	0,838	-5,4	-2,9	1259	11	1219	8	1197	10
A47-98	329	68,2	0,00E+00	3198	0,1047	0,00073	3,23081	0,04158	0,223792	0,002423	0,841	-26,3	-24,4	1709	12	1465	10	1302	13
A47-99	564	52,8	0,00E+00	3004	0,08489	0,00051	1,19409	0,01607	0,102018	0,001228	0,894	-54,8	-53,6	1313	11	798	7	626	7
A47-100	90	20,2	0,00E+00	8811	0,10219	0,00072	3,40998	0,04495	0,242016	0,00269	0,843	-17,8	-15,6	1664	13	1507	10	1397	14
A47-101	850	52,8	1,10E+00	1477	0,08168	0,0007	0,7552	0,01822	0,067053	0,001512	0,935	-68,3	-67	1238	16	571	11	418	9
A47-102	189	21,5	0,00E+00	8444	0,07421	0,00045	1,26995	0,01467	0,12411	0,001217	0,849	-29,6	-27,4	1047	12	832	7	754	7
A47-103	371	76,1	0,00E+00	13727	0,12191	0,00088	3,7	0,04693	0,222393	0,002289	0,82	-38,3	-36,8	1984	13	1580	10	1295	12
A47-104	222	34,1	0,00E+00	9828	0,07814	0,00049	1,80105	0,02966	0,167171	0,002543	0,924	-14,4	-11,6	1150	12	1046	11	997	14
A47-105	60	13	0,00E+00	2947	0,10148	0,00076	3,29504	0,05132	0,235483	0,003222	0,878	-19,4	-17	1651	13	1480	12	1363	17
A47-106	781	273,3	0,00E+00	70170	0,19172	0,00187	9,84465	0,16356	0,372412	0,005007	0,809	-30,2	-28,3	2757	16	2420	15	2041	24
A47-107	154	71,6	0,00E+00	18377	0,18345	0,0017	12,46528	0,21174	0,492804	0,007014	0,838	-4,6	-2	2684	15	2640	16	2583	30
A47-108	581	140,4	0,00E+00	22499	0,10365	0,00069	3,69521	0,04583	0,258553	0,002711	0,845	-13,8	-11,6	1691	12	1570	10	1482	14
A47-109	827	203,9	0,00E+00	9357	0,12215	0,00087	4,42635	0,08112	0,262822	0,004437	0,921	-27,2	-25,4	1988	12	1717	15	1504	23
A47-110	554	131	0,00E+00	32428	0,11881	0,00084	4,16381	0,07926	0,254173	0,004493	0,929	-27,5	-25,7	1938	12	1667	16	1460	23

Sample	*ppm*				Ratios							Discordance		Ages					
Name	U	^{206}Pb	$^{206}Pb_c$(%)	206/204	$^{207}Pb/^{206}Pb$*	1SE	$^{207}Pb/^{235}U$*	1SE	$^{206}Pb/^{238}U$*	1SE	Rho	Central (%)	Minimum rim (%)	207/206	1σ	207/235	1σ	206/238	1σ
A47-111	206	43,5	0,00E+00	5833	0,10074	0,00069	3,13686	0,04138	0,225842	0,002542	0,853	-21,9	-19,8	1638	12	1442	10	1313	13
A47-112	242	43,4	0,00E+00	79753	0,07832	0,00052	2,0754	0,02454	0,192185	0,001881	0,828	-2,1	.	1155	13	1141	8	1133	10
A47-113	278	37,6	0,00E+00	6837	0,07744	0,00051	1,55286	0,02083	0,145437	0,001695	0,869	-24,3	-21,7	1132	13	952	8	875	10
A47-114	776	97,6	0,00E+00	21412	0,10538	0,00072	1,97233	0,04197	0,135748	0,002735	0,947	-55,6	-54,4	1721	12	1106	14	821	16
A47-115	163	40,2	0,00E+00	12658	0,09752	0,0007	3,55234	0,04544	0,264186	0,002797	0,828	-4,7	-2	1577	13	1539	10	1511	14
A47-116	85	11,4	0,00E+00	2438	0,07595	0,00134	1,51777	0,03541	0,144943	0,002214	0,655	-21,6	-15,2	1094	34	938	14	873	12
A47-117	176	13,8	0,00E+00	2406	0,06399	0,00062	0,74607	0,01064	0,084559	0,000884	0,734	-30,6	-26	741	20	566	6	523	5
A47-118	258	15,6	0,00E+00	2207	0,06404	0,00051	0,65627	0,04995	0,074322	0,005625	0,994	-39,2	-35,6	743	17	512	31	462	34
A47-119B	130	18,8	0,00E+00	8396	0,09	0,00104	1,99477	0,09043	0,16075	0,007049	0,967	-35	-31,6	1426	21	1114	31	961	39
A47-120	143	14,1	0,00E+00	2911	0,07758	0,00058	1,15047	0,02975	0,107558	0,002665	0,958	-44,2	-41,9	1136	14	777	14	659	16
A47-121	594	65,2	1,10E-01	47980	0,09858	0,00058	1,59309	0,02994	0,117206	0,002091	0,949	-58,3	-57,3	1597	11	968	12	714	12
A47-122	39	2,8	0,00E+00	1584	0,05917	0,00069	0,63248	0,02956	0,07752	0,00351	0,969	-16,7	-6,9	574	26	498	18	481	21
A47-123	140	23,1	0,00E+00	7740	0,08937	0,00056	2,18467	0,02888	0,177289	0,002068	0,882	-27,6	-25,6	1412	12	1176	9	1052	11
A47-124	252	19,3	0,00E+00	4323	0,06258	0,00039	0,7122	0,00909	0,082537	0,000918	0,872	-27,4	-23,9	694	13	546	5	511	5
A47-125	105	32,5	0,00E+00	16289	0,11331	0,00075	5,19041	0,0767	0,332211	0,004385	0,893	-0,3	.	1853	11	1851	13	1849	21
A47-126	244	64,6	0,00E+00	13827	0,10135	0,0006	3,96649	0,05423	0,283851	0,003501	0,902	-2,6	-0,3	1649	11	1627	11	1611	18
A47-127	615	91,3	0,00E+00	22291	0,07333	0,00038	1,61701	0,0202	0,159932	0,001815	0,908	-7	-4,2	1023	10	977	8	956	10
A47-128	654	191,9	0,00E+00	56277	0,11472	0,00069	4,98013	0,07032	0,314839	0,004019	0,904	-6,8	-4,7	1876	11	1816	12	1764	20
A47-129	242	73,5	0,00E+00	4036	0,16657	0,00128	7,50869	0,13468	0,326939	0,005295	0,903	-31,8	-30,1	2523	13	2174	16	1824	26
A47-130	97	22	0,00E+00	5785	0,0997	0,00067	3,34993	0,04752	0,243691	0,00305	0,882	-14,6	-12,3	1618	12	1493	11	1406	16
A47-131	231	37	0,00E+00	7154	0,08248	0,00051	1,96348	0,02607	0,172643	0,002024	0,883	-19,8	-17,4	1257	12	1103	9	1027	11
A47-133	767	157,6	0,00E+00	21686	0,08627	0,00048	2,63035	0,03451	0,221123	0,002627	0,905	-4,6	-2,2	1344	10	1309	10	1288	14
A47-132	405	99,3	0,00E+00	18846	0,21137	0,00187	7,70359	0,13224	0,264327	0,003888	0,857	-53,8	-52,6	2916	14	2197	15	1512	20
A47-134	226	64,5	0,00E+00	19320	0,10701	0,00066	4,53948	0,06507	0,307666	0,003974	0,901	-1,3	.	1749	11	1738	12	1729	20

Sample AA16-49

Sample	*ppm*				Ratios							Discordance		Ages					
Name	U	^{206}Pb	$^{206}Pb_c$(%)	206/204	$^{207}Pb/^{206}Pb$*	1SE	$^{207}Pb/^{235}U$*	1SE	$^{206}Pb/^{238}U$*	1SE	Rho	Central (%)	Minimum rim (%)	207/206	1σ	207/235	1σ	206/238	1σ
A49-02	168	6,8	0,00E+00	2479	0,05734	0,00076	0,29597	0,00488	0,037435	0,000364	0,589	-54	-47,1	505	28	263	4	237	2
A49-03	108	9,4	0,00E+00	2699	0,0585	0,0006	0,66978	0,00935	0,083044	0,000788	0,680	-6,5	.	548	21	521	6	514	5
A49-04	70	4,5	0,00E+00	1699	0,0541	0,00072	0,46227	0,00761	0,061972	0,000601	0,589	3,4	.	375	28	386	5	388	4
A49-01	341	21,6	0,00E+00	6338	0,05527	0,00052	0,46322	0,00648	0,060784	0,000629	0,740	-10,4	.	423	21	386	4	380	4
A49-06	95	3,5	0,00E+00	890	0,05464	0,00089	0,27115	0,00518	0,03599	0,000362	0,527	-43,4	-28,1	398	36	244	4	228	2
A49-05	321	16,1	5,60E-01	2342	0,05296	0,0006	0,34799	0,00508	0,047653	0,000439	0,632	-8,5	.	327	25	303	4	300	3
A49-07	674	47,5	0,00E+00	7994	0,05822	0,00053	0,54886	0,00784	0,068374	0,000748	0,766	-21,5	-14,6	538	19	444	5	426	5
A49-08	646	169,5	0,00E+00	413089	0,10036	0,00136	3,48531	0,06322	0,251863	0,003027	0,663	-12,5	-8,7	1631	25	1524	14	1448	16
A49-09	103	6,9	0,00E+00	1249	0,05677	0,00068	0,51694	0,00815	0,066042	0,000673	0,647	-15	-3,6	483	26	423	5	412	4
A49-10	167	6,4	0,00E+00	2268	0,05307	0,00072	0,3	0,00457	0,037704	0,000357	0,573	-28,6	-9,6	332	29	247	4	239	2
A49-11	404	18,4	0,00E+00	1161	0,07252	0,00235	0,4486	0,01517	0,044862	0,000426	0,281	-73,3	-67,8	1001	62	376	11	283	3
A49-13	778	59,6	0,00E+00	2163	0,06369	0,00062	0,66182	0,00946	0,075365	0,000789	0,733	-37,3	-33,1	731	19	516	6	468	5
A49-14	335	21,1	0,00E+00	6875	0,05607	0,00104	0,49617	0,01127	0,064174	0,000849	0,582	-12,3	.	455	39	409	8	401	5
A49-15	528	37,1	0,00E+00	5917	0,0592	0,00124	0,58359	0,0145	0,071501	0,000964	0,543	-23,3	-5,9	574	45	467	9	445	6
A49-16	178	8,3	0,00E+00	2265	0,05715	0,00137	0,37675	0,01031	0,047808	0,000627	0,480	-40,4	-20	498	52	325	8	301	4
A49-17	176	12	0,00E+00	8474	0,05449	0,00106	0,52226	0,0124	0,069512	0,000948	0,574	11,1	.	391	43	427	8	433	6
A49-18	469	27,9	0,00E+00	20800	0,05756	0,00121	0,47563	0,01234	0,059934	0,000914	0,588	-27,6	-8,9	513	45	395	8	375	6
A49-19	47	2,8	0,00E+00	973	0,0537	0,00126	0,43604	0,01219	0,058891	0,000895	0,543	3	.	359	51	367	9	369	5
A49-20	247	10	0,00E+00	3962	0,05307	0,00105	0,29782	0,00739	0,040699	0,000609	0,602	-23	.	332	43	265	6	257	4
A49-21	482	17,8	0,00E+00	6171	0,04974	0,00097	0,25533	0,00632	0,037228	0,000568	0,616	29,3	.	183	45	231	5	236	4
A49-22	312	12,8	0,00E+00	3881	0,05083	0,00103	0,28934	0,0075	0,041288	0,00067	0,626	12,2	.	233	46	258	6	261	4
A49-23	85	3,4	0,00E+00	1898	0,05033	0,00114	0,27688	0,00765	0,039902	0,000635	0,576	20,5	.	210	52	248	6	252	4
A49-24	179	11,6	0,00E+00	7407	0,0539	0,00111	0,5	0,01262	0,06508	0,001037	0,611	11,1	.	367	43	401	9	406	6
A49-26B	1625	34,4	0,00E+00	4952	0,05968	0,0013	0,16276	0,004	0,019778	0,000228	0,468	-79,4	-74,6	592	44	153	3	126	1
A49-27	445	35,2	0,00E+00	4700	0,0588	0,00063	0,59448	0,00819	0,073327	0,000635	0,628	-19,2	-11,1	560	23	474	5	456	4
A49-28	707	193,5	0,00E+00	16587	0,09277	0,00046	3,19069	0,03406	0,249451	0,002355	0,884	-3,6	-1,5	1483	9	1455	8	1436	12
A49-29	730	28,3	0,00E+00	1870	0,05822	0,00043	0,28977	0,00304	0,0361	0,000268	0,706	-58,5	-55,6	538	15	258	2	229	2
A49-30	529	19	0,00E+00	19549	0,05204	0,00042	0,24089	0,00299	0,033571	0,000316	0,757	-26,3	-14,9	287	18	219	2	213	2
A49-31	215	11,1	0,00E+00	2620	0,05338	0,0004	0,35508	0,00403	0,048245	0,000412	0,751	-12,2	-2,2	345	17	309	3	304	3
A49-32	209	8,1	0,00E+00	3277	0,05127	0,00047	0,25734	0,00309	0,036404	0,000287	0,656	-9	.	253	20	233	2	231	2
A49-33	296	12,9	0,00E+00	3225	0,0518	0,00041	0,29165	0,00335	0,040839	0,000336	0,717	-6,8	.	276	17	260	3	258	2
A49-34B	639	25,4	0,00E+00	16690	0,05028	0,00028	0,3	0,00235	0,037232	0,000266	0,784	13,6	2,6	208	13	233	2	236	2
A49-34A	409	17,5	0,00E+00	4210	0,05126	0,00035	0,28355	0,0031	0,040122	0,000346	0,788	0,5	.	252	15	253	2	254	2
A49-35	929	58,9	0,00E+00	632	0,07405	0,00119	0,60783	0,01138	0,059532	0,000572	0,513	-66,1	-63,4	1043	30	482	7	373	3
A49-36	199	11,2	0,00E+00	2569	0,05301	0,00046	0,38452	0,00442	0,05261	0,000396	0,656	0,4	.	329	18	330	3	331	2
A49-37	32	2,7	0,00E+00	1023	0,05931	0,0009	0,657	0,01155	0,080341	0,00071	0,503	-14,4	-1,1	579	32	513	7	498	4

Sample	*ppm*				Ratios							Discordance		Ages					
Name	U	^{206}Pb	$^{206}Pb_c$(%)	206/204	$^{207}Pb/^{206}Pb$*	1SE	$^{207}Pb/^{235}U$*	1SE	$^{206}Pb/^{238}U$*	1SE	Rho	Central (%)	Minimum rim (%)	207/206	1σ	207/235	1σ	206/238	1σ
A49-38	421	80,1	0,00E+00	20188	0,07646	0,00037	1,86042	0,02047	0,176473	0,001743	0,898	-5,8	-3,4	1107	9	1067	7	1048	10
A49-39	608	29,4	0,00E+00	14737	0,05168	0,00032	0,32461	0,00319	0,045553	0,00035	0,781	5,9	.	271	13	285	2	287	2
A49-40	76	3,9	0,00E+00	1104	0,05409	0,00069	0,36085	0,00551	0,048383	0,000411	0,557	-19,2	-2,1	375	28	313	4	305	3
A49-41	1164	39	0,00E+00	510	0,0778	0,00303	0,3	0,01392	0,031557	0,000421	0,324	-83,7	-80,2	1142	77	296	11	200	3
A49-42	549	21,5	0,00E+00	5389	0,05085	0,00033	0,25958	0,00272	0,037026	0,000302	0,778	0,2	.	234	14	234	2	234	2
A49-43	408	31,6	0,00E+00	4559	0,05867	0,00033	0,58988	0,006	0,072925	0,00062	0,836	-18,8	-14,7	555	12	471	4	454	4
A49-44	68	2,9	0,00E+00	724	0,05692	0,00078	0,32037	0,00517	0,040821	0,000352	0,535	-48,1	-39,5	488	29	282	4	258	2
A49-45	29	2,6	0,00E+00	1144	0,05975	0,00112	0,68776	0,01453	0,08348	0,000814	0,461	-13,6	.	595	39	531	9	517	5
A49-46	449	18,1	0,00E+00	7726	0,05084	0,00035	0,2678	0,00285	0,038202	0,000312	0,767	3,5	.	234	16	241	2	242	2
A49-47	299	13,3	0,00E+00	1670	0,06221	0,0008	0,36087	0,00583	0,042073	0,000414	0,609	-62,3	-58,6	681	27	313	4	266	3
A49-48	207	42,8	0,00E+00	18298	0,08402	0,00046	2,24803	0,02603	0,19405	0,001984	0,883	-12,6	-10,4	1293	11	1196	8	1143	11
A49-49	218	46,6	0,00E+00	11870	0,08032	0,00043	2,21523	0,02318	0,200028	0,001802	0,861	-2,7	-0,2	1205	10	1186	7	1175	10
A49-50	401	62,9	0,00E+00	33878	0,07016	0,00036	1,42711	0,01482	0,147534	0,001332	0,869	-5,3	-2,4	933	10	900	6	887	7
A49-51	389	29,4	0,00E+00	7293	0,05614	0,00031	0,55634	0,00559	0,071869	0,000607	0,840	-2,4	.	458	12	449	4	447	4
A49-52	402	29,3	0,00E+00	10014	0,05655	0,00036	0,53917	0,00561	0,069146	0,000571	0,794	-9,4	-3,3	474	13	438	4	431	3
A49-53	207	13,6	0,00E+00	2473	0,05471	0,00039	0,47135	0,00523	0,062483	0,000533	0,769	-2,5	.	400	15	392	4	391	3
A49-54	304	163,4	0,00E+00	44851	0,18546	0,00146	12,56969	0,19576	0,491563	0,006612	0,864	-5,6	-3,4	2702	12	2648	15	2577	29
A49-55	144	7,3	0,00E+00	1091	0,0709	0,00153	0,47457	0,0111	0,048547	0,000443	0,39	-69,6	-65,6	954	42	394	8	306	3
A49-56	37	16,7	0,00E+00	6414	0,18317	0,00162	11,68802	0,25109	0,462787	0,009063	0,912	-10,3	-7,9	2682	14	2580	20	2452	40
A49-57	476	32,4	0,00E+00	5197	0,06054	0,00099	0,61408	0,01185	0,073572	0,00075	0,528	-27,5	-16,4	623	34	486	7	458	5
A49-58	93	3,2	0,00E+00	840	0,05301	0,00059	0,27361	0,00432	0,037435	0,000418	0,706	-28,6	-14,9	329	24	246	3	237	3
A49-60	83	3,2	0,00E+00	1109	0,05136	0,00048	0,29406	0,00412	0,041529	0,000435	0,748	2,2	.	257	20	262	3	262	3
A49-61	37	1,5	0,00E+00	370	0,06142	0,00173	0,38325	0,01152	0,045252	0,000482	0,354	-57,6	-45	654	57	329	8	285	3
A49-62	545	37,4	0,00E+00	18622	0,05611	0,00029	0,5764	0,00683	0,074499	0,000796	0,903	1,4	.	457	11	462	4	463	5
A49-63	150	6,9	0,00E+00	2959	0,05371	0,00045	0,37249	0,00495	0,050303	0,000518	0,775	-12,1	-1,2	359	19	321	4	316	3
A49-64	83	5	0,00E+00	1835	0,05782	0,00052	0,52306	0,00717	0,065607	0,000676	0,751	-22,4	-15,5	523	19	427	5	410	4
A49-65	629	46,5	0,00E+00	31747	0,0571	0,00029	0,6	0,00732	0,080254	0,000838	0,901	0,4	.	496	10	497	5	498	5
A49-66	1011	32,4	0,00E+00	4389	0,05415	0,00047	0,26236	0,00399	0,035136	0,000439	0,821	-41,7	-34,6	377	18	237	3	223	3
A49-67	934	31,7	0,00E+00	13678	0,05102	0,00029	0,26102	0,00307	0,037107	0,000383	0,877	-2,8	.	242	12	235	2	235	2
A49-68	96	10,8	0,00E+00	2212	0,07588	0,00075	1,27473	0,01978	0,121837	0,001456	0,77	-34	-30,8	1092	19	835	9	741	8
A49-69	511	22,2	0,00E+00	8068	0,05269	0,00031	0,3444	0,00404	0,047408	0,000482	0,868	-5,4	.	315	12	300	3	299	3
A49-70	115	4	0,00E+00	1940	0,05359	0,00051	0,28245	0,0043	0,038222	0,000456	0,784	-32,3	-22,5	354	20	253	3	242	3
A49-71	260	8,8	0,00E+00	3020	0,05076	0,00035	0,25954	0,00324	0,037086	0,000385	0,83	2,2	.	230	15	234	3	235	2
A49-72	182	6,3	0,00E+00	1654	0,05323	0,00063	0,27791	0,00436	0,037869	0,000387	0,651	-29,7	-15,1	338	25	249	3	240	2
A49-73	622	22,1	0,00E+00	9177	0,05119	0,0003	0,27469	0,00324	0,038921	0,000398	0,867	-1,3	.	249	13	246	3	246	2
A49-74	994	33,7	0,00E+00	11132	0,05104	0,00028	0,2618	0,00302	0,037201	0,000379	0,884	-3	.	243	12	236	2	235	2

Sample	*ppm*				Ratios							Discordance		Ages					
Name	U	^{206}Pb	$^{206}Pb_c$(%)	206/204	$^{207}Pb/^{206}Pb$*	1SE	$^{207}Pb/^{235}U$*	1SE	$^{206}Pb/^{238}U$*	1SE	Rho	Central (%)	Minimum rim (%)	207/206	1σ	207/235	1σ	206/238	1σ
A49-75	773	23,4	0,00E+00	2016	0,0638	0,00142	0,31749	0,01316	0,036091	0,00126	0,842	-70,1	-64,9	735	45	280	10	229	8
A49-76	353	49,8	0,00E+00	20249	0,07013	0,0004	1,47491	0,01912	0,152534	0,00178	0,9	-2	.	932	11	920	8	915	10
A49-77	401	23,3	0,00E+00	6944	0,05492	0,00033	0,48265	0,00596	0,063733	0,000691	0,878	-2,7	.	409	13	400	4	398	4
A49-78	399	18,7	0,00E+00	6107	0,05426	0,00036	0,38439	0,00473	0,051384	0,000536	0,847	-15,8	-8,2	382	14	330	3	323	3
A49-79	328	11,2	0,00E+00	3935	0,05143	0,00037	0,26678	0,0034	0,037624	0,000397	0,827	-8,6	.	260	16	240	3	238	2
A49-80	514	33,5	0,00E+00	7722	0,05585	0,00031	0,54864	0,00666	0,071251	0,000766	0,886	-0,6	.	446	12	444	4	444	5
A49-81	843	45,1	0,00E+00	5701	0,06033	0,00067	0,4889	0,00855	0,058772	0,000791	0,770	-41,3	-35,8	616	24	404	6	368	5
A49-82	847	29,3	0,00E+00	3542	0,05649	0,0007	0,29728	0,00491	0,038168	0,000415	0,658	-49,7	-42,6	472	27	264	4	241	3
A49-83	118	9,2	0,00E+00	3356	0,05752	0,00041	0,67359	0,00895	0,084931	0,000949	0,841	2,8	.	512	16	523	5	525	6
A49-84	301	13,3	0,00E+00	4690	0,0531	0,00038	0,35615	0,00466	0,048647	0,000532	0,835	-8,2	.	333	16	309	3	306	3
A49-85	764	107,9	0,00E+00	761	0,07363	0,00049	1,55657	0,02118	0,153322	0,001819	0,872	-11,6	-8,4	1031	13	953	8	920	10
A49-86	448	15,5	0,00E+00	6462	0,05366	0,00036	0,28225	0,0036	0,03815	0,000413	0,849	-33	-26,3	357	15	252	3	241	3
A49-87	336	11,5	0,00E+00	3913	0,05122	0,00036	0,26695	0,00355	0,037798	0,000425	0,846	-4,7	.	251	16	240	3	239	3
A49-88	129	4,5	0,00E+00	1299	0,05644	0,00123	0,2994	0,00731	0,038476	0,000425	0,452	-49,1	-32,4	470	46	266	6	243	3
A49-89	122	4,2	0,00E+00	1047	0,05899	0,00099	0,30892	0,00633	0,037982	0,000448	0,575	-58,7	-51,5	567	35	273	5	240	3
A49-90	892	29,5	0,00E+00	4987	0,05577	0,00057	0,28032	0,00442	0,036454	0,000439	0,764	-48,8	-42,6	443	22	251	4	231	3
A49-91	1084	39,1	0,00E+00	252	0,10475	0,00328	0,575	0,01915	0,039812	0,000452	0,341	-86,9	-85,6	1710	55	461	12	252	3
A49-92	431	18	0,00E+00	4971	0,05276	0,00035	0,33603	0,00433	0,04619	0,000514	0,862	-8,8	.	319	14	294	3	291	3
A49-93	342	11,2	0,00E+00	3679	0,05039	0,00034	0,25171	0,00336	0,036225	0,000416	0,861	7,7	.	213	16	228	3	229	3
A49-94	140	6,7	0,00E+00	1049	0,07112	0,00275	0,52337	0,02106	0,053371	0,000603	0,281	-66,8	-57,8	961	79	427	14	335	4
A49-96	238	13	2,90E+00	519	0,05032	0,00123	0,43469	0,01294	0,062654	0,001068	0,573	89,4	42	210	54	367	9	392	6